Evaluation of bioreductively-activated Tirapazamine (TPZ) prodrugs for the management of hypoxic solid tumors

by

Sindhuja Pattabhi Raman

A thesis submitted in partial fulfillment of the requirements for the degree of

Master of Science

in

Cancer Sciences

Department of Oncology
University of Alberta

Abstract

Solid tumors often have large areas with low levels of oxygen (termed hypoxic regions), which are associated with poor prognosis and treatment response. Tirapazamine (TPZ), a hypoxia targeting anticancer drug, started as a promising candidate to deal with this issue. However, it was withdrawn from the clinic due to severe neurotoxic side effects and poor target delivery. Hypoxic cells overexpress glucose transporters (GLUT) - a key feature during hypoxic tumor progression. Our project aims at conjugating TPZ with glucose to exploit the upregulated GLUTs for its delivery, and thereby facilitate the therapeutic management of hypoxic tumors. We hypothesized that glucose-conjugated TPZ (G_6-TPZ) would be selectively recruited to these receptors, facilitating its entrapment in poorly oxygenated cells only, with minimal damage to their oxygenated counterparts. However, our results reveal that the addition of the glucose moiety to TPZ was counterproductive since G_6-TPZ displayed selective hypoxic cytotoxicity only at very high concentrations of the compound. We speculate that the reduced cytotoxicity of G_6-TPZ might be due to the fact that the compound was not taken up by the cells. In order to monitor the cellular uptake of TPZ, we developed a click chemistry-based approach by incorporating an azido (N_3) group to our parent compound (N_3-TPZ). We observed that the azido-conjugated TPZ was highly hypoxia selective and the compound successfully tracks cellular hypoxia. Using a similar methodology, we went on to isolate and identify the proteins that are modified by N_3-TPZ under hypoxia in order to obtain a better understanding of the potential underlying molecular mechanism of TPZ cytotoxicity. In addition, we exploited the property of monitoring TPZ uptake by N_3-TPZ to study the uptake and localization of G_6-TPZ by synthesizing a new derivative of TPZ, which incorporated both glucose and azido moieties. Overall, we carried out the above specified structural modifications on TPZ as an attempt to overcome the limitations of TPZ therapy.

Acknowledgements

I owe sincere gratitude to my co-supervisors, Dr. Michael Weinfeld and Dr. Piyush Kumar for their constant support and motivation without which this dissertation would not be possible. I wish to thank them for providing me the opportunity to work in their team and providing mentorship, motivation, invaluable guidance and encouragement throughout the project, which set the direction for my research.

I would like to sincerely thank Dr. Lynne Postovit for kindly letting me work in her laboratory for a year and supervising me in my earlier days. I am indebted to her for all her constructive suggestions and advice in various meetings throughout the research. I also would like to extend my thanks to her lab members who were kind and friendly towards me.

My sincere thanks to Dr. Richard Fahlman for letting us perform mass spectrometry in his laboratory and am deeply grateful for his kind assistance and valuable suggestions with the data analysis. I also would like to extend my gratitude to Jack Moore who helped us with the proteomics.

My special thanks to Dr. Hassan Elsaidi for designing and synthesizing all the drugs that have been used in this project. Without his effort, it would have been impossible to carry out this work smoothly. I also owe a lot to Faisal Bin Rashed, who is a very good friend and has been a great constant support throughout the entire project. His friendly talks, continual encouragement, valuable discussions and timely help made this journey considerably easier.

Most importantly, I would like to thank all the CRIO group members for their warmth of kindness and interesting discussions in our monthly meetings which have been very beneficial. I am delighted and indebted to Dr. Dawn McDonald and Xiao-Hong Yang who constantly helped

and guided me with their technical expertise. I heartily thank Mesfin Fanta and Xiaoyan Yang who were always welcoming, amicable and willing to help.

Furthermore, I am immensely pleased to thank my best friends in the lab Zahra Shire, Diana Diaz, Bingcheng Jiang and Wisdom Kate who made my research experience cheerful and uplifting by providing a great positive working environment. In addition, I would like to thank Dr. Feridoun Karimi-Busheri and Dr. Aghdass Rasouli-Nia for their genuine support and advice. I also extend my thanks to the imaging facility, especially Geraldine Barron.

Lastly, I take great pleasure to acknowledge my parents and my husband for always being there patiently by my side throughout this endeavour and for their immense love, moral support and persistent prayers which made this journey worthwhile.

Table of Contents

List of Tables

List of Figures

List of Abbreviations

Abbreviation	Full name
ºC	degree Celsius
%	percent
AV	arteriovenous
Ab	antibody
AP-1	activator protein 1
ATP	adenosine protein 1
ARCON	accelerated radiotherapy with carbogen and nicotinamide
ARNT	aryl hydrocarbon receptor nuclear translator
AQ4N	banoxantrone
ATCC	American type culture collection
bHlH	basic helix-loop-helix
BSA	bovine serum albumin
BTZ	benzotriazinyl radical
CAIX	carbonic anhydrase-IX
CATAPULT	CIS and TPZ in subjects with advanced previously untreated NSCL tumours
CBP	CREB-binding protein
cDNA	complementary protein
CEBP	CCAAT-enhancer-binding protein
CO_2	carbon dioxide
CIS	cisplatin
CFA	colony formation assay
CSC	cancer stem cell
Cu-ATSM	Copper (II)-diacetyl-bis(N-methylthiosemicarbazone)
CuAAC	Copper(I)-Catalyzed Azide-Alkyne Cycloaddition
CVS	Crystal violet staining
CYP450R	cytochrome p450 oxideroductase
DAHANCA	Danish Head and Neck Cancer group
DAPI	4'.6-diamidino-2-phenylindole
DFS	Disease-free survival
DMEM	Dulbecco's Modified Eagle Medium
DMEM/F12	Dulbecco's Modified Eagle Medium: nutrient mixture F-12
DMSO	Dimethyl sulfoxide
DNA	deoxyribonucleic acid
DSB	double strand break
EBV	Epstein-bar virus
EDTA	ethylenediaminetetraacetic acid
EF5	pentafluorinated etanidazole
eIF2α	eukaryotic translation initiation factor 2 subunit alpha
ELISA	enzyme linked immunosorbent assay
EO9	apaziquone

ERK	extracellular signal-regulated kinase
FAZA	fluoroazomycin arabinofuranoside
FBS	fetal bovine serum
FDG	fluorodeoxyglucose
FETA	fluoroetanidazole
FIH-1	factor-inhibiting HIF-1
FMISO	fluoromisonidazole
FU	fluorouracil
G	gravity (units)
GOG	Gynecologic Oncology Group
GLUT-1	glucose transporter-1
G_6-TPZ	glucose-conjugated TPZ
HAP	hypoxia activated prodrug
HBOT	hyperbaric oxygen therapy
HCl	hydrochloric acid
HCR	hypoxic cytotoxic ratio
HIF	hypoxia inducible factor
HNC	head and neck cancer
HNSCC	head and neck squamous cell carcinoma
Hg	millimeters of mercury
HPV	human papilloma virus
HRE	hypoxia-response element
HRP	horseradish peroxidase
hrs	hours
IAZA	iodoazomycin arabinoside
ICH	intracellular helix
IC_{50}	half maximal inhibitory concentration
IHC	immunohistochemistry
IR	ionizing radiation
LC-MS/MS	liquid chromatography coupled mass spectrometry
LDHA	lactate dehydrogenase- A
LOX-1	lysyl oxidase-1
LRC	locoregional control
LSCLC	limited-stage small-cell lung cancer
MDR	multidrug resistance
MFS	major facilitator superfamily
mg	milligram
mm	millimeter
mM	millimolar
mRNA	messenger ribonucleic acid
mTOR	mammalian target of rapamycin
mTORC1/4E-BP1	mTOR complex 1/eukaryotic initiation factor 4E-binding protein-1
MTT	3-(4,5-dimethylthiazol-2-Yl)-2,5-diphenyltetrazolium bromide

NF-kβ	nuclear factor kappa beta
NI	nitroimidazole
NIRS	near-infrared spectroscopy
nm	nanometer
NaCl	sodium chloride
NADPH	nicotinamide adenine dinucleotide phosphate hydrogen
NaF	sodium fluoride
Na_3VO_4	sodium orthovanadate
N_2	nitrogen
N_3	azido
N_3-TPZ	azido-conjugated TPZ
N_3-G_6-TPZ	azido-glucose-conjugated TPZ
NSCLC	non-small-cell lung cancer
O_2	oxygen
OS	overall survival
PAS	per-arnt-sim
PBS	phosphate buffered saline
PE	etoposide
PET	positron emission tomography
PFA	paraformaldehyde
PFS	progression free survival
pH	potential hydrogen
PHD	prolyl hydroxylase domain enzyme
PHD2	prolyl hydroxylase domain protein 2
PI3K	phosphatidylinositide-3-kinase
POR	porfiromycin
PSM	peptide-spectrum match
p16	cyclin-dependent kinase inhibitor 2A
Real-Time RT-PCR	real-time reverse transcription polymerase chain reaction
RIPA	radioimmunoprecipitation buffer
RNA	ribonucleic acid
ROS	reactive oxygen species
RPLP0	ribosomal protein lateral stalk subunit P0
Rpm	revolutions per minute
RT	radiation therapy
SCCVII	squamous cell mouse carcinoma
SDS	sodium dodecyl sulfate
SDS-PAGE	sodium dodecyl sulfate-polyacrylamide gel electrophoresis
SEM	standard error of mean
SGLT	sodium-glucose linked transporters
SLC2A	solute carriers 2A gene family
SPECT	single photon emission computed tomography
SSB	single strand break
STRING	search tool for the retrieval of interacting genes/proteins
SWOG	Southwest Oncology Group
TBS-T	tris buffered saline with tween
TH-302	evofosfamide

TPZ	tirapazamine
Tris-HCl	tris(hydroxymethyl)aminomethane-hydrochloric acid
TROG	Trans-Tasman Radiation Oncology Group
VEGF	vascular endothelial growth factor
VHL	von hippel-lindau
V	volt
Mg	microgram
µg/ml	microgram/milliliter
µl	microliter
µM	micromolar
α	alpha
β	beta
δ	delta

Copyright licenses

Licensee: Sindhuja Pattabhi Raman. License Date: Nov 9, 2018. License Number: 4465011315984. Publication: Nature. Title: Crystal structure of the human glucose transporter GLUT1. Type of use: Thesis/dissertation. Total: 0.00 CAD.

Licensee: Sindhuja Pattabhi Raman. License Date: Nov 9, 2018. License Number: 4465020499624. Publication: Nature Reviews Cancer. Title: Exploiting tumour hypoxia in cancer treatment. Type of use: Thesis/dissertation. Total: 0.00 USD.

Licensee: Sindhuja Pattabhi Raman. License Date: Nov 9, 2018. License Number: 4465020778672. Publication: Cell. Title: A Lactate-Induced Response to Hypoxia. Type of use: Reuse in a thesis/dissertation. Total: 0.00 USD.

Licensee: Sindhuja Pattabhi Raman. License Date: Dec 3, 2018. License Number: 4481340596748. Publication: Elsevier Books. Title: Medicinal Chemistry of Anticancer Drugs. Type of use: Reuse in a thesis/dissertation. Total: 0.00 CAD.

Licensee: Sindhuja Pattabhi Raman. License Date: Dec 4, 2018. License Number: 4482050213742. Publication: British Journal of Cancer. Title: The Histological Structure of Some Human Lung Cancers and the Possible Implications for Radiotherapy. Type of use: Thesis/dissertation. Total: 0.00 CAD.

Chapter I - Introduction

1.1. Tumor Hypoxia

Tumor Hypoxia is a physiological state where cells within a tumor are sub-optimally oxygenated [1]. Reduction in oxygen level is mainly due to poor vascularization in tumor tissues, which renders it difficult to satisfy the high demand for oxygen created due to rapid and aggressive proliferation of cancer cells [2,3]. The estimated level of oxygenation in normal tissues is 40-60 mm Hg, whereas the partial O_2 pressure reduces to 10 mm Hg or lower in hypoxic conditions [4]. Tumor hypoxia is a common feature that occurs in almost all types of human solid tumors, heterogeneously compromising 50-60% of a tumor mass [5-11]. Hypoxia alters cellular metabolism, which can trigger the activation of genes involved in glycolysis, cell survival, replication, angiogenesis, tissue invasion, metastasis and loss of genomic stability [12,13]. As a consequence, the malignant potency of hypoxic tumors is amplified enabling them to withstand conventional radio [14] and chemotherapy [15] and thereby leading to treatment failure. Therefore, tumor hypoxia presents significant human health challenges and contributes to poor overall survival of cancer patients. Hence, development of novel approaches that molecularly target tumor hypoxia is of utmost need.

1.1.1. Different types of tumor hypoxia

Tumor hypoxia is broadly classified into two types namely, acute and chronic, which contribute to the different hypoxia related responses within the tumor leading to variable effects on tumor development and therapeutic response [16]. The first scientific study documenting hypoxia was published by Thomlinson and Gray in 1955 [17]. They suggested that cells within a tumor could remain viable under chronic levels of hypoxia for hours to a few days when located at a distance of 70 μm from the vasculature (Figure 1.1). This sets the basis for description of diffusion-limited hypoxia or chronic hypoxia, as the distance to which oxygen can diffuse is largely limited by the

rapid rate at which it is consumed by respiring tumor cells [18]. In the early 1980s, Brown and co-workers proposed that hypoxia in tumors can also arise through another mechanism. They demonstrated that oxygenation levels within a tumor can vary by fluctuating levels of blood flowing through the vessels to the tumor. This arises as a consequence of temporary closing/opening or blockage of a blood vessel due to malformed tumor vasculature resulting in transient periods of severe hypoxia within the tumor [19] (Figure 1.2). The phenomenon is known as acute hypoxia and is also quoted with different names such as perfusion-limited, cyclic, repetitive, transient, short-term, intermittent and fluctuating hypoxia by several authors [19-21]. Targeting acute hypoxia is said to be difficult when compared to chronic hypoxia due to lack of blood flow and in addition, acute hypoxic cells are also said to demonstrate high metastatic potential [22]. Since then, immense research has been conducted in order to control the hypoxic effects in solid tumors thereby to improve the efficacy of treatment given to cancer patients.

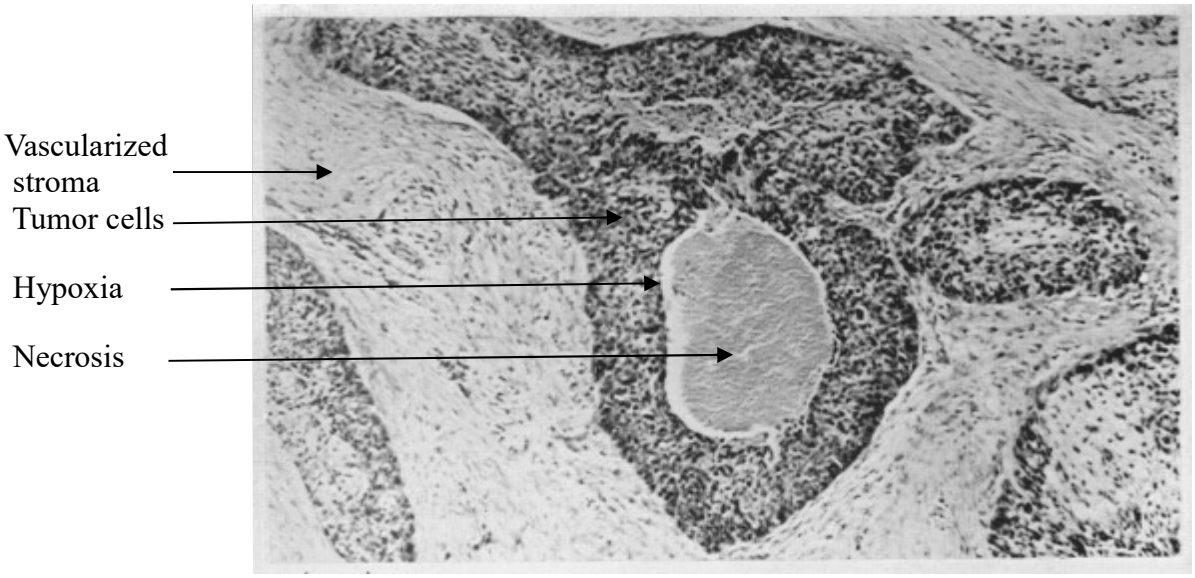

Figure 1.1 Diffusion-limited or chronic hypoxia

Diagram shows a transverse section of a tumor cord surrounded by vascularized stroma. It also shows large areas of necrosis which is separated from stroma by a narrow band of tumor cells. The study indicates that even though the necrotic centre grows with respect to the enlargement of the

tumor cord, the thickness of tumor cells remains constant. They identified that the cells bordering necrosis were viable, but hypoxic. This is due to the limited diffusion distance of oxygen through the respiring tissue since hypoxic cells are located farthest from the blood vessel. The condition was termed as diffusion-limited hypoxia, now also known as chronic hypoxia [17]. Reproduced and modified by permission from Nature Publishing Group: British Journal of Cancer. The Histological Structure of Some Human Lung Cancers and the Possible Implications for Radiotherapy. Thomlinson, R. H. and Gray, L. H., Copyright © 1955.

(a) Normal tissue **(b) Tumor tissue**

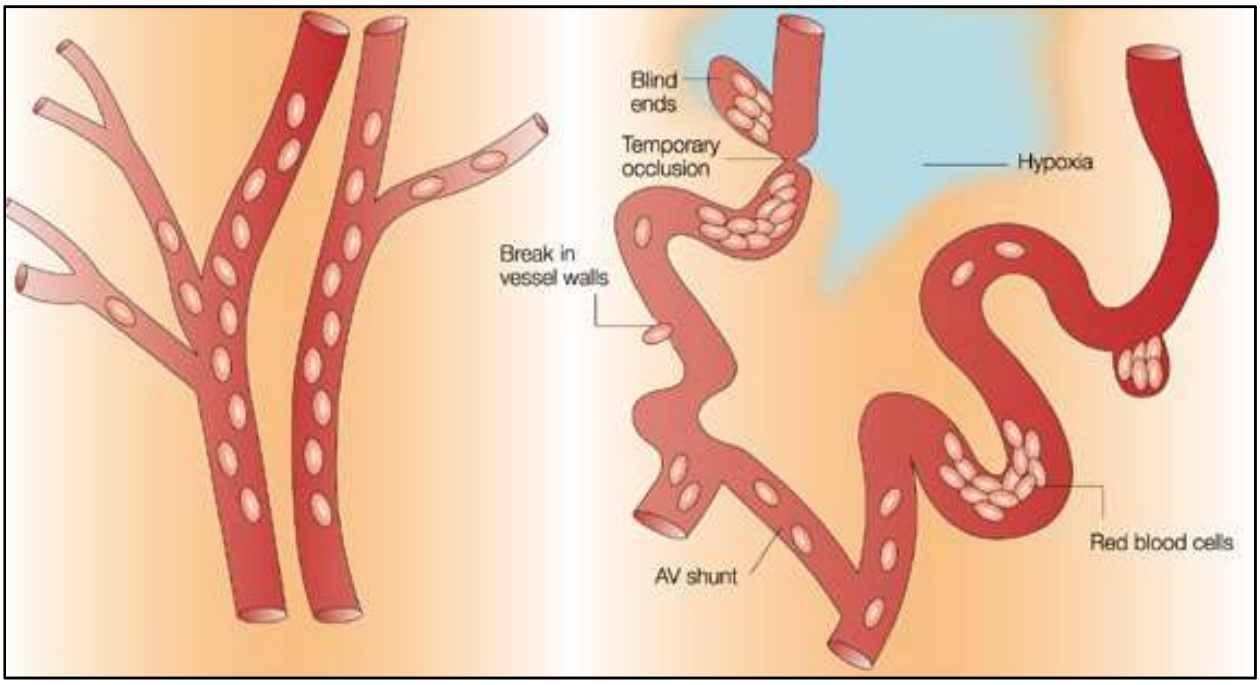

Figure 1.2 Vasculature of normal tissue versus tumor tissue.

Diagram showing the differences between normal and tumor vasculature (a) normal tissue has uniform, highly organized, evenly spaced blood vessels close enough to provide nutrient and oxygen supply to all the cells. (b) In tumor tissue, hypoxic regions are present between the blood vessels, which are complex, dilated, irregular with lots of twists, blind ends, temporary occlusion, and AV shunt. In addition, the vessels are far apart from each other, which leads to transient blockage of blood delivery resulting in acute (perfusion-limited) hypoxia along with chronic (diffusion-limited) hypoxia [23]. Reproduced by permission from Nature Publishing Group: Nature Reviews Cancer. Exploiting tumour hypoxia in cancer treatment. Brown, J. M. and Wilson, W. R., Copyright © 2004.

1.1.2. Head and Neck Cancer

Head and Neck Cancer (HNC) comprises a diverse group of malignant tumors that arise from the epithelial lining of the head and neck regions. They are distinguished based on the primary site of origin as malignancies of the oral cavity, nasal cavity, pharynx, larynx and salivary glands [24]. HNC is the sixth most common cancer worldwide with an incidence rate of ~ 550,000 cases and accounts for ~ 380,000 deaths annually. The male to female ratio for the likelihood of developing HNC ranges from 2:1 to 4:1 and the disease is more prevalent in people who are over 50 years of age [25]. Over recent years, human papilloma virus (HPV) infection has been reported to be the primary risk factor associated with HNC [26]. The other leading causes are smoking, alcohol abuse and Epstein-Barr virus (EBV) infection (for nasopharyngeal cancer). Most common treatment modalities for HNC are surgery, radiation therapy and chemotherapy. The treatment efficacy is said to be improved with altered fractionated radiotherapy [27] and concomitant cisplatin chemotherapy [28]. However, regardless of therapeutic measures, the 5 year overall survival rate of HNC patients still remains only 40-50% [29]. Locoregional recurrence is demonstrated as one of the major contributors to morbidity in 15-50% of HNC patients [30]. Approximately, 90% of all HNCs are squamous cell carcinomas (HNSCC) [31]. Even though, the HNSCC share similar histology, the disease is highly heterogeneous with respect to pathogenesis, clinical progression and management strategy [32]. In spite of the diversity, the common feature that leads to locoregional recurrence and eventually treatment failure in HNC is the presence of tumor hypoxia [33]. The effect of pretreatment tumor oxygenation status on the radiation therapy related response in HNSCC was first documented in 1996 [34]. Since then, numerous studies have demonstrated that HNC patients bearing a higher degree of hypoxic fractions show poor response to radio- and chemotherapy and the effectiveness of surgery is limited as well [35]. Hence, tumor hypoxia is considered as a strong

independent negative prognostic factor in HNC resulting in decreased locoregional control (LRC), overall survival (OS) and long term disease-free survival (DFS) [36]. Therefore, unravelling the mechanistic relationship between tumor hypoxia and treatment outcome in HNC is of great clinical importance and will play a major role in improving the quality of life of HNC patients. Since HNC is a well-documented tumor type for hypoxia studies [37], we chose it as our ideal model of study.

1.1.3. Tumor hypoxia as a therapeutic barrier in HNC

As discussed above, low partial O_2 pressure is a key component in HNC and is associated with increased resistance to treatment (radiotherapy and anti-tumor drug delivery).

1.1.3.1. Hypoxia induced radioresistance

The influence of oxygen on radiotherapy was recognized back in 1900 and hypoxic radioresistance was first discussed in detail by Schwartz and colleagues in 1909 [38]. Now, it is a well-established concept that hypoxic cells exhibit up to three times more resistance to radiation therapy when compared to aerobic cells [39]. Radiation is delivered to patients through different means; the notable ones are external beam radiation (widely used), brachytherapy/internal radiation and through use of radiopharmaceuticals [40]. In solid tumors, radiosensitivity is characterized by two factors namely, intrinsic radiosensitivity displayed by the tumor cells and the degree/extent of hypoxia [41]. Ionizing radiation (IR) kills rapidly dividing cells by generating reactive hydroxyl free radicals either by direct or indirect action [42]. In the presence of oxygen, the reactive free radicals target the DNA strand inducing irreversible DNA damage. We can say, oxygen acts as a potent chemical radiosensitizer by enhancing the efficiency of ionizing radiation dose during radiotherapy by formation of DNA damaging free radicals in cancer cells [42]. In hypoxia, due to a lack of electron supply from oxygen, the DNA damage induced by radiation would be repaired by the tumor cells. In addition, free radicals generated by radiation are reduced

and repaired by sulfhydryl containing macromolecules, a phenomenon known as chemical restitution. Hypoxic cells use the above said mechanism to withstand the damaging effect of radiotherapy [43]. Acute hypoxic cells are said to show high radioresistance when compared to chronic hypoxic cells [44]. However, the exact therapeutic significance of acute hypoxia in radiation therapy still remains unclear. Since there has been only limited success to overcome radioresistance of hypoxic cells, employing a hypoxia modified multi-fractionated radiotherapy (RT) regimen with precise delivery of escalated radiation doses to hypoxic tumor cells and utilizing multimodality functional imaging in RT planning might result in better outcomes when used in combination with surgical resection and novel adjuvants.

1.1.3.2. Hypoxia induced chemoresistance

Hypoxic stress promotes cancer cells to develop resistance against chemotherapeutic agents. Hypoxia-induced chemoresistance was first elucidated in 1950s, suggesting that tumor cells present in severe hypoxic conditions are resistant to chemotherapy [17]. The relation between hypoxia and chemoresistance in HNC was evident when a sub-population of hypoxic cells showed selective survival after chemotherapy [45]. It is believed that various reasons contribute to impaired chemosensitivity. The major reason why these anti-cancer drugs are less effective is due to the inefficient delivery of the cytotoxic drugs to the specific tumor site [46]. Since hypoxic cells are located far from the blood vessel and the vascular organization in hypoxic tumors is abnormal, the diffusion distance between the drug and tumor increases suggesting that the drug might get metabolized before reaching the target cells, which would ultimately result in delivering therapeutically ineffective dose of the drug to the tumor [47,48]. It was also identified that hypoxic tumors are resistant to chemotherapeutic agents that target rapidly proliferating cells [49]. This might be due to the fact that some cells reduce their proliferation rate while they develop within a hypoxic

tumor contributing to reduced response to the anti-cancer agents [46,48]. Anti-cancer drugs that induce DNA damage such as doxorubicin exhibit low efficacy towards hypoxic cells due to decreased free-radical generation [47]. Hence, in most of the cases it is not the tumor that exhibits resistance towards the therapeutic agent, it is the limitation of the drug due to hypoxic conditions which results in poor therapeutic efficiency. Moreover, recent evidence suggests that cancer stem cell (CSC) populations present in HNC might contribute to drug resistance [50]. This is due to the fact that these stem-cell-like cell fractions residing in hypoxic conditions possess the ability to survive in fluctuating blood flow. Also, the low proliferation rate of CSC with infrequent cell cycling patterns results in failure to respond to division-dependent chemo drugs [51]. Further, the upregulation of multidrug resistance (MDR) genes and the over expression of gene product p-glycoprotein (known to be involved in MDR) under hypoxia is linked to the poorer response towards anti-cancer drugs since MDR causes extrusion of drugs [52]. In addition, hypoxia also promotes genetic instability in cancer cells due to mutation of p53 resulting in loss of upregulation of p53 apoptotic target genes which ultimately leads to a rapid development of drug resistance in cells [44]. Hence, hypoxia-induced chemoresistance could only be overcome by using novel drugs such as hypoxic cytotoxins that exploit hypoxia thereby converting a hypoxic problem into a therapeutic advantage.

1.2. Cellular response to hypoxia at the molecular level

The cellular response to hypoxia is mainly mediated by the hypoxia inducible factor (HIF) family, which regulates the expression of multiple genes associated in processes such as adaptation and rapid progression of cancer cells [53]. However, in recent years, new players have been identified in regulating hypoxia at the molecular level [54].

1.2.1. Hypoxia Inducible Factor dependent and independent mechanism

1.2.1.1. HIF-dependent mechanism

Hypoxic tumor cells undergo a lot of adaptive and cellular changes in order to survive in the low intra-tumoral pH of the tumor microenvironment [55]. Approximately 1-1.5% of the genome is transcriptionally regulated by hypoxia often through a Hypoxia-Inducible Factor (HIF) dependent pathway [56]. Even though HIF related response does not solely contribute to all the alterations that occur to gene expression in hypoxia, it plays a major part in the above said alterations and adaptations to low oxygen. Its essential role is strongly evident as the HIF signalling pathway is reported to be present in almost all cell types and all higher eukaryotes [57]. HIF, a transcription factor identified in 1991 [58], is a heterodimeric protein comprising of two sub-units namely, α (HIF-α) and β (HIF-β/ aryl hydrocarbon receptor nuclear translocator- ARNT) that binds to the hypoxia-responsive element (HRE) in the erythropoietin gene. In HIF-1 protein, HIF-1α is the oxygen sensitive sub-unit whereas HIF-1β is constitutively expressed. Both sub-units belong to the basic helix-loop-helix (bHLH)-per-arnt-sim (PAS) protein family [59]. There are three paralogs of HIF-α subunit (HIF-1, HIF-2, HIF-3) of which HIF-1 and HIF-2 are extensively studied [60]. Both HIF-1α and HIF-2α display high sequence similarity and possess the ability to heterodimerize with ARNT and bind to HRE [61].

Under normoxia, HIF-1α protein levels are said to be low due to hydroxylation by active prolyl hydroxylase domain protein 2 (PHD2) and factor-inhibiting HIF-1 (FIH-1), in the presence of co-substrate (2-oxoglutarate) and cofactors namely ferrous iron and ascorbate. Hydroxylation of HIF-1α leads to its binding to the Von Hippel-Lindau tumor suppressor protein (VHL), initiating ubiquitination by E3 ubiquitin ligase, which results in the proteosomal degradation of HIF-1α by the 26S proteasome [62]. As a result, HIF-1α has a very short half-life of < 5 min in the cytoplasm

at normal oxygen levels [63]. In contrast, under hypoxic conditions, the hydroxylases are inhibited as a result of substrate limitation. HIF-1α gets stabilized and translocates from the cytoplasm to the nucleus and heterodimerizes with HIF-β/ARNT, thus evading the VHL- regulated proteasomal degradation [64]. Hence, the stable transcriptionally active heterodimerized complex (HIF-1α + HIF-1β/ARNT) induces gene expression by binding to the core DNA sequence 5'-TACGTG-3' at HRE regions in target genes [65]. These effects result in the activation of the transcription of oxygen-dependent genes by binding with co-activators p300 and CBP [64]. Some notable target genes that are stimulated are glucose transporter-1 (GLUT-1), lysyl oxidase-1 (LOX-1), vascular endothelial growth factor (VEGF), carbonic anhydrase-9 (CAIX), and glycolytic enzymes such as phospho-glycerate kinase and lactate dehydrogenase- A (LDHA) [66] (Figure 1.3).

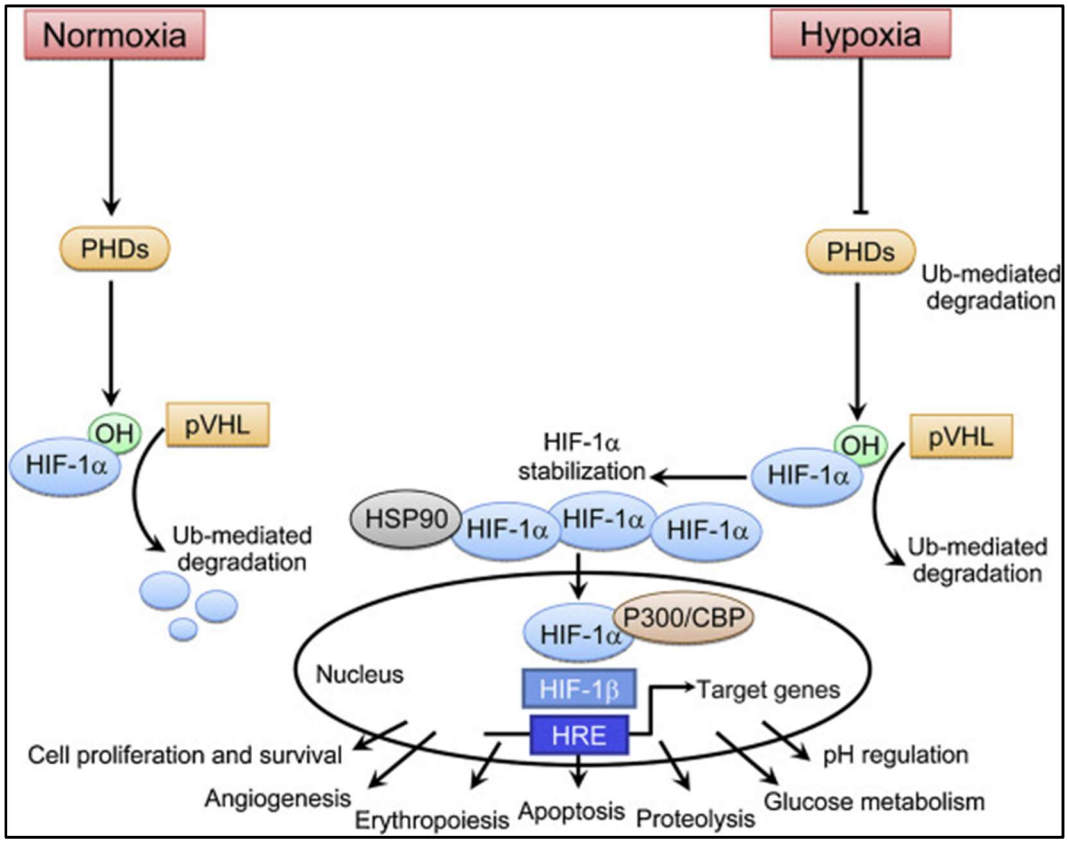

Figure 1.3 Hypoxia-Inducible Factor-1 signalling pathway

The diagram depicts how HIF-1α is regulated in different oxygen levels. Under normoxia, HIF-1α is hydroxylated by prolyl hydroxylases which leads to its binding to Von Hippel-Lindau tumor suppressor protein. VHL bound HIF-1α in turn is targeted for ubiquitination and degradation. In hypoxia, HIF-1α is stabilized, translocates to the nucleus and heterodimerizes with its partner HIF-1β. HIF-1(α-β) complex, in turn, binds to the hypoxia responsive elements upstream of various target genes leading to activation of their transcription [67]. Reproduced by permission from Elsevier: Critical Reviews in Oncology/Hematology. Past approaches and future directions for targeting tumor hypoxia in squamous cell carcinomas of the head and neck. Curtis, K. K., Wong, W. W. & Ross, H. J., Copyright © 2016.

1.2.1.2. HIF independent mechanism

Although HIF is critical for hypoxia response, recent studies have demonstrated that it is not the only master regulator of hypoxia response suggesting the existence of a HIF-1 independent hypoxia related response. Multiple pathways like tumor angiogenesis and several oxygen-relatable transcription factors such as NF-kβ, AP-1, CEBP are reported to respond to hypoxia in a HIF independent manner [68]. As a result, hypoxic regulation of a few genes occurs independent of HIF indicating the existence of other oxygen-regulated pathways that are controlled by PHD enzymes in a similar fashion as HIF pathways [69]. In 2015, Lee at al. discovered NDRG3, an oxygen-regulated substrate of the PHD2/VHL pathway [70]. NDRG3 protein levels were found to be elevated in several cell types under oxygen limited conditions resulting in increased angiogenesis, motility, proliferative and anti-apoptotic activity [71]. Moreover, these authors demonstrated that NDRG3 becomes proteasomally degraded through PHD2/VHL under normoxia, but under hypoxia, lactate binds to the protein, boosts and stabilises it thereby escaping the VHL associated degradation. The stable NDRG3 protein then binds to c-Raf thereby mediating hypoxia induced activation of Raf/Erk pathway triggering signals for cell growth and angiogenesis [70] (Figure 1.4). Since the

inhibition of lactate production abolishes the hypoxia induced expressions, we can say that lactate plays a critical role in promoting hypoxic response independent of HIF. Furthermore, the authors proposed a model which suggests that during prolonged hypoxia, although the mRNA expression of NDGR3 is independent of HIF levels, the protein becomes active and accumulates only when it is bound to the glycolytic end product lactate, which in turn boosts NDRG3 mediated signalling pathways [70]. Thus, even though NDRG3 activity is not directly HIF dependent, it is coupled with the HIF mediated response since HIF1-α regulates the expression of LDHA. Therefore, targeting NDRG3 combined with HIF might be an effective anti-hypoxia strategy and could improve the treatment efficacy of hypoxia-induced diseases.

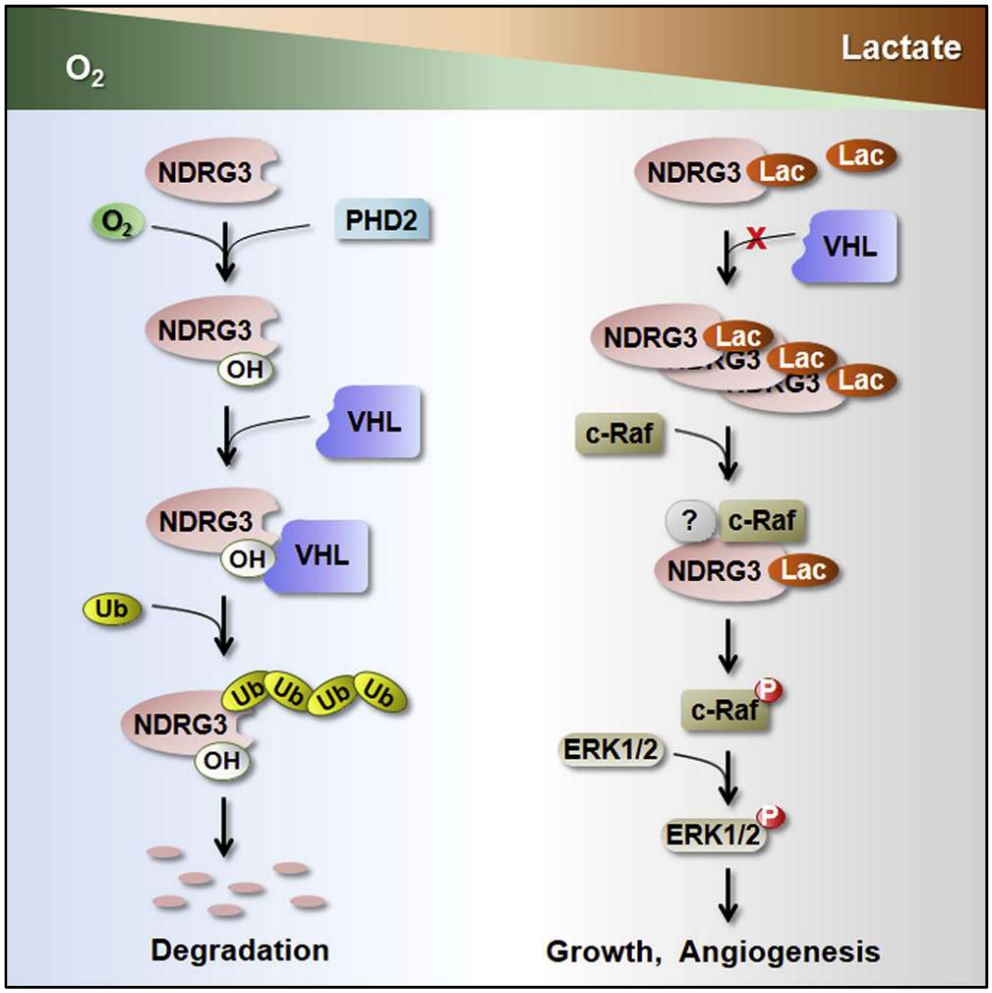

Figure 1.4 Lactate induced hypoxic response (HIF independent mechanism)

NDRG3, an oxygen-regulated substrate of VHL pathway regulates hypoxia independent of HIF. In normoxia, NDRG3 protein is hydroxylated by prolyl hydroxylases and is degraded in a PHD2/VHL-dependent manner. In contrast, under low oxygen the protein evades VHL degradation by binding to lactate which allows it to accumulate. The stabilized NDRG3 protein then binds to c-Raf, mediating hypoxia-induced activation of the Raf-ERK pathway thereby promoting angiogenesis and cell growth [70]. Reproduced by permission from Elsevier: Cell. A Lactate-Induced Response to Hypoxia. Lee, D. C. *et al,* Copyright © 2015.

1.3. Hypoxia responsive gene: Glucose transporter (GLUT)

In general, all cells need a constant flow of glucose as a source of energy for normal physiological function. Since glucose is highly polar, passive transportation across the plasma membrane is very limited and hence structurally relatable transport proteins known as glucose transporters act as carrier proteins by binding to glucose for easier cellular uptake [72,73]. Glucose transporters are broadly classified into two classes namely, sodium-glucose linked transporters or symporters (SGLTs) and facilitated diffusion glucose transporters (GLUTs) on the basis of substrate specificity, distribution and regulatory mechanism [74]. The SGLT family consists of 12 members and are usually expressed by cells in the small intestine and renal proximal tubes. These proteins aid in the active transport of glucose against the electrochemical gradient [75].

GLUTs are a group of integral transmembrane proteins responsible for bidirectional glucose transport in cells and tissues through a facilitative diffusion mechanism against a concentration gradient [76]. These proteins contain two substrate binding sites exposed towards either the outside or inside of the cell. Glucose binding on either side results in a conformational change which helps to ease transport from one side of the membrane to the other, and the phenomenon is termed as the alternate access mechanism [77]. On the basis of sequence similarity,

GLUTs encoded by solute carriers 2A gene family (SLC2A) of membrane transport proteins are grouped into three classes which comprises of 14 members in total [78]. The isoforms vary in tissue specificity and glucose affinity. Among these transporters, the highly conserved GLUT-1 is regarded as the principal isoform and was the first characterized GLUT and most intensively studied [79]. GLUT-1 belongs to the sugar porter subfamily of a larger superfamily of proteins known as the major facilitator superfamily (MFS) [80]. The MFS family in common is comprised of 12 transmembrane helices organized into two domains namely amino and carboxy, which are exposed to the cytoplasm of the cell [81]. It is also reported that the first six and the latter six helices might exhibit pseudo symmetry [82]. Structurally, GLUT-1 is composed of ~500 amino acids and contains a single site for N-linked glycosylation [83]. In adults, GLUT-1 is expressed in erythrocytes, placenta, endothelial cells of blood-tissue barrier such as the blood-brain barrier and is known to be widely distributed in fetal tissue [84]. The main role of GLUT-1 is to transport glucose back and forth between blood and organs that have less access due to passive diffusion [85]. Although, GLUT-1 is ubiquitously expressed in normal tissues, GLUT-1 levels are increased dramatically under hypoxia making it one of the major genes over-expressed in hypoxic tumor cells [86-91]. Elevated expression has been observed in almost all hypoxic tumors rendering GLUT-1 an excellent prognostic and diagnostic marker [92-95]. In particular, GLUT-1 expression has been associated with lymph node metastasis, poor survival and increased tumor growth in HNC [96,97].

Although the structure of bacterial GLUT-1 homologues had been revealed earlier [98-100], it was essential to identify the detailed structure of human GLUT-1 since bacterial GLUT-1 is a proton-driven symporter [101] whereas human GLUT-1 is a proton-independent uniporter [81,102]. Immense research has been carried out over several decades to characterize the atomic structure for a better understanding of the transport mechanism and functions. In 2014, Deng et al, elucidated

the crystal structure of GLUT-1 in an inward open conformation [103] (Figure 1.5). They succeeded in crystallizing full length GLUT-1 structure at 3.2 Å resolution containing two point mutations N45T and E329Q in order to eliminate heterogeneity due to glycosylation [104]. Also, in order to prevent multiple interchangeable conformations caused due to the high activity of GLUT-1, the abovesaid mutations were introduced so as to lock and stabilize the protein in a certain conformation. Similar to other MFS membrane transporters, the amino and carboxy terminal domains of GLUT-1 exhibits pseudo symmetry [81,105]. The N and C domains are connected through an intracellular helix (ICH), which is an unique feature of the sugar porter subfamily. The C-terminal segment seems to be invisible and this might be due to the flexibility in the abovesaid conformation [103]. Both the domains are predicted to enclose a cavity in the structure which opens to the intracellular side of the protein. Interestingly, the crystal structure also defines a glucose binding site in the cavity. Hence the authors suggest that, depending upon the angle at which the domains meet each other, the exposure of the glucose binding site from one side of the membrane to the other varies [103]. Overall, since GLUT-1 is regarded as a hypoxic target, unravelling the structure of GLUT-1 might provide clues for developing potential therapeutic agents that target GLUT-1.

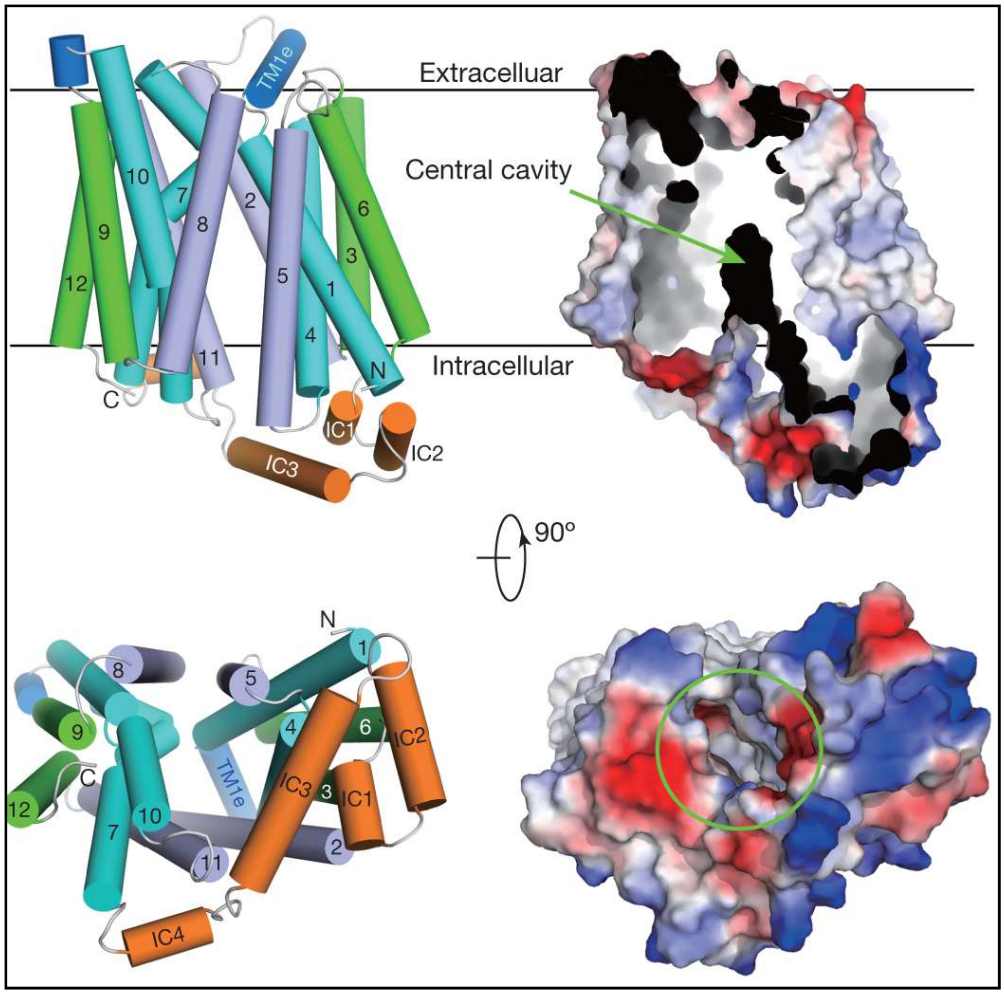

Figure 1.5 Structure of human glucose transporter GLUT-1

The diagram shows the structure of full-length human GLUT-1 in an inward-open conformation. The side and cytoplasmic views are shown on the left. A slab of cut-open view of the surface electrostatic potential, is shown on the right so that the inward-facing enclosed cavity can be seen easily. The full length GLUT-1 structure was crystallized containing two point mutations- N45T and E329Q [103]. GLUT-1 is comprised of 12 transmembrane segments, organized into two domains namely amino and carboxy terminal. The corresponding transmembrane segments in the four 3-helix repeats are displayed in the same colour. The extracellular and intracellular helices are coloured blue and orange, respectively. IC indicates intracellular helix. All figures were generated with PyMol. Reproduced by permission from Nature Publishing Group: Nature. Crystal structure of the human glucose transporter GLUT1. Deng, D. *et al*, Copyright © 2014.

1.3.1. Regulation of glucose transport by hypoxia

Although GLUT-1 induced by HIF-1α serves as an energy provider to malignant tumor cells, the correlation between GLUT-1 and HIF-1α expression varies in different carcinomas. Hence, it is critical to study the involvement of hypoxic HIF-1 signaling in GLUT-1 regulation. Oxidative phosphorylation is the crucial step in the production of ATP in cells where hydrogen atoms and electrons are transferred to oxygen [106]. But in hypoxic atmosphere, cells choose anaerobic glycolysis to release energy and this pathway is regulated by HIF-1α [107]. Basically, hypoxia induces a shift from aerobic to anaerobic glycolysis in order to maintain the energy supply in a rapidly growing tumor tissue, which leads to an increase in the expression of genes encoding key glycolytic enzymes and glucose transporters such as GLUT-1 [107,108]. Regulation of glucose transport by hypoxia is said to be triphasic. Initially under hypoxia, GLUT-1 gets activated on the pre-existing plasma membrane, due to decreased ATP production [109]. If hypoxia still exists, GLUT-1 molecules are said to be translocated from intracellular vesicles to plasma membrane [110]. In chronically hypoxic cells, de novo synthesis of GLUT-1 takes place and the pathway is mediated by HIF-1α [111]. GLUT-1 was the first gene discovered whose rate of transcription is dually regulated in hypoxia by HIF-1α and by inhibition of oxidative phosphorylation [112]. This renders GLUT-1 as an intrinsic cellular marker for targeting hypoxic cells in tumors [113-115]. The activation of GLUTs at the plasma membrane is found to be regulated by PI3-kinase (PI3K) signaling pathway, which in turn is linked to HIF-1α since PI3K can upregulate HIF-1α mRNA translation [116,117]. There is also evidence that an inverse relationship exists between VHL and GLUT-1 expression [118] which in turn highlights the critical role of HIF-1α since we know loss of VHL protein activity increases HIF-1α activity resulting in glucose uptake [119].

In addition to hypoxia, GLUT-1 expression is known to be regulated by mitogens, growth factors, phorbol esters and oncogenes such as *H-ras, src, and c-myc* [120-122]. Studies have indicated that the *ras* oncogene upregulates GLUT-1 mRNA and protein levels and HIF-1 plays a crucial role in the upregulation [123-125]. HIF-1 has been proved to bind to the *cis* acting binding sites located within the 5' flanking region of GLUT-1 mRNA and H-*ras* is said to upregulate GLUT-1 when HIF-1 is bound to it [126,127]. The authors suggest that the HIF-1 binding site located in the GLUT-1 promoter is sufficient to mediate the upregulation of promoter activity by H-*ras* [128]. Taken together, H-*ras* helps the cells to survive in a hypoxic tumor microenvironment by enhancing GLUT-1 expression through upregulation of HIF-1α protein levels.

1.4. Evaluation of hypoxia

1.4.1. Invasive and Non- Invasive methods

As discussed above, tumor hypoxia is established as a strong indicator for poor prognosis in HNC leading to poor patient outcome and therapeutic response [129-131]. Due to the heterogeneity in hypoxia, there is an acute need to stratify patients according to their hypoxic status [132]. The degree and extent of hypoxia should be assessed before initiating the treatment plan so that an appropriate personalized hypoxia-based treatment modality can be offered with an intent to improve the curative outcome. Several techniques have been identified to measure oxygen levels in hypoxia and they are broadly classified into invasive and non-invasive methods.

1.4.1.1. Invasive methods to assess tumor hypoxia

Invasive polarographic needle electrodes was used as a gold standard technique in routine clinical management to measure pO_2 and to predict tumor response [133-135]. Even though the electrodes can access a variety of tumor sites such as head and neck, cervix, prostate, lung and pancreas, its insertion into the tumor disrupts tissues limiting the capacity to differentiate between

varying hypoxic patterns [136,137]. Oxygen distribution in tissues is also measured by another approach called phosphorescence quenching where an oxyphor, a phosphorescent probe is injected into the vasculature which successfully maps oxygen concentration in a variety of physiological environments [138,139]. In addition, near-infrared spectroscopy (NIRS) can be used to analyse tumor oxygenation *in vivo* through tracking spectral changes by haemoglobin in the vasculature [140]. Although, initially, phosphorescence imaging and NIRS had certain limitations such as low sensitivity, resolution, limited tissue penetration and path length hindering its clinical translation, the latest developments in those modalities have led to its approval in clinical practise [141]. A few 2-nitroimidazole derivatives such as misonidazole and pimonidazole act as exogenous probes to detect tumor hypoxia by forming stable adducts with intracellular macromolecules under hypoxic conditions [142]. The hypoxic adducts are detected by tumor biopsy and immunohistochemistry (IHC) by specific antibodies raised against these probes. The most widely used exogenous marker, pimonidazole, is demonstrated to be more sensitive in severe hypoxic conditions when compared to other methods [143-145].

1.4.1.2. Non-invasive methods to assess tumor hypoxia

Of late special emphasis is on non-invasive hypoxic imaging with new reagents and sophisticated imaging techniques which help in deciphering the molecular events related to hypoxia. Positron emission tomography (PET) imaging is a highly preferred methodology in the clinic that traces hypoxia using radiolabelled reporters [146-148]. In PET imaging, organic molecular markers labelled with positron-emitting radioisotopes such as ^{18}F, ^{124}I, or $^{60/64}Cu$ are used to visualize the hypoxic status of tumors in a three dimensional manner [149]. The notable molecular markers that are used to attach to these isotopes can either be 2-nitroimidazole derivatives such as fluoromisonidazole (FMISO), pentafluorinated etanidazole (EF5), fluoroetanidazole (FETA) or

nucleoside conjugates of 2-nitroimidazole such as iodoazomycin arabinoside (IAZA), fluoroazomycin arabinofuranoside (FAZA), and metal chelated ligands, for example Cu(II)-diacetyl-bis(N-methylthiosemicarbazone) (Cu-ATSM) [149,150]. These markers bind to the contents in a hypoxic cell selectively generating adducts to cellular macromolecules which are detected by PET scanner. ^{18}F-FMISO was the first-generation nitroimidazole biomarker known to detect hypoxia in glioma, HNC, renal tumor and non-small cell lung cancer [151-158]. However, owing to its high lipophilicity, slow clearance rate and variability in the rate of retention in different cancers led to the development of second generation nitroimidazole based PET hypoxia biomarkers [159]. EF5 is reported to be one of the most stable hypoxia biomarkers as it is more water soluble thereby evading degradation by oxidizing mechanisms in the body [160,161]. Although ^{18}F-EF5 showed positive outcome in identifying high-risk patients in clinical trials, the major drawback of the compound is its complex labelling chemistry which results in low radiochemical yield [162,163]. The radio-iodinated azomycin arabinoside ^{123}I-IAZA has been tested as a hypoxia tracer using single photon emission computed tomography (SPECT) imaging and has been clinically validated in HNC, small cell lung cancer and glioblastoma [164,165]. ^{18}F-FAZA, another sugar-coupled 2-nitroimidazole derivative was developed based on promising results from the use of ^{123}I-IAZA in SPECT imaging [166]. ^{18}F-FAZA is considered to be a very effective hypoxic PET imaging agent with faster diffusion, quick clearance rates in normal tissues and high tumor-to-background ratios when compared to other markers [167]. Due to its superior biokinetics, ^{18}F-FAZA imaging had been successful in identifying malignancies of head and neck, lung, lymphoma and glioma [168-170]. In addition, Cu-ATSM (a hypoxic tracer) which has garnered considerable interest in recent times exploits the oxidation/reduction ability of chelated copper ions for its selective

accumulation in hypoxic areas when coupled with dithiosemicarbazone, which is already known for its antioxidant properties [171].

The concept of elevated glucose transporters in malignant and hypoxic tumors was taken advantage of in hypoxic imaging. But many physiological pitfalls have been observed to be associated with ^{18}F-FDG (fluoro-2-deoxyglucose) PET imaging since FDG uptake by tumor cells reflects the metabolic activity rather than being hypoxia selective, which eventually results in inconsistent results while detecting tumor hypoxia [172-176]. In addition, IHC staining of several endogenous proteins such as HIF-1α [177-179], GLUT-1 [113,114,180], CAIX [181-184] and VEGF [185,186] induced by hypoxia have also been demonstrated to play a significant role in monitoring hypoxia. Also, bioluminescence-based detection of HIF-1α has been found to be effective in imaging hypoxic fractions *in vivo* [187,188]. But these imaging strategies need further investigation due to the complex heterogeneity of tumor hypoxia. Hence use of combination of these markers could result in accurate quantification of tumor hypoxia.

1.5. Radiosensitization of hypoxic cells

Over the past several decades, various attempts have been made to radiosensitize hypoxic cells which withstand conventional therapy. Numerous studies focused mostly on either elevating the oxygen supply so as to improve radiosensitivity/curability or by administration of oxygen mimetic radiosensitizers which selectively sensitizes hypoxic cells to ionizing radiation by replacing oxygen.

1.5.1. Increase in oxygen delivery

Efforts to increase the oxygen delivery to tumor lesions through blood flow in order to overcome intratumoral hypoxia have been carried out through different methods. Hyperbaric oxygen therapy (HBOT) is an approach used since the 1960s where patients inhale pure oxygen at

elevated pressures ranging from 1.5-2.5 atmospheres [189]. Although several reports indicate a positive outcome in HBOT when combined with radiation in solid tumors of head and neck, cervix and bladder, the benefit of the modality still remains controversial [190-194]. The efficacy of HBOT varies depending on the tumor type, size and extent of lesion [195]. Another attempt to overcome tumor hypoxia was carried out by breathing carbogen, a modified gas mixture which contains 5% CO_2 in oxygen. Addition of CO_2 improved tumor oxygenation and the technique showed better outcomes by reoxygenating chronic hypoxic cells [196]. Nicotinamide, a vitamin B3 analogue is proven to target perfusion-related acute hypoxia by preventing transient fluctuations in tumor blood flow. In addition, nicotinamide is said to enhance tumor radiosensitivity since it is known to inhibit poly ADP-ribose polymerase 1, a crucial enzyme involved in DNA repair [197-200]. The combination of nicotinamide to overcome acute hypoxia and carbogen breathing to overcome chronic hypoxia led to the basis for the studies involving accelerated radiotherapy with carbogen and nicotinamide (ARCON) [201-205]. Early results from ARCON trials did not show any significant improvement in overall survival (OS) among patients with HNC, glioblastoma and non-small cell lung cancer [206-209]. However, recent clinical trials with ARCON, at low doses showed promising potential by exhibiting improved LCR, OS and DFS in squamous laryngeal cancer patients with hypoxic tumors [210]. Despite the ongoing research to control tumor hypoxia by elevating oxygen levels, special emphasis is on hypoxic radiosensitizers and hypoxic cell cytotoxins that preferentially sensitizes and kills hypoxic cells respectively.

1.5.2. Hypoxic cell radiosensitizers

In early 1960s, hypoxic-cell radiosensitizers were developed as a result of an immense research to find an alternative approach to use of high-pressure oxygen tanks in radiosensitizing hypoxic cells [211]. These oxygen-substitutes possess the ability to diffuse into poorly vascularized

areas within the tumor and are said to achieve the desired radiosensitizing effect by chemical means [212]. The major reason for success of these molecules over oxygen is that they can penetrate further than oxygen and reach the hypoxic fractions within the tumor since they do not get rapidly metabolized by tumor cells through which they diffuse [213]. The mechanism of action behind this class of sensitizers is based on the principle of 'oxygen fixation' theory [214-216]. An ideal hypoxic cell radiosensitizer must be able to selectively sensitize hypoxic cells at a tolerable dose that would exert only minimum toxicity to normoxic tissues and must possess an optimum reduction potential which plays a crucial factor in the hypoxia selectivity. In addition, it must be chemically stable with optimal lipophilicity and efficient even at fairly low doses of radiation. Nitroimidazoles (NI) are the most common members of this class as their electron-affinic nitro group was designed to react with DNA radicals induced by ionizing radiation in a similar fashion as oxygen does [217]. 2-NI were established as better radiosensitizers as they exhibit higher reduction potential when compared to 4- and 5-NI [218]. Metronidazole and misonidazole which belong to 2-NI class were among the first few compounds that were identified for their hypoxic radiosensitization properties in both *in vitro* and animal models [213,219-221]. Although, both the molecules started as attractive promising agents in hypoxia directed cancer therapy, they eventually failed at clinical trials as an adjunct to radiotherapy by showing no survival benefits when compared to radiotherapy alone [213,222,223]. The treated patients also experienced a high incidence of peripheral neuropathy and convulsions at fractionated radiation doses [202,222,224]. The major reason behind the failure of these compounds is that only low radiosensitizing effect was achieved at tolerable doses of these drugs [213]. Hence, in an effort to improve the therapeutic benefit of NI, more polar analogues such as pimonidazole and etanidazole were developed [225,226]. Even though both the compounds showed improved therapeutic indices in preclinical models, their clinical application was again limited in

combination with radiotherapy by showing no significant benefit in patients with cervical carcinoma and HNC respectively [227-229]. Currently, nimorazole is the most successful example of a C5-derived NI-based radiosensitizer, which was reported to be less toxic when compared to other members of the class permitting use of tolerable high dosage [230]. The drug shows promise in clinical trials by exhibiting a significant overall improvement in LRC and DFS of HNSCC patients when combined with standard fractionated radiotherapy in a study conducted by the Danish Head and Neck Cancer group (DAHANCA) [230,231]. Recently, a novel class of NI alkylsulfonamide radiosensitizers has been identified and their potential in therapy is being explored [232,233]. In addition, the use of glycididazole (novel NI polymeric compound) as an efficient hypoxic radiosensitizer is underway [234]. Hence, several studies with new approaches are being carried out in the field of hypoxic-cell radiosensitizers in order to identify a potential clinical candidate.

1.6. Hypoxic-cell Cytotoxins

1.6.1. Different classes of bioreductive drugs

The development of hypoxic-cell radiosensitizers led to the discovery of hypoxic-cell cytotoxins, also widely known as bioreductive drugs or hypoxia activated prodrugs (HAPs). Unlike the hypoxic-cell radiosensitizers which render solid tumors more radio-responsive during radiotherapy, HAPs preferentially kill the hypoxic cells within a tumor by cytotoxic metabolites that are generated through bioreductive activation. [235-238]. These prodrugs are considered superior to conventional anti-cancer agents in cancer therapy since they specifically target a unique subpopulation of cells within a solid tumor hence lowering the toxicity related side effects in well-oxygenated tissues [3,239]. With better drug delivery properties, an ideal HAP also possesses the potential of overcoming a major cause of hypoxia-induced radio- and chemo-resistance by exerting maximum cytotoxicity to the cells located farthest from the blood vessels [16,240]. This unique

characteristic feature of HAP makes it an attractive targeted strategy to turn tumor hypoxia into a therapeutic advantage either by acting alone or in combination with radiation and other existing chemotherapeutic drugs resulting in a synergistic response [241-250]. Based on their chemical moieties, HAPs are broadly classified into five main types namely, quinones, nitroaromatic compounds, aromatic N-oxides, aliphatic N-oxides and transition metal complexes [251,252]. In addition, the molecules are also grouped into two classes depending on the hypoxic threshold required for their activation by specific reductases. Class I HAPs include benzotriazine N,N-dioxides such as Tirapazamine (TPZ) and SN 30000 which are activated under relatively mild hypoxia to generate short-lived cytotoxic radicals that are restricted within the cell where they are formed [253,254]. Whereas nitro compounds such as PR-104 and evofosfamide (TH-302) fall under Class II HAPs which require severe hypoxia for enzymatic reduction and subsequent activation to produce stable prodrug radicals that are known to have longer lifetimes and these cytotoxins possess the added advantage of diffusing into moderately hypoxic cells and eliminating them, thus exerting a bystander effect [241,248,255,256]. In general, most HAPs (nitro compounds, benzotriazine di-oxides and quinones) are activated through one-electron reduction by flavin-oxidoreductases resulting in the formation of an oxygen-sensitive radical intermediate. Subsequently, the radical undergoes further reduction in hypoxia generating active toxic drug; whereas in the presence of oxygen, the intermediate is back-oxidized to the prodrug resulting in a futile metabolic cycle thus ensuring minimal toxicity to normoxic tissues [257,258]. In contrast, a few bioreductive prodrugs (PR-104 and AQ4N) are activated in an oxygen-independent manner, catalysed by certain two-electron oxidoreductases [259]. Since, the two-electron reduction of the prodrug fails to generate an oxygen-sensitive radical intermediate, the process is irreversible and occurs in both normoxic and hypoxic tissues [259].

Basically, the concept of HAPs arose from early studies in the 1980s which reported the bioreductive potential of mitomycin C, a quinone based derivative in a hypoxic environment *in vitro* [260]. The drug's low hypoxia selectivity in preclinical studies [261] led to the development of its analogues such as porfiromycin (POR) and apaziquone (EO9) with superior hypoxia selectivity over the lead compound [262-264]. However, although both the compounds demonstrated differential toxicity in early preclinical and clinical trials, unfortunately they were not explored further since it was concluded that POR was inferior to mitomycin C in a follow-up Phase III trial [265]; EO9 trials were restricted to study designs where only local administration of the drug was possible [266]. This was due to the drug's poor pharmacokinetic profile, but the possibility that EO9 might be effective in a loco-regional setting remains to be explored [267].

In addition to sensitizing hypoxic cells to radiotherapy, nitroimidazoles also exhibit hypoxia-selective cytotoxicity in regard to their high electron affinity [217,268]. The dual functionality of NI was reported in several members of the class such as misonidazole, etanidazole, and doranidazole; these compounds having been shown to undergo oxygen-sensitive redox cycling, which is a typical feature of a bioreductive prodrug [269-271]. As discussed earlier, although these compounds except nimorazole did not show clinical promise in hypoxia therapy, a few molecules from this class are being successfully used as bioreductive hypoxia markers on the basis of their hypoxia-selective uptake property [227,272-277]. Moving forward, new generation cytotoxic nitroaromatic compounds such as TH-302 and PR-104 were discovered in an attempt to develop more effective NI based compounds [246,278]. These prodrugs bind selectively to hypoxic cells through complex reductive chemistry and eventually become activated to cytotoxic products which mediate cell killing predominantly through DNA damage [256,279]. Despite the advancement, several

clinical trials on both PR-104 and TH-302 yielded mixed results in various tumors; currently their potential to sensitize tumors to radiation is being assessed in ongoing trials [279-284].

TPZ, an aromatic-N-oxide is the lead compound in the benzotriazine family and is one of the best characterized HAPs [257]. The mechanism behind the cytotoxic action of TPZ and its success in clinical trials will be discussed in detail in the upcoming section. In contrast to aromatic-N-oxides, aliphatic N-oxides induce hypoxia selective cytotoxicity through a different mechanism and the most clinically advanced molecule in that class is banoxantrone (AQ4N) [285]. A notable unique feature in AQ4N when compared to other bioreductive drugs, is that it exhibits hypoxia selectivity in an oxygen sensitive two electron-reduction rather than generation of ROS through redox cycling [285]. Even though the drug displayed a significant efficacy in preclinical mouse models and Phase I clinical trials, AQ4N unfortunately is yet to progress further than Phase II trials [246,286,287]. Mentionable examples of transition metal complexes which fall under the fifth class of HAPs include cobalt (III) and copper (II) complexes that undergo hypoxia selective one-electron reduction to form unstable cobalt (II) and copper (I) complexes, which in turn become dissociated to release cytotoxic ligands [288-290]; the clinical usability of these compounds is currently being explored.

Overall, in spite of ongoing advancements in HAPs, most of the molecules failed to show significant clinical benefit, but a major limitation responsible for the failure may be a lack of sufficient patient stratification on the basis of tumor hypoxia [36,291-294]. Therefore, we can say that future clinical trials with promising HAPs would be worthwhile only if the abovementioned issue is addressed.

1.6.2. Drug of Interest: Tirapazamine (TPZ)

Although several hypoxia targeted cytotoxic agents have been developed in the past, ongoing studies are being vigorously pursued to identify better bioreductive agents that possess high hypoxic differential. Our drug of interest, TPZ (3-amino-1,2,4-benzotriazine-1,4 dioxide [alternatively known as tirazone, SR 4233, SR 259075 and WIN 59075]) emerged as a promising drug by satisfying this criteria as it exerts a relatively high hypoxic cytotoxic ratio (HCR) [295]. TPZ, a well-known anticancer drug, was first synthesized by Robbins and Schofield in 1957 as a derivative of 1,2,4-benzotriazines [296]. Even though TPZ was initially used during screening for herbicides in 1972, the drug was later found to target hypoxic tumor cells [295]. TPZ was the first HAP to be successfully tested in the clinic based on its high killing efficacy in hypoxic cells [297]. The drug, under very low oxygen levels, is thought to be activated by multiple reductases to form free radicals, which subsequently induce single and double strand breaks (SSB and DSBs), base damage and cell death [298]. TPZ is also known for its remarkable potential as an efficient adjunct to irradiation and chemotherapeutic agents [299].

1.6.2.1. Molecular mechanism of preferential toxicity

The mechanism for the selective toxicity of TPZ towards hypoxic cells occurs as a result of intracellular enzymatic one electron reduction of the parent molecule to a free radical species, which in turn interacts with DNA and eventually causes cell death [238]. The reduction of TPZ under both aerobic and hypoxic conditions is mainly catalysed by NADPH-dependent cytochrome 450 reductase (P450R) enzymes resulting in the formation of a highly reactive oxygen-sensitive radical intermediate [300-302]. Other enzymes such as xanthine oxidase, aldehyde oxidase and cytochrome P450, DT-diaphorase are also reported to play a limited role in reducing TPZ [303-306]. In normal cells and tissues, oxygen removes the free electron from the TPZ radical thereby back-oxidizing it

to the non-toxic parent compound along with the production of other reactive oxygen species (ROS), including superoxide, which is moderately reactive by nature [246,307-309]. In contrast, in a hypoxic environment, the TPZ radical readily undergoes homolytic cleavage to the reduced product SR 4317 (mono-N-oxide metabolite) and a hydroxyl radical [310-315]. Although both the radicals can degrade DNA, the pattern of TPZ induced damages is characteristic of hydroxyl radicals, in which damage to both the DNA backbone and the heterocyclic bases occur [312,314,316]. Moreover, the TPZ radical is also said to undergo a different type of fragmentation reaction in a low oxygen state resulting in the generation of another DNA-damaging species, termed the benzotriazinyl radical (BTZ), formed by loss of a water molecule [317]. Similar to the hydroxyl radical, the BTZ radical is proven to be responsible for DNA strand cleavage and poisoning of topoisomerase II [318-320]. Topoisomerase II poisoning results either by direct damage from TPZ radicals or from radicals produced on the DNA molecules, which act as topoisomerase II substrates [321]. In addition to TPZ's ability to generate DNA damaging radicals under hypoxia, the drug also reacts with these DNA radicals, thereby acting as a substitute for molecular oxygen [322]. Basically, addition of TPZ to a DNA radical generates intermediates, which further undergo reduction and protonation, finally resulting in hydroxylation of the DNA molecule, which in turn leads to strand breaks [323-325]. Hence, the dual role of TPZ is the reason why the drug is highly efficient specifically in hypoxic cells. Besides the above factors, it has also been identified that TPZ selectively produces other DNA lesions such as abortive topoisomerase I-DNA complex and unligatable DNA ends during hypoxia which get converted to DSBs during replication [298]. Taken together, the overall level of TPZ radical-induced DNA damage under hypoxia; double-strand breaks in particular cause cell death. Even though the cytotoxicity of TPZ in hypoxic conditions has been examined in detail, that under normoxic conditions remained largely unexplored.

However, recent reports indicate that the ROS derived from superoxide through the reoxidation of TPZ under normoxic conditions causes oxidative DNA damage and DSBs [298]. Despite the fact that TPZ induces cell death under oxic conditions, the drug's cytotoxicity is markedly lower under normoxia when compared to hypoxia due to decreased efficacy of cell killing by normoxia-specific ROS rendering TPZ as a promising HAP candidate [298].

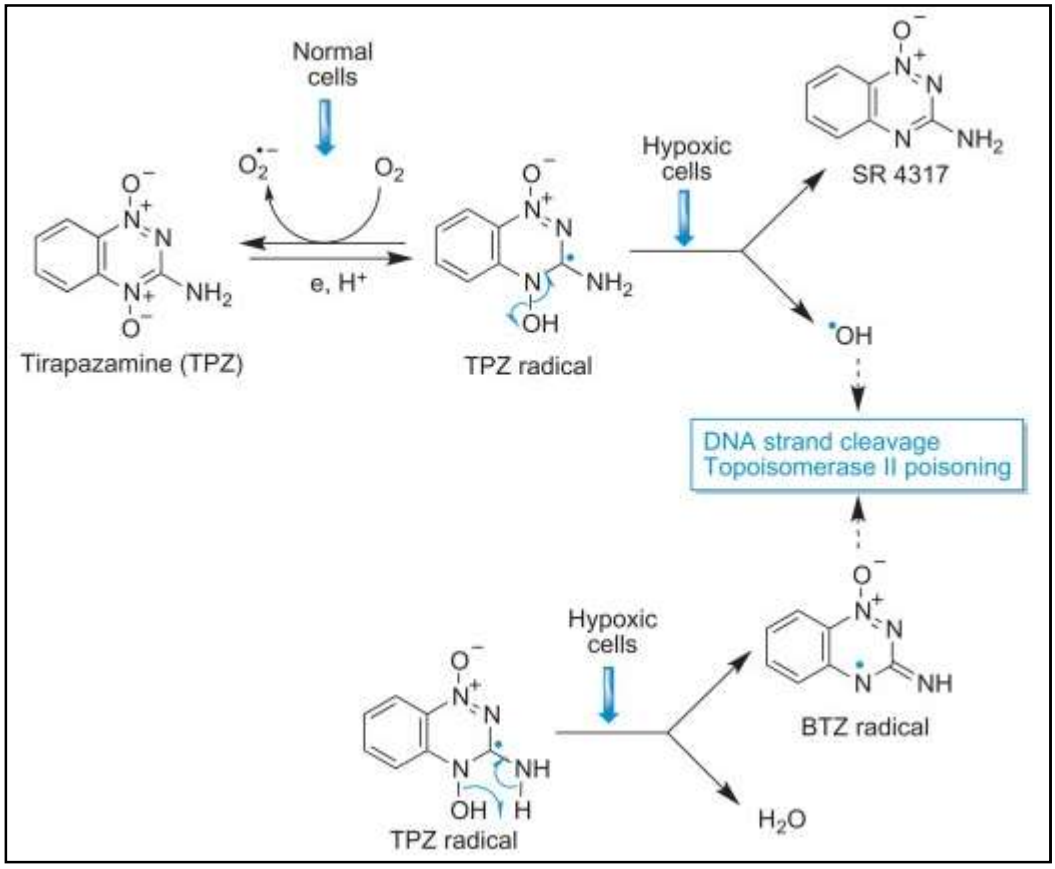

Figure 1.6 Hypoxia-selective activation of TPZ

The diagram shows how the radical species derived from TPZ metabolism exhibit anticancer activity. Initially, the prodrug gets reduced to a reactive TPZ radical intermediate in the presence of CYP450R enzyme. In aerobic conditions, the radical intermediate is back-oxidized resulting in a futile cycle, whereas under hypoxia, the TPZ radical undergoes two different types of fragmentation reactions yielding hydroxyl and benzotriazinyl radicals, which causes DNA strand

cleavage and topoisomerase II poisoning [326]. Reproduced by permission from Elsevier Books: Medicinal Chemistry of Anticancer Drugs. Chapter 4 Anticancer Drugs Acting via Radical Species Radiotherapy and Photodynamic Therapy of Cancer. Carmen Avendaño and J. Carlos Menéndez, Copyright © 2015.

1.6.2.2. Early studies of TPZ

The first experimental study of TPZ conducted in 1986 by Zeman *et al*., reported that the drug was a selective killer of hypoxic cells by exhibiting a high HCR ranging from 50-300 in mouse and Chinese hamster cells and 15-50 in human cell lines [295]. The decreased cytotoxicity ratio of TPZ in cells of human origin reflects the fact that the drug gets activated by different levels of enzymes in varying cell lines [295,327]. Durand and Olive demonstrated that TPZ shows minimum activity against cells in the centre of hypoxic spheroids, which suggested the possibility that the drug might get bioreductively inactivated before reaching the chronic hypoxic cells [328]. The above finding also explains why TPZ exhibits low cytotoxicity in *in vivo* models when compared to *in vitro*. Also, the variability in the sensitivity of TPZ within each tumor type depends strongly on its oxygenation status [329,330]. Apart from showing hypoxia selective cytotoxicity, TPZ also possesses radiosensitizing properties. The synergistic response of TPZ and radiation was initially demonstrated in (SCCVII) transplantable squamous cell mouse carcinoma by Brown and Lemmon [331]. The combined therapy drastically delayed tumor growth and the treatment was found to be more effective when TPZ was administered prior to radiotherapy rather than the reverse order, thereby confirming the fact that TPZ potentiates the effect of radiation [331]. Similar results had been reported in human colon cancer cell lines and melanoma cells [332-334]. It has also been demonstrated that the use of electric pulses along with TPZ and radiotherapy shows better outcome when compared to only radiochemotherapy (TPZ and radiation) [335]. Although, initially TPZ was designed to be used as an adjunct to irradiation, the drug has shown great efficacy when combined

with other chemotherapeutic agents, notably cisplatin (CIS) [4]. Besides better tumor control, a low level of toxicity was observed in normoxic tissues when TPZ was administered prior to cisplatin [336]. TPZ is said to potentiate the anti-cancer effects of CIS by inhibiting the repair of CIS-DNA adducts which is believed to be the major pathway by which the two drugs interact resulting in complementary cytotoxicity [337]. The dual sensitizing effect of TPZ in combinatorial therapy (radiation and other chemo drugs, especially CIS) was tested in most solid tumor types and its promising outcome led to the drug's entry into clinical trials.

1.6.2.3. TPZ Clinical trials and the setbacks

Phase I clinical trials of TPZ in combination with cisplatin or etoposide demonstrated safety of TPZ [338,339]. The studies also reported a significant outcome on tumor control in HNC, non-small cell lung cancer (NSCLC) and cervical cancer [338-341]. However, poor response was reported in studies where TPZ was the only therapeutic agent, suggesting that TPZ performs best when it is used as an adjunct to other cancer treatments rather than a monotherapy [342]. The most common side effects such as muscle cramping, nausea, vomiting, diarrhoea, weight loss, skin rash and acute reversible hearing loss were associated with the chemical dose of TPZ used for treatment [342-345]. However, since the TPZ-induced toxicities were reversible at tolerable chemical doses, the drug advanced to further trials.

Phase II trials with combined modality (either TPZ and radiation or TPZ and CIS) showed clinical advantages by improving overall outcome in advanced HNC, NSCLC, metastatic melanoma, ovarian cancer, cervical cancer and glioblastoma [249,345-352]. A notable result was achieved by Rischin *et al*., in a randomized Phase II trial of the Trans-Tasman Radiation Oncology Group (TROG 98.02) in locally advanced HNC where they compared the effectiveness of two concurrent chemoradiotherapy regimens namely TPZ, CIS and radiation versus Fluorouracil

[FU- chemodrug], CIS and radiation [353]. The group which received TPZ/CIS regimen showed promising results by exhibiting better LRC and overall survival (OS) when compared to the other arm [353]. In addition, ^{18}F-FMISO PET imaging was used in a sub-study of TROG 98.02 (Phase II trial) to scan hypoxic tumors in HNC patients prior to the therapeutic regimen [158]. As expected, patients with hypoxic tumors who received TPZ/CIS regimen showed better benefit with fewer local recurrences when compared to the non-TPZ treated patients, supporting the fact that TPZ specifically targets hypoxic cells [158]. The possibility of using TPZ in combination with multiagent chemotherapy was examined by the Southwest Oncology Group (SWOG 0004) in limited-stage small-cell lung cancer (LSCLC) [354]. The results of the SWOG 0004 pilot study (Phase II trial) showed that TPZ when combined with CIS, etoposide (PE) and concurrent thoracic radiotherapy yielded promising survival rates indicating the potential use of TPZ with other therapeutic agents in future trials [354]. Despite, the success of TPZ in Phase-II trials, only a limited number of Phase III trials on TPZ were carried out. Due to the remarkable synergy between TPZ and CIS, two subsequent Phase III clinical trials CATAPULT I (CIS and TPZ in Subjects with Advanced Previously Untreated NSCL Tumors) and CATAPULT II were carried out. CATAPULT I showed improved clinical response and increased median survival time in NSCLC patients who received TPZ/CIS regimen when compared to only CIS arm thereby reconfirming the fact that TPZ enhances CIS activity [355]. Although CATAPULT II was initiated with a lot of expectations, unfortunately low OS and increased toxicity were observed in the CIS/TPZ arm when compared to CIS/PE resulting in early patient drop out; thus suggesting that TPZ might be useful in triple agent combination chemotherapy [356]. But the major reasons behind TPZ-arm related toxicity was using a generalized population without pre-identifying a hypoxic population and the use of concentrations as high as 390 mg/m^2 in the above study, even though the majority of Phase I and

II trials considered 330 mg/m^2 TPZ as the maximum tolerable concentration [344,347,357]. Moreover, the results of the Phase III trial conducted by SWOG S0003 were disappointing, as addition of TPZ to a combination of paclitaxel and carboplatin in NSCLC patients showed increased toxicity and failed to demonstrate any survival benefit [358]. Similarly, a randomized multi-centre Phase III trial conducted by TROG 02.02 showed no therapeutic benefit of TPZ in advanced HNC patients, which was quite surprising considering the earlier promising results from Phase II trials conducted by the same group [359]. In addition, a recent Phase III randomized trial conducted by the Gynecologic Oncology Group (GOG 219) in 2014, which was closed early for accrual revealed that TPZ/CIS chemoradiotherapy was not superior to CIS chemoradiotherapy in terms of progression free survival (PFS) or OS in cervix cancer patients although the combination was fairly well tolerated in terms of dose [299]. The plausible explanation for the failure of the above studies (SWOG S0003, TROG 02.02 and GOG 219) would be mainly due to inadequate hypoxia within the tumors [299,358,359]. As mentioned earlier, TPZ benefit is most likely restricted to patients with hypoxic primaries and therefore only a well-defined group of patients who have a certain degree of hypoxia should be recruited for future TPZ clinical trials. Hence, a strict hypoxic patient stratification must be performed using either PET imaging or biomarkers such as p16 prior to treatment in order to achieve the best TPZ therapeutic benefit. Nevertheless, since TPZ is highly dependent on chemical dose and schedule [336,360], these factors also should be considered for a better outcome along with the best combination of radio and chemotherapeutic agent that would boost the TPZ efficacy.

1.6.2.4. Recent advancements in TPZ studies

In addition to the above mentioned reasons with regard to TPZ failure in clinical trials, another major limitation that was highlighted in almost all TPZ trials was the drug's inability to

penetrate deeply into severely hypoxic tissue [328,361-364]. As discussed earlier, this would be due to the excessive metabolic consumption of TPZ as the drug is activated even at mild hypoxia thereby limiting its access to hypoxic zones [361,362,365,366]. Hence, in order to achieve an optimum TPZ efficacy, the drug's transport issue was addressed by development of several TPZ analogues with improved penetration and metabolism properties [361,365]. Of these analogues, SN30000 (also known as CEN-209) shows promise by exhibiting a better diffusion profile and efficient extravascular transport in multiple xenograft models when compared to the lead compound, but the compound is yet to enter clinical trials [367-369]. In addition, researchers have also tried to overcome the penetration issues of TPZ by encapsulating the drug into nanoparticles [370,371]. A recent study has reported that nanoparticles loaded with TPZ along with a photosensitizer exhibits significantly improved penetration properties ultimately resulting in enhanced anticancer activity of TPZ in both *in vitro* and *in vivo* models [372]. Although several researchers have addressed the limitations of TPZ, many groups have also developed analogues of the drug by exploiting desirable properties of the lead compound; few notable advancements have been discussed as follows**.** In 2014, Johnson and coworkers synthesized TPZ analogues containing nitrogen mustard units (DNA-alkylating agents), and these new agents showed potential by exerting both DNA-oxidizing and DNA-alkylating effect simultaneously on hypoxic tumor cells [373]. Their work was based on the idea of activating a DNA-alkylating species selectively in hypoxic tumor tissue by utilizing the electronic changes which resulted from the metabolic deoxygenation of TPZ analogues [303,374,375]. Hence, this remarkable union of two anticancer drugs is said to overcome the common limitation of TPZ displaying cytotoxicity only in a small subset of tumor cells where it undergoes bioreductive metabolism. The authors have shown that these new agents possess the superior ability to diffuse and kill neighbouring tumor cells present in both more moderate and severe hypoxic

conditions [373]. Most recently, a group exploited the inherent fluorescent property of mono-N-oxide metabolite generated during hypoxic TPZ metabolism to detect the presence of bioreductive enzymes in tumor tissue [376,377]. Accordingly, they developed TPZ analogues which act as profluorescent substrates of one-electron reductases and thus may serve as diagnostic probes in identifying the enzymes involved in hypoxia-selective one-electron bioactivation of the drug [378]. Taken together, these profluorescent compounds can provide a basis for fluorescent based bioassays which would aid in identifying tumors that are highly responsive to hypoxic cytotoxins [378].

1.7. Research objectives

Our research aims at transforming TPZ structurally in order to increase its cellular uptake and tissue penetration properties. As discussed earlier, hypoxic cells express abundant GLUTs, a key feature that we have exploited in our project. We have synthesized a glucose-conjugated TPZ (G_6-TPZ) derivative in an effort to improve the delivery of TPZ selectively to poorly oxygenated cells. We hypothesize that the addition of a glucose moiety to TPZ would render G_6-TPZ to be selectively recruited by the upregulated GLUT receptors, facilitating its entrapment in hypoxic cancer cells. Molecular modelling-based conformational analysis of G_6-TPZ docked into the binding pocket of GLUT-1 revealed binding kinetics similar to 2-deoxyglucose (Elsaidi *et al*, unpublished), which supports the targeting of our compound to the abundantly expressed GLUT receptors on hypoxic tumor cells. Subsequently, bioreductive activation of our molecules will take place selectively in a hypoxic environment, to generate cytotoxic drug species in oxygen-deficient cells, with minimal damage to their oxygenated counterparts. Together our approach aims to overcome the limitations of TPZ therapy. All the drug and/or chemical compounds, except G_6-TPZ which was synthesized by Naeja Pharmaceuticals (Kumar P., unpublished), used in this

study were designed and synthesized by Dr Hassan Elsaidi, a senior researcher in our group. The efficacy of G_6-TPZ was tested using several cytotoxicity assays. Structures of the parent compound and G_6-TPZ are as follows.

TPZ

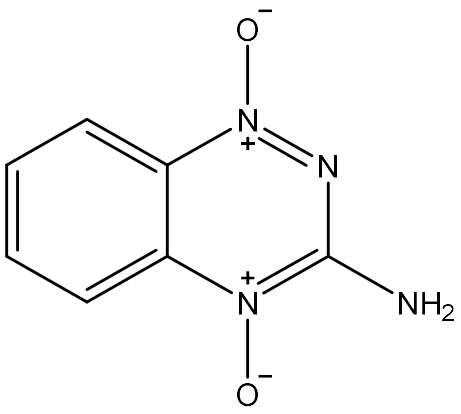

3-Amino-1,2,4-benzotriazine 1,4-dioxide
Chemical Formula: $C_7H_6N_4O_2$
Exact Mass: 178.0491
Molecular Weight: 178.1510

G_6-TPZ

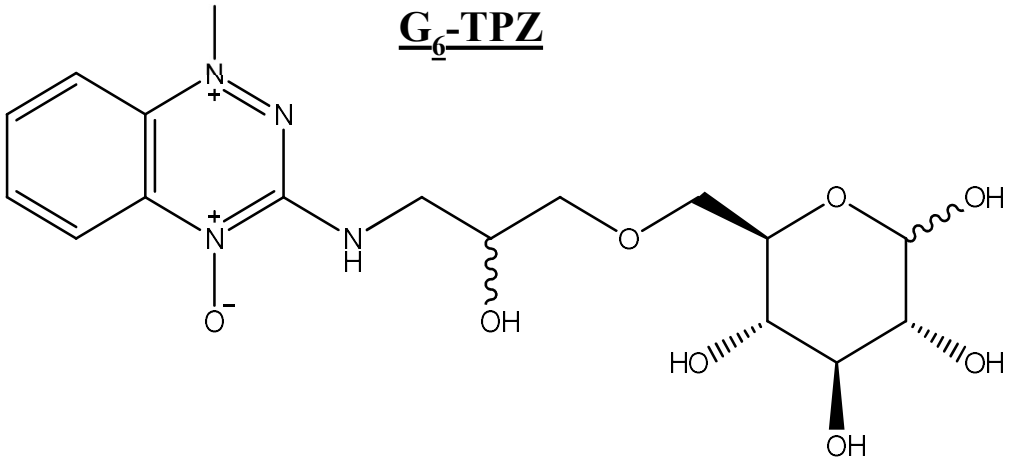

Chemical Formula: $C_{16}H_{22}N_4O_9$
Exact Mass: 414.1387
Molecular Weight: 414.3710

Although inducing DNA damage is considered as the major mechanism behind TPZ's cytotoxicity, we hypothesize that binding of bioreduced TPZ to cellular proteins under hypoxia would play a role in altering the drug's efficacy. Hence identifying the proteins bound to TPZ under hypoxic conditions could help to determine the pathway by which TPZ causes toxicity. This was addressed by incorporating an azido (N_3) group to our parent compound (N_3-TPZ) to exploit a click chemistry-based protocol. The azido group of N_3-TPZ reacts with an alkyne in the presence of a copper catalyst at room temperature (RT) to form a stable triazole conjugate. Depending on the type of alkyne labelling (fluorophore or biotin), the drug-protein adducts can either be imaged using immunofluorescence staining or be pulled down with mutein streptavidin beads. Thus, we aimed to use our clickable prodrug of TPZ as a tool for mapping and imaging hypoxic cells *in vitro* in addition to isolating potential protein candidates that get modified by N_3-TPZ under hypoxia.

N_3-TPZ

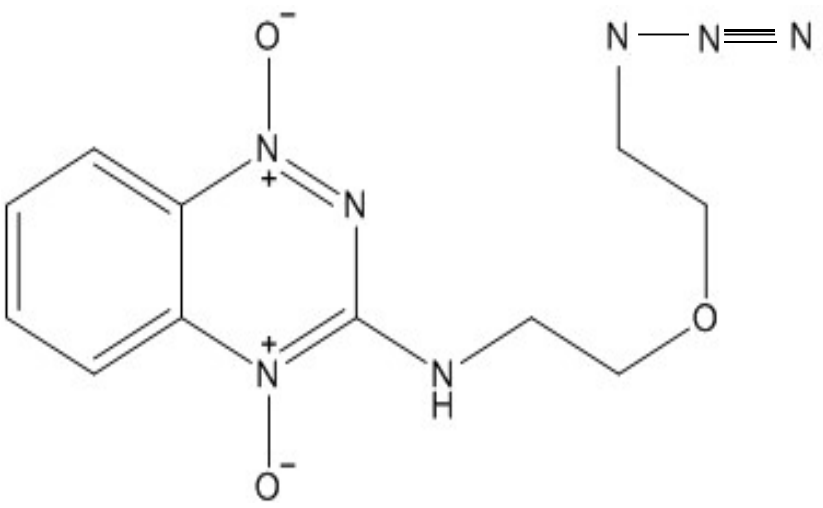

3-{[2-(2-azidoethoxy)ethyl]amino}-1,2,4-benzotriazine 1,4-dioxide
Chemical Formula: $C_{11}H_{13}N_7O_3$
Exact Mass: 291.1080
Molecular Weight: 291.2710

As we knew the uptake of N_3-TPZ in a hypoxic cell can be monitored by click chemistry, we set out to exploit this property of the reagent to examine the localization of G_6-TPZ. Accordingly, we designed a new derivative of TPZ by conjugation of both glucose and azido moieties (N_3-G_6-TPZ) to our parent compound. The efficacy and localization of the compound were studied.

N_3-G_6-TPZ

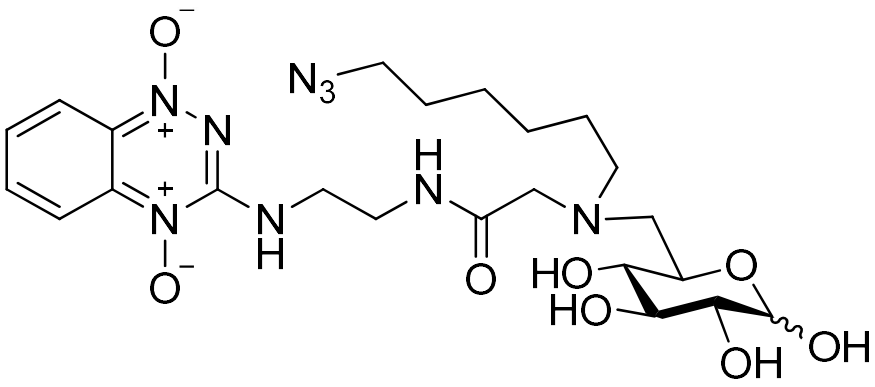

Chemical Formula: $C_{23}H_{35}N_9O_8$
Exact Mass: 565.2609
Molecular Weight: 565.5880

Overall, we carried out the above specified structural modifications on TPZ as an attempt to increase its clinical potential as an anticancer drug and our research goal was to examine the potency of these TPZ derivatives.

Chapter II - Materials and Methods

2.1. Cell Culture

The FaDu head and neck squamous cell carcinoma cell line was obtained from American Type Culture Collection (ATCC, Manassas, VA). The cells were cultured in a 1:1 mixture of Dulbecco's Modified Eagle's Medium and Ham's F12 medium (DMEM/F12) supplemented with 10% fetal bovine serum (FBS), 1% L-glutamine, 1% penicillin/streptomycin and were maintained at 37°C under 5% CO_2 in a humidified incubator. All culture supplements were purchased from Invitrogen (Waltham, MA).

2.2. Hypoxic condition

To establish hypoxic conditions, treated/untreated cells cultured in media were placed in airtight chambers flushed with a gas mixture of 5% CO_2 / 95% N_2. Oxygen concentrations within these chambers were maintained using Pro-Ox model O_2 regulators (BioSpherix, NY). We also followed another methodology to establish hypoxic conditions by pumping air out and replacing it with a gas mixture of 5% CO_2 / 95% N_2 to canisters which had treated/untreated cells cultured in media. The procedure was carried out for five cycles with an interval of 30 seconds in between. Another round of five cycles were repeated with a longer interval of 10 minutes in between. Thereafter, canisters were placed in the incubators at 37°C with 5% CO_2, for the required duration according to the experimental set-up.

2.3. Drug and/or chemical compounds

Tirapazamine (TPZ) used in the study was obtained from Sigma-Aldrich Canada Co, Oakville, ON, Canada (Product No: SML0552, CAS-No: 27314-97-2). Glucose-conjugated TPZ (G_6-TPZ) was synthesized by Naeja Pharmaceuticals (Kumar P., unpublished). Other chemical compounds used in this study such as Azido-conjugated TPZ (N_3-TPZ) and Azido-glucose-conjugated TPZ

(N_3-G_6-TPZ) were designed, synthesized and their respective structures (presented in the prior chapter) were corroborated by Dr Hassan Elsaidi, a senior researcher in our group.

2.4. Cytotoxicity assays

2.4.1. MTT assay

Cytotoxicity/cytostasis evaluation of TPZ and its derivatives was performed using the MTT [3-(4,5-dimethylthiazol-2-yl)-2,5-diphenyl-2H-tetrazolium bromide] assay as described by Mosmann *et al*.,[379] with slight modifications. Cell Proliferation Kit I (MTT) was purchased from Roche Diagnostics, Manheim, Germany (Catalogue No: 11465007001). FaDu cells (~3000 cells/well) were seeded in 96-well microtitre plates and incubated overnight at 37°C with 5% CO_2, allowing the cells to adhere to the surface. Next day, the cells were treated with varying concentrations of compound and the plates were incubated under normoxic (20% O_2) and hypoxic (0.1% O_2) conditions for 72 hours. Culture medium (DMEM/F12 and low glucose DMEM) without cells was set for background, according to the experimental set-up. In brief, after the required incubation period, a final volume of 50 µl MTT reagent was added to each well and the plates were further incubated for 3-5 hours at 37°C to form formazan crystals. DMSO was added to the wells to dissolve the formazan products and absorbance of the samples was measured spectrophotometrically using an ELISA plate reader at a wavelength of 564 nm. For optimal results, the absorbance of background wavelength (media only) was subtracted from other absorbance results.

2.4.2. Crystal Violet Staining (CVS) assay

FaDu cells (~3000 cells/well) were seeded in 96-well microtitre plates and incubated overnight at 37°C with 5% CO_2, allowing the cells to adhere to the surface. The cells were then treated with varying concentrations of compound and the plates were incubated under normoxic

(20% O_2) and hypoxic (0.1% O_2) conditions for 72 hours. Culture medium (DMEM/F12 and low glucose DMEM) without cells was set for background, according to the experimental set-up. After the required incubation period, media was aspirated and the plates were left to dry for a few minutes. This was followed by addition of crystal violet solution to the wells in order to stain the cells. Subsequently, the dye was discarded, plates were washed with water and left to dry overnight. Finally, methanol was added to the wells and the plates were further incubated for 20 minutes so as to dissolve the crystals. Absorbance of the samples was measured spectrophotometrically using an ELISA plate reader at a wavelength of 520 nm. For optimal results, the absorbance of background wavelength (media only) was subtracted from other absorbance results.

2.4.3. Colony formation assay

FaDu cells (optimum density ranging from 300-3000 cells) were seeded in 60-mm tissue culture plates and incubated overnight at 37°C with 5% CO_2, allowing the cells to adhere to the surface. The cells were then treated with varying concentrations of compound and the plates were incubated under normoxic (20% O_2) and hypoxic (0.5% O_2) conditions for 24 hours. Next day, the media was changed and the plates were incubated further for 14 days (at 37°C with 5% CO_2) to let the colonies develop. After 14 days, the colonies were stained with crystal violet solution and counted.

2.5. Western blot analysis

FaDu cells were seeded in 60-mm tissue culture plates and incubated overnight at 37°C with 5% CO_2, allowing the cells to adhere to the surface. The treated/untreated cells were then exposed to both normoxic (20% O_2) and variable hypoxic conditions for various time durations depending on the experimental set-up. Cells were washed twice with ice cold PBS and resuspended

in RIPA buffer (50 mM Tris-HCl pH 7.6, 150 mM NaCl, 1% deoxycholate, 1% Triton X-100, 1 mM Na_3VO_4, 50 mM NaF, 1 mM phenylmethylsulfonyl fluoride, protease and phosphatase inhibitor cocktail). Later, the cell lysates were sonicated and centrifuged at 20,000 g for 20 minutes at 4°C. Protein was quantified using the Bradford assay according to the manufacturer's protocol (Bio-Rad, USA). Protein (15-20 µg) was added to sample buffer (2% SDS, 10% glycerol, 0.02% bromophenol blue, 50 mM Tris HCl pH 6.8, 12.5 mM EDTA, 1% β-mercaptoethanol) and boiled for 5 minutes. Samples were separated in a 10% SDS-PAGE gel at 180 V for 1 hour at RT. The proteins were then transferred to a nitrocellulose membrane by wet transfer at 100 V for 2 hours at room temperature. In order to prevent non-specific protein binding, membranes were blocked in 5% non-fat milk in TBS-T (Tris buffered saline, 0.1% Tween-20) for 1 hour. Membranes were then immunostained with the following primary antibodies: rabbit anti-GLUT-1 (Abcam-ab652, 1:1000), mouse anti-HIF-1α (Novus biologicals-NB100-449, 1:1000) and mouse anti-actin (Santa Cruz-sc 47778, 1:2000) overnight at 4°C. Next day, membranes were washed 5 times for 7 minutes each in TBS-T and then were incubated with appropriate HRP-conjugated secondary antibody (goat anti-rabbit and goat anti-mouse) at 1:10,000 dilution in 5% milk for 1 hour at room temperature. Membranes were again washed 5 times for 7 minutes each in TBS-T followed by a 1X 5 minute PBS wash. Finally, the membranes were incubated with chemiluminescence reagent (Thermo Scientific SuperSignal West Pico Plus Chemiluminescent substrate) for 5 minutes prior to autoradiography.

2.6. Real-time reverse transcription polymerase chain reaction (Real-Time RT-PCR)

FaDu cells were seeded in 6-well tissue culture plates and incubated overnight at 37°C with 5% CO_2, allowing the cells to adhere to the surface. Cells were then exposed to both normoxic

(20% O_2) and variable hypoxic conditions (5, 2, 1, 0.5% O_2) for various time durations (6, 12, 24 and 48 hour), depending on the experimental set-up. Total RNA was extracted using RNA extraction Manual PerfectPure RNA Cell and Tissue kit (5 Prime Inc, MD) according to manufacturer's protocol. RNAs were quantified by measuring the absorbance at 260 nm and respective cDNA was synthesized using the High Capacity cDNA Reverse Transcription Kit (Applied Biosystems, CA). Real time RT-PCR analysis was performed using 2 µg of cDNA and TaqMan gene expression human primer/probe sets. The following primer/probes were used: GLUT-1 (Life Technologies-Hs00892681_m1), LOX (Applied Biosystems- Hs00184706), and RPLPO (Applied Biosystems- 4333761). Relative fold changes were normalized to the control gene RPLPO and gene expression was quantified using comparative threshold cycle method ($2^{-\Delta\Delta Ct}$) as described by Pfaffl [380].

2.7. Click Chemistry

FaDu cells (~0.5 million) were seeded on coverslips in 30-mm tissue culture plates and incubated overnight at 37°C with 5% CO_2, allowing the cells to adhere to the surface. Cells were then treated with varying concentrations of compound and incubated under normoxic (20% O_2) and hypoxic (<0.1% O_2) conditions for 24 hours. Post-treatment, cells were fixed with 4% paraformaldehyde (PFA) in PBS for 20 minutes at RT and cells were washed thrice with PBS. This was followed by blocking and permeabilization of cells with PBS containing 1% BSA and 0.1% Triton-X-100 for 20 minutes and cells were again rinsed thrice with PBS. Click reaction was performed for 30 minutes at room temperature in the presence of Alexa Fluor 594 alkyne (Life Technologies, A10275) using the Click-iT Cell Reaction Buffer Kit (Thermo Fisher Scientific, Catalogue No: C10269) following the manufacturer's protocol. The cells were then washed thrice with PBS containing 0.01% Triton X-100 followed by a 3X PBS wash. Nuclei were counterstained

with Hoechst at room temperature for 5 minutes in the dark and cells were rinsed thrice with PBS. Finally, the coverslips were mounted on slides and images were obtained using a Zeiss LSM 710 laser scanning confocal microscopy (Carl Zeiss, Inc).

2.8. Affinity Purification assay

FaDu cells were seeded on coverslips in 60-mm tissue culture plates and incubated overnight at 37°C with 5% CO_2, allowing the cells to adhere to the surface. Cells were then treated with varying concentrations of the compound and incubated under normoxic (20% O_2) and hypoxic (<0.1% O_2) conditions for 24 hours. Cells were washed twice with ice cold PBS and re-suspended in RIPA buffer. The cell lysates were sonicated and centrifuged at 14,000 rpm for 20 minutes at 4ºC. Protein was quantified using the Bradford assay according to the manufacturer's protocol. Later, click reaction was performed on the lysate for 30 minutes at room temperature in the presence of a non-PEGylated Biotin-Alkyne (Lumiprobe, Catalogue No: C37B0) using Click-iT Cell Reaction Buffer Kit following the manufacturer's protocol. The lysate was also blocked simultaneously with 0.1% BSA in PBS. Meanwhile, streptavidin mutein matrix was prepared according to the manufacturer's protocol (Roche Diagnostics, Catalogue No: 03708152001) and the beads were blocked for 1 hour with 1% BSA in PBS at room temperature. This was followed by incubating the clicked lysate with streptavidin mutein matrix overnight at 4°C and next day, the protein complexes were eluted four times with biotin (Sigma-Aldrich, B4501). Eluates were run on 10% SDS-PAGE gel and transferred to a nitrocellulose membrane. The membrane was blocked in 5% non-fat milk in TBS-T (Tris buffered saline, 0.1% Tween-20) for 1 hour to prevent non-specific binding, and then immunostained with the Streptavidin-HRP antibody (Thermo Fisher Scientific, RPN1231VS, 1:2000) overnight at 4°C. Next day, the membrane was washed 5 times for 7 minutes each in TBS-T followed by a 5 minute

PBS wash. Finally, the membrane was incubated with chemiluminescence reagent (Thermo Scientific SuperSignal West Pico Plus Chemiluminescent substrate) for 5 minutes prior to autoradiography.

2.9. Statistical Analysis

The experiments in the study were conducted in at least three independent runs. Data are presented as mean value ± standard error of mean (SEM). The statistical analysis was performed with GraphPad Prism 7 Software (GraphPad Software Inc., USA) using an unpaired t-test. $p < 0.05$ was considered statistically significant.

Chapter III - Results

3.1. Determination of optimum time and oxygen concentration for GLUT-1 upregulation

In spite of the well-established fact that GLUT-1 has been regarded as a diagnostic hallmark of tumor hypoxia, we set out to investigate how GLUT-1 responds to various hypoxic conditions. Prior to testing the potential of glucose-conjugated TPZ (G_6-TPZ), preliminary experiments were performed to determine the optimum hypoxic conditions at which GLUT-1 experiences the best upregulation. As discussed earlier, since HNC is a well-established tumor type for hypoxia studies, we chose FaDu cells (derived from a hypopharyngeal carcinoma cell line) as our model of study. A well-known hypoxia marker, LOX was used as a control gene in our studies in order to ensure that we attained appropriate hypoxia-induced gene responses in our study set up.

To study how GLUT-1 responds to decreasing O_2 concentrations, experiments were performed to determine the optimum oxygen concentration and time point at which GLUT-1 is maximally upregulated. FaDu cells exposed to varying levels of oxygen (20, 5, 2, 1 and 0.5% O_2) for 24 hours, resulted in a progressive increase of GLUT-1 mRNA levels at decreasing O_2 concentrations, showing a significant increase at 0.5% O_2 when compared to 20% O_2 (ie., normoxic condition) [Figure 3.1 A]. As mentioned earlier, LOX was used as a control to ensure a caninocal hypoxia-induced response. Accordingly, LOX mRNA levels increased with decreasing O_2 concentrations with a maximal increase at 0.5% O_2 similarly as GLUT-1 mRNA levels [Figure 3.1 B]. GLUT-1 protein levels demonstrated a similar trend by showing a high induction of GLUT-1 protein at hypoxic conditions such as 1% and 0.5% O_2 when compared to normoxic control [Figure 3.2 A]. HIF-1α protein was also induced at 0.5% O_2, confirming the response of HIF-1α to hypoxia in our study [Figure 3.2 B]. Taken together, 0.5% O_2 was

considered for future hypoxic experiments since the concentration exhibited a constant increase of GLUT-1 at both the mRNA and protein levels.

In order to determine the response of GLUT-1 to varying exposure times in hypoxia, FaDu cells were exposed to 0.5% O_2 for 6, 12, 24 and 48 hours, which revealed that GLUT-1 mRNA levels increased with increasing exposure time reaching a maximum at 24 hours and later the levels declined sharply [Figure 3.3 A]. LOX mRNA levels were observed to be upregulated at the longer exposure time points, i.e. 24 and 48 hours [Figure 3.3 B]. Considering the fact that GLUT-1 mRNA showed a maximum upregulation at 24 hours and LOX mRNA levels correlates with the same, 24 hours was chosen as the optimum exposure time to hypoxia. Taken together, 0.5% O_2 and 24 hours incubation were considered as optimum conditions for further hypoxic experiments.

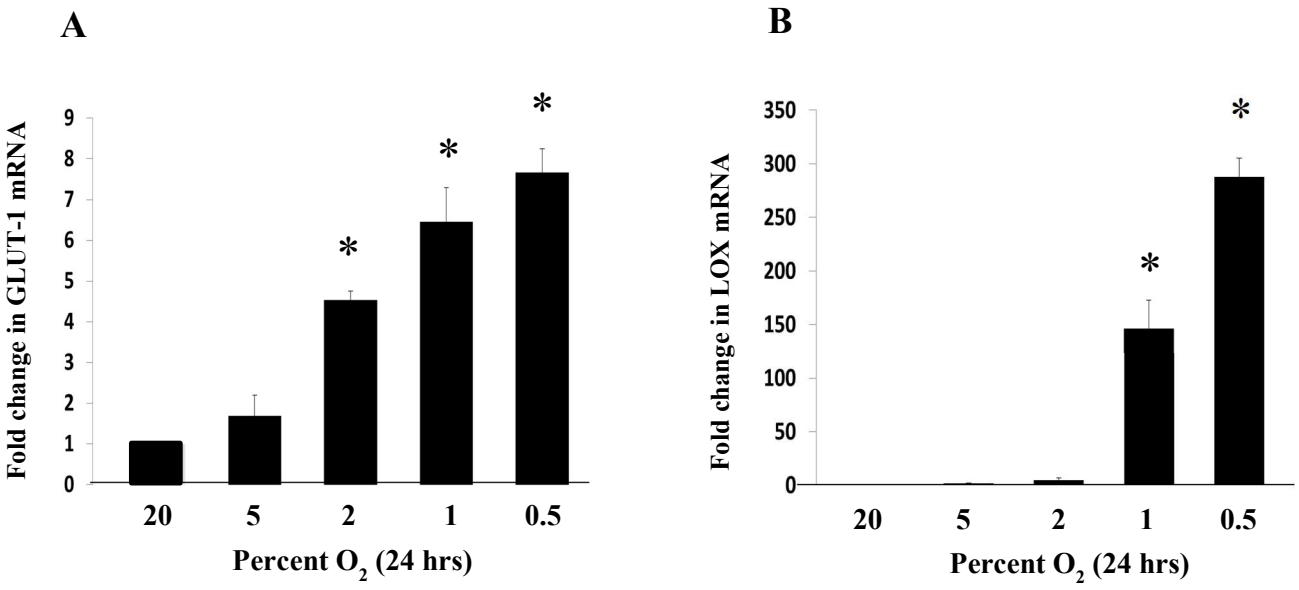

Figure 3.1 GLUT-1 is inversely regulated in an oxygen-concentration dependent manner

FaDu cells were seeded in 6-well plates and incubated overnight to adhere. The cells were then exposed to varying oxygen conditions for 24 hours. (A) Real time RT-PCR data shows that GLUT-1 mRNA levels increase progressively with a decrease in O_2 concentration in FaDu cells. (B) Real time RT-PCR of LOX mRNA levels reveals that LOX mRNA is highly upregulated with decreasing levels of O_2 with a maximal upregulation at 0.5% O_2. The mRNA levels were measured by Real time RT-PCR and relative fold changes were normalized to the control gene RPLPO. The experiment was repeated twice and the error bars represent the standard error of the mean. The difference between different O_2 concentration versus 20% O_2 control was analyzed with an unpaired t-test; (*) indicates statistical significance of $p < 0.05$. Thus, 0.5% O_2 was chosen as an optimum oxygen concentration for further experiments since mRNA levels of both GLUT-1 and LOX showed maximal upregulation at that oxygen concentration.

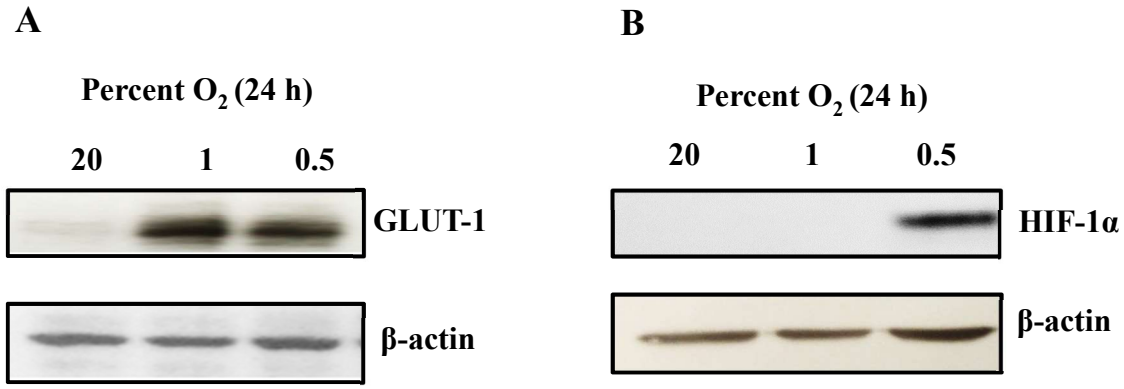

Figure 3.2 GLUT-1 and HIF-1α protein are regulated by hypoxia in an oxygen concentration-dependent manner

FaDu cells were seeded in 60-mm dishes and incubated overnight to adhere. The cells were then exposed to 20%, 1% and 0.5% O_2 for 24 hours. (A) Western blot analysis of FaDu cells exposed to various oxic conditions for 24 hours shows that GLUT-1 protein levels increase with decreasing levels of O_2. β-actin was used as a loading control. (B) Western blot analysis confirms upregulated HIF-1α expression at 0.5% hypoxia and β-actin was used as a loading control. Hence, 0.5% O_2 was chosen as an optimum oxygen concentration for further experiments since we observed a strong induction of GLUT-1 and HIF-1α protein level at that oxygen concentration.

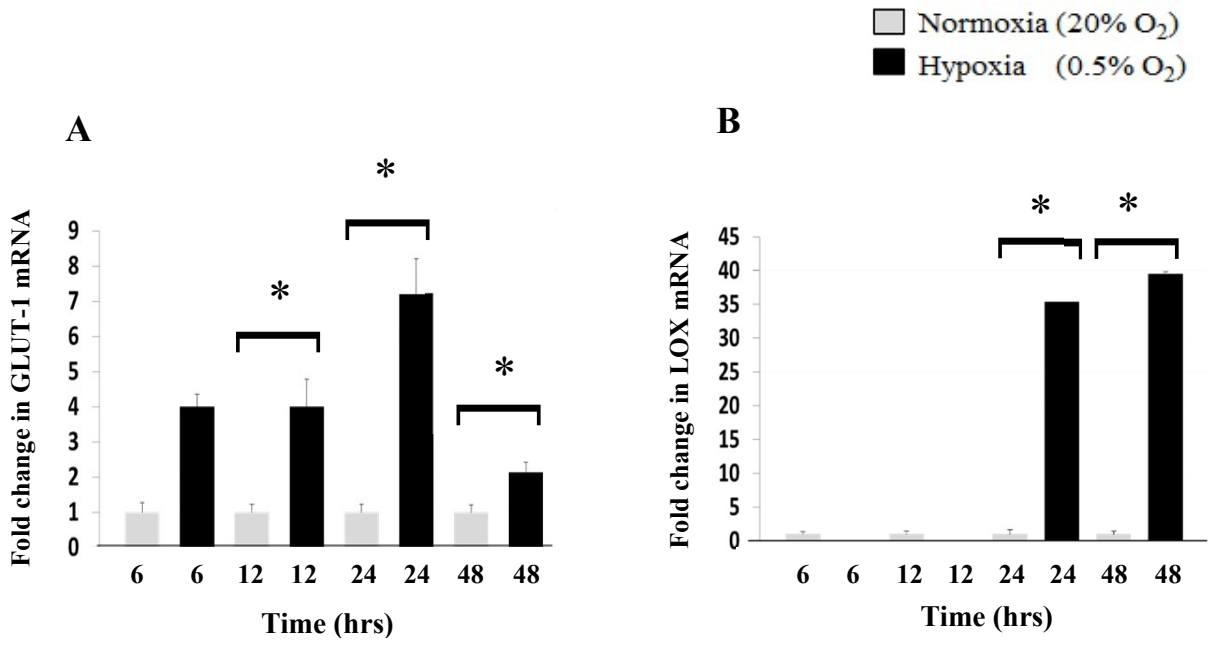

Figure 3.3 Time course of GLUT-1 response

FaDu cells were seeded in 6-well plates and incubated overnight to adhere. The cells were then exposed to either 20% or 0.5% O_2 for 6, 12, 24 and 48 hours. (A) Real time RT-PCR data reveals that GLUT-1 mRNA levels increase linearly up to 24 hours with exposure to 0.5% O_2 when compared to GLUT-1 mRNA levels at 20% O_2 and later declines sharply at 48 hours in FaDu cells. (B) Real time RT-PCR shows that LOX mRNA levels are upregulated with increasing exposure time in 0.5% O_2 compared to 20% O_2 control levels. The mRNA levels were measured by Real time RT-PCR and relative fold changes were normalized to the control gene RPLPO. The experiment was repeated twice and the error bars represent the standard error of the mean. The difference between normoxia and hypoxia within each time point was analyzed with an unpaired t-test; (*) indicates statistical significance of $p < 0.05$. We chose 24 hours as an optimum time for further experiments since mRNA levels of both GLUT-1 and LOX showed maximal upregulation during that time point at 0.5% O_2.

3.2. TPZ exhibits preferential hypoxic cytotoxicity in a concentration-dependent manner

Following the determination of optimum hypoxic conditions, cytotoxicity of the parent compound (TPZ) was assessed using different assays such as the MTT, crystal violet staining and colony formation assay. We used three different approaches to screen cytotoxicity in order to validate the efficacy of the drug since each assay employs different parameters as a basis to assess cell death. In the MTT assay, which measures cellular metabolic activity, TPZ showed preferential cytotoxicity at low oxygen levels (0.5% O_2) in a concentration-dependent manner with minimal toxicity under normoxia [Figure 3.4 A]. A similar trend of hypoxic cytotoxicity was observed in TPZ when assessed using crystal violet staining assay, which measures the DNA mass of living cells, and the IC_{50} of the drug in hypoxia was observed to be approximately 10 μM, which is lower compared to treatment under normoxia [Figure 3.4 B]. We also evaluated the colony forming ability of cells treated with TPZ and the results correlated with the prior cytotoxicity data thereby reconfirming the hypoxia selective cytotoxicity of the parent compound [Figure 3.4 C]. Therefore, the cytotoxicity data of TPZ strongly establishes that the parent compound is highly hypoxia selective.

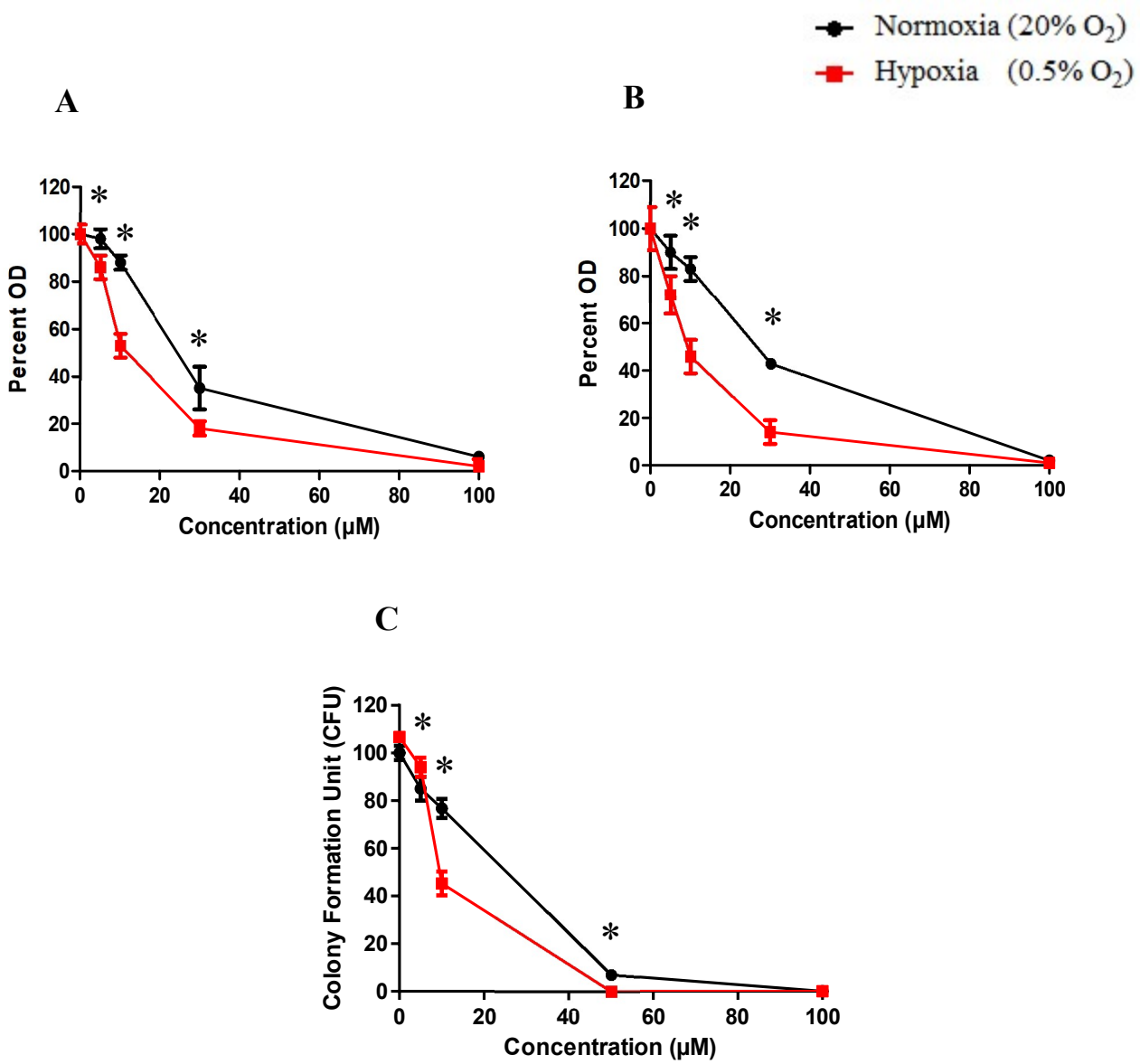
Normoxia (20% O2)
Hypoxia (0.5% O2)
A
B
C
Percent OD
Concentration (μM)
Colony Formation Unit (CFU)
0
20
40
60
80
100
120
*

Figure 3.4 TPZ shows hypoxia-selective cytotoxicity in a concentration-dependent manner

Cytotoxicity of TPZ treated cells as observed using the MTT assay (A), crystal violet staining assay (CVS) (B) and colony forming assay (CFA) (C). In the MTT assay (A), FaDu cells (3000 cells/well) were seeded in 96-well plates and incubated overnight to adhere. The cells were then treated with increasing concentrations of TPZ and the plates were exposed to both normoxic (20% O_2) and hypoxic (0.5% O_2) conditions for 72 hours. Culture medium (DMEM) without cells was set for background. MTT was added to each well and the plates were further incubated for 3-5 hours to form formazan crystals. DMSO was added to dissolve the formazan products and absorbance of the samples was measured spectrophotometrically. Error bars represent the standard error of the mean. The difference between normoxia and hypoxia within each TPZ concentration was analyzed with an unpaired t-test; (*) indicates statistical significance of $p < 0.05$. In the CVS assay (B), FaDu cells (3000 cells/well) were seeded in 96-well plates and incubated overnight to adhere. The cells were then treated with increasing concentrations of TPZ and the plates were exposed to both normoxic (20% O_2) and hypoxic (0.5% O_2) conditions for 72 hours. Culture medium (DMEM) without cells was set for background. Media was aspirated post-treatment followed by addition of crystal violet solution to stain the cells. Crystals were dissolved using methanol and absorbance of the samples was measured spectrophotometrically. Error bars represent the standard error of the mean. The difference in percent colony formation between normoxia and hypoxia within each TPZ concentration was analyzed with an unpaired t-test; (*) indicates statistical significance of $p < 0.05$. In CFA, (C), FaDu cells (optimum density-ranging from 300 to 3000 cells) were seeded in 60-mm plates and incubated overnight to adhere. Next day, the cells were treated with increasing TPZ concentrations and the plates were exposed to both normoxic (20% O_2) and hypoxic (0.5% O_2) conditions for 24 hours. The media was changed and the plates were incubated for 14 days (at 37°C with 5% CO_2) to let the colonies develop. Colonies were stained with crystal violet solution and counted. Error bars represent the standard error of the mean. The difference in percent colony formation between normoxia and hypoxia within each TPZ concentration was analyzed with an unpaired t-test; (*) indicates statistical significance of $p < 0.05$. The cytotoxicity data of TPZ (A, B, C) as assessed using these assays correlated with each other by displaying an IC_{50} of approximately 10 μM under hypoxia.

3.3. G_6-TPZ displays hypoxia-selective cytotoxicity at high concentrations

Following the toxicity studies with TPZ, we went on to examine the potential of glucose-conjugated TPZ (G_6-TPZ) by examining the cytotoxicity of the compound in FaDu cells. As previously described, G_6-TPZ was synthesized in an attempt to improve the delivery of TPZ selectively to poorly oxygenated cells by taking advantage of the upregulated GLUT receptors in hypoxic cancer cells. Initially, G_6-TPZ did not show any hypoxic cytotoxicity in FaDu cells cultured in DMEM up to 100 μM concentration. Later, the cells were glucose- starved by culturing them in low glucose DMEM prior to treatment with high concentrations of G_6-TPZ. As shown in Figure 3.5A, the MTT assay of G_6-TPZ displayed hypoxic cytotoxicity in low oxygen levels (0.1% O_2) at very high concentrations of the compound (500 and 1000 μM) whereas minimal toxicity was seen in the normoxic group. A similar, but slightly amplified, response of G_6-TPZ was observed when assessed using CVS assay [Figure 3.5 B]. Since, we observed a hypoxia-specific response only at high concentrations of G_6-TPZ in FaDu cells, the compound was not used in the future studies.

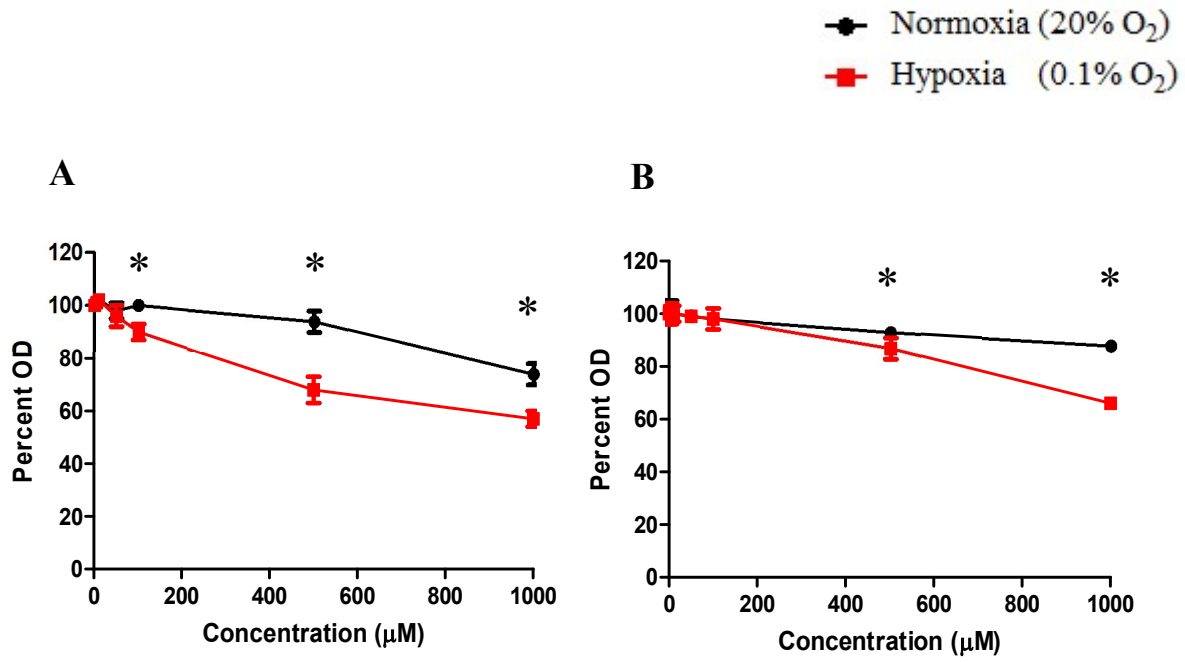

Figure 3.5 G_6-TPZ displays hypoxia-selective cytotoxicity at high concentrations

Cytotoxicity of G_6-TPZ as observed using the MTT assay (A) and CVS assay (B). In the MTT assay (A), FaDu cells (3000 cells/well) were seeded in 96-well plates and incubated overnight to adhere. The cells were then treated with increasing concentrations of G_6-TPZ and the plates were exposed to both normoxic (20% O_2) and hypoxic (0.1% O_2) conditions for 72 hours. Culture medium (low glucose DMEM) without cells was set for background. MTT was added to each well and the plates were further incubated for 3-5 hours to form formazan crystals. DMSO was added to dissolve the formazan products and absorbance of the samples was measured spectrophotometrically. Error bars represent the standard error of the mean. The difference between normoxia and hypoxia within each G_6-TPZ concentration was analyzed with an unpaired t-test; (*) indicates statistical significance of $p < 0.05$. In the CVS assay (B), FaDu cells (3000 cells/well) were seeded in 96-well plates and incubated overnight to adhere. The cells were then treated with increasing concentrations of G_6-TPZ and the plates were exposed to both normoxic (20% O_2) and hypoxic (0.1% O_2) conditions for 72 hours. Culture medium (low glucose DMEM) without cells was set for background. Media was aspirated post-treatment followed by addition of crystal violet solution to stain the cells. Crystals were dissolved using methanol and absorbance of the samples was measured spectrophotometrically. Error bars represent the standard

error of the mean. The difference between normoxia and hypoxia within each G_6-TPZ concentration was analyzed with an unpaired t-test; (*) indicates statistical significance of $p < 0.05$. The cytotoxicity data of G_6-TPZ (A & B) as assessed using both MTT and CVS assays demonstrated a similar trend which correlated with each other by exhibiting hypoxia-selective cytotoxicity at very high concentrations of the compound.

3.4. Effect of TPZ on the expression of HIF-1α

As discussed earlier, we hypothesize that binding of bioreduced TPZ to cellular proteins under hypoxia might contribute to the drug's cytotoxicity besides induction of DNA damage. Although we had a hint that TPZ is stabilized at protein level, it is still uncertain whether the drug binds directly to HIF-1α protein or it is bound to the proteins which stabilize HIF-1α. In order to investigate this effect, we performed a western blot analysis on proteins isolated from FaDu cells which were treated with increasing concentrations of TPZ and incubated at normoxic and hypoxic (0.5% O_2) conditions for 24 hours [Figure 3.6]. A sharp decrease in the expression of HIF-1α level was observed at 10 μM TPZ treated hypoxic sample. This result is in accordance with our prior data which suggested the IC_{50} of TPZ in hypoxia to be approximately 10 μM when assessed using several cytotoxicity assays [Figure 3.4]. As expected, the HIF-1α expression was observed to be low in normoxic TPZ treated samples. The data indicates the fact that TPZ inhibits the hypoxic stabilization of HIF- 1α and therefore, we speculate that the drug might either bind directly to the HIF-1α protein, or to the proteins that stabilize HIF-1α and thereby let HIF-1 be proteasomally degraded. This stimulated our interest in identifying proteins that bind TPZ under hypoxia.

3.5. Click chemistry-based protocol using azido conjugated TPZ

As mentioned earlier, we designed an azido conjugated TPZ (N_3-TPZ) derivative in an effort to identify TPZ binding proteins using a click chemistry-based approach. In addition, we also used our clickable prodrug of TPZ to image hypoxic cell content *in vitro* and to trace tumor hypoxia. The general principle of how N_3-TPZ can be used to image hypoxic cells using click chemistry is illustrated in Figure 3.7. As our drug is hypoxia selective, it will get bioreductively activated under hypoxia thereby binding to cellular proteins. Subsequently, the azide group (N_3) of N_3-TPZ can react with an alkyne by click chemistry in the presence of a copper catalyst resulting in the formation a stable triazole conjugate. The labelling of the alkyne to a fluorophore would allow us to trace where the drug accumulates. Thus, N_3-TPZ can be used as a tool to monitor TPZ uptake.

3.6. N_3-TPZ exhibits selective hypoxic cytotoxicity in a concentration-dependent manner

The hypoxic selectivity of N_3-TPZ was initially assessed by examining the cytotoxicity of the compound using different assays in FaDu cells. As shown in Figure 3.8A, the MTT assay of N_3-TPZ displayed selective cytotoxicity in low oxygen levels (0.1% O_2) in a concentration-dependent manner whereas minimal toxicity was seen in the normoxic group. Similar, but a slightly amplified response of N_3-TPZ was observed when assessed using the CVS and CFA assays [Figure 3.8B & C]. The IC_{50} of N_3-TPZ in hypoxia lies between 20-25 μM, which was lower than the response to the compound in normoxia treated cells. Taken together, N_3-TPZ appeared to be hypoxia selective but slightly less toxic when compared to the parent compound (TPZ)

[Figure 3.4]. This indicated that N_3-TPZ is a good model to study TPZ interactions since the azide modification did not seem to drastically alter the toxicity of the parent compound. Next, we went on to examine the response of N_3-TPZ on HIF-1α expression. Western blot analysis performed on proteins isolated from FaDu cells, which were treated with increasing concentrations of N_3-TPZ and incubated under normoxic and hypoxic (0.5% O_2) conditions for 24 hours, revealed that HIF-1α protein levels decreased with increasing concentrations of N_3-TPZ in hypoxic samples [Figure 3.8D]. A sharp decrease in the expression of HIF-1α level was observed at 30 μM N_3-TPZ treated hypoxic sample. This result correlates with our prior data which suggested that the IC_{50} of N_3-TPZ under hypoxia to lie between 20-25 μM when assessed using different cytotoxicity assays [Figure 3.8A, B & C].

3.7. Hypoxia selective sub-cellular localization of N_3-TPZ

Next, we went on to examine the localization of N_3-TPZ using click chemistry. The click reaction was performed on FaDu cells that were treated with increasing concentrations of N_3-TPZ for 24 hours under normoxic and hypoxic (<0.1 O_2) conditions. Fluorescence images obtained from confocal microscopy reveals selective sub-cellular localization of N_3-TPZ in cells exposed to hypoxia (<0.1 O_2) [Figure 3.9]. It is evident that the compound displays cytoskeletal staining with nucleolar and nuclear localization. The click signal intensity was observed to be concentration dependent in hypoxic N_3-TPZ treated cells [Figure 3.9B, C & D]. On the other hand, minimal to no background signal was detected in normoxic N_3-TPZ treated cells even at high concentrations of the reagent [Figure 3.9A], which reconfirms the hypoxia selectivity of the compound. In addition, the Z-stack images acquired through confocal microscopy shows that N_3-TPZ efficiently enters the cell under hypoxia [Figure 3.10], reconfirming the hypoxia selective sub-cellular

localization of the compound. Overall, we can say this methodology provides an approach to monitor TPZ cellular uptake.

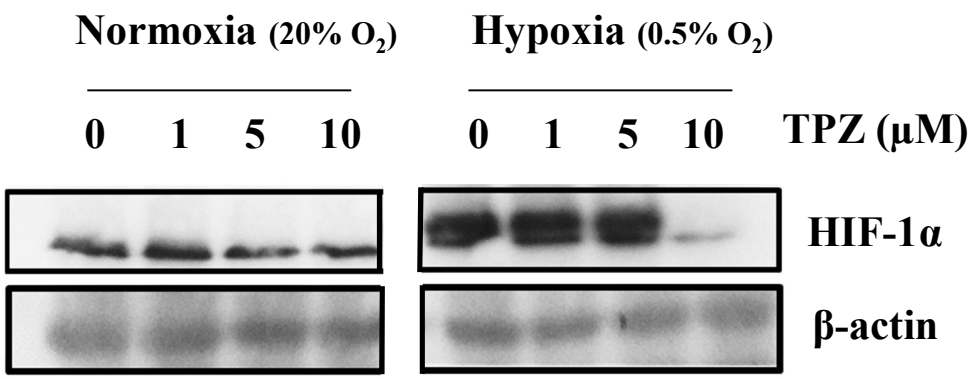

Figure 3.6 TPZ inhibits hypoxic stabilization of HIF-1α

FaDu cells were seeded in 60-mm dishes and incubated overnight to adhere. The cells were then treated with increasing concentrations of TPZ under normoxic (20% O_2) or hypoxic (0.5% O_2) conditions for 24 hours. Following treatment, cell lysates were extracted and loaded on 10% SDS-PAGE gel. Later, the proteins that were transferred to a nitrocellulose membrane were immunostained overnight with anti-HIF-1α antibody. β-actin was used as a loading control. Western blot analysis indicates a sharp decrease in the expression of HIF-1α level in 10 μM TPZ treated hypoxic cells whereas the HIF-1α levels were elevated at lower concentrations (1 and 5 μM) of TPZ treated hypoxic samples. In contrast, HIF-1α expression was observed to be low in normoxic TPZ treated samples. This data suggests that higher concentrations of TPZ inhibits the hypoxic stabilization of HIF-1α.

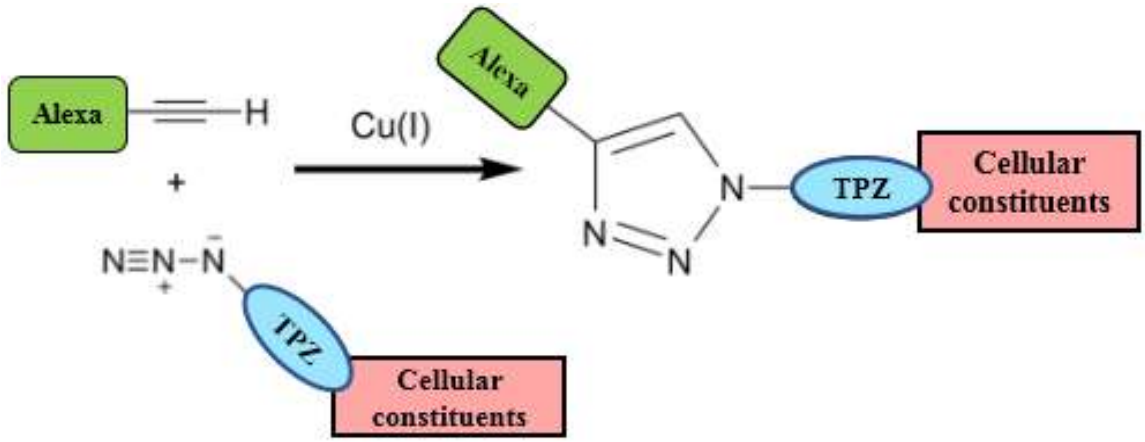

Figure 3.7 Experimental principle to image hypoxic cells using N_3-TPZ click chemistry

Schematic diagram depicting the general principle of imaging hypoxic cells using N_3-TPZ click chemistry. TPZ, being hypoxia selective, will become bioreductively activated under hypoxia, leading to its binding to cellular constituents including proteins. Subsequently, the azide group (N_3) of N_3-TPZ reacts with an alkyne and the molecule undergoes a rapid click reaction in the presence of a copper catalyst resulting in the formation a stable triazole conjugate. The labelling of the alkyne to a fluorophore (Alexa) eventually allows us to detect where the compound accumulates.

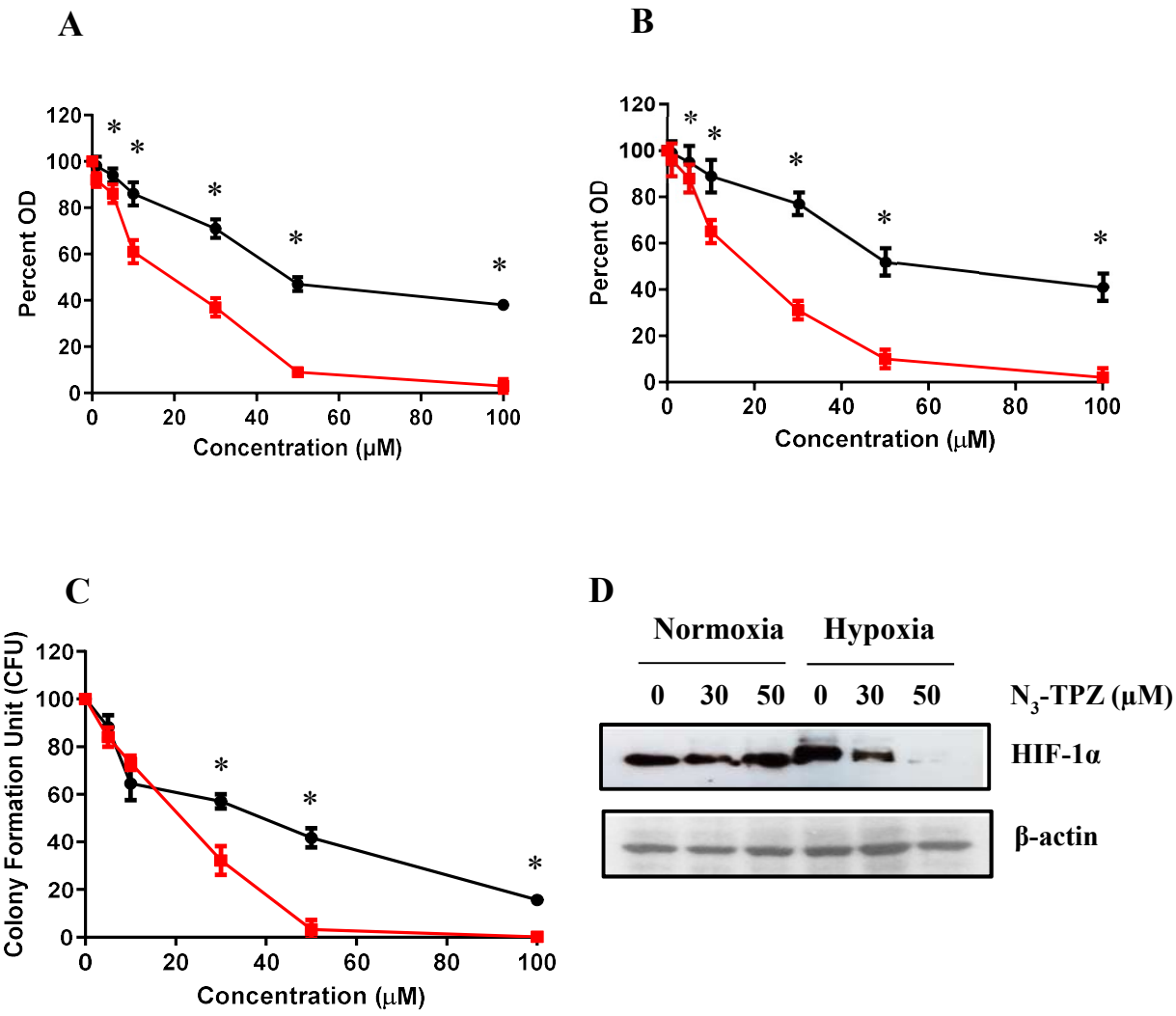
A
B
C
D
Percent OD
Concentration (μM)
Colony Formation Unit (CFU)
Normoxia
Hypoxia
0 30 50 0 30 50
N3-TPZ (μM)
HIF-1α
β-actin

Figure 3.8 N_3-TPZ shows hypoxic cytotoxicity in a concentration-dependent manner

Cytotoxicity of N_3-TPZ treated FaDu cells as observed using the MTT assay (A), CVS assay (B) and colony formation assay (CFA) (C). In the MTT assay (A), FaDu cells (3000 cells/well) were seeded in 96-well plates and incubated overnight to adhere. The cells were then treated with increasing concentrations of N_3-TPZ and the plates were exposed to both normoxic (20% O_2) and hypoxic (0.1% O_2) conditions for 72 hours. Culture medium (DMEM) without cells was set for background. MTT was added to each well and the plates were further incubated for 3-5 hours to form formazan crystals. DMSO was added to dissolve the formazan products and absorbance of the samples was measured spectrophotometrically. Error bars represent the standard error of the mean. The difference between normoxia and hypoxia at each N_3-TPZ concentration was analyzed with an unpaired t-test; (*) indicates statistical significance of $p < 0.05$. In the CVS assay (B), FaDu cells (3000 cells/well) were seeded in 96-well plates and incubated overnight to adhere. The cells were then treated with increasing concentrations of N_3-TPZ and the plates were exposed to both normoxic (20% O_2) and hypoxic (0.1% O_2) conditions for 72 hours. Culture medium (DMEM) without cells was set for background. Media was aspirated post-treatment followed by addition of crystal violet solution to stain the cells. Crystals were dissolved using methanol and absorbance of the samples was measured spectrophotometrically. Error bars represent the standard error of the mean. The difference between normoxia and hypoxia within each N_3-TPZ concentration was analyzed with an unpaired t-test; (*) indicates statistical significance of $p < 0.05$. In the CFA (C), FaDu cells (optimum density-ranging from 300 to 3000 cells) were seeded in 60-mm plates and incubated overnight to adhere. Next day, the cells were treated with increasing N_3-TPZ concentrations and the plates were exposed to both normoxic (20% O_2) and hypoxic (0.5% O_2) conditions for 24 hours. The media was changed and the plates were incubated for 14 days (at 37°C with 5% CO_2) to let the colonies develop. Colonies were stained with crystal violet solution and counted. Error bars represent the standard error of the mean. The difference in percent colony formation between normoxia and hypoxia within each N_3-TPZ concentration was analyzed with an unpaired t-test; (*) indicates statistical significance of $p < 0.05$. The cytotoxicity data of N_3-TPZ as assessed using these assays demonstrated a similar trend which correlated with each other by displaying an IC_{50} value under hypoxia ranging between 20-25 μM. (D) FaDu cells were seeded in 60-mm dishes and incubated overnight to adhere. The cells were then treated with varying concentrations of N_3-TPZ and were exposed to both normoxic (20% O_2) and hypoxic

(0.5% O_2) conditions for 24 hours. Following treatment, cell lysates were extracted and run on 10% gel. Western blot analysis reveals that HIF-1α protein levels decrease at increasing concentrations of N_3-TPZ in hypoxic samples. β-actin was used as a loading control.

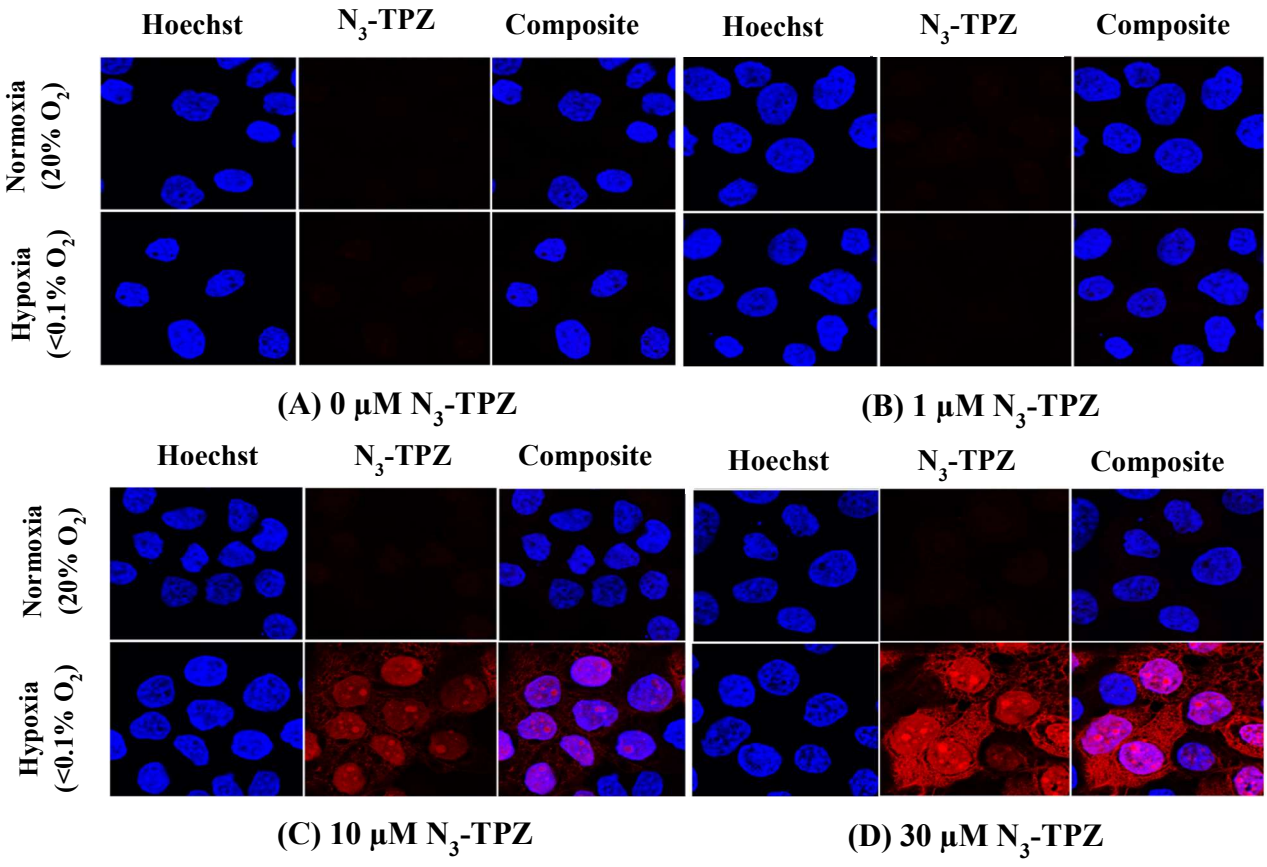

Figure 3.9 N_3-TPZ click chemistry signal is concentration-dependent

FaDu cells were seeded on coverslips and incubated overnight to adhere. The cells were then treated with increasing concentrations of N_3-TPZ for 24 hours under normoxic and hypoxic (<0.1% O_2) conditions. Cells were fixed in 2% paraformaldehyde and click chemistry was performed at room temperature for 30 minutes using Alexa 594-alkyne. Nuclei were counterstained with Hoechst and images were obtained using confocal microscopy. The signal intensity was observed to be concentration dependent in hypoxic N_3-TPZ treated cells whereas normoxic N_3-TPZ treated cells exhibited minimum to no background signal.

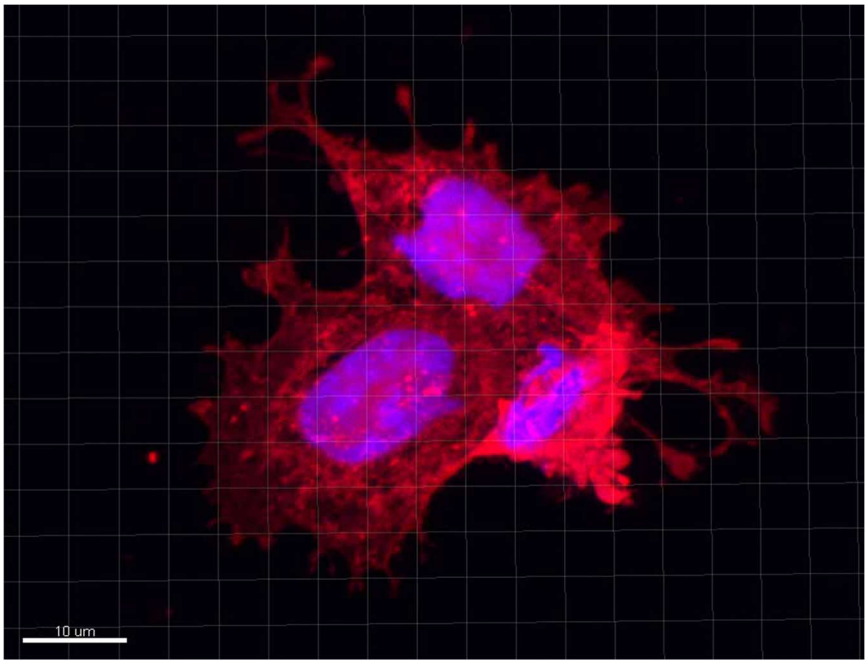

Figure 3.10 Localization of N_3-TPZ

Confocal microscopy reveals localization of N_3-TPZ. FaDu cells were treated with 30 μM N_3-TPZ for 24 hours under hypoxic (<0.1% O_2) conditions. Cells were fixed in 2% paraformaldehyde and click chemistry was performed at room temperature for 30 minutes using Alexa 594 alkyne. Nuclei were counterstained with Hoechst, and a range of Z-stack images were obtained. The image shows that the entrapment of N_3-TPZ is cytoplasmic with nucleolar and nuclear localization.

3.8. Identification of potential protein binding partners of N_3-TPZ

Following the success of imaging hypoxic cells using N_3-TPZ click chemistry, we set out to identify the proteins that are bound to N_3-TPZ using the same principle but with a biotin-conjugated alkyne rather than an Alexa-alkyne. The click reaction was performed on whole cell lysates isolated from FaDu cells that were treated with 30 μM N_3-TPZ for 24 hours under normoxic

and hypoxic (<0.1 O_2) conditions. Use of biotin alkyne enabled us to pull down the N_3-TPZ bound proteins with a streptavidin column. As shown in Figure 3.11, the schematic diagram illustrates the general principle of isolating potential protein candidates that get modified by N_3-TPZ under hypoxia using click chemistry. The biotinylated N_3-TPZ protein adducts that were eluted from the column using free biotin were run on SDS-PAGE along with clicked lysates, transferred to nitrocellulose membrane and were analysed using horseradish peroxidase (HRP)-coupled streptavidin to detect biotinylated proteins and a β-tubulin antibody. In this analysis, streptavidin-HRP signal was detected only in hypoxic N_3-TPZ treated clicked lysates and eluates indicating the specificity of protein modification by N_3-TPZ [Figure 3.12 A & B]. The β-tubulin signal confirms the efficiency of the streptavidin pull down and also highlights the low background non-specific binding to the beads.

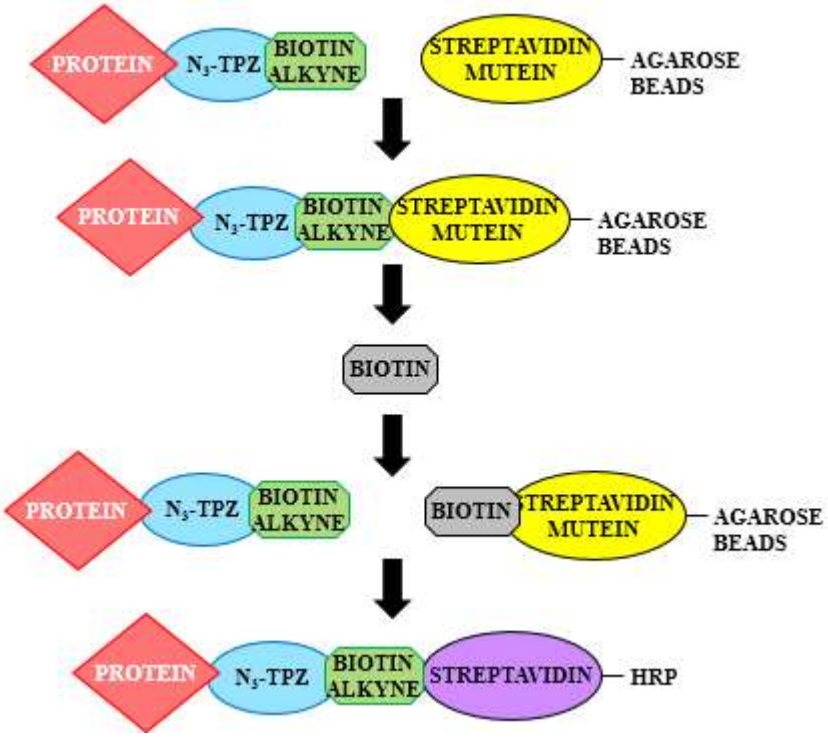

Figure 3.11 Experimental principle of isolating potential N_3-TPZ binding partners using click chemistry principle

A similar N_3-TPZ click chemistry principle described earlier for imaging hypoxic cells is used here to identify proteins that are bound to N_3-TPZ, but biotin-alkyne is used in place of an alexa-alkyne. Use of biotin-alkyne enables us to pull down the N_3-TPZ bound proteins with a streptavidin column. The biotin-alkyne bound N_3-TPZ proteins were loaded on streptavidin beads, where the biotin binds to streptavidin. Subsequently, the biotinylated proteins were eluted using free biotin and the eluates run on an SDS-PAGE gel is finally probed and visualized with streptavidin HRP.

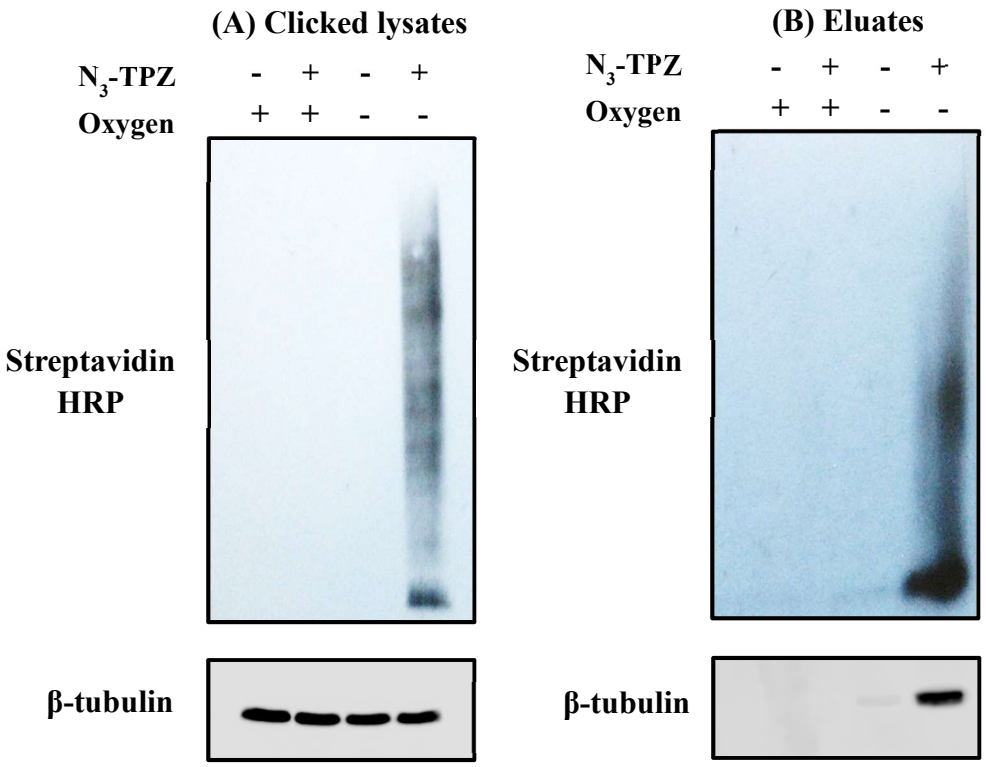

Figure 3.12 Isolation of potential binding partners of N_3-TPZ using click chemistry

Click chemistry with a biotin labelled alkyne was performed on the cell lysates isolated from FaDu cells that had been treated with 30 μM N_3-TPZ for 24 hours under normoxic and hypoxic (< 0.1%) conditions. This was followed by pull down of potential binding partners using streptavidin mutein beads. Clicked lysates (a) and eluates (b) were run on SDS-PAGE, transferred to nitrocellulose membrane and biotinylated proteins were detected with streptavidin-HRP, and β-tubulin by standard western blot. In both clicked lysate and eluates, streptavidin-HRP signal was detected only in hypoxic N_3-TPZ treated lane indicating the specificity of protein modification by N_3-TPZ. The β-tubulin signal validated the efficiency of pull down and highlighted the low background non-specific binding to the beads.

Since streptavidin-HRP signal was detected only in hypoxic N_3-TPZ treated cell eluates, they were further analyzed by liquid chromatography coupled mass spectrometry (LC-MS/MS) along with controls consisting of the eluate from hypoxic, but otherwise untreated, cells, and the whole cell lysate from hypoxic cells that underwent the click reaction without being treated with N_3-TPZ (Table 3.1-3.3). Since many proteins appeared in the latter control, only the common proteins found between this group and hypoxic N_3-TPZ treated eluate are tabulated in Table 3.3 and the rest of the proteins identified in the hypoxic whole cell clicked lysate are expanded in the appendix (Table A1).

As MS/MS-based proteomic studies are based on peptides, the proteins within a group are ranked depending on (a) the number of peptide sequences unique to a protein group, (b) the number of PSMs [(peptide-spectrum match)- total number of identified peptide spectra match for the protein], (c) their protein score (the sum of ion scores of all peptides that were identified), and (d) sequence coverage (% of the protein sequence covered by identified peptides). Ultimately, the top ranking protein of a group becomes the master protein of that group and is displayed in the search results report. As shown in Table 3.1, the analysis of the eluate from the hypoxic untreated cells (control) contains far fewer proteins when compared to Table 3.2, which showcases the analysis of hypoxic N_3-TPZ treated eluate. In addition, we also observed that the score, coverage and PSMs are considerably lower in the hypoxic control (Table 3.1) when compared to the cells treated with N_3-TPZ under hypoxia (Table 3.2). Since in the hypoxic control, the proteins adhere to the column in the absence of a streptavidin interaction, the few proteins identified in that group (Table 3.1) presumably bind to the column through an alternative non-specific interaction. The fact that many more proteins were recovered from the N_3-TPZ treated cells than the untreated cells

provides strong evidence that the proteins listed in Table 3.2 are biotinylated, which is in agreement with what we visually observed in the gel (Figure 3.12).

Furthermore, our proteomic analysis demonstrates that although the labeling of the proteins is enriched for a sub fraction of the proteome, we observed that the labeling is not highly specific. Figure 3.13 graphically displays the comparison of data sets of the whole proteome (obtained from the hypoxic whole cell clicked lysate) versus the N_3-TPZ treated cell eluate. We observed that the N_3-TPZ adducted proteins are proportional to their abundance as viewed by the positive slope of the data in Figure 3.13 A, which demonstrates the signal intensity of each protein from each sample versus each other. In addition, we also identified that some very high abundance proteins are not observed in the hypoxic N_3-TPZ treated cell eluates, which implies that many high abundance proteins do not react with TPZ. A similar trend was observed in Figure 3.13 B, which displays the alignment of all proteins with their respective observed ion intensities from the hypoxic N_3-TPZ treated cell eluate and hypoxic whole cell lysate (highlighted by red and black lines respectively). The relative ion intensity denotes the amount of ion produced with respect to the amount of the most abundant ion in the mass spectrum. Again, we observed that a large number of proteins are demonstrated to not be detected in the drug association experiment. Collectively, we could say that although N_3-TPZ labels diverse proteins, numerous high abundance proteins escape such labelling for a reason, which is unknown. Few notable examples of those highly abundant proteins that escaped N_3-TPZ labelling are heat shock protein 75 kDa, peroxiredoxin-4, plectin and ubiquitin-40S ribosomal protein. In contrast, we also observed several low abundance proteins that were preferentially labelled by N_3-TPZ, for example junction plakoglobin, desmoplakin, T-complex protein 1 subunit delta and proliferating cell nuclear antigen.

We identified a few highly abundant proteins that were labelled by N_3-TPZ under hypoxia. Since it is possible that modification of some of these proteins may contribute to the toxicity of TPZ we used STRING (Search Tool for the Retrieval of Interacting Genes/Proteins) database to examine potential protein-protein interactions among the 13 most highly ranked proteins (Figure 3.14). Although our protein network was enriched in variable biological processes, molecular functions, reactome pathways and several protein domains, we specifically focussed on the cellular component since we were interested in examining the localization of the compound. As shown in Figure 3.14, we observed enrichment of our input proteins in both nucleus and cytoplasm moderately in our network as estimated by STRING; and the result correlated with our prior data observed during N_3-TPZ imaging studies (Figure 3.9 and 3.10). In addition, we also identified that eukaryotic translation initiation factor 4A-I and II were labelled by N_3-TPZ under hypoxia (Figure 3.14). This finding is interesting given that a previous TPZ study found an association of TPZ with another eukaryotic translation initiation factor (eIf2α) [392]. It was reported that the down-regulation of HIF-1α by TPZ was largely dependent on the phosphorylation of this translation initiation factor [392].

Table 3.1 LC-MS/MS analysis for hypoxic cell control eluate (untreated with N_3-TPZ)

Accession	Description	Score	Coverage	# Proteins	# Unique Peptides	# Peptides	# PSMs	# AAs	MW [kDa]	calc. pI
P08238	Heat shock protein HSP 90-beta	34.34	7.04	1	4	4	10	724	83.2	5.03
P06733	Alpha-enolase	34.06	12.90	1	4	4	10	434	47.1	7.39
E7EUT5	Glyceraldehyde-3- phosphate dehydrogenase	21.20	17.69	2	3	3	7	260	27.9	6.95
Q5ST81	Tubulin beta chain	18.80	5.91	7	2	2	6	372	41.7	4.91
A0A0A0MSI0	Peroxiredoxin-1 (Fragment)	14.97	27.49	2	4	4	5	171	19.0	6.92
P63104	14-3-3 protein zeta/delta	10.71	10.61	2	2	2	3	245	27.7	4.79
A6NMY6	Putative annexin A2-like protein	9.30	6.19	2	2	2	3	339	38.6	6.95
A8MW50	L-lactate dehydrogenase (Fragment)	9.11	18.10	2	3	3	3	232	25.2	5.81
P16403	Histone H1.2	8.83	15.96	3	3	3	3	213	21.4	10.93
P10809	60 kDa heat shock protein, mitochondrial	8.62	5.76	1	3	3	3	573	61.0	5.87

Table 3.2 LC-MS/MS analysis for hypoxic N_3-TPZ treated cell eluate

Accession	Description	Score	Coverage	# Proteins	# Unique Peptides	# Peptides	# PSMs	# AAs	MW [kDa]	calc. pI
P04406	Glyceraldehyde-3-phosphate dehydrogenase	197.29	23.28	1	6	6	91	335	36.0	8.46
P08238	Heat shock protein HSP 90-beta	185.60	14.78	1	3	10	66	724	83.2	5.03
P07900	Heat shock protein HSP 90-alpha	184.99	13.39	1	3	9	65	732	84.6	5.02
P11142	Heat shock cognate 71 kDa protein	131.70	18.58	1	7	10	52	646	70.9	5.52
P07437	Tubulin beta chain	126.89	30.63	1	3	11	49	444	49.6	4.89
H3BTN5	Pyruvate kinase (Fragment)	116.44	18.97	2	8	8	39	485	53.0	6.84
P68104	Elongation factor 1-alpha 1	113.30	14.50	2	5	5	41	462	50.1	9.01
P68371	Tubulin beta-4B chain	106.02	30.56	1	3	11	41	445	49.8	4.89
P11021	78 kDa glucose-regulated protein	89.65	19.72	1	7	9	33	654	72.3	5.16
P0DMV8	Heat shock 70 kDa protein	86.80	9.98	2	3	5	31	641	70.0	5.66
P60174	Triosephosphate isomerase	82.44	18.88	1	4	4	27	286	30.8	5.92
P60709	Actin, cytoplasmic 1	80.24	29.60	2	8	8	29	375	41.7	5.48
P10809	60 kDa heat shock protein, mitochondrial	78.10	18.67	1	8	8	29	573	61.0	5.87

Accession	Description	Score	Coverage	# Proteins	# Unique Peptides	# Peptides	# PSMs	# AAs	MW [kDa]	calc. pI
P07195	L-lactate dehydrogenase B chain	77.27	24.25	1	6	7	32	334	36.6	6.05
P63104	14-3-3 protein zeta/delta	68.07	17.96	2	3	4	24	245	27.7	4.79
P07355	Annexin A2	65.81	24.48	1	7	7	24	339	38.6	7.75
P06733	Alpha-enolase	61.87	20.05	1	6	6	21	434	47.1	7.39
P09211	Glutathione S-transferase P	58.76	36.19	1	6	6	47	210	23.3	5.64
P38646	Stress-70 protein, mitochondrial	56.97	17.82	1	9	9	20	679	73.6	6.16
P68363	Tubulin alpha-1B chain	56.62	22.39	1	7	7	21	451	50.1	5.06
E7EQG2	Eukaryotic initiation factor 4A-II	52.05	6.63	3	2	2	17	362	41.3	5.64
A0A0U1RQ	Fatty acid synthase	50.44	5.06	2	11	11	20	2509	273.0	6.47
H3BUH7	Fructose-bisphosphate aldolase A (Fragment)	48.64	34.19	5	4	4	18	155	16.9	8.56
P62258	14-3-3 protein epsilon	46.50	17.65	1	3	4	19	255	29.2	4.74
A0A0B4J1	Transketolase	41.95	17.51	2	5	5	13	457	49.9	7.91
C9J9K3	40S ribosomal protein SA (Fragment)	40.04	15.59	3	3	3	12	263	29.4	5.25
P25705	ATP synthase subunit alpha, mitochondrial	37.98	11.93	1	5	5	15	553	59.7	9.13
O43175	D-3-phosphoglycerate dehydrogenase	37.21	9.19	1	4	4	14	533	56.6	6.71
P14625	Endoplasmin	37.19	5.73	1	3	4	14	803	92.4	4.84
P00505	Aspartate aminotransferase, mitochondrial	36.27	9.53	1	3	3	13	430	47.5	9.01
P07737	Profilin-1	36.25	31.43	1	3	3	17	140	15.0	8.27
P27348	14-3-3 protein theta	35.01	13.06	1	1	3	14	245	27.7	4.78
P61981	14-3-3 protein gamma	34.72	17.00	1	2	4	14	247	28.3	4.89
P11586	C-1-tetrahydrofolate synthase, cytoplasmic	32.93	7.17	2	5	5	12	935	101.5	7.30
A0A0A0MS	Peroxiredoxin-1	31.60	32.16	2	5	5	13	171	19.0	6.92
D6RF44	Heterogeneous nuclear ribonucleoprotein D0 (Fragment)	31.25	28.83	5	2	3	12	111	12.5	8.57
Q14247	Src substrate cortactin	31.19	10.55	1	4	4	11	550	61.5	5.40
P04083	Annexin A1	28.90	18.79	1	5	5	11	346	38.7	7.02
A0A087WV	Filamin-A	27.72	4.58	4	7	7	11	2315	245.7	5.97
E9PPU1	40S ribosomal protein S3	25.58	27.85	4	4	4	10	158	17.4	9.50
Q5T6W2	Heterogeneous nuclear ribonucleoprotein K (Fragment)	25.02	12.66	2	3	3	9	379	41.8	5.59
P35579	Myosin-9	24.95	2.35	1	3	3	9	1960	226.4	5.60

Accession	Description	Score	Coverage	# Proteins	# Unique Peptides	# Peptides	# PSMs	# AAs	MW [kDa]	calc. pI
G3V1A4	Cofilin 1 (Non-muscle), isoform CRA_a	23.86	26.17	3	3	3	9	149	16.8	8.35
H0Y2X5	Aldehyde dehydrogenase 1 family, member A3, isoform CRA_b	23.72	12.10	2	4	4	9	405	44.2	7.56
F8W0G4	Poly(rC)-binding protein 2 (Fragment)	23.04	24.05	6	2	3	9	158	16.6	7.77
P23526	Adenosylhomocysteinase	22.40	8.10	1	3	3	9	432	47.7	6.34
G3V576	Heterogeneous nuclear ribonucleoproteins C1/C2	21.24	16.45	7	3	3	8	231	25.2	9.82
H0YH81	ATP synthase subunit beta, mitochondrial (Fragment)	21.18	20.99	2	5	5	8	362	38.2	5.55
Q9UQ80	Proliferation-associated protein 2G4	20.36	10.41	1	3	3	7	394	43.8	6.55
P13639	Elongation factor 2	19.49	4.08	1	3	3	8	858	95.3	6.83
G3V203	60S ribosomal protein L18	18.52	22.56	4	3	3	7	164	18.7	11.59
Q15365	Poly(rC)-binding protein 1	18.14	11.24	1	2	3	7	356	37.5	7.09
H0Y400	Spliceosome RNA helicase DDX39B (Fragment)	18.10	12.83	4	2	2	7	187	21.8	5.12
D6R9P3	Heterogeneous nuclear ribonucleoprotein A/B	18.06	8.57	3	1	2	7	280	30.3	7.91
F5GY37	Prohibitin-2	17.93	9.36	3	2	2	7	267	29.7	9.88
P40925	Malate dehydrogenase, cytoplasmic	17.16	8.08	1	2	2	6	334	36.4	7.36
P00338	L-lactate dehydrogenase A chain	16.70	12.65	1	3	4	7	332	36.7	8.27
P24534	Elongation factor 1-beta	16.16	12.44	1	2	2	5	225	24.7	4.67
Q3BDU5	Prelamin-A/C	15.65	9.65	2	4	4	6	487	55.6	6.65
H9KV75	Alpha-actinin-1	15.37	3.16	3	2	2	6	822	94.8	5.69
P50991	T-complex protein 1 subunit delta	15.34	5.01	1	2	2	6	539	57.9	7.83
P49411	Elongation factor Tu, mitochondrial	15.00	7.96	1	3	3	6	452	49.5	7.61
P62937	Peptidyl-prolyl cis-trans isomerase A	15.00	12.12	1	2	2	6	165	18.0	7.81
H7C3I1	Hsc70-interacting protein (Fragment)	14.71	16.44	5	2	2	5	146	16.3	4.88
E7EQR4	Ezrin	14.09	4.78	2	2	2	5	586	69.3	6.16
B1AHC9	X-ray repair cross-complementing protein 6	12.64	4.83	2	2	2	4	559	64.2	9.28
Q9Y277	Voltage-dependent anion-selective channel protein 3	12.41	8.13	1	1	2	5	283	30.6	8.66

Accession	Description	Score	Coverage	# Proteins	# Unique Peptides	# Peptides	# PSMs	# AAs	MW [kDa]	calc. pI
A0A0J9YX	Glucose-6-phosphate isomerase (Fragment)	12.15	11.94	6	2	2	4	268	30.4	9.01
F8VPE8	60S acidic ribosomal protein P0 (Fragment)	11.75	30.07	6	3	3	4	153	16.7	9.33
P30050	60S ribosomal protein L12	11.66	18.79	1	2	2	4	165	17.8	9.42
P00558	Phosphoglycerate kinase 1	11.14	6.71	1	2	2	4	417	44.6	8.10
P15924	Desmoplakin	10.83	1.08	1	3	3	4	2871	331.6	6.81
P12004	Proliferating cell nuclear antigen	10.47	12.26	1	2	2	5	261	28.8	4.69
P23284	Peptidyl-prolyl cis-trans isomerase B	10.40	12.04	1	2	2	7	216	23.7	9.41
P13667	Protein disulfide-isomerase A4	10.31	3.57	1	2	2	4	645	72.9	5.07
P50395	Rab GDP dissociation inhibitor beta	10.07	5.17	1	2	2	4	445	50.6	6.47
B4DUR8	T-complex protein 1 subunit gamma	9.79	6.60	2	3	3	4	500	55.6	5.64
P26641	Elongation factor 1-gamma	9.78	5.95	1	2	2	3	437	50.1	6.67
H7BZ94	Protein disulfide-isomerase	9.72	5.17	2	2	2	3	464	52.5	4.87
P62269	40S ribosomal protein S18	9.43	11.18	1	2	2	4	152	17.7	10.99
F5GZS6	4F2 cell-surface antigen heavy chain	8.03	6.51	3	3	3	3	599	64.8	5.10
Q92598	Heat shock protein 105 kDa	7.82	4.90	1	3	3	3	858	96.8	5.39
P50990	T-complex protein 1 subunit theta	7.65	3.83	1	2	2	3	548	59.6	5.60
Q00610	Clathrin heavy chain 1	7.59	1.91	2	3	3	3	1675	191.5	5.69
P14923	Junction plakoglobin	7.56	5.10	1	3	3	3	745	81.7	6.14
Q02790	Peptidyl-prolyl cis-trans isomerase FKBP4	7.43	5.01	1	2	2	3	459	51.8	5.43
C9JZ20	Prohibitin (Fragment)	7.41	15.92	5	3	3	3	201	22.3	5.96
P21796	Voltage-dependent anion-selective channel protein 1	7.11	8.13	1	1	2	3	283	30.8	8.54
Q15084	Protein disulfide-isomerase A6	5.61	7.05	1	2	2	2	440	48.1	5.08
Q92928	Putative Ras-related protein Rab-1C	4.91	13.43	3	2	2	2	201	22.0	5.43
P27824	Calnexin	4.79	3.21	1	2	2	2	592	67.5	4.60
P04181	Ornithine aminotransferase, mitochondrial	4.79	4.78	1	2	2	2	439	48.5	7.03
Q9NR30	Nucleolar RNA helicase 2	4.70	3.32	1	2	2	2	783	87.3	9.28
G3XAL0	Malate dehydrogenase	4.69	11.69	2	2	2	2	231	24.6	7.99

Accession	Description	Score	Coverage	# Proteins	# Unique Peptides	# Peptides	# PSMs	# AAs	MW [kDa]	calc. pI
H0YIZ0	Serine hydroxymethyltransferase (Fragment)	4.63	8.33	2	2	2	2	264	28.8	9.44

Table 3.3: LC-MS/MS analysis for hypoxic whole cell clicked lysate (common proteins found between this group and hypoxic N_3-TPZ treated eluate)

Accession	Description	Score	Coverage	# Proteins	# Unique Peptides	# Peptides	# PSMs	# AAs	MW [kDa]	calc. pI
P49327	Fatty acid synthase	545.71	46.12	1	84	84	355	2511	273.3	6.44
P14618	Pyruvate kinase PKM	342.95	56.87	1	26	26	196	531	57.9	7.84
P04406	Glyceraldehyde-3-phosphate dehydrogenase	324.82	67.46	1	17	17	233	335	36.0	8.46
P07900	Heat shock protein HSP 90-alpha	318.27	52.60	1	25	39	271	732	84.6	5.02
P10809	60 kDa heat shock protein, mitochondrial	314.92	55.67	1	29	29	212	573	61.0	5.87
P08238	Heat shock protein HSP 90-beta	311.65	55.80	1	23	38	273	724	83.2	5.03
P68371	Tubulin beta-4B chain	286.39	53.03	1	4	21	198	445	49.8	4.89
P68363	Tubulin alpha-1B chain	285.93	60.31	1	4	19	181	451	50.1	5.06
P07437	Tubulin beta chain	281.82	59.23	1	6	22	189	444	49.6	4.89
P35579	Myosin-9	274.88	41.99	1	59	68	178	1960	226.4	5.60
P60709	Actin, cytoplasmic 1	270.07	75.47	2	9	18	200	375	41.7	5.48
P11142	Heat shock cognate 71 kDa protein	244.67	48.45	1	16	25	163	646	70.9	5.52
Q60FE5	Filamin A	225.32	37.90	2	63	66	167	2620	278.1	6.06
P13639	Elongation factor 2	205.20	44.99	1	31	32	135	858	95.3	6.83
P68104	Elongation factor 1-alpha 1	194.17	40.48	2	12	12	180	462	50.1	9.01
P07355	Annexin A2	191.10	61.06	1	22	22	117	339	38.6	7.75
P06733	Alpha-enolase	186.46	69.35	1	21	25	141	434	47.1	7.39
P0DMV8	Heat shock 70 kDa protein 1A	178.38	58.66	2	21	29	132	641	70.0	5.66
P12814	Alpha-actinin-1	159.09	56.61	1	26	39	120	892	103.0	5.41
P04075	Fructose-bisphosphate aldolase A	157.20	74.73	2	17	18	103	364	39.4	8.09
P09211	Glutathione S-transferase P	145.00	56.67	1	9	9	119	210	23.3	5.64
P06576	ATP synthase subunit beta, mitochondrial	131.31	59.55	1	20	20	106	529	56.5	5.40
P11021	78 kDa glucose-regulated protein	128.46	40.21	1	22	24	89	654	72.3	5.16

Accession	Description	Score	Coverage	# Proteins	# Unique Peptides	# Peptides	# PSMs	# AAs	MW [kDa]	calc. pI
P25705	ATP synthase subunit alpha, mitochondrial	120.29	44.67	1	18	18	69	553	59.7	9.13
P29401	Transketolase	119.23	43.02	1	15	15	94	623	67.8	7.66
P04083	Annexin A1	119.14	49.42	1	15	15	76	346	38.7	7.02
P38646	Stress-70 protein, mitochondrial	117.72	39.47	1	19	19	80	679	73.6	6.16
P11586	C-1-tetrahydrofolate synthase, cytoplasmic	117.10	41.28	1	29	29	90	935	101.5	7.30
Q00610	Clathrin heavy chain 1	114.89	35.82	2	40	40	90	1675	191.5	5.69
P07237	Protein disulfide-isomerase	112.63	48.43	1	19	19	74	508	57.1	4.87
P14625	Endoplasmin	109.84	34.12	1	21	23	88	803	92.4	4.84
P02545	Prelamin-A/C	102.23	39.31	1	24	24	68	664	74.1	7.02
Q14247	Src substrate cortactin	100.01	33.82	1	18	18	73	550	61.5	5.40
F5GZS6	4F2 cell-surface antigen heavy chain	95.04	36.39	3	19	19	57	599	64.8	5.10
P26641	Elongation factor 1-gamma	85.30	46.68	1	16	16	53	437	50.1	6.67
P62937	Peptidyl-prolyl cis-trans isomerase A	74.60	65.45	1	8	8	64	165	18.0	7.81
P50991	T-complex protein 1 subunit delta	70.82	49.35	1	17	18	56	539	57.9	7.83
P49411	Elongation factor Tu, mitochondrial	70.44	32.08	1	10	11	37	452	49.5	7.61
P60174	Triosephosphate isomerase	64.26	59.09	1	14	14	51	286	30.8	5.92
P50395	Rab GDP dissociation inhibitor beta	63.76	36.40	1	6	13	36	445	50.6	6.47
Q06830	Peroxiredoxin-1	62.99	58.79	1	9	12	50	199	22.1	8.13
P12956	X-ray repair cross-complementing protein 6	62.87	45.16	1	21	21	63	609	69.8	6.64
G3V1A4	Cofilin 1 (Non-muscle), isoform CRA_a	61.44	60.40	4	12	12	55	149	16.8	8.35
J3KPX7	Prohibitin-2	60.58	48.66	2	11	11	41	298	33.2	9.83
O43175	D-3-phosphoglycerate dehydrogenase	59.63	36.02	1	13	13	41	533	56.6	6.71
P61978	Heterogeneous nuclear ribonucleoprotein K	59.30	32.61	1	14	14	60	463	50.9	5.54
P23396	40S ribosomal protein S3	58.08	56.38	1	14	14	33	243	26.7	9.66
P35232	Prohibitin	57.84	48.90	1	9	9	27	272	29.8	5.76
P04181	Ornithine aminotransferase, mitochondrial	57.58	29.61	1	11	11	33	439	48.5	7.03
P50990	T-complex protein 1 subunit theta	56.79	44.71	1	20	20	47	548	59.6	5.60

Accession	Description	Score	Coverage	# Proteins	# Unique Peptides	# Peptides	# PSMs	# AAs	MW [kDa]	calc. pI
Q15084	Protein disulfide-isomerase A6	56.70	27.73	1	10	10	29	440	48.1	5.08
P00338	L-lactate dehydrogenase A chain	56.30	58.73	1	16	17	61	332	36.7	8.27
P07195	L-lactate dehydrogenase B chain	55.89	56.59	1	16	17	73	334	36.6	6.05
P00558	Phosphoglycerate kinase 1	55.01	42.45	1	12	12	49	417	44.6	8.10
P62258	14-3-3 protein epsilon	54.89	43.14	1	10	11	39	255	29.2	4.74
P21796	Voltage-dependent anion-selective channel protein 1	51.98	70.67	1	14	15	42	283	30.8	8.54
Q15365	Poly(rC)-binding protein 1	50.97	42.70	1	7	9	25	356	37.5	7.09
C9J9K3	40S ribosomal protein SA (Fragment)	50.88	50.95	3	10	10	32	263	29.4	5.25
P27824	Calnexin	49.15	20.95	1	10	10	36	592	67.5	4.60
Q92598	Heat shock protein 105 kDa	48.62	23.78	1	15	15	35	858	96.8	5.39
P63104	14-3-3 protein zeta/delta	48.06	55.10	1	13	15	45	245	27.7	4.79
P49368	T-complex protein 1 subunit gamma	45.71	35.23	2	14	15	35	545	60.5	6.49
P05388	60S acidic ribosomal protein P0	45.02	50.47	1	10	10	35	317	34.3	5.97
E7EQR4	Ezrin	44.53	36.35	2	13	18	45	586	69.3	6.16
P06744	Glucose-6-phosphate isomerase	43.49	33.87	2	13	13	47	558	63.1	8.32
Q02790	Peptidyl-prolyl cis-trans isomerase FKBP4	41.89	40.74	1	14	14	26	459	51.8	5.43
P00505	Aspartate aminotransferase, mitochondrial	39.35	32.33	1	10	10	35	430	47.5	9.01
P61981	14-3-3 protein gamma	39.24	39.68	1	5	6	23	247	28.3	4.89
P40925	Malate dehydrogenase, cytoplasmic	34.60	42.81	1	10	10	28	334	36.4	7.36
Q14240	Eukaryotic initiation factor 4A-II	33.25	30.47	2	2	8	25	407	46.4	5.48
P23526	Adenosylhomocysteinase	32.71	31.94	1	12	12	32	432	47.7	6.34
P07737	Profilin-1	32.27	49.29	1	6	6	28	140	15.0	8.27
Q15366	Poly(rC)-binding protein 2	32.15	31.78	1	5	7	18	365	38.6	6.79
P27348	14-3-3 protein theta	31.05	35.51	1	10	11	26	245	27.7	4.78
H	Nucleolar RNA helicase 2	30.39	19.03	1	11	11	23	783	87.3	9.28
Q13838	Spliceosome RNA helicase DDX39B	27.05	24.77	1	9	9	24	428	49.0	5.67
P13667	Protein disulfide-isomerase A4	25.73	28.68	1	13	13	28	645	72.9	5.07

Accession	Description	Score	Coverage	# Proteins	# Unique Peptides	# Peptides	# PSMs	# AAs	MW [kDa]	calc. pI
Q9UQ80	Proliferation-associated protein 2G4	21.47	37.31	1	11	11	17	394	43.8	6.55
P24534	Elongation factor 1-beta	20.29	30.67	1	4	4	14	225	24.7	4.67
P50502	Hsc70-interacting protein	20.05	15.18	1	4	4	14	369	41.3	5.27
P62269	40S ribosomal protein S18	18.66	32.89	1	6	6	16	152	17.7	10.99
P14923	Junction plakoglobin	17.44	9.13	1	4	4	9	745	81.7	6.14
P12004	Proliferating cell nuclear antigen	16.86	35.25	1	6	6	11	261	28.8	4.69
H0YHA7	60S ribosomal protein L18 (Fragment)	16.08	43.71	4	6	7	10	167	19.0	11.78
P30050	60S ribosomal protein L12	15.65	45.45	1	5	5	14	165	17.8	9.42
Q9Y277	Voltage-dependent anion-selective channel protein 3	11.94	34.63	1	5	7	16	283	30.6	8.66
P23284	Peptidyl-prolyl cis-trans isomerase B	11.50	44.44	1	9	9	20	216	23.7	9.41
G3V576	Heterogeneous nuclear ribonucleoproteins C1/C2	5.35	20.35	7	4	4	6	231	25.2	9.82
H0YA96	Heterogeneous nuclear ribonucleoprotein D0 (Fragment)	4.23	21.43	4	2	3	6	210	23.9	9.58
D6R9P3	Heterogeneous nuclear ribonucleoprotein A/B	3.70	26.07	4	4	5	9	280	30.3	7.91

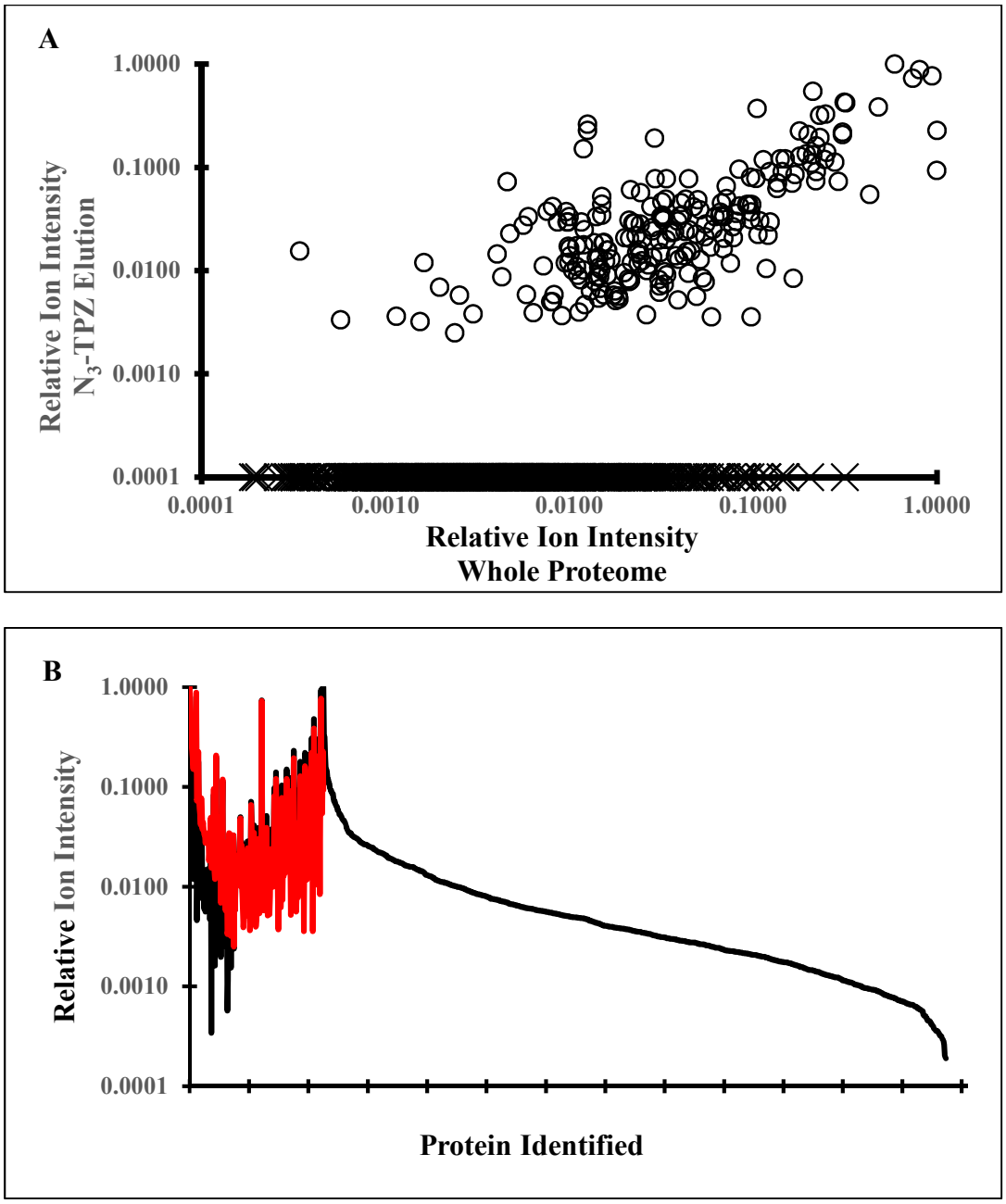

Figure 3.13 Comparison of relative ion intensity of proteins in the whole proteome and the drug-pulldowns

(A) The graph shows the comparison of signal intensity of each protein from each sample versus each other. (B) The graph shows the alignment of all proteins with their respective ion intensity. The red and black lines reveal the measured ion intensities of each protein in both experiments (drug-pulldown and whole proteome respectively). Over all the data suggests that even though N_3-TPZ labels diverse proteins, numerous high abundance proteins escape the labelling.

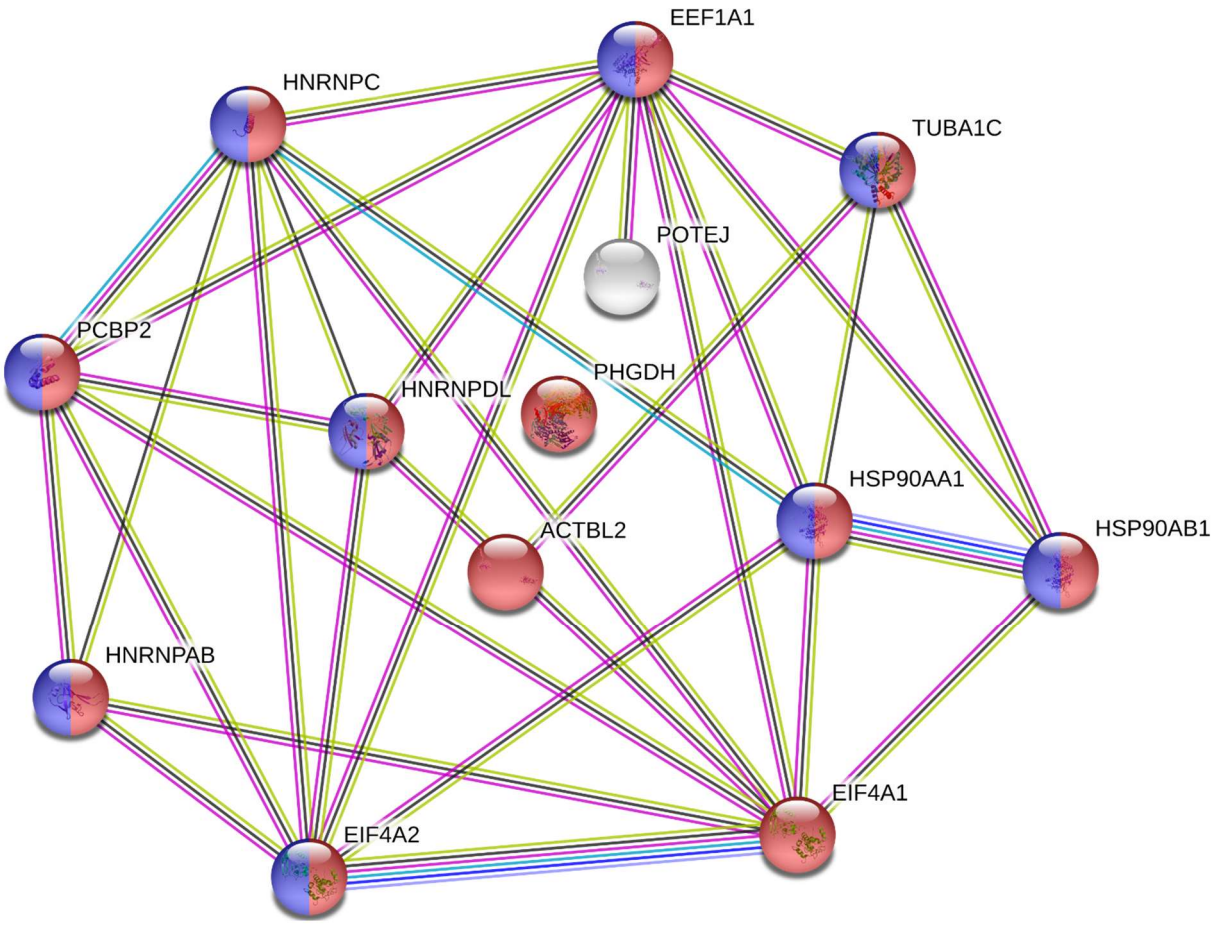

Figure 3.14 Functional enrichment in protein network of N_3-TPZ targets under hypoxia using STRING database

Screenshot from the STRING website shows the protein-protein association of 13 highly abundant proteins that were labelled by N_3-TPZ under hypoxia. Specifically, the Figure shows the functional enrichment of the protein network based on the cellular component. Node colour differentiates the protein enrichment in the cellular component by red and blue colours representing cytoplasm and nucleus respectively; white node represents the weaker association to the input protein. Coloured lines in between the proteins represents the different types of interaction evidence (pink- experimentally determined, cyan- curated databases, yellow- textmining, black – co-expression, purple - cooccurrence, blue - protein homology.

Input proteins are as follows: **EIF4A1**- Eukaryotic initiation factor 4A-I, **TUBA1C-** Tubulin alpha-1C chain, **EIF4A2**- Eukaryotic initiation factor 4A-II, **HSP90AA1**- Heat shock protein HSP 90-alpha, **EEF1A1**- Elongation factor 1 alpha 1, **HNRNPAB**- Heterogeneous nuclear ribonucleoprotein A/B, **PCBP2**- Poly (rC)-binding protein 2, **PHGDH**- D-3-phosphoglycerate dehydrogenase, **HSP90AB1**- Heat shock protein HSP 90-beta, **POTEJ**- POTE ankyrin domain family member J, **ACTBL2**- Beta-actin-like protein 2, **HNRNPC**- Heterogeneous nuclear ribonucleoprotein C1/C2, **HNRNPDL**- Heterogeneous nuclear ribonucleoprotein D-like.

3.9. Hypoxia selective cytotoxicity of N_3-G_6-TPZ

We proceeded to test the efficacy of a new compound, N_3-G_6-TPZ, a derivative of TPZ which contains both glucose and azido moieties conjugated to it. Our prior results indicated the utility of N_3-TPZ to monitor TPZ uptake. Therefore, N_3-G_6-TPZ was synthesized in an effort to study the uptake and localization of G_6-TPZ, since the compound exhibited hypoxic sensitization only at higher concentrations [Figure 3.5]. The efficacy of N_3-G_6-TPZ was assessed by examining its cytotoxicity using the crystal violet staining assay in FaDu cells cultured in both DMEM and low glucose DMEM [Figure 3.15]. Two different media were used in order to compare and study the response of N_3-G_6-TPZ on glucose-starved FaDu cells. As shown in Figure 3.15 A, N_3-G_6-TPZ treated cells cultured in DMEM displayed selective cytotoxicity in low oxygen levels (0.1% O_2) when compared to its normoxic counterparts. A similar trend was observed in N_3-G_6-TPZ treated cells cultured in low glucose DMEM [Figure 3.15 B]. Since there was no significant difference in the cytotoxicity of N_3-G_6-TPZ treated cells cultured in both media, further experiments with the compound were performed on cells cultured in DMEM. Although N_3-G_6-TPZ demonstrated concentration dependent hypoxia-selective cytotoxicity, it is evident that the compound seems to be less toxic in comparison to N_3-TPZ [Figure 3.8] and the parent compound TPZ [Figure 3.4], but was markedly more toxic when compared to G_6-TPZ [Figure 3.5].

3.10. Hypoxia selective sub-cellular localization of N_3-G_6-TPZ

Using fluorescence imaging, we investigated whether N_3-G_6-TPZ was either taken up by FaDu cells or remains bound to the GLUT-1 transporter. The click reaction was performed on FaDu cells that had been treated with increasing concentrations of N_3-G_6-TPZ for 24 hours under normoxic and hypoxic (<0.1 O_2) conditions. Fluorescence images obtained by confocal microscopy reveal selective sub-cellular localization of N_3-G_6-TPZ in cells exposed to hypoxia (<0.1 O_2). In addition, it is evident that considerably less N_3-G_6-TPZ [Figure 3.16 B, C & D] was taken up by the hypoxic cells when compared to N_3-TPZ [Figure 3.9 B, C & D]. The click signal intensity was observed to be concentration dependent in hypoxic N_3-G_6-TPZ treated cells [Figure 3.16 B, C & D]. In contrast, minimum to no background signal was detected in normoxic N_3-G_6-TPZ treated cells even at high concentrations of the reagent, which reconfirms the hypoxia selectivity of the compound [Figure 3.16 A].

Since the N_3-G_6-TPZ signal was low, we checked the localization of the compound. The Z-stack images acquired through confocal microscopy suggest that N_3-G_6-TPZ enters the cells and the entrapment is predominantly nucleolar and nuclear with cytoskeleton staining [Figure 3.17]. In addition, we also observed that the localization of N_3-G_6-TPZ under hypoxia was quite similar to the localization of hypoxic N_3-TPZ treated cells [Figure 3.10].

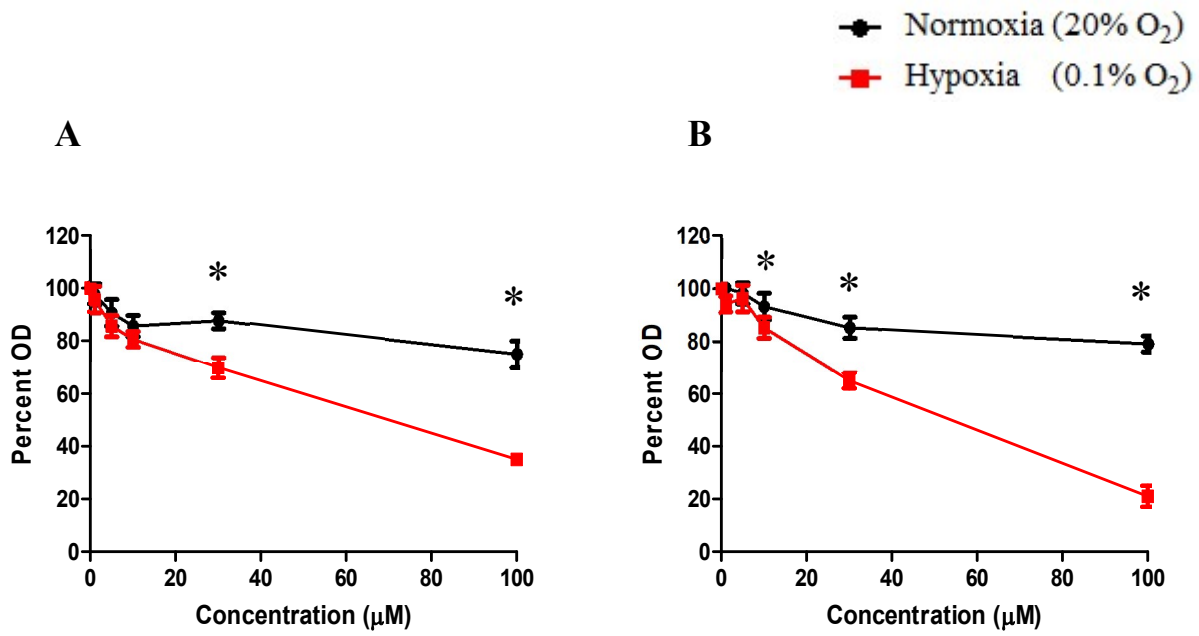

Figure 3.15 Hypoxia selective cytotoxicity of N_3-G_6-TPZ

Cytotoxicity of N_3-G_6-TPZ treated cells as observed using the CVS assay in DMEM (A) and low glucose DMEM (B). In the CVS assay, FaDu cells (3000 cells/well) were seeded in 96-well plates and incubated overnight to adhere. The cells were then treated with increasing concentrations of N_3-G_6-TPZ and the plates were exposed to either normoxic (20% O_2) or hypoxic (0.1% O_2) conditions for 72 hours. Culture medium [DMEM-(A)], [DMEM low glucose-(B)] without cells was set for background respectively. The media was aspirated post-treatment, followed by addition of crystal violet solution to stain the cells. Crystals were dissolved using methanol and absorbance of the samples was measured spectrophotometrically. Error bars represent the standard error of the mean. The difference between normoxia and hypoxia within each N_3-G_6-TPZ concentration was analyzed with an unpaired t-test; (*) indicates statistical significance of $p < 0.05$. The cytotoxicity data of N_3-G_6-TPZ (A, B) treated cells cultured in both DMEM and low glucose DMEM exhibited a similar trend of significant hypoxia selective toxicity.

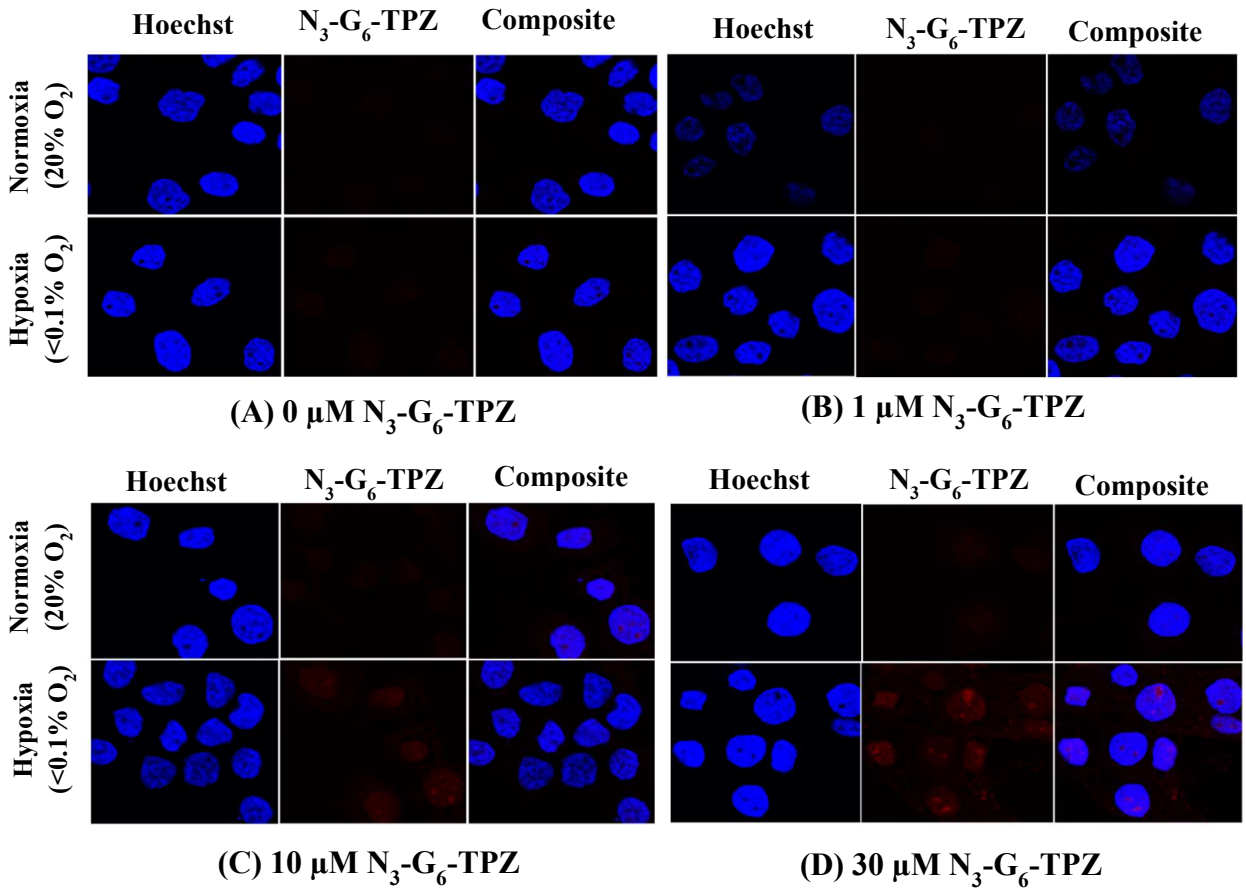

Figure 3.16 N_3-G_6-TPZ click chemistry signal is concentration-dependent

FaDu cells were seeded on coverslips and incubated overnight to adhere. The cells were then treated with increasing concentrations of N_3-G_6-TPZ for 24 hours under normoxic or hypoxic (<0.1% O_2) conditions. Cells were fixed in 2% paraformaldehyde and click chemistry was performed at room temperature for 30 minutes using Alexa 594 alkyne. Nuclei were counterstained with Hoechst, and images were obtained using confocal microscopy. The signal intensity was observed to be concentration dependent in hypoxic N_3-G_6-TPZ treated cells whereas normoxic N_3-G_6-TPZ treated cells exhibited minimum to no background signal.

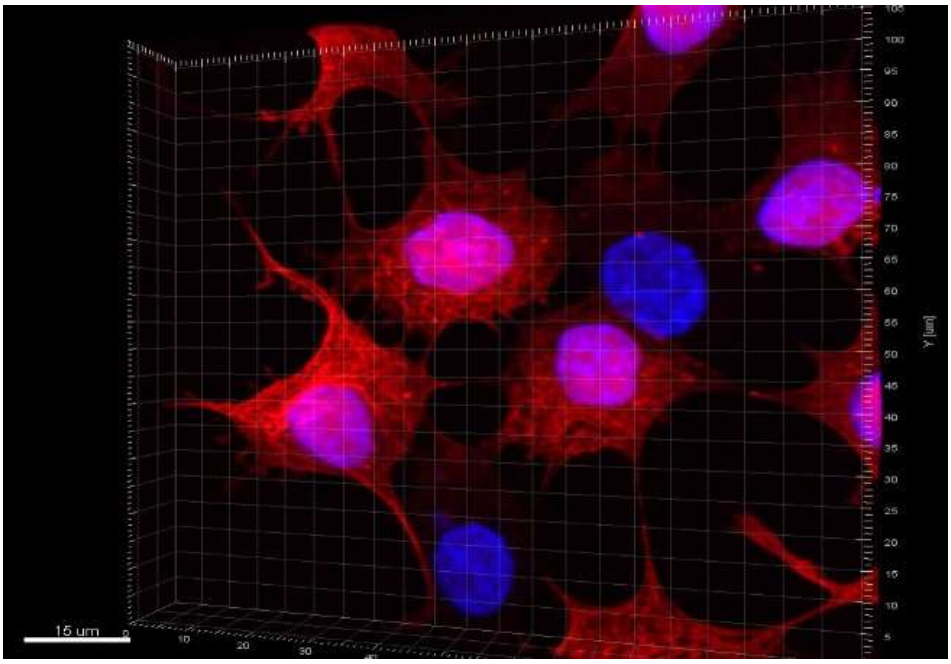

Figure 3.17 Localization of N_3-G_6-TPZ

Confocal microscopy reveals localization of N_3-G_6-TPZ. FaDu cells were treated with 30 μM N_3-G_6-TPZ for 24 hours under hypoxic (<0.1% O_2) conditions. Cells were fixed in 2% paraformaldehyde and click chemistry was performed at room temperature for 30 minutes using Alexa 594 alkyne. Nuclei were counterstained with Hoechst, and a range of Z-stack images were obtained. The image shows that the entrapment of N_3-G_6-TPZ is mostly cytoplasmic with nucleolar and nuclear staining.

Chapter IV- Discussion

Over the decades, it has been well established that major metabolic alterations occur in mammalian cells that undergo oncogenic transformation [381]. Cancer cells are known to produce energy by displaying increased glycolytic metabolism even in aerobic conditions; a phenomenon known as the Warburg effect [382,383]. Under hypoxia, due to inhibition of oxidative phosphorylation, malignant tumor cells choose anaerobic glycolysis to release energy in order to maintain the energy supply in a rapidly growing tumor tissue [112]. Eventually, hypoxic cells undergo metabolic adaptation, which in turn leads to upregulation of genes that encode the enzymes required for anaerobic glycolysis [108]. As a consequence, the acute stimulation of glucose transport by hypoxia is mediated by the upregulation of facilitative glucose transporters, primarily by GLUT-1, thus making it an intrinsic cellular marker of hypoxia [113-115]. Therefore, the idea to exploit the abundance of GLUTs in hypoxia formed the basis of our objective to transform TPZ structurally by adding a glucose moiety to it. This was carried out in an effort to improve the delivery of TPZ selectively to oxygen deficient cells. Our initial objective in this study was to determine the effect of glucose-conjugated TPZ (G_6-TPZ) on poorly oxygenated FaDu cells using several cytotoxicity assays.

4.1. Regulation of GLUT-1 protein and mRNA levels by hypoxia

Our data indicates that hypoxia regulates GLUT-1 protein and mRNA levels in FaDu cells. We observed that both GLUT-1 protein and mRNA levels were inversely regulated in an oxygen-concentration dependent manner (Figure 3.1 A & Figure 3.2 A). Our result is in accordance with prior reports, which have shown that hypoxia regulates GLUT-1 by increasing the activity of the sodium-independent transport of glucose in an oxygen-concentration dependent manner [384]. The increase in glucose transport has been demonstrated to be dependent on protein

synthesis and is known to be linked with a rise in GLUT-1 protein units at the membrane level [384]. In addition, the upregulation of GLUT-1 mRNA transcript in response to hypoxia is said to occur as a result of either reduced oxygen concentration per se or inhibition of oxidative phosphorylation [112,127]. We observed a high induction of HIF-1α protein in whole cell lysates isolated from FaDu cells which were exposed to 0.5% O_2, thereby demonstrating a similar trend as GLUT-1 protein (Figure 3.2 B). Since, HIF-1α is the oxygen sensitive subunit of HIF-1 protein, the expression of HIF-1α is said to be specifically induced under hypoxic conditions in an oxygen dependent manner, whereas the protein becomes proteasomally degraded by ubiquitination in oxygenated cells [59,62]. In addition, since we observed induction of GLUT-1 protein at both 0.5 and 1% O_2 and HIF-1α protein only at 0.5% O_2, we speculate that GLUT-1 would also be regulated through other oxygen- regulated pathways independent of HIF. Previous studies have suggested that lactate plays a critical role in promoting hypoxic response independent of HIF and this mechanism is said to be controlled by PHD enzymes in a similar fashion as HIF pathways [69].

Although GLUT-1 mRNA levels displayed a positive linear correlation with decreasing oxygen concentrations, a slightly different trend of GLUT-1 mRNA was observed when FaDu cells were exposed to 0.5% O_2 for varying time points. The mRNA levels of GLUT-1 increased with increasing exposure time reaching a maximum at 24 hours and later the levels declined sharply (Figure 3.3 A). The decrease in GLUT-1 mRNA levels following 24 hours was surprising, but intriguing since we observed the mRNA levels of another hypoxia-responsive gene, *LOX* to be upregulated at longer exposure time points, i.e. 24 and 48 hours (Figure 3.3 B).

4.2. Determining the cytotoxicity of TPZ

Initially, the effect of the parent compound (TPZ) on FaDu cells was investigated prior to determining the effect of G_6-TPZ on poorly oxygenated FaDu cells. It is well-established that TPZ

displays anticancer activity on tumor cells through induction of apoptosis [385]. As mentioned earlier, cytotoxicity of TPZ was evaluated using three different assays so as to validate the efficacy of the drug since each assay uses different parameters to assess cell death. The response of TPZ, when determined based on the measurement of cellular metabolic activity (MTT assay) was reported to display a concentration-dependent cytotoxicity in FaDu cells when treated only under hypoxic conditions (Figure 3.4 A). The hypoxia selective cytotoxicity of TPZ arises as a consequence of activation by intracellular reductive enzymes that adds a single electron to the parent molecule resulting in the production of a free radical species, which in turn induces DNA single and double strand breaks (SSB and DSBs), base damage and ultimately cell death [298]. However, minimal cytotoxicity was observed in normoxic TPZ treated cells (Figure 3.4) since the unstable TPZ radical gets rapidly back oxidized to the non-toxic parent molecule in the presence of oxygen [246]. Further, TPZ was observed to exhibit a similar trend of toxicity when evaluated using the crystal violet staining assay and the clonogenic assay, which measure cytotoxicity of the compound based on the DNA mass of the living cells and the ability to form colonies, respectively (Figure 3.4 B & C). Collectively, the above results reconfirm the fact that the parent compound gets bioreductively activated selectively under hypoxic conditions.

4.3. Determining the cytotoxicity of G_6-TPZ

Following the assessment of TPZ cytotoxicity, the potential of G_6-TPZ was investigated by examining the cytotoxicity of the compound in FaDu cells. We hypothesized that the addition of a glucose moiety to TPZ would enhance the selective recruitment of G_6-TPZ through interaction with the upregulated GLUT receptors, facilitating its entrapment in hypoxic cancer cells. The recently published crystal structure of human GLUT-1 reveals that, aside from the hydroxyl group at position 6 of D-glucose, all of the other hydroxyl groups are involved in stabilizing

hydrogen-bonding interactions with various amino acid residues within the transporter [103]. Earlier studies have reported that the C6 position of glucose could tolerate addition of various functional groups and simultaneously retain the substrate specificity and internalization by GLUT-1 since the modification at C6 position does not interfere with receptor binding [386,387]. In addition, it has been reported that anticancer agents conjugated to the C6 position of D-glucose can bind to GLUT-1 with high affinity [386-388], which further added support to our hypothesis. Based on these observations, we designed and synthesized glucose-conjugated TPZ (G_6-TPZ: C6 end of glucose conjugated to TPZ). Although, our molecular modelling based conformational analysis of G_6-TPZ docked into the binding pocket of GLUT-1 revealed binding kinetics similar to 2-deoxyglucose (Elsaidi *et al*. unpublished data), unexpectedly, G_6-TPZ up to 100 μM concentration failed to show any hypoxic sensitization in FaDu cells cultured in DMEM. Moving forward, we tried to glucose-starve the cells by culturing them in low glucose DMEM prior to treatment with high concentrations of G_6-TPZ. Glucose starvation in tumor cells has recently been shown to impair DNA DSB repair by inhibiting histone acetylation [389]. We expected a cytotoxic effect of G_6-TPZ on hypoxic glucose starved cells since TPZ is known to cause cytotoxicity primarily by induction of DNA DSBs [298]. Even though we observed that G_6-TPZ was considerably less potent than TPZ, it still retained its selective hypoxic cytotoxicity at very high concentrations of the compound (500 and 1000 μM) when assessed using MTT and CVS assay (Figure 3.5 A & B). We speculate that even though our conjugate may have high-affinity for GLUT-1, the low cytotoxicity of G_6-TPZ could be due to the bulky substituent at C6 which makes transport of the compound through GLUT-1 difficult. Another plausible explanation would be that the conjugate might bind to GLUT-1 very strongly, thus blocking the transporter and in turn preventing glucose uptake,

rather than competing for facilitated transport. Hence, in order to determine the underlying reason, we were interested to study the cellular uptake and localization of the compound under hypoxia.

4.4. Effect of TPZ on the expression of HIF-1α

As briefly discussed in the results section, we postulated that the binding of bioreduced TPZ to cellular proteins might contribute to drug's cytotoxicity in addition to induction of cytotoxic DNA DSBs through a topoisomerase-II dependent process [321]. Even though we had an indication that TPZ binds to proteins, we were still uncertain whether the drug binds directly to HIF-1α protein or if it is bound to the proteins that stabilize HIF-1α. Based on the observations, we went on to investigate the effect of TPZ on HIF-1α activity. Our results revealed that TPZ at 10 μM decreases the cellular HIF-1α protein levels under hypoxic conditions (Figure 3.6). The above result was in line with our prior data which suggested that the IC_{50} of TPZ in hypoxia to be approximately 10 μM when assessed using several cytotoxicity assays (Figure 3.4). TPZ has been identified to be associated in HIF-1α translational regulation without affecting HIF-1α mRNA expression or protein degradation [390]. In addition, prior studies have revealed that the down-regulation of HIF-1α by TPZ is largely dependent on the phosphorylation of translation initiation factor 2α (eIF2α) rather than the mTOR complex 1/eukaryotic initiation factor 4E-binding protein-1 (mTORC1/4E-BP1) signalling pathway [390]. In addition, the inhibitory effect of TPZ on HIF-1α protein synthesis under hypoxic conditions is said to be a topoisomerase-II independent phenomenon [390]. Overall, our findings and prior studies reiterate the fact that TPZ inhibits the hypoxic stabilization of HIF- 1α; thereby being a potent regulator. This also strongly adds support to our hypothesis that TPZ might either bind directly to the HIF-1α protein, or to the proteins that stabilize HIF-1α. Therefore, we set out to identify the proteins bound to TPZ under

hypoxic conditions in order to gain new insight in determining the pathway by which TPZ causes toxicity.

4.5. Determining the cytotoxicity of N_3-TPZ

We designed a new derivative of TPZ by incorporating an azido (N_3) group into our parent compound to exploit a click chemistry-based protocol. The copper (I)-catalyzed alkyne-azide cycloaddition (CuAAC) click reaction has become very popular over the past decade and is considered a reliable method since it links molecules covalently [391]. When the azido group of N_3-TPZ is paired with an alkyne in the presence of a copper catalyst, an irreversible, hydrolytically stable triazole conjugate is formed [392]. Notable advantages of click reaction include its fast reaction rate with high efficiency under physiological conditions in any solvent over a wide range of temperatures, chemo-selectivity, tolerance to other functional groups and the robust nature of the products [393]. Based on the type of alkyne labelling (fluorophore or biotin), we used our clickable prodrug of TPZ to image hypoxic cell content *in vitro* and to identify TPZ-binding proteins.

We observed that N_3-TPZ displayed hypoxia-selective cytotoxicity in a concentration-dependent manner, when examined using MTT, CVS and CFA assay (Figure 3.8 A, B & C). The IC_{50} of N_3-TPZ in hypoxia ranged between 20-25 μM, which was lower than the response of the compound in normoxia. Overall, N_3-TPZ appeared to be hypoxia selective but slightly less cytotoxic when compared to the parent compound, which exhibited an IC_{50} of approximately 10 μM under hypoxia (Figure 3.6). The data suggests that N_3-TPZ is a reasonable model to study TPZ interactions since the azide modification did not drastically alter the toxicity of the parent compound. Furthermore, we went on to examine the response of N_3-TPZ on HIF-1α expression. Our results revealed that under hypoxia, N_3-TPZ causes a reduction in the HIF-1α protein levels in a concentration-dependent manner (Figure 3.8 D). Interestingly, we

observed a sharp decline in the expression of HIF-1α level at 30 μM N_3-TPZ treated hypoxic sample, which is consistent with our observation that the IC_{50} of N_3-TPZ under hypoxia lies between 20-25 μM when assessed using different cytotoxicity assays (Figure 3.8 A, B & C).

4.6. Determining the localization of N_3-TPZ

Using click-chemistry approach, we observed the hypoxia selective sub-cellular localization of N_3-TPZ (Figure 3.9). Our results reveal that the compound displays cytoskeletal staining as well as nucleolar and nuclear localization. The click signal intensity in hypoxic N_3-TPZ treated cells was observed to be concentration dependent whereas minimal to no background signal was detected in normoxic N_3-TPZ treated cells even at high concentrations of the reagent (Figure 3.9 A), reconfirming the hypoxia selectivity of the compound. Moreover, we are the first to report an easy, robust, sensitive and straightforward methodology, which only requires standard laboratory and microscopy setup to image cellular hypoxia and monitor TPZ uptake within a few hours. It is also noteworthy to mention that we are the first to design and chemically modify TPZ by conjugating it with an azido moiety and to successfully use this unique approach to trace cellular hypoxia.

4.7. Identification of potential binding partners of N_3-TPZ

We used a similar methodology with a biotin-conjugated alkyne rather than an Alexa-alkyne to isolate the potential protein candidates that are modified by N_3-TPZ under hypoxia. As mentioned earlier, use of biotin-alkyne enabled us to pull down the N_3-TPZ bound proteins with a mutein-streptavidin column. Western blot analysis was performed on the clicked lysates and eluates and subsequently the biotinylated proteins were detected using (HRP)-coupled streptavidin and a β-tubulin antibody. Our data reveals that streptavidin-HRP signal was detected only in hypoxic N_3-TPZ treated clicked lysates and eluates indicating the specificity of protein

modification by N_3-TPZ (Figure 3.12). The β-tubulin signal validated the efficiency of streptavidin pull down and highlighted the low background non-specific binding to the beads. Interestingly, the N_3-TPZ concentration used in the above experiment was 30 μM, a concentration at which the compound exhibited hypoxia specific protein modification and which was in accord with our finding that N_3-TPZ displays hypoxia-specific cytotoxicity (Figure 3.8 A, B & C). Although we know TPZ induces toxicity by DNA damage, we went on to explore the protein modifications associated with the drug, which we speculated could also play a role in altering the drug's efficacy. Since streptavidin-HRP signal was detected only in hypoxic N_3-TPZ treated eluates, they were further analyzed by liquid chromatography coupled mass spectrometry (LC-MS/MS) along with hypoxic control eluates and hypoxic whole cell clicked lysate. Our analyses revealed that although labeling was not highly specific, the labeling was enriched for a sub fraction of the proteome. In addition, we observed that numerous high abundance proteins escape such labelling. The explanation for these observations are unknown, but presumably are related to the chemistry of TPZ interaction with proteins and the subcellular localization of the compound.

Even though several high abundance proteins escaped the drug labelling, we identified a few highly abundant proteins that were labelled by N_3-TPZ under hypoxia. Interestingly, our proteomic analysis revealed tubulin alpha-1C chain as one of the highly abundant protein labelled by N_3-TPZ under hypoxia, which correlates with the β-tubulin signal that we observed specifically in the western blot of hypoxic N_3-TPZ treated cell eluate (Figure 3.12). In addition, we observed a filamentous pattern in the N_3-TPZ click imaging studies under hypoxia (Figure 3.9), which further validates our proteomic analysis data and strongly suggests that TPZ might interact with tubulin that has to be explored in detail in future. Furthermore, we used these highly ranked proteins to study the predicted protein-protein interactions associated with the drug using STRING

database. STRING has been recommended as the first choice in assessing functional and physical associations between proteins on a global scale when compared to other protein-protein interaction databases on the basis of data comprehensiveness, use of confidence scores and visualization features [394-396]. Apart from obtaining information through known interactions such as experimental data and curated databases on protein-protein interactions [397-399], STRING surpasses other databases by collecting predicted interactions through variable sources such as co-expression analysis, text-mining of scientific literature, gene fusions, neighbourhood and co-occurrence; thus rendering the database as a more reliable resource [400-402]. Therefore, using STRING, we observed the functional association of our input proteins (highly abundant proteins that were labelled by N_3-TPZ under hypoxia) in variable biological processes, molecular functions, cellular component, reactome pathways and several protein domains (Figure 3.14). Since we were interested in the localization of the compound, we examined the cellular localization of the proteins. Interestingly, we observed the enrichment of our input proteins in both the nucleus and cytoplasm as shown in Figure 3.14 and the result estimated by STRING was in accord with our cell imaging during the hypoxia selective sub-cellular localization studies of N_3-TPZ (Figure 3.9 and 3.10). Our imaging results revealed that the compound displayed both cytoskeletal staining as well as nucleolar and nuclear localization, which fairly correlates with our STRING findings; hence corroborating the localization of N_3-TPZ.

As mentioned, we are the first to explore the protein modifications associated with TPZ and isolate the potential protein candidates that are modified by the drug under hypoxia. Interestingly, a fellow graduate student in our group has studied another class of hypoxia-specific compounds based on 2-nitroimidazole (NI) and has made use of an azido derivative. We observed that the abundance and set of proteins associated with the azido-conjugated NI differs from the

proteins associated with our compound, N_3-TPZ, which belongs to an N-oxide class of drugs. For instance, glyceraldehyde-3-phosphate dehydrogenase was observed to be highly abundant in azido-conjugated NI, whereas the abundance of the same protein was remarkably very low with our compound. The striking difference in the protein interactions between the different classes of the drug (N-oxide and nitroimidazole) establishes the fact that TPZ interacts with proteins differently when compared to nitroimidazoles. However, we also need to highlight that our samples were analysed by LC-MS/MS only once and the experiment should be repeated further and additional experiments will be required to validate our observations so as to unravel the basis underlying protein-N_3-TPZ interactions.

4.8. Determining the cytotoxicity of N_3-G_6-TPZ

Since we found that N_3-TPZ was a useful reagent for monitoring drug uptake, we went on to utilize a similar approach to study the uptake and localization of G_6-TPZ, since we observed that this compound displayed hypoxic sensitization only at higher concentrations. Consequently, we designed and synthesized a new derivative of G_6-TPZ (N_3-G_6-TPZ), which incorporates both glucose and azido moieties.

Our data revealed that N_3-G_6-TPZ exhibited hypoxia-selective cytotoxicity in a concentration-dependent manner when examined using the CVS assay with FaDu cells cultured in both DMEM and low glucose DMEM (Figure 3.15). We used two different media in order to compare and study the response of N_3-G_6-TPZ on glucose-starved FaDu cells. However, our results indicate that there was no significant difference in the cytotoxicity of N_3-G_6-TPZ treated cells cultured in both media. Our results also indicate that N_3-G_6-TPZ is less toxic than N_3-TPZ (Figure 3.8) and the parent compound TPZ (Figure 3.4), but was remarkably more toxic when compared to G_6-TPZ (Figure 3.5). We speculate that the addition of glucose moiety has an impact

on N_3-G_6-TPZ since its hypoxia selective cytotoxicity is reduced when compared to the toxicity of N_3-TPZ, where only azido moiety is conjugated to TPZ. Therefore, we think that the comparatively low hypoxic cytotoxicity of N_3-G_6-TPZ when compared to TPZ and N_3-TPZ, might be due to either reduced transporter efficiency of the compound resulting from addition of the glucose moiety or maybe the compound remains bound to the GLUT-1 transporter.

4.9. Determining the localization of N_3-G_6-TPZ

In order to explore the underlying reason, we went on to study the cellular uptake and localization of N_3-G_6-TPZ under hypoxia using click chemistry. Fluorescence images reveal the hypoxia selective sub-cellular localization of N_3-G_6-TPZ (Figure 3.16). Although, the click signal intensity in hypoxic N_3-G_6-TPZ treated cells was observed to be concentration dependent, it was clearly evident that considerably less N_3-G_6-TPZ was taken up by the hypoxic cells when compared to N_3-TPZ (Figure 3.9). Contrastingly, minimum to no background signal was detected in normoxic N_3-G_6-TPZ treated cells even at high concentrations of the reagent, which reconfirms the hypoxia selectivity of the compound (Figure 3.16 A). Due to low click signal intensity under hypoxia, the localization of the compound was further investigated. The Z-stack images acquired through confocal microscopy indicates that N_3-G_6-TPZ efficiently penetrates into the cellular membrane and the entrapment of the compound is predominantly nucleolar and nuclear with some cytoskeleton staining (Figure 3.17). In addition, we also observed that the localization of N_3-G_6-TPZ was quite similar to the localization of N_3-TPZ under hypoxia (Figure 3.10). Therefore, even though the localizations of N_3-G_6-TPZ and N_3-TPZ are quite similar, the difference between the toxicities of the compounds might be due to their distinct chemical structures, and notably both the compounds have different amine linkages which might also contribute to their different cellular properties.

4.10. Overall impact on the objective

Our initial objective in this study was to improve the delivery of TPZ selectively to oxygen deficient cells by adding a glucose moiety to it which was based on the idea of exploiting the abundance of GLUTs in hypoxia. However, our results reveal that the addition of glucose moiety to TPZ did not work fairly well since glucose-conjugated TPZ displayed selective hypoxic cytotoxicity only at very high concentrations. We speculate that the reduced cytotoxicity of G_6-TPZ might be due to the fact that the compound was not taken up by the cells or it was cleared out faster due to higher hydrophilicity in comparison to TPZ. Our next objective was to devise a TPZ derivative that would monitor the cellular uptake of TPZ which led to the incorporation of an azido group to our parent compound. Subsequently, we observed that the azido-conjugated TPZ was highly hypoxia selective and in addition, using click-chemistry approach we observed that the compound successfully traces tumor hypoxia and binds to proteins. Next, using similar methodology we went on to isolate the potential protein candidates that are modified by N_3-TPZ under hypoxia using a biotin alkyne. The drug-protein adducts were pulled down with mutein streptavidin beads and were analysed further by LC-MS/MS. Our analyses revealed that although the N_3-TPZ labeling was not highly specific, it was enriched for a sub fraction of the proteome. In addition, we also observed that numerous high abundance proteins escape such labelling for some reason that is unknown. However, using a few highly abundant proteins that were labelled by N_3-TPZ under hypoxia, using STRING database, we observed that those proteins were enriched in both nucleus and cytoplasm suggesting the localization of the compound. Furthermore, we exploited the property of monitoring TPZ uptake by N_3-TPZ to study the uptake and localization of G_6-TPZ by synthesizing a new derivative of TPZ which incorporated both glucose and azido moieties. Apparently, our results reveal that N_3-G_6-TPZ was considerably more potent when

compared to G_6-TPZ. We speculate that the difference between the toxicities of the compounds might be due to the structural difference in the linkage between glucose and TPZ in G_6-TPZ when compared to N_3-G_6-TPZ. On the contrary, N_3-TPZ, which had a rather simpler addition to TPZ turned out to be a relatively good model to study TPZ interactions since the azide modification did not seem to drastically alter the toxicity of the parent compound.

Chapter V - Future Directions

With regard to determining the potential of TPZ and its derivatives, we plan to measure the uptake of G_6-TPZ by labelling it with C_{14}. We prefer intrinsic radiolabelling of the compound rather than tagging it with a fluorescent dye so that the structure, conformation and property of the compound is unaltered, thus making it identical to its unlabelled counterpart. The direct measure of the radiolabelled compound uptake or binding will be determined through a radioactive assay. We also plan to determine whether the cellular uptake of these glucose-conjugated TPZ derivatives (G_6-TPZ and N_3-G_6-TPZ) are GLUT-1 mediated. In general, even though all the glyoconjugates are designed to be taken up by facilitated diffusion, a few compounds are known to be transported through passive diffusion. Hence, in order to study the transport mechanism of our glucose-conjugated TPZ derivatives, we plan to monitor the cellular uptake of these compounds in the presence and absence of an exofacial GLUT-1 inhibitor. We could confirm that the entry of G_6-TPZ and N_3-G_6-TPZ into cells are GLUT-1 receptor mediated if their co-treatment with a GLUT-1 inhibitor significantly reduces their cellular uptake. In addition, since D-glucose is the main substrate of GLUT-1, its inhibitory effect on our glucose-compounds would be assessed too.

A recent study suggests that varying the position of substitution of glucose to anticancer compounds does not only contribute to the alteration of cellular uptake and cytotoxicity, but also plays a major role in the GLUT-1 specificity of the glyoconjugates [403]. Since, substituents at C_2 of glucose are considered to be stronger substrates for GLUT-1 when compared to C_6 of glucose, we plan to test our hypothesis on G_2-TPZ, which has been synthesized as an alternative approach by our group.

Following our success in using N_3-TPZ to image cellular hypoxia, we plan to further validate the hypoxia selectivity of N_3-TPZ using click chemistry approach by co-staining them with pimonidazole, a commercially available hypoxia marker. Furthermore, we also plan to

confirm our *in vitro* imaging results of N_3-TPZ by performing *in vivo* studies of N_3-TPZ click chemistry along with pimonidazole co-staining. We aim to encapsulate N_3-TPZ into nanoparticles and use them in *in vivo* studies for a better outcome since encapsulation would elevate the delivery properties of the compound. We intend to use orthotopic xenograft model to validate our *in vitro* findings since it is known to effectively reproduce the tumor microenvironment of HNSCC [404] and has been well established over the years as a clinically relevant tumor model [405]. In addition, these studies would be conducted with FaDu cells as it has been previously reported that the FaDu cell line is associated with high incidence of cervical lymph node metastasis in orthotopic HNC models [406-408]. We also would like to incorporate periodic monitoring of hypoxia in animals by using ^{18}F-FAZA PET scan in order to obtain a more complete analysis.

We carried out affinity purification studies with N_3-TPZ in an effort to explore the protein modifications associated with TPZ. But since the analysis of our samples by LC-MS/MS was carried out only once, the experiment needs to be repeated to reconfirm the pattern of abundance in the identified set of proteins and its cellular localization in order to get a better picture of TPZ binding partners.

We still have a lingering question about TPZ - whether it binds to HIF-1α directly or to the proteins that stabilize HIF-1α? We plan to use immunoprecipitation to determine the interaction between TPZ and HIF-1α. Accordingly, initially the N_3-TPZ treated and untreated cells will be clicked with a biotin alkyne. Later the lysates would be incubated with an anti-HIF-1α antibody, which would be followed by a pull down with secondary antibody-coated beads. Western blot of the eluates would be performed to determine whether HIF-1α was modified by the immunoprecipitated N_3-TPZ or not. As discussed earlier in the introduction, cytochrome c P450 reductase (CYP450R), a one-electron reducing enzyme, is known to play a major role in the

metabolic activation of TPZ. As prior studies suggest that high levels of P450R activity increases the sensitivity to TPZ, in future we plan to use cells that express high levels of catalytically active CYP450R by transfecting the cells with P450 reductase cDNA. It is highly likely that the overexpression of CYP450R activity in cells would efficiently elevate the cytotoxic response of TPZ and its derivatives in oxygen-deficient cells. We would like to use this model to study and compare the cytotoxic response of N_3-TPZ and TPZ to confirm whether N_3-TPZ undergoes a similar mechanism of activation when compared to the parent compound.

In conclusion, we would like to emphasize the fact that TPZ still holds great promise with recent developments in identifying tumors that are highly responsive to hypoxic cytotoxins. Therefore, employing a strict hypoxic patient stratification using either PET imaging or biomarkers prior to the treatment plan along with the use of an ideal combinatorial therapy would boost the TPZ efficacy, which would ultimately result in attaining the best therapeutic benefit of TPZ, thereby aiding in enhancing the quality of life of cancer patients.

References

1 Pahlman, S. & Mohlin, S. Hypoxia and hypoxia-inducible factors in neuroblastoma. *Cell Tissue Res* **372**, 269-275, doi:10.1007/s00441-017-2701-1 (2018).

2 Bennewith, K. L. & Dedhar, S. Targeting hypoxic tumour cells to overcome metastasis. *BMC Cancer* **11**, 504, doi:10.1186/1471-2407-11-504 (2011).

3 Minchinton, A. I. & Tannock, I. F. Drug penetration in solid tumours. *Nat Rev Cancer* **6**, 583-592, doi:10.1038/nrc1893 (2006).

4 Brown, J. M. The Hypoxic Cell. *Cancer Research* **59**, 5863 (1999).

5 Kim, Y., Lin, Q., Glazer, P. M. & Yun, Z. Hypoxic tumor microenvironment and cancer cell differentiation. *Curr Mol Med* **9**, 425-434 (2009).

6 Birner, P. *et al.* Overexpression of Hypoxia-inducible Factor 1α Is a Marker for an Unfavorable Prognosis in Early-Stage Invasive Cervical Cancer. *Cancer Research* **60**, 4693 (2000).

7 Zhong, H., Semenza, G. L., Simons, J. W. & De Marzo, A. M. Up-regulation of hypoxia-inducible factor 1α is an early event in prostate carcinogenesis. *Cancer Detection and Prevention* **28**, 88-93, doi:10.1016/j.cdp.2003.12.009 (2004).

8 Duffy, J. P., Eibl, G., Reber, H. A. & Hines, O. J. Influence of hypoxia and neoangiogenesis on the growth of pancreatic cancer. *Mol Cancer* **2**, 12 (2003).

9 Wei, J. *et al.* Hypoxia potentiates glioma-mediated immunosuppression. *PLoS One* **6**, e16195, doi:10.1371/journal.pone.0016195 (2011).

10 Nordsmark, M. *et al.* Hypoxia in human soft tissue sarcomas: Adverse impact on survival and no association with p53 mutations. *British Journal Of Cancer* **84**, 1070, doi:10.1054/bjoc.2001.1728 (2001).

11 Hartmann, A. *et al.* Hypoxia-induced up-regulation of angiogenin in human malignant melanoma. *Cancer Res* **59**, 1578-1583 (1999).

12 Keith, B. & Simon, M. C. Hypoxia-inducible factors, stem cells, and cancer. *Cell* **129**, 465-472, doi:10.1016/j.cell.2007.04.019 (2007).

13 Padhani, A. R. Where are we with imaging oxygenation in human tumours? *Cancer imaging : the official publication of the International Cancer Imaging Society* **5**, 128-130, doi:10.1102/1470-7330.2005.0103 (2005).

14 Bar, E. E., Lin, A., Mahairaki, V., Matsui, W. & Eberhart, C. G. Hypoxia Increases the Expression of Stem-Cell Markers and Promotes Clonogenicity in Glioblastoma Neurospheres. *The American Journal of Pathology* **177**, 1491-1502, doi:10.2353/ajpath.2010.091021 (2010).

15 Lara, P. C. *et al.* Severe hypoxia induces chemo-resistance in clinical cervical tumors through MVP over-expression. *Radiation Oncology* **4**, 29, doi:10.1186/1748-717X-4-29 (2009).

16 Höckel, M. & Vaupel, P. Tumor Hypoxia: Definitions and Current Clinical, Biologic, and Molecular Aspects. *JNCI: Journal of the National Cancer Institute* **93**, 266-276, doi:10.1093/jnci/93.4.266 (2001).

17 Thomlinson, R. H. & Gray, L. H. The histological structure of some human lung cancers and the possible implications for radiotherapy. *British journal of cancer* **9**, 539-549 (1955).

18 West, J. B. Physiological Effects of Chronic Hypoxia. *New England Journal of Medicine* **376**, 1965-1971, doi:10.1056/NEJMra1612008 (2017).

19 Brown, J. M. Evidence for acutely hypoxic cells in mouse tumours, and a possible mechanism of reoxygenation. *Br J Radiol* **52**, 650-656, doi:10.1259/0007-1285-52-620-650 (1979).
20 Bayer, C., Shi, K., Astner, S. T., Maftei, C.-A. & Vaupel, P. Acute Versus Chronic Hypoxia: Why a Simplified Classification is Simply Not Enough. *International Journal of Radiation Oncology • Biology • Physics* **80**, 965-968, doi:10.1016/j.ijrobp.2011.02.049 (2011).
21 Rofstad, E. K., Galappathi, K., Mathiesen, B. & Ruud, E. B. Fluctuating and diffusion-limited hypoxia in hypoxia-induced metastasis. *Clin Cancer Res* **13**, 1971-1978, doi:10.1158/1078-0432.Ccr-06-1967 (2007).
22 Horsman, M. R. & Overgaard, J. The impact of hypoxia and its modification of the outcome of radiotherapy. *Journal of radiation research* **57 Suppl 1**, i90-i98, doi:10.1093/jrr/rrw007 (2016).
23 Brown, J. M. & Wilson, W. R. Exploiting tumour hypoxia in cancer treatment. *Nature Reviews Cancer* **4**, 437, doi:10.1038/nrc1367 (2004).
24 Stoyanov, G. S., Kitanova, M., Dzhenkov, D. L., Ghenev, P. & Sapundzhiev, N. Demographics of Head and Neck Cancer Patients: A Single Institution Experience. *Cureus* **9**, e1418-e1418, doi:10.7759/cureus.1418 (2017).
25 Beck, T. N. & Golemis, E. A. Genomic insights into head and neck cancer. *Cancers of the Head & Neck* **1**, 1, doi:10.1186/s41199-016-0003-z (2016).
26 Blitzer, G. C., Smith, M. A., Harris, S. L. & Kimple, R. J. Review of the clinical and biologic aspects of human papillomavirus-positive squamous cell carcinomas of the head and neck. *International journal of radiation oncology, biology, physics* **88**, 761-770, doi:10.1016/j.ijrobp.2013.08.029 (2014).
27 De Felice, F. *et al.* Radiotherapy Controversies and Prospective in Head and Neck Cancer: A Literature-Based Critical Review. *Neoplasia (New York, N.Y.)* **20**, 227-232, doi:10.1016/j.neo.2018.01.002 (2018).
28 Iqbal, M. S. *et al.* Primary Concurrent Chemoradiation in Head and Neck Cancers with Weekly Cisplatin Chemotherapy: Analysis of Compliance, Toxicity and Survival. *International archives of otorhinolaryngology* **21**, 171-177, doi:10.1055/s-0036-1594020 (2017).
29 Boscolo-Rizzo, P. *et al.* The evolution of the epidemiological landscape of head and neck cancer in Italy: Is there evidence for an increase in the incidence of potentially HPV-related carcinomas? *PloS one* **13**, e0192621-e0192621, doi:10.1371/journal.pone.0192621 (2018).
30 Gilyoma, J. M., Rambau, P. F., Masalu, N., Kayange, N. M. & Chalya, P. L. Head and neck cancers: a clinico-pathological profile and management challenges in a resource-limited setting. *BMC research notes* **8**, 772-772, doi:10.1186/s13104-015-1773-9 (2015).
31 Vigneswaran, N. & Williams, M. D. Epidemiologic trends in head and neck cancer and aids in diagnosis. *Oral and maxillofacial surgery clinics of North America* **26**, 123-141, doi:10.1016/j.coms.2014.01.001 (2014).
32 Klussmann, J. P. Head and Neck Cancer - New Insights into a Heterogeneous Disease. *Oncology Research and Treatment* **40**, 318-319, doi:10.1159/000477255 (2017).
33 Leeman, J. E., Li, J., Pei, X. & et al. Patterns of treatment failure and postrecurrence outcomes among patients with locally advanced head and neck squamous cell carcinoma after chemoradiotherapy using modern radiation techniques. *JAMA Oncology* **3**, 1487-1494, doi:10.1001/jamaoncol.2017.0973 (2017).

34 Nordsmark, M., Overgaard, M. & Overgaard, J. Pretreatment oxygenation predicts radiation response in advanced squamous cell carcinoma of the head and neck. *Radiotherapy and Oncology* **41**, 31-39, doi:10.1016/S0167-8140(96)91811-3 (1996).
35 Méry, B. *et al.* Targeting head and neck tumoral stem cells: From biological aspects to therapeutic perspectives. *World journal of stem cells* **8**, 13-21, doi:10.4252/wjsc.v8.i1.13 (2016).
36 Walsh, J. C. *et al.* The clinical importance of assessing tumor hypoxia: relationship of tumor hypoxia to prognosis and therapeutic opportunities. *Antioxidants & redox signaling* **21**, 1516-1554, doi:10.1089/ars.2013.5378 (2014).
37 Bittner, M.-I. & Grosu, A.-L. Hypoxia in Head and Neck Tumors: Characteristics and Development during Therapy. *Frontiers in oncology* **3**, 223-223, doi:10.3389/fonc.2013.00223 (2013).
38 Bertout, J. A., Patel, S. A. & Simon, M. C. The impact of O2 availability on human cancer. *Nature reviews. Cancer* **8**, 967-975, doi:10.1038/nrc2540 (2008).
39 Rockwell, S., Dobrucki, I. T., Kim, E. Y., Marrison, S. T. & Vu, V. T. Hypoxia and radiation therapy: past history, ongoing research, and future promise. *Curr Mol Med* **9**, 442-458 (2009).
40 Dietrich, A. *et al.* Improving external beam radiotherapy by combination with internal irradiation. *The British journal of radiology* **88**, 20150042-20150042, doi:10.1259/bjr.20150042 (2015).
41 Liu, C., Lin, Q. & Yun, Z. Cellular and molecular mechanisms underlying oxygen-dependent radiosensitivity. *Radiation research* **183**, 487-496, doi:10.1667/RR13959.1 (2015).
42 Riley, P. A. Free radicals in biology: oxidative stress and the effects of ionizing radiation. *International journal of radiation biology* **65**, 27-33 (1994).
43 Willers, H., Azzoli, C. G., Santivasi, W. L. & Xia, F. Basic mechanisms of therapeutic resistance to radiation and chemotherapy in lung cancer. *Cancer journal (Sudbury, Mass.)* **19**, 200-207, doi:10.1097/PPO.0b013e318292e4e3 (2013).
44 Muz, B., de la Puente, P., Azab, F. & Azab, A. K. The role of hypoxia in cancer progression, angiogenesis, metastasis, and resistance to therapy. *Hypoxia (Auckland, N.Z.)* **3**, 83-92, doi:10.2147/HP.S93413 (2015).
45 Gabalski, E. C. *et al.* Pretreatment and midtreatment measurement of oxygen tension levels in head and neck cancers. *Laryngoscope* **108**, 1856-1860 (1998).
46 Durand, R. E. The influence of microenvironmental factors during cancer therapy. *In Vivo* **8**, 691-702 (1994).
47 Teicher, B. A. Hypoxia and drug resistance. *Cancer Metastasis Rev* **13**, 139-168 (1994).
48 Durand, R. E. & Raleigh, J. A. Identification of nonproliferating but viable hypoxic tumor cells in vivo. *Cancer Res* **58**, 3547-3550 (1998).
49 Sullivan, R., Pare, G. C., Frederiksen, L. J., Semenza, G. L. & Graham, C. H. Hypoxia-induced resistance to anticancer drugs is associated with decreased senescence and requires hypoxia-inducible factor-1 activity. *Molecular cancer therapeutics* **7**, 1961-1973, doi:10.1158/1535-7163.Mct-08-0198 (2008).
50 Prince, M. E. *et al.* Identification of a subpopulation of cells with cancer stem cell properties in head and neck squamous cell carcinoma. *Proc Natl Acad Sci U S A* **104**, 973-978, doi:10.1073/pnas.0610117104 (2007).

51 Duarte, S. *et al.* Isolation of head and neck squamous carcinoma cancer stem-like cells in a syngeneic mouse model and analysis of hypoxia effect. *Oncol Rep* **28**, 1057-1062, doi:10.3892/or.2012.1904 (2012).
52 Shen, X. *et al.* Hypoxia Induces Multidrug Resistance via Enhancement of Epidermal Growth Factor-Like Domain 7 Expression in Non-Small Lung Cancer Cells. *Chemotherapy* **62**, 172-180, doi:10.1159/000456066 (2017).
53 Ortmann, B., Druker, J. & Rocha, S. Cell cycle progression in response to oxygen levels. *Cellular and molecular life sciences : CMLS* **71**, 3569-3582, doi:10.1007/s00018-014-1645-9 (2014).
54 Nakayama, K. & Ronai, Z. Siah: new players in the cellular response to hypoxia. *Cell cycle (Georgetown, Tex.)* **3**, 1345-1347, doi:10.4161/cc.3.11.1207 (2004).
55 Riffle, S. & Hegde, R. S. Modeling tumor cell adaptations to hypoxia in multicellular tumor spheroids. *Journal of experimental & clinical cancer research : CR* **36**, 102-102, doi:10.1186/s13046-017-0570-9 (2017).
56 Matsushima, S. *et al.* Broad suppression of NADPH oxidase activity exacerbates ischemia/reperfusion injury through inadvertent downregulation of hypoxia-inducible factor-1α and upregulation of peroxisome proliferator-activated receptor-α. *Circulation research* **112**, 1135-1149, doi:10.1161/CIRCRESAHA.111.300171 (2013).
57 Franke, K., Gassmann, M. & Wielockx, B. Erythrocytosis: the HIF pathway in control. *Blood* **122**, 1122 (2013).
58 Wang, G. L. & Semenza, G. L. Purification and characterization of hypoxia-inducible factor 1. *The Journal of biological chemistry* **270**, 1230-1237 (1995).
59 Salceda, S. & Caro, J. Hypoxia-inducible Factor 1α (HIF-1α) Protein Is Rapidly Degraded by the Ubiquitin-Proteasome System under Normoxic Conditions: ITS STABILIZATION BY HYPOXIA DEPENDS ON REDOX-INDUCED CHANGES. *Journal of Biological Chemistry* **272**, 22642-22647 (1997).
60 Graham, A. M. & Presnell, J. S. Hypoxia Inducible Factor (HIF) transcription factor family expansion, diversification, divergence and selection in eukaryotes. *PloS one* **12**, e0179545-e0179545, doi:10.1371/journal.pone.0179545 (2017).
61 Hu, C. J. *et al.* Differential regulation of the transcriptional activities of hypoxia-inducible factor 1 alpha (HIF-1alpha) and HIF-2alpha in stem cells. *Molecular and cellular biology* **26**, 3514-3526, doi:10.1128/mcb.26.9.3514-3526.2006 (2006).
62 Hagg, M. & Wennstrom, S. Activation of hypoxia-induced transcription in normoxia. *Experimental cell research* **306**, 180-191, doi:10.1016/j.yexcr.2005.01.017 (2005).
63 Ke, Q. & Costa, M. Hypoxia-Inducible Factor-1 (HIF-1). *Molecular Pharmacology* **70**, 1469 (2006).
64 Ziello, J. E., Jovin, I. S. & Huang, Y. Hypoxia-Inducible Factor (HIF)-1 regulatory pathway and its potential for therapeutic intervention in malignancy and ischemia. *The Yale journal of biology and medicine* **80**, 51-60 (2007).
65 Gu, Y. Z., Moran, S. M., Hogenesch, J. B., Wartman, L. & Bradfield, C. A. Molecular characterization and chromosomal localization of a third alpha-class hypoxia inducible factor subunit, HIF3alpha. *Gene expression* **7**, 205-213 (2018).
66 Seeber, L. M. S. *et al.* Hypoxia-Inducible Factor-1 as a Therapeutic Target in Endometrial Cancer Management %J Obstetrics and Gynecology International. **2010**, doi:10.1155/2010/580971 (2010).

67 Curtis, K. K., Wong, W. W. & Ross, H. J. Past approaches and future directions for targeting tumor hypoxia in squamous cell carcinomas of the head and neck. *Critical reviews in oncology/hematology* **103**, 86-98, doi:10.1016/j.critrevonc.2016.05.005 (2016).
68 Cummins, E. P. & Taylor, C. T. Hypoxia-responsive transcription factors. *Pflugers Archiv : European journal of physiology* **450**, 363-371, doi:10.1007/s00424-005-1413-7 (2005).
69 Elvidge, G. P. *et al.* Concordant Regulation of Gene Expression by Hypoxia and 2-Oxoglutarate-dependent Dioxygenase Inhibition: THE ROLE OF HIF-1α, HIF-2α, AND OTHER PATHWAYS. **281**, 15215-15226, doi:10.1074/jbc.M511408200 (2006).
70 Lee, D. C. *et al.* A lactate-induced response to hypoxia. *Cell* **161**, 595-609, doi:10.1016/j.cell.2015.03.011 (2015).
71 Park, K. C., Lee, D. C. & Yeom, Y. I. NDRG3-mediated lactate signaling in hypoxia. *BMB reports* **48**, 301-302 (2015).
72 Baldwin, J. M., Gorga, J. C. & Lienhard, G. E. The monosaccharide transporter of the human erythrocyte. Transport activity upon reconstitution. *The Journal of biological chemistry* **256**, 3685-3689 (1981).
73 Kasahara, M. & Hinkle, P. C. Reconstitution and purification of the D-glucose transporter from human erythrocytes. *The Journal of biological chemistry* **252**, 7384-7390 (1977).
74 Navale, A. M. & Paranjape, A. N. Glucose transporters: physiological and pathological roles. *Biophysical reviews* **8**, 5-9, doi:10.1007/s12551-015-0186-2 (2016).
75 Sala-Rabanal, M. *et al.* Bridging the gap between structure and kinetics of human SGLT1. *American journal of physiology. Cell physiology* **302**, C1293-C1305, doi:10.1152/ajpcell.00397.2011 (2012).
76 Jurcovicova, J. Glucose transport in brain - effect of inflammation. *Endocrine regulations* **48**, 35-48 (2014).
77 Kapoor, K. *et al.* Mechanism of inhibition of human glucose transporter GLUT1 is conserved between cytochalasin B and phenylalanine amides. *Proceedings of the National Academy of Sciences of the United States of America* **113**, 4711-4716, doi:10.1073/pnas.1603735113 (2016).
78 Joost, H. G. *et al.* Nomenclature of the GLUT/SLC2A family of sugar/polyol transport facilitators. *American journal of physiology. Endocrinology and metabolism* **282**, E974-976, doi:10.1152/ajpendo.00407.2001 (2002).
79 Mueckler, M. & Thorens, B. The SLC2 (GLUT) family of membrane transporters. *Molecular aspects of medicine* **34**, 121-138, doi:10.1016/j.mam.2012.07.001 (2013).
80 Pao, S. S., Paulsen, I. T. & Saier, M. H., Jr. Major facilitator superfamily. *Microbiology and molecular biology reviews : MMBR* **62**, 1-34 (1998).
81 Mueckler, M. *et al.* Sequence and structure of a human glucose transporter. *Science (New York, N.Y.)* **229**, 941-945 (1985).
82 Abramson, J. *et al.* Structure and mechanism of the lactose permease of Escherichia coli. *Science (New York, N.Y.)* **301**, 610-615, doi:10.1126/science.1088196 (2003).
83 Thorens, B. & Mueckler, M. Glucose transporters in the 21st Century. *American journal of physiology. Endocrinology and metabolism* **298**, E141-E145, doi:10.1152/ajpendo.00712.2009 (2010).
84 Stokkel, M. P., Linthorst, M. F., Borm, J. J., Taminiau, A. H. & Pauwels, E. K. A reassessment of bone scintigraphy and commonly tested pretreatment biochemical parameters in newly diagnosed osteosarcoma. *Journal of cancer research and clinical oncology* **128**, 393-399, doi:10.1007/s00432-002-0350-5 (2002).

85 Shah, K., Desilva, S. & Abbruscato, T. The role of glucose transporters in brain disease: diabetes and Alzheimer's Disease. *International journal of molecular sciences* **13**, 12629-12655, doi:10.3390/ijms131012629 (2012).
86 Chung, F.-Y. *et al.* GLUT1 gene is a potential hypoxic marker in colorectal cancer patients. *BMC cancer* **9**, 241-241, doi:10.1186/1471-2407-9-241 (2009).
87 Sadlecki, P. *et al.* The role of Hypoxia-inducible factor-1 α , glucose transporter-1, (GLUT-1) and carbon anhydrase IX in endometrial cancer patients. *BioMed research international* **2014**, 616850-616850, doi:10.1155/2014/616850 (2014).
88 Airley, R. *et al.* Glucose Transporter Glut-1 Expression Correlates with Tumor Hypoxia and Predicts Metastasis-free Survival in Advanced Carcinoma of the Cervix. *Clinical Cancer Research* **7**, 928 (2001).
89 Carvalho, K. C. *et al.* GLUT1 expression in malignant tumors and its use as an immunodiagnostic marker. *Clinics (Sao Paulo, Brazil)* **66**, 965-972, doi:10.1590/S1807-59322011000600008 (2011).
90 Hayashi, M. *et al.* Induction of glucose transporter 1 expression through hypoxia-inducible factor 1alpha under hypoxic conditions in trophoblast-derived cells. *The Journal of endocrinology* **183**, 145-154, doi:10.1677/joe.1.05599 (2004).
91 Ouiddir, A., Planes, C., Fernandes, I., VanHesse, A. & Clerici, C. Hypoxia upregulates activity and expression of the glucose transporter GLUT1 in alveolar epithelial cells. *American journal of respiratory cell and molecular biology* **21**, 710-718, doi:10.1165/ajrcmb.21.6.3751 (1999).
92 Eckert, A. W., Lautner, M. H., Taubert, H., Schubert, J. & Bilkenroth, U. Expression of Glut-1 is a prognostic marker for oral squamous cell carcinoma patients. *Oncol Rep* **20**, 1381-1385 (2008).
93 Carvalho, K. C. *et al.* GLUT1 expression in malignant tumors and its use as an immunodiagnostic marker. *Clinics (Sao Paulo)* **66**, 965-972 (2011).
94 Yu, M. *et al.* The prognostic value of GLUT1 in cancers: a systematic review and meta-analysis. *Oncotarget* **8**, 43356-43367, doi:10.18632/oncotarget.17445 (2017).
95 Blayney, J. K. *et al.* Glucose transporter 1 expression as a marker of prognosis in oesophageal adenocarcinoma. *Oncotarget* **9**, 18518-18528, doi:10.18632/oncotarget.24906 (2018).
96 Zhou, S., Wang, S., Wu, Q., Fan, J. & Wang, Q. Expression of glucose transporter-1 and -3 in the head and neck carcinoma--the correlation of the expression with the biological behaviors. *ORL; journal for oto-rhino-laryngology and its related specialties* **70**, 189-194, doi:10.1159/000124293 (2008).
97 Wu, X.-H. *et al.* Expression and significance of hypoxia-inducible factor-1α and glucose transporter-1 in laryngeal carcinoma. *Oncology letters* **5**, 261-266, doi:10.3892/ol.2012.941 (2013).
98 Sun, L. *et al.* Crystal structure of a bacterial homologue of glucose transporters GLUT1-4. *Nature* **490**, 361-366, doi:10.1038/nature11524 (2012).
99 Quistgaard, E. M., Löw, C., Moberg, P., Trésaugues, L. & Nordlund, P. Structural basis for substrate transport in the GLUT-homology family of monosaccharide transporters. *Nature Structural &Amp; Molecular Biology* **20**, 766, doi:10.1038/nsmb.2569 https://www.nature.com/articles/nsmb.2569#supplementary-information (2013).

100 Iancu, C. V., Zamoon, J., Woo, S. B., Aleshin, A. & Choe, J.-y. Crystal structure of a glucose/H⁺ symporter and its mechanism of action. *Proceedings of the National Academy of Sciences* **110**, 17862 (2013).
101 Madej, M. G., Sun, L., Yan, N. & Kaback, H. R. Functional architecture of MFS D-glucose transporters. *Proc Natl Acad Sci U S A* **111**, E719-727, doi:10.1073/pnas.1400336111 (2014).
102 Olson, A. L. & Pessin, J. E. Structure, function, and regulation of the mammalian facilitative glucose transporter gene family. *Annual review of nutrition* **16**, 235-256, doi:10.1146/annurev.nu.16.070196.001315 (1996).
103 Deng, D. *et al.* Crystal structure of the human glucose transporter GLUT1. *Nature* **510**, 121, doi:10.1038/nature13306 (2014).
104 Schürmann, A. *et al.* Role of Conserved Arginine and Glutamate Residues on the Cytosolic Surface of Glucose Transporters for Transporter Function. *Biochemistry* **36**, 12897-12902, doi:10.1021/bi971173c (1997).
105 Manolescu, A. R., Witkowska, K., Kinnaird, A., Cessford, T. & Cheeseman, C. Facilitated hexose transporters: new perspectives on form and function. *Physiology (Bethesda, Md.)* **22**, 234-240, doi:10.1152/physiol.00011.2007 (2007).
106 Eales, K. L., Hollinshead, K. E. R. & Tennant, D. A. Hypoxia and metabolic adaptation of cancer cells. *Oncogenesis* **5**, e190, doi:10.1038/oncsis.2015.50 (2016).
107 Lum, J. J. *et al.* The transcription factor HIF-1alpha plays a critical role in the growth factor-dependent regulation of both aerobic and anaerobic glycolysis. *Genes & development* **21**, 1037-1049, doi:10.1101/gad.1529107 (2007).
108 Li, X.-B., Gu, J.-D. & Zhou, Q.-H. Review of aerobic glycolysis and its key enzymes - new targets for lung cancer therapy. *Thoracic cancer* **6**, 17-24, doi:10.1111/1759-7714.12148 (2015).
109 Jing, M., Cheruvu, V. K. & Ismail-Beigi, F. Stimulation of glucose transport in response to activation of distinct AMPK signaling pathways. *American journal of physiology. Cell physiology* **295**, C1071-C1082, doi:10.1152/ajpcell.00040.2008 (2008).
110 Widnell, C. C. Control of glucose transport by GLUT1: Regulated secretion in an unexpected environment. *Bioscience Reports* **15**, 427-443, doi:10.1007/BF01204347 (1995).
111 Zhang, J.-Z., Behrooz, A. & Ismail-Beigi, F. Regulation of glucose transport by hypoxia. *American Journal of Kidney Diseases* **34**, 189-202, doi:10.1016/S0272-6386(99)70131-9 (1999).
112 Behrooz, A. & Ismail-Beigi, F. Dual control of glut1 glucose transporter gene expression by hypoxia and by inhibition of oxidative phosphorylation. *The Journal of biological chemistry* **272**, 5555-5562 (1997).
113 Hoskin, P. J., Sibtain, A., Daley, F. M. & Wilson, G. D. GLUT1 and CAIX as intrinsic markers of hypoxia in bladder cancer: relationship with vascularity and proliferation as predictors of outcome of ARCON. *Br J Cancer* **89**, 1290-1297, doi:10.1038/sj.bjc.6601260 (2003).
114 Airley, R. E. *et al.* GLUT-1 and CAIX as intrinsic markers of hypoxia in carcinoma of the cervix: relationship to pimonidazole binding. *International journal of cancer* **104**, 85-91, doi:10.1002/ijc.10904 (2003).
115 Gillies, R. M., Robinson, S. P., McPhail, L. D., Carter, N. D. & Murray, J. F. Immunohistochemical assessment of intrinsic and extrinsic markers of hypoxia in

reproductive tissue: differential expression of HIF1α and HIF2α in rat oviduct and endometrium. *Journal of Molecular Histology* **42**, 341-354, doi:10.1007/s10735-011-9338-2 (2011).

116 Melstrom, L. G. *et al.* Apigenin inhibits the GLUT-1 glucose transporter and the phosphoinositide 3-kinase/Akt pathway in human pancreatic cancer cells. *Pancreas* **37**, 426-431, doi:10.1097/MPA.0b013e3181735ccb (2008).

117 Volker, H. U. *et al.* Expression of p-AKT characterizes adenoid cystic carcinomas of head and neck with a higher risk for tumor relapses. *Diagnostic pathology* **4**, 18, doi:10.1186/1746-1596-4-18 (2009).

118 Fukuzumi, M., Hamakawa, H., Onishi, A., Sumida, T. & Tanioka, H. Gene expression of GLUT isoforms and VHL in oral squamous cell carcinoma. *Cancer letters* **161**, 133-140 (2000).

119 Ramakrishnan, S. K. *et al.* Loss of von Hippel-Lindau protein (VHL) increases systemic cholesterol levels through targeting hypoxia-inducible factor 2alpha and regulation of bile acid homeostasis. *Molecular and cellular biology* **34**, 1208-1220, doi:10.1128/mcb.01441-13 (2014).

120 Jun, Y. J. *et al.* Clinicopathologic significance of GLUT1 expression and its correlation with Apaf-1 in colorectal adenocarcinomas. *World journal of gastroenterology* **17**, 1866-1873, doi:10.3748/wjg.v17.i14.1866 (2011).

121 Merrall, N. W., Plevin, R. & Gould, G. W. Growth factors, mitogens, oncogenes and the regulation of glucose transport. *Cellular signalling* **5**, 667-675 (1993).

122 Driedger, P. E. & Blumberg, P. M. The effect of phorbol diesters on chicken embryo fibroblasts. *Cancer Res* **37**, 3257-3265 (1977).

123 Flier, J. S., Mueckler, M. M., Usher, P. & Lodish, H. F. Elevated levels of glucose transport and transporter messenger RNA are induced by ras or src oncogenes. *Science (New York, N.Y.)* **235**, 1492 (1987).

124 Birnbaum, M. J., Haspel, H. C. & Rosen, O. M. Transformation of rat fibroblasts by FSV rapidly increases glucose transporter gene transcription. *Science (New York, N.Y.)* **235**, 1495 (1987).

125 Racker, E., Resnick, R. J. & Feldman, R. Glycolysis and methylaminoisobutyrate uptake in rat-1 cells transfected with ras or myc oncogenes. *Proceedings of the National Academy of Sciences* **82**, 3535 (1985).

126 Murakami, T. *et al.* Identification of two enhancer elements in the gene encoding the type 1 glucose transporter from the mouse which are responsive to serum, growth factor, and oncogenes. *Journal of Biological Chemistry* **267**, 9300-9306 (1992).

127 Ebert, B. L., Firth, J. D. & Ratcliffe, P. J. Hypoxia and Mitochondrial Inhibitors Regulate Expression of Glucose Transporter-1 via Distinct Cis-acting Sequences. *Journal of Biological Chemistry* **270**, 29083-29089 (1995).

128 Chen, C., Pore, N., Behrooz, A., Ismail-Beigi, F. & Maity, A. Regulation of glut1 mRNA by Hypoxia-inducible Factor-1: INTERACTION BETWEEN H-ras AND HYPOXIA. *Journal of Biological Chemistry* **276**, 9519-9525 (2001).

129 Janssen, H. L., Haustermans, K. M., Balm, A. J. & Begg, A. C. Hypoxia in head and neck cancer: how much, how important? *Head & neck* **27**, 622-638, doi:10.1002/hed.20223 (2005).

130 Nordsmark, M. *et al.* Prognostic value of tumor oxygenation in 397 head and neck tumors after primary radiation therapy. An international multi-center study. *Radiotherapy and*

oncology : journal of the European Society for Therapeutic Radiology and Oncology **77**, 18-24, doi:10.1016/j.radonc.2005.06.038 (2005).
131 Stadler, P. *et al.* Influence of the hypoxic subvolume on the survival of patients with head and neck cancer. *Int J Radiat Oncol Biol Phys* **44**, 749-754 (1999).
132 Nakajima, E. C. *et al.* Quantifying metabolic heterogeneity in head and neck tumors in real time: 2-DG uptake is highest in hypoxic tumor regions. *PLoS One* **9**, e102452, doi:10.1371/journal.pone.0102452 (2014).
133 Flenley, D. C. Arterial blood gas tensions and pH. *British journal of clinical pharmacology* **9**, 129-135 (1980).
134 Gaertner, F. C., Souvatzoglou, M., Brix, G. & Beer, A. J. Imaging of hypoxia using PET and MRI. *Current pharmaceutical biotechnology* **13**, 552-570 (2012).
135 Stone, H. B., Brown, J. M., Phillips, T. L. & Sutherland, R. M. Oxygen in human tumors: correlations between methods of measurement and response to therapy. Summary of a workshop held November 19-20, 1992, at the National Cancer Institute, Bethesda, Maryland. *Radiat Res* **136**, 422-434 (1993).
136 Shaw, A. D., Li, Z., Thomas, Z. & Stevens, C. W. Assessment of tissue oxygen tension: comparison of dynamic fluorescence quenching and polarographic electrode technique. *Critical care (London, England)* **6**, 76-80 (2002).
137 Vaupel, P., Hockel, M. & Mayer, A. Detection and characterization of tumor hypoxia using pO2 histography. *Antioxid Redox Signal* **9**, 1221-1235, doi:10.1089/ars.2007.1628 (2007).
138 Esipova, T. V. *et al.* Two new "protected" oxyphors for biological oximetry: properties and application in tumor imaging. *Analytical chemistry* **83**, 8756-8765, doi:10.1021/ac2022234 (2011).
139 Wilson, D. F., Lee, W. M., Makonnen, S., Apreleva, S. & Vinogradov, S. A. Oxygen pressures in the interstitial space of skeletal muscle and tumors in vivo. *Advances in experimental medicine and biology* **614**, 53-62, doi:10.1007/978-0-387-74911-2_7 (2008).
140 Boushel, R. *et al.* Monitoring tissue oxygen availability with near infrared spectroscopy (NIRS) in health and disease. *Scandinavian journal of medicine & science in sports* **11**, 213-222 (2001).
141 Zheng, X. *et al.* Hypoxia-specific ultrasensitive detection of tumours and cancer cells in vivo. *Nature communications* **6**, 5834, doi:10.1038/ncomms6834 (2015).
142 Dische, S. *et al.* A comparison of the tumour concentrations obtainable with misonidazole and Ro 03-8799. *Br J Radiol* **59**, 911-917, doi:10.1259/0007-1285-59-705-911 (1986).
143 Varia, M. A. *et al.* Pimonidazole: a novel hypoxia marker for complementary study of tumor hypoxia and cell proliferation in cervical carcinoma. *Gynecologic oncology* **71**, 270-277, doi:10.1006/gyno.1998.5163 (1998).
144 Ragnum, H. B. *et al.* The tumour hypoxia marker pimonidazole reflects a transcriptional programme associated with aggressive prostate cancer. *British journal of cancer* **112**, 382-390, doi:10.1038/bjc.2014.604 (2015).
145 Aguilera, K. Y. & Brekken, R. A. Hypoxia Studies with Pimonidazole in vivo. *Bio-protocol* **4**, e1254 (2014).
146 Wang, W. *et al.* Pharmacokinetic analysis of hypoxia (18)F-fluoromisonidazole dynamic PET in head and neck cancer. *Journal of nuclear medicine : official publication, Society of Nuclear Medicine* **51**, 37-45, doi:10.2967/jnumed.109.067009 (2010).
147 Price, J. M., Robinson, S. P. & Koh, D. M. Imaging hypoxia in tumours with advanced MRI. *The quarterly journal of nuclear medicine and molecular imaging : official*

publication of the Italian Association of Nuclear Medicine (AIMN) [and] the International Association of Radiopharmacology (IAR), [and] Section of the So **57**, 257-270 (2013).
148 Kelada, O. J. & Carlson, D. J. Molecular imaging of tumor hypoxia with positron emission tomography. *Radiation research* **181**, 335-349, doi:10.1667/RR13590.1 (2014).
149 Lopci, E. *et al.* PET radiopharmaceuticals for imaging of tumor hypoxia: a review of the evidence. *American journal of nuclear medicine and molecular imaging* **4**, 365-384 (2014).
150 Fleming, I. N. *et al.* Imaging tumour hypoxia with positron emission tomography. *British Journal Of Cancer* **112**, 238, doi:10.1038/bjc.2014.610 (2014).
151 Laking, G. & Price, P. Radionuclide imaging of perfusion and hypoxia. *Eur J Nucl Med Mol Imaging* **37 Suppl 1**, S20-29, doi:10.1007/s00259-010-1453-x (2010).
152 Rajendran, J. G. *et al.* Tumor hypoxia imaging with [F-18] fluoromisonidazole positron emission tomography in head and neck cancer. *Clinical cancer research : an official journal of the American Association for Cancer Research* **12**, 5435-5441, doi:10.1158/1078-0432.CCR-05-1773 (2006).
153 Eschmann, S. M. *et al.* Prognostic impact of hypoxia imaging with 18F-misonidazole PET in non-small cell lung cancer and head and neck cancer before radiotherapy. *Journal of nuclear medicine : official publication, Society of Nuclear Medicine* **46**, 253-260 (2005).
154 Koh, W. J. *et al.* Evaluation of oxygenation status during fractionated radiotherapy in human nonsmall cell lung cancers using [F-18]fluoromisonidazole positron emission tomography. *Int J Radiat Oncol Biol Phys* **33**, 391-398, doi:10.1016/0360-3016(95)00170-4 (1995).
155 Cheng, J. *et al.* 18F-fluoromisonidazole PET/CT: a potential tool for predicting primary endocrine therapy resistance in breast cancer. *Journal of nuclear medicine : official publication, Society of Nuclear Medicine* **54**, 333-340, doi:10.2967/jnumed.112.111963 (2013).
156 Segard, T. *et al.* Detection of hypoxia with 18F-fluoromisonidazole (18F-FMISO) PET/CT in suspected or proven pancreatic cancer. *Clinical nuclear medicine* **38**, 1-6, doi:10.1097/RLU.0b013e3182708777 (2013).
157 Kim, B. W. *et al.* Prognostic assessment of hypoxia and metabolic markers in cervical cancer using automated digital image analysis of immunohistochemistry. *Journal of translational medicine* **11**, 185, doi:10.1186/1479-5876-11-185 (2013).
158 Rischin, D. *et al.* Prognostic significance of [18F]-misonidazole positron emission tomography-detected tumor hypoxia in patients with advanced head and neck cancer randomly assigned to chemoradiation with or without tirapazamine: a substudy of Trans-Tasman Radiation Oncology Group Study 98.02. *Journal of clinical oncology : official journal of the American Society of Clinical Oncology* **24**, 2098-2104, doi:10.1200/jco.2005.05.2878 (2006).
159 Sorger, D. *et al.* [18F]Fluoroazomycinarabinofuranoside (18FAZA) and [18F]Fluoromisonidazole (18FMISO): a comparative study of their selective uptake in hypoxic cells and PET imaging in experimental rat tumors. *Nucl Med Biol* **30**, 317-326 (2003).
160 Evans, S. M. *et al.* Comparative measurements of hypoxia in human brain tumors using needle electrodes and EF5 binding. *Cancer Res* **64**, 1886-1892 (2004).
161 Komar, G. *et al.* 18F-EF5: a new PET tracer for imaging hypoxia in head and neck cancer. *Journal of nuclear medicine : official publication, Society of Nuclear Medicine* **49**, 1944-1951, doi:10.2967/jnumed.108.053785 (2008).

162 Mahy, P. *et al.* Comparative pharmacokinetics, biodistribution, metabolism and hypoxia-dependent uptake of [18F]-EF3 and [18F]-MISO in rodent tumor models. *Radiotherapy and oncology : journal of the European Society for Therapeutic Radiology and Oncology* **89**, 353-360, doi:10.1016/j.radonc.2008.06.008 (2008).
163 Laughlin, K. M. *et al.* Biodistribution of the nitroimidazole EF5 (2-[2-nitro-1H-imidazol-1-yl]-N-(2,2,3,3,3-pentafluoropropyl) acetamide) in mice bearing subcutaneous EMT6 tumors. *The Journal of pharmacology and experimental therapeutics* **277**, 1049-1057 (1996).
164 Urtasun, R. C. *et al.* Measurement of hypoxia in human tumours by non-invasive spect imaging of iodoazomycin arabinoside. *The British journal of cancer. Supplement* **27**, S209-212 (1996).
165 Stypinski, D. *et al.* Dosimetry estimations for 123I-IAZA in healthy volunteers. *Journal of nuclear medicine : official publication, Society of Nuclear Medicine* **42**, 1418-1423 (2001).
166 Kumar, P., Wiebe, L. I., Atrazheva, E. & Tandon, M. An improved synthesis of α-AZA, α-AZP and α-AZG, the precursors to clinical markers of tissue hypoxia. *Tetrahedron Letters* **42**, 2077-2078, doi:https://doi.org/10.1016/S0040-4039(01)00099-5 (2001).
167 Reischl, G. *et al.* Imaging of tumor hypoxia with [124I]IAZA in comparison with [18F]FMISO and [18F]FAZA--first small animal PET results. *Journal of pharmacy & pharmaceutical sciences : a publication of the Canadian Society for Pharmaceutical Sciences, Societe canadienne des sciences pharmaceutiques* **10**, 203-211 (2007).
168 Souvatzoglou, M. *et al.* Tumour hypoxia imaging with [18F]FAZA PET in head and neck cancer patients: a pilot study. *Eur J Nucl Med Mol Imaging* **34**, 1566-1575, doi:10.1007/s00259-007-0424-3 (2007).
169 Verwer, E. E. *et al.* Parametric methods for quantification of 18F-FAZA kinetics in non-small cell lung cancer patients. *Journal of nuclear medicine : official publication, Society of Nuclear Medicine* **55**, 1772-1777, doi:10.2967/jnumed.114.141846 (2014).
170 Postema, E. J. *et al.* Initial results of hypoxia imaging using 1-alpha-D: -(5-deoxy-5-[18F]-fluoroarabinofuranosyl)-2-nitroimidazole (18F-FAZA). *Eur J Nucl Med Mol Imaging* **36**, 1565-1573, doi:10.1007/s00259-009-1154-5 (2009).
171 Bowen, S. R., van der Kogel, A. J., Nordsmark, M., Bentzen, S. M. & Jeraj, R. Characterization of positron emission tomography hypoxia tracer uptake and tissue oxygenation via electrochemical modeling. *Nuclear medicine and biology* **38**, 771-780, doi:10.1016/j.nucmedbio.2011.02.002 (2011).
172 Gagel, B. *et al.* pO polarography, contrast enhanced color duplex sonography (CDS), [18F] fluoromisonidazole and [18F] fluorodeoxyglucose positron emission tomography: validated methods for the evaluation of therapy-relevant tumor oxygenation or only bricks in the puzzle of tumor hypoxia? *BMC Cancer* **7**, 113, doi:10.1186/1471-2407-7-113 (2007).
173 Gagel, B. *et al.* pO(2) Polarography versus positron emission tomography ([(18)F] fluoromisonidazole, [(18)F]-2-fluoro-2'-deoxyglucose). An appraisal of radiotherapeutically relevant hypoxia. *Strahlentherapie und Onkologie : Organ der Deutschen Rontgengesellschaft ... [et al]* **180**, 616-622, doi:10.1007/s00066-004-1229-y (2004).
174 Zimny, M. *et al.* FDG--a marker of tumour hypoxia? A comparison with [18F]fluoromisonidazole and pO2-polarography in metastatic head and neck cancer. *Eur J Nucl Med Mol Imaging* **33**, 1426-1431, doi:10.1007/s00259-006-0175-6 (2006).

175 Dierckx, R. A. & Van de Wiele, C. FDG uptake, a surrogate of tumour hypoxia? *Eur J Nucl Med Mol Imaging* **35**, 1544-1549, doi:10.1007/s00259-008-0758-5 (2008).
176 Li, X.-F., Du, Y., Ma, Y., Postel, G. C. & Civelek, A. C. (18)F-fluorodeoxyglucose uptake and tumor hypoxia: revisit (18)f-fluorodeoxyglucose in oncology application. *Translational oncology* **7**, 240-247, doi:10.1016/j.tranon.2014.02.010 (2014).
177 Beasley, N. J. *et al.* Hypoxia-inducible factors HIF-1alpha and HIF-2alpha in head and neck cancer: relationship to tumor biology and treatment outcome in surgically resected patients. *Cancer Res* **62**, 2493-2497 (2002).
178 Baba, Y. *et al.* HIF1A overexpression is associated with poor prognosis in a cohort of 731 colorectal cancers. *The American journal of pathology* **176**, 2292-2301, doi:10.2353/ajpath.2010.090972 (2010).
179 Seeber, L. M. *et al.* The role of hypoxia inducible factor-1alpha in gynecological cancer. *Critical reviews in oncology/hematology* **78**, 173-184, doi:10.1016/j.critrevonc.2010.05.003 (2011).
180 Rademakers, S. E., Lok, J., van der Kogel, A. J., Bussink, J. & Kaanders, J. H. Metabolic markers in relation to hypoxia; staining patterns and colocalization of pimonidazole, HIF-1alpha, CAIX, LDH-5, GLUT-1, MCT1 and MCT4. *BMC Cancer* **11**, 167, doi:10.1186/1471-2407-11-167 (2011).
181 Loncaster, J. A. *et al.* Carbonic anhydrase (CA IX) expression, a potential new intrinsic marker of hypoxia: correlations with tumor oxygen measurements and prognosis in locally advanced carcinoma of the cervix. *Cancer Res* **61**, 6394-6399 (2001).
182 Tanaka, N. *et al.* Expression of carbonic anhydrase 9, a potential intrinsic marker of hypoxia, is associated with poor prognosis in oesophageal squamous cell carcinoma. *Br J Cancer* **99**, 1468-1475, doi:10.1038/sj.bjc.6604719 (2008).
183 Chia, S. K. *et al.* Prognostic significance of a novel hypoxia-regulated marker, carbonic anhydrase IX, in invasive breast carcinoma. *Journal of clinical oncology : official journal of the American Society of Clinical Oncology* **19**, 3660-3668, doi:10.1200/jco.2001.19.16.3660 (2001).
184 Ilie, M. *et al.* High levels of carbonic anhydrase IX in tumour tissue and plasma are biomarkers of poor prognostic in patients with non-small cell lung cancer. *Br J Cancer* **102**, 1627-1635, doi:10.1038/sj.bjc.6605690 (2010).
185 E, G. *et al.* Endogenous vascular endothelial growth factor-A (VEGF-A) maintains endothelial cell homeostasis by regulating VEGF receptor-2 transcription. *The Journal of biological chemistry* **287**, 3029-3041, doi:10.1074/jbc.M111.293985 (2012).
186 Kusumanto, Y. H., Meijer, C., Dam, W., Mulder, N. H. & Hospers, G. A. P. Circulating vascular endothelial growth factor (VEGF) levels in advanced stage cancer patients compared to normal controls and diabetes mellitus patients with critical ischemia. *Drug target insights* **2**, 105-109 (2007).
187 Viola, R. J. *et al.* In vivo bioluminescence imaging monitoring of hypoxia-inducible factor 1alpha, a promoter that protects cells, in response to chemotherapy. *AJR. American journal of roentgenology* **191**, 1779-1784, doi:10.2214/ajr.07.4060 (2008).
188 Saha, D. *et al.* In vivo bioluminescence imaging of tumor hypoxia dynamics of breast cancer brain metastasis in a mouse model. *Journal of visualized experiments : JoVE*, 3175, doi:10.3791/3175 (2011).
189 Boerema, I. High Tension Oxygen Therapy: Hyperbaric Oxygen. *Proceedings of the Royal Society of Medicine* **57**, 817-818, doi:10.1177/003591576405700924 (1964).

190 Watson, E. R. *et al.* Hyperbaric oxygen and radiotherapy: a Medical Research Council trial in carcinoma of the cervix. *The British Journal of Radiology* **51**, 879-887, doi:10.1259/0007-1285-51-611-879 (1978).
191 Brady, L. W. *et al.* Hyperbaric oxygen therapy for carcinoma of the cervix—Stages IIB, IIIA, IIIB and IVA: Results of a randomized study by the radiation therapy oncology group. *International Journal of Radiation Oncology • Biology • Physics* **7**, 991-998, doi:10.1016/0360-3016(81)90149-8 (1981).
192 Beppu, T. *et al.* A Phase II Study of Radiotherapy after Hyperbaric Oxygenation Combined with Interferon-beta and Nimustine Hydrochloride to Treat Supratentorial Malignant Gliomas. *Journal of Neuro-Oncology* **61**, 161-170, doi:10.1023/A:1022169107872 (2003).
193 Haffty, B. G., Hurley, R. & Peters, L. J. Radiation therapy with hyperbaric oxygen at 4 atmospheres pressure in the management of squamous cell carcinoma of the head and neck: results of a randomized clinical trial. *Cancer J Sci Am* **5**, 341-347 (1999).
194 Hoskin, P. J., Saunders, M. I. & Dische, S. Hypoxic radiosensitizers in radical radiotherapy for patients with bladder carcinoma. **86**, 1322-1328, doi:doi:10.1002/(SICI)1097-0142(19991001)86:7<1322::AID-CNCR30>3.0.CO;2-E (1999).
195 Stępień, K., Ostrowski, R. P. & Matyja, E. Hyperbaric oxygen as an adjunctive therapy in treatment of malignancies, including brain tumours. *Medical oncology (Northwood, London, England)* **33**, 101-101, doi:10.1007/s12032-016-0814-0 (2016).
196 Horsman, M. R. *et al.* Reducing acute and chronic hypoxia in tumours by combining nicotinamide with carbogen breathing. *Acta oncologica (Stockholm, Sweden)* **33**, 371-376 (1994).
197 Surjana, D., Halliday, G. M. & Damian, D. L. Role of Nicotinamide in DNA Damage, Mutagenesis, and DNA Repair %J Journal of Nucleic Acids. **2010**, 13, doi:10.4061/2010/157591 (2010).
198 Albert, J. M. *et al.* Inhibition of Poly(ADP-Ribose) Polymerase Enhances Cell Death and Improves Tumor Growth Delay in Irradiated Lung Cancer Models. *Clinical Cancer Research* **13**, 3033 (2007).
199 Calabrese, C. R. *et al.* Anticancer Chemosensitization and Radiosensitization by the Novel Poly(ADP-ribose) Polymerase-1 Inhibitor AG14361. *JNCI: Journal of the National Cancer Institute* **96**, 56-67, doi:10.1093/jnci/djh005 (2004).
200 Khan, K. *et al.* Head and neck cancer radiosensitization by the novel poly(ADP-ribose) polymerase inhibitor GPI-15427. **32**, 381-391, doi:doi:10.1002/hed.21195 (2010).
201 Bussink, J. Clinical Outcome and Tumour Microenvironmental Effects of Accelerated Radiotherapy with Carbogen and Nicotinamide. *Acta Oncologica* **38**, 875-882, doi:10.1080/028418699432563 (1999).
202 Saunders, M. & Dische, S. Clinical results of hypoxic cell radiosensitisation from hyperbaric oxygen to accelerated radiotherapy, carbogen and nicotinamide. *The British journal of cancer. Supplement* **27**, S271-S278 (1996).
203 Stern, S. & Guichard, M. Efficacy of agents counteracting hypoxia in fractionated radiation regimes. *Radiotherapy and Oncology* **41**, 143-149, doi:https://doi.org/10.1016/S0167-8140(96)01787-2 (1996).
204 Aquino-Parsons, C., Lim, P., Green, A. & Minchinton, A. I. Carbogen Inhalation in Cervical Cancer: Assessment of Oxygenation Change. *Gynecologic oncology* **74**, 259-264, doi:https://doi.org/10.1006/gyno.1999.5443 (1999).

205 Stüben, G., Stuschke, M., Knühmann, K., Horsman, M. R. & Sack, H. The effect of combined nicotinamide and carbogen treatments in human tumour xenografts: oxygenation and tumour control studies. *Radiotherapy and Oncology* **48**, 143-148, doi:https://doi.org/10.1016/S0167-8140(98)00006-1 (1998).
206 Miralbell, R. *et al.* Accelerated Radiotherapy, Carbogen, and Nicotinamide in Glioblastoma Multiforme: Report of European Organization for Research and Treatment of Cancer Trial 22933. *Journal of Clinical Oncology* **17**, 3143-3149, doi:10.1200/JCO.1999.17.10.3143 (1999).
207 Bernier, J. *et al.* ARCON: accelerated radiotherapy with carbogen and nicotinamide in non small cell lung cancer: a phase I/II study by the EORTC. *Radiotherapy and Oncology* **52**, 149-156, doi:10.1016/S0167-8140(99)00106-1 (1999).
208 Bernier, J. *et al.* ARCON: accelerated radiotherapy with carbogen and nicotinamide in head and neck squamous cell carcinomas. The experience of the Co-operative Group of Radiotherapy of the European Organization for Research and Treatment of Cancer (EORTC). *Radiotherapy and Oncology* **55**, 111-119, doi:10.1016/S0167-8140(00)00165-1 (2000).
209 Simon, J.-M. *et al.* Radiotherapy and chemotherapy with or without carbogen and nicotinamide in inoperable biopsy-proven glioblastoma multiforme. *Radiotherapy and Oncology* **67**, 45-51, doi:10.1016/S0167-8140(03)00007-0 (2003).
210 Janssens, G. O. *et al.* Accelerated Radiotherapy With Carbogen and Nicotinamide for Laryngeal Cancer: Results of a Phase III Randomized Trial. *Journal of Clinical Oncology* **30**, 1777-1783, doi:10.1200/JCO.2011.35.9315 (2012).
211 Adams, G. E. & Cooke, M. S. Electron-affinic sensitization. I. A structural basis for chemical radiosensitizers in bacteria. *International journal of radiation biology and related studies in physics, chemistry, and medicine* **15**, 457-471 (1969).
212 Adams, G. E. *et al.* Electron-affinic sensitization. VII. A correlation between structures, one-electron reduction potentials, and efficiencies of nitroimidazoles as hypoxic cell radiosensitizers. *Radiat Res* **67**, 9-20 (1976).
213 Dische, S. Chemical sensitizers for hypoxic cells: A decade of experience in clinical radiotherapy. *Radiotherapy and Oncology* **3**, 97-115, doi:10.1016/S0167-8140(85)80015-3 (1985).
214 Alper, T. The modification of damage caused by primary ionization of biological targets. *Radiat Res* **5**, 573-586 (1956).
215 Howard-Flanders, P. Effect of oxygen on the radiosensitivity of bacteriophage in the presence of sulphydryl compounds. *Nature* **186**, 485-487 (1960).
216 Chapman, J. D., Greenstock, C. L., Reuvers, A. P., McDonald, E. & Dunlop, I. Radiation chemical studies with nitrofurazone as related to its mechanism of radiosensitization. *Radiat Res* **53**, 190-203 (1973).
217 Wardman, P. Chemical Radiosensitizers for Use in Radiotherapy. *Clinical Oncology* **19**, 397-417, doi:10.1016/j.clon.2007.03.010 (2007).
218 Kizaka-Kondoh, S. & Konse-Nagasawa, H. Significance of nitroimidazole compounds and hypoxia-inducible factor-1 for imaging tumor hypoxia. *Cancer Science* **100**, 1366-1373, doi:10.1111/j.1349-7006.2009.01195.x (2009).
219 Chapman, J. D., Reuvers, A. P. & Borsa, J. Effectiveness of nitrofuran derivatives in sensitizing hypoxic mammalian cells to X rays. *The British Journal of Radiology* **46**, 623-630, doi:10.1259/0007-1285-46-548-623 (1973).

220 Ahn, G. O. & Brown, M. Targeting tumors with hypoxia-activated cytotoxins. *Front Biosci* **12**, 3483-3501 (2007).
221 Kappen, L. S., Lee, T. R., Yang, C. C. & Goldberg, I. H. Oxygen transfer from the nitro group of a nitroaromatic radiosensitizer to a DNA sugar damage product. *Biochemistry* **28**, 4540-4542, doi:10.1021/bi00437a004 (1989).
222 Dische, S., Saunders, M. I., Lee, M. E., Adams, G. E. & Flockhart, I. R. Clinical testing of the radiosensitizer Ro 07-0582: experience with multiple doses. *British journal of cancer* **35**, 567-579 (1977).
223 Urtasun, R. *et al.* Radiation and nitroimidazoles in supratentorial high grade gliomas: a second clinical trial. *British Journal Of Cancer* **46**, 101, doi:10.1038/bjc.1982.171 (1982).
224 Grigsby, P. W. *et al.* Irradiation with or without misonidazole for patients with stages IIIb and IVa carcinoma of the cervix: final results of RTOG 80-05. *International Journal of Radiation Oncology • Biology • Physics* **44**, 513-517, doi:10.1016/S0360-3016(99)00054-1 (1999).
225 Brown, J. M., Yu, N. Y., Brown, D. M. & Lee, W. W. SR-2508: a 2-nitroimidazole amide which should be superior to misonidazole as a radiosensitizer for clinical use. *Int J Radiat Oncol Biol Phys* **7**, 695-703 (1981).
226 Saunders, M. I. *et al.* The clinical testing of Ro 03-8799--pharmacokinetics, toxicology, tissue and tumor concentrations. *Int J Radiat Oncol Biol Phys* **10**, 1759-1763 (1984).
227 Dische, S. *et al.* A trial of Ro 03-8799 (pimonidazole) in carcinoma of the uterine cervix: an interim report from the Medical Research Council Working Party on advanced carcinoma of the cervix. *Radiotherapy and Oncology* **26**, 93-103, doi:https://doi.org/10.1016/0167-8140(93)90089-Q (1993).
228 Urtasun, R. C. *et al.* Intervention with the hypoxic tumor cell sensitizer etanidazole in the combined modality treatment of limited stage small-cell lung cancer. A one-institution study. *International Journal of Radiation Oncology*Biology*Physics* **40**, 337-342, doi:https://doi.org/10.1016/S0360-3016(97)00771-2 (1998).
229 Eschwège, F. *et al.* Results of a european randomized trial of Etanidazole combined with radiotherapy in head and neck carcinomas. *International Journal of Radiation Oncology*Biology*Physics* **39**, 275-281, doi:https://doi.org/10.1016/S0360-3016(97)00327-1 (1997).
230 Overgaard, J. *et al.* A randomized double-blind phase III study of nimorazole as a hypoxic radiosensitizer of primary radiotherapy in supraglottic larynx and pharynx carcinoma. Results of the Danish Head and Neck Cancer Study (DAHANCA) Protocol 5-85. *Radiotherapy and Oncology* **46**, 135-146, doi:https://doi.org/10.1016/S0167-8140(97)00220-X (1998).
231 Overgaard, J. & Horsman, M. R. Modification of hypoxia-induced radioresistance in tumors by the use of oxygen and sensitizers. *Seminars in Radiation Oncology* **6**, 10-21, doi:https://doi.org/10.1016/S1053-4296(96)80032-4 (1996).
232 Bonnet, M. *et al.* Novel nitroimidazole alkylsulfonamides as hypoxic cell radiosensitisers. *Bioorganic & Medicinal Chemistry* **22**, 2123-2132, doi:https://doi.org/10.1016/j.bmc.2014.02.039 (2014).
233 Hong, C. R., Wang, J., Hicks, K. O. & Hay, M. P. in *Tumor Microenvironment.* (eds Constantinos Koumenis, Lisa M. Coussens, Amato Giaccia, & Ester Hammond) 269-290 (Springer International Publishing).

234 Yasui, H. *et al.* Preclinical study on hypoxic radiosensitizing effects of glycididazole in comparison with those of doranidazole in vitro and in vivo. *Oncol Lett* **15**, 1993-1998, doi:10.3892/ol.2017.7481 (2018).
235 Denny, W. A. The role of hypoxia-activated prodrugs in cancer therapy. *The Lancet. Oncology* **1**, 25-29, doi:10.1016/s1470-2045(00)00006-1 (2000).
236 Sun, J. D. *et al.* Selective tumor hypoxia targeting by hypoxia-activated prodrug TH-302 inhibits tumor growth in preclinical models of cancer. *Clin Cancer Res* **18**, 758-770, doi:10.1158/1078-0432.Ccr-11-1980 (2012).
237 Hu, J. *et al.* Targeting the multiple myeloma hypoxic niche with TH-302, a hypoxia-activated prodrug. *Blood* **116**, 1524-1527, doi:10.1182/blood-2010-02-269126 (2010).
238 Phillips, R. M. Targeting the hypoxic fraction of tumours using hypoxia-activated prodrugs. *Cancer Chemotherapy and Pharmacology* **77**, 441-457, doi:10.1007/s00280-015-2920-7 (2016).
239 Lee, C. T., Boss, M. K. & Dewhirst, M. W. Imaging tumor hypoxia to advance radiation oncology. *Antioxid Redox Signal* **21**, 313-337, doi:10.1089/ars.2013.5759 (2014).
240 Foehrenbacher, A., Secomb, T. W., Wilson, W. R. & Hicks, K. O. Design of optimized hypoxia-activated prodrugs using pharmacokinetic/pharmacodynamic modeling. *Front Oncol* **3**, 314, doi:10.3389/fonc.2013.00314 (2013).
241 Foehrenbacher, A. *et al.* The Role of Bystander Effects in the Antitumor Activity of the Hypoxia-Activated Prodrug PR-104. *Front Oncol* **3**, 263, doi:10.3389/fonc.2013.00263 (2013).
242 Hu, J. *et al.* Synergistic induction of apoptosis in multiple myeloma cells by bortezomib and hypoxia-activated prodrug TH-302, in vivo and in vitro. *Molecular cancer therapeutics* **12**, 1763-1773, doi:10.1158/1535-7163.Mct-13-0123 (2013).
243 Liapis, V. *et al.* Hypoxia-activated pro-drug TH-302 exhibits potent tumor suppressive activity and cooperates with chemotherapy against osteosarcoma. *Cancer letters* **357**, 160-169, doi:10.1016/j.canlet.2014.11.020 (2015).
244 Meng, F. *et al.* Enhancement of hypoxia-activated prodrug TH-302 anti-tumor activity by Chk1 inhibition. *BMC Cancer* **15**, 422, doi:10.1186/s12885-015-1387-6 (2015).
245 McKeown, S. R., Hejmadi, M. V., McIntyre, I. A., McAleer, J. J. & Patterson, L. H. AQ4N: an alkylaminoanthraquinone N-oxide showing bioreductive potential and positive interaction with radiation in vivo. *Br J Cancer* **72**, 76-81 (1995).
246 Patterson, L. H. *et al.* Enhancement of chemotherapy and radiotherapy of murine tumours by AQ4N, a bioreductively activated anti-tumour agent. *Br J Cancer* **82**, 1984-1990, doi:10.1054/bjoc.2000.1163 (2000).
247 Abbattista, M. R. *et al.* Pre-clinical activity of PR-104 as monotherapy and in combination with sorafenib in hepatocellular carcinoma. *Cancer biology & therapy* **16**, 610-622, doi:10.1080/15384047.2015.1017171 (2015).
248 Patterson, A. V. *et al.* Mechanism of action and preclinical antitumor activity of the novel hypoxia-activated DNA cross-linking agent PR-104. *Clin Cancer Res* **13**, 3922-3932, doi:10.1158/1078-0432.Ccr-07-0478 (2007).
249 Treat, J. *et al.* Tirapazamine with cisplatin in patients with advanced non-small-cell lung cancer: a phase II study. *Journal of clinical oncology : official journal of the American Society of Clinical Oncology* **16**, 3524-3527, doi:10.1200/jco.1998.16.11.3524 (1998).
250 Marcu, L. & Olver, I. Tirapazamine: from bench to clinical trials. *Current clinical pharmacology* **1**, 71-79 (2006).

251 Guise, C. P. *et al.* Bioreductive prodrugs as cancer therapeutics: targeting tumor hypoxia. *Chinese journal of cancer* **33**, 80-86, doi:10.5732/cjc.012.10285 (2014).
252 Denny, W. A., Wilson, W. R. & Hay, M. P. Recent developments in the design of bioreductive drugs. *The British journal of cancer. Supplement* **27**, S32-38 (1996).
253 Yin, J., Glaser, R. & Gates, K. S. On the reaction mechanism of tirapazamine reduction chemistry: unimolecular N-OH homolysis, stepwise dehydration, or triazene ring-opening. *Chem Res Toxicol* **25**, 634-645, doi:10.1021/tx200546u (2012).
254 Shinde, S. S. *et al.* Characterization of radicals formed following enzymatic reduction of 3-substituted analogues of the hypoxia-selective cytotoxin 3-amino-1,2,4-benzotriazine 1,4-dioxide (tirapazamine). *Journal of the American Chemical Society* **132**, 2591-2599, doi:10.1021/ja908689f (2010).
255 Wilson, W. R. *et al.* Bystander effects of bioreductive drugs: potential for exploiting pathological tumor hypoxia with dinitrobenzamide mustards. *Radiat Res* **167**, 625-636, doi:10.1667/rr0807.1 (2007).
256 Meng, F. *et al.* Molecular and cellular pharmacology of the hypoxia-activated prodrug TH-302. *Molecular cancer therapeutics* **11**, 740-751, doi:10.1158/1535-7163.Mct-11-0634 (2012).
257 Wilson, W. R. & Hay, M. P. Targeting hypoxia in cancer therapy. *Nat Rev Cancer* **11**, 393-410, doi:10.1038/nrc3064 (2011).
258 Wardman, P. Electron transfer and oxidative stress as key factors in the design of drugs selectively active in hypoxia. *Current medicinal chemistry* **8**, 739-761 (2001).
259 Workman, P. Enzyme-directed bioreductive drug development revisited: a commentary on recent progress and future prospects with emphasis on quinone anticancer agents and quinone metabolizing enzymes, particularly DT-diaphorase. *Oncology research* **6**, 461-475 (1994).
260 Lin, A. J., Cosby, L. A., Shansky, C. W. & Sartorelli, A. C. Potential bioreductive alkylating agents. 1. Benzoquinone derivatives. *Journal of medicinal chemistry* **15**, 1247-1252 (1972).
261 Stratford, I. J. & Stephens, M. A. The differential hypoxic cytotoxicity of bioreductive agents determined in vitro by the MTT assay. *International Journal of Radiation Oncology*Biology*Physics* **16**, 973-976, doi:https://doi.org/10.1016/0360-3016(89)90898-5 (1989).
262 Rockwell, S., Keyes, S. R. & Sartorelli, A. C. Preclinical Studies of Porfiromycin as an Adjunct to Radiotherapy. *Radiation Research* **116**, 100-113, doi:10.2307/3577481 (1988).
263 Hendriks, H. R. *et al.* EO9: A novel bioreductive alkylating indoloquinone with preferential solid tumour activity and lack of bone marrow toxicity in preclinical models. *European Journal of Cancer* **29**, 897-906, doi:https://doi.org/10.1016/S0959-8049(05)80434-4 (1993).
264 Adams, G. E., Stratford, I. J., Edwards, H. S., Bremner, J. C. M. & Cole, S. Bioreductive drugs as post-irradiation sensitizers: Comparison of dual function agents with SR 4233 and the mitomycin C analogue EO9. *International Journal of Radiation Oncology*Biology*Physics* **22**, 717-720, doi:https://doi.org/10.1016/0360-3016(92)90510-O (1992).
265 Haffty, B. G. *et al.* Concurrent chemo-radiotherapy with mitomycin C compared with porfiromycin in squamous cell cancer of the head and neck: Final results of a randomized

clinical trial. *International Journal of Radiation Oncology*Biology*Physics* **61**, 119-128, doi:https://doi.org/10.1016/j.ijrobp.2004.07.730 (2005).

266 Phillips, R. M., Hendriks, H. R. & Peters, G. J. EO9 (Apaziquone): from the clinic to the laboratory and back again. *British Journal of Pharmacology* **168**, 11-18, doi:10.1111/j.1476-5381.2012.01996.x (2012).

267 Workman, P., Binger, M. & Kooistra, K. L. Pharmacokinetics, distribution, and metabolism of the novel bioreductive alkylating indoloquinone EO9 in rodents. *International Journal of Radiation Oncology*Biology*Physics* **22**, 713-716, doi:https://doi.org/10.1016/0360-3016(92)90509-G (1992).

268 Moeller, B. J., Richardson, R. A. & Dewhirst, M. W. Hypoxia and radiotherapy: opportunities for improved outcomes in cancer treatment. *Cancer and Metastasis Reviews* **26**, 241-248, doi:10.1007/s10555-007-9056-0 (2007).

269 Palcic, B. & Skarsgard, L. D. Cytotoxicity of misonidazole and DNA damage in hypoxic mammalian cells. *The British journal of cancer. Supplement* **3**, 54-59 (1978).

270 DeGraff, W. G., Russo, A., Friedman, N. & Mitchell, J. B. Misonidazole hypoxic cytotoxicity and chemosensitization in two cell lines with different intracellular glutathione levels. *European journal of cancer (Oxford, England : 1990)* **26**, 17-20 (1990).

271 Jin, C., Bai, L., Wu, H., Tian, F. & Guo, G. Radiosensitization of paclitaxel, etanidazole and paclitaxel+etanidazole nanoparticles on hypoxic human tumor cells in vitro. *Biomaterials* **28**, 3724-3730, doi:https://doi.org/10.1016/j.biomaterials.2007.04.032 (2007).

272 Chapman, J. D., Engelhardt, E. L., Stobbe, C. C., Schneider, R. F. & Hanks, G. E. Measuring hypoxia and predicting tumor radioresistance with nuclear medicine assays. *Radiotherapy and oncology : journal of the European Society for Therapeutic Radiology and Oncology* **46**, 229-237 (1998).

273 Nunn, A., Linder, K. & Strauss, H. W. Nitroimidazoles and imaging hypoxia. *European journal of nuclear medicine* **22**, 265-280 (1995).

274 Arteel, G. E., Thurman, R. G., Yates, J. M. & Raleigh, J. A. Evidence that hypoxia markers detect oxygen gradients in liver: pimonidazole and retrograde perfusion of rat liver. *Br J Cancer* **72**, 889-895 (1995).

275 Russell, J. *et al.* Immunohistochemical detection of changes in tumor hypoxia. *Int J Radiat Oncol Biol Phys* **73**, 1177-1186, doi:10.1016/j.ijrobp.2008.12.004 (2009).

276 Evans, S. M., Jenkins, W. T., Joiner, B., Lord, E. M. & Koch, C. J. 2-Nitroimidazole (EF5) binding predicts radiation resistance in individual 9L s.c. tumors. *Cancer Res* **56**, 405-411 (1996).

277 Raleigh, J. A. *et al.* Hypoxia and vascular endothelial growth factor expression in human squamous cell carcinomas using pimonidazole as a hypoxia marker. *Cancer Res* **58**, 3765-3768 (1998).

278 Duan, J. X. *et al.* Potent and highly selective hypoxia-activated achiral phosphoramidate mustards as anticancer drugs. *Journal of medicinal chemistry* **51**, 2412-2420, doi:10.1021/jm701028q (2008).

279 Guise, C. P. *et al.* The Bioreductive Prodrug PR-104A Is Activated under Aerobic Conditions by Human Aldo-Keto Reductase 1C3. *Cancer Research* **70**, 1573 (2010).

280 McKeage, M. J. *et al.* PR-104 a bioreductive pre-prodrug combined with gemcitabine or docetaxel in a phase Ib study of patients with advanced solid tumours. *BMC Cancer* **12**, 496, doi:10.1186/1471-2407-12-496 (2012).

281 Guise, C. P. *et al.* Identification of human reductases that activate the dinitrobenzamide mustard prodrug PR-104A: a role for NADPH:cytochrome P450 oxidoreductase under hypoxia. *Biochemical pharmacology* **74**, 810-820, doi:10.1016/j.bcp.2007.06.014 (2007).
282 Larue, R. T. *et al.* A phase 1 'window-of-opportunity' trial testing evofosfamide (TH-302), a tumour-selective hypoxia-activated cytotoxic prodrug, with preoperative chemoradiotherapy in oesophageal adenocarcinoma patients. *BMC Cancer* **16**, 644, doi:10.1186/s12885-016-2709-z (2016).
283 Peeters, S. G. J. A. *et al.* TH-302 in Combination with Radiotherapy Enhances the Therapeutic Outcome and Is Associated with Pretreatment [¹⁸F]HX4 Hypoxia PET Imaging. *Clinical Cancer Research* **21**, 2984 (2015).
284 Van Cutsem, E. *et al.* Evofosfamide (TH-302) in combination with gemcitabine in previously untreated patients with metastatic or locally advanced unresectable pancreatic ductal adenocarcinoma: Primary analysis of the randomized, double-blind phase III MAESTRO study. *Journal of Clinical Oncology* **34**, 193-193, doi:10.1200/jco.2016.34.4_suppl.193 (2016).
285 Patterson, L. H. & McKeown, S. R. AQ4N: a new approach to hypoxia-activated cancer chemotherapy. *British Journal Of Cancer* **83**, 1589, doi:10.1054/bjoc.2000.1564 (2000).
286 Albertella, M. R. *et al.* Hypoxia-Selective Targeting by the Bioreductive Prodrug AQ4N in Patients with Solid Tumors: Results of a Phase I Study. *Clinical Cancer Research* **14**, 1096 (2008).
287 Steward, W. P. *et al.* The use of pharmacokinetic and pharmacodynamic end points to determine the dose of AQ4N, a novel hypoxic cell cytotoxin, given with fractionated radiotherapy in a phase I study. *Annals of Oncology* **18**, 1098-1103, doi:10.1093/annonc/mdm120 (2007).
288 Ahn, G. O. *et al.* Radiolytic and cellular reduction of a novel hypoxia-activated cobalt(III) prodrug of a chloromethylbenzindoline DNA minor groove alkylator. *Biochemical pharmacology* **71**, 1683-1694, doi:https://doi.org/10.1016/j.bcp.2006.03.007 (2006).
289 Parker, L. L. *et al.* A Novel Design Strategy for Stable Metal Complexes of Nitrogen Mustards as Bioreductive Prodrugs. *Journal of medicinal chemistry* **47**, 5683-5689, doi:10.1021/jm049866w (2004).
290 Ware, D. C., Palmer, B. D., Wilson, W. R. & Denny, W. A. Hypoxia-selective antitumor agents. 7. Metal complexes of aliphatic mustards as a new class of hypoxia-selective cytotoxins. Synthesis and evaluation of cobalt(III) complexes of bidentate mustards. *Journal of medicinal chemistry* **36**, 1839-1846, doi:10.1021/jm00065a006 (1993).
291 Dubois, L. *et al. Current preclinical and clinical applications of hypoxia PET imaging using 2-nitroimidazoles*. Vol. 59 (2015).
292 Dhani, N. C. *et al.* Analysis of the intra- and intertumoral heterogeneity of hypoxia in pancreatic cancer patients receiving the nitroimidazole tracer pimonidazole. *British Journal Of Cancer* **113**, 864, doi:10.1038/bjc.2015.284
https://www.nature.com/articles/bjc2015284#supplementary-information (2015).
293 Toustrup, K. *et al.* Validation of a 15-gene hypoxia classifier in head and neck cancer for prospective use in clinical trials. *Acta Oncologica* **55**, 1091-1098, doi:10.3109/0284186X.2016.1167959 (2016).

294 Eustace, A. *et al.* A 26-Gene Hypoxia Signature Predicts Benefit from Hypoxia-Modifying Therapy in Laryngeal Cancer but Not Bladder Cancer. *Clinical Cancer Research* **19**, 4879 (2013).
295 Zeman, E. M., Brown, J. M., Lemmon, M. J., Hirst, V. K. & Lee, W. W. SR-4233: a new bioreductive agent with high selective toxicity for hypoxic mammalian cells. *Int J Radiat Oncol Biol Phys* **12**, 1239-1242 (1986).
296 Robbins, R. F. & Schofield, K. 623. Polyazabicyclic compounds. Part II. Further derivatives of benzo-1 : 2 : 4-triazine. *Journal of the Chemical Society (Resumed)*, 3186-3194, doi:10.1039/JR9570003186 (1957).
297 Brown, J. M. Hypoxic cytotoxic agents: a new approach to cancer chemotherapy. *Drug resistance updates : reviews and commentaries in antimicrobial and anticancer chemotherapy* **3**, 7-13, doi:10.1054/drup.2000.0120 (2000).
298 Moriwaki, T. *et al.* Cytotoxicity of Tirapazamine (3-Amino-1,2,4-benzotriazine-1,4-dioxide)-Induced DNA Damage in Chicken DT40 Cells. *Chemical Research in Toxicology* **30**, 699-704, doi:10.1021/acs.chemrestox.6b00417 (2017).
299 DiSilvestro, P. A. *et al.* Phase III Randomized Trial of Weekly Cisplatin and Irradiation Versus Cisplatin and Tirapazamine and Irradiation in Stages IB2, IIA, IIB, IIIB, and IVA Cervical Carcinoma Limited to the Pelvis: A Gynecologic Oncology Group Study. *Journal of Clinical Oncology* **32**, 458-464, doi:10.1200/JCO.2013.51.4265 (2014).
300 Patterson, A. V. *et al.* Overexpression of human NADPH:cytochrome c (P450) reductase confers enhanced sensitivity to both tirapazamine (SR 4233) and RSU 1069. *Br J Cancer* **76**, 1338-1347 (1997).
301 Chinje, E. C. *et al.* Does reductive metabolism predict response to tirapazamine (SR 4233) in human non-small-cell lung cancer cell lines? *Br J Cancer* **81**, 1127-1133, doi:10.1038/sj.bjc.6690819 (1999).
302 Saunders, M. P., Patterson, A. V., Chinje, E. C., Harris, A. L. & Stratford, I. J. NADPH:cytochrome c (P450) reductase activates tirapazamine (SR4233) to restore hypoxic and oxic cytotoxicity in an aerobic resistant derivative of the A549 lung cancer cell line. *Br J Cancer* **82**, 651-656, doi:10.1054/bjoc.1999.0977 (2000).
303 Laderoute, K. R. & Rauth, A. M. Identification of two major reduction products of the hypoxic cell toxin 3-amino-1,2,4-benzotriazine-1,4-dioxide. *Biochemical pharmacology* **35**, 3417-3420 (1986).
304 Laderoute, K., Wardman, P. & Rauth, A. M. Molecular mechanisms for the hypoxia-dependent activation of 3-amino-1,2,4-benzotriazine-1,4-dioxide (SR 4233). *Biochemical pharmacology* **37**, 1487-1495 (1988).
305 Riley, R. J. & Workman, P. DT-diaphorase and cancer chemotherapy. *Biochemical pharmacology* **43**, 1657-1669 (1992).
306 McLane, K. E., Fisher, J. & Ramakrishnan, K. Reductive Drug Metabolism. *Drug Metabolism Reviews* **14**, 741-799, doi:10.3109/03602538308991408 (1983).
307 Elwell, J. H., Siim, B. G., Evans, J. W. & Brown, J. M. Adaptation of human tumor cells to tirapazamine under aerobic conditions: implications of increased antioxidant enzyme activity to mechanism of aerobic cytotoxicity. *Biochemical pharmacology* **54**, 249-257 (1997).
308 Wouters, B. G. *et al.* Mitochondrial dysfunction after aerobic exposure to the hypoxic cytotoxin tirapazamine. *Cancer Res* **61**, 145-152 (2001).

309 Lloyd, R. V., Duling, D. R., Rumyantseva, G. V., Mason, R. P. & Bridson, P. K. Microsomal reduction of 3-amino-1,2,4-benzotriazine 1,4-dioxide to a free radical. *Mol Pharmacol* **40**, 440-445 (1991).
310 Baker, M. A., Zeman, E. M., Hirst, V. K. & Brown, J. M. Metabolism of SR 4233 by Chinese hamster ovary cells: basis of selective hypoxic cytotoxicity. *Cancer Res* **48**, 5947-5952 (1988).
311 Walton, M. I. & Workman, P. Pharmacokinetics and bioreductive metabolism of the novel benzotriazine di-N-oxide hypoxic cell cytotoxin tirapazamine (WIN 59075; SR 4233; NSC 130181) in mice. *The Journal of pharmacology and experimental therapeutics* **265**, 938-947 (1993).
312 Daniels, J. S. & Gates, K. S. DNA Cleavage by the Antitumor Agent 3-Amino-1,2,4-benzotriazine 1,4-Dioxide (SR4233): Evidence for Involvement of Hydroxyl Radical. *Journal of the American Chemical Society* **118**, 3380-3385, doi:10.1021/ja9510774 (1996).
313 Birincioglu, M. *et al.* DNA base damage by the antitumor agent 3-amino-1,2,4-benzotriazine 1,4-dioxide (tirapazamine). *Journal of the American Chemical Society* **125**, 11607-11615, doi:10.1021/ja0352146 (2003).
314 Zagorevskii, D. *et al.* A mass spectrometry study of tirapazamine and its metabolites. insights into the mechanism of metabolic transformations and the characterization of reaction intermediates. *Journal of the American Society for Mass Spectrometry* **14**, 881-892, doi:10.1016/s1044-0305(03)00334-9 (2003).
315 Chowdhury, G., Junnotula, V., Daniels, J. S., Greenberg, M. M. & Gates, K. S. DNA strand damage product analysis provides evidence that the tumor cell-specific cytotoxin tirapazamine produces hydroxyl radical and acts as a surrogate for O(2). *Journal of the American Chemical Society* **129**, 12870-12877, doi:10.1021/ja074432m (2007).
316 Kotandeniya, D., Ganley, B. & Gates, K. S. Oxidative DNA base damage by the antitumor agent 3-amino-1,2,4-benzotriazine 1,4-dioxide (tirapazamine). *Bioorganic & medicinal chemistry letters* **12**, 2325-2329 (2002).
317 Anderson, R. F., Shinde, S. S., Hay, M. P., Gamage, S. A. & Denny, W. A. Activation of 3-amino-1,2,4-benzotriazine 1,4-dioxide antitumor agents to oxidizing species following their one-electron reduction. *Journal of the American Chemical Society* **125**, 748-756, doi:10.1021/ja0209363 (2003).
318 Biedermann, K. A., Wang, J., Graham, R. P. & Brown, J. M. SR 4233 cytotoxicity and metabolism in DNA repair-competent and repair-deficient cell cultures. *British journal of cancer* **63**, 358-362 (1991).
319 Wang, J., Biedermann, K. A. & Brown, J. M. Repair of DNA and chromosome breaks in cells exposed to SR 4233 under hypoxia or to ionizing radiation. *Cancer Res* **52**, 4473-4477 (1992).
320 Delahoussaye, Y. M., Evans, J. W. & Brown, J. M. Metabolism of tirapazamine by multiple reductases in the nucleus. *Biochemical pharmacology* **62**, 1201-1209 (2001).
321 Peters, K. B. & Brown, J. M. Tirapazamine: a hypoxia-activated topoisomerase II poison. *Cancer Res* **62**, 5248-5253 (2002).
322 Jones, G. D. & Weinfeld, M. Dual action of tirapazamine in the induction of DNA strand breaks. *Cancer Res* **56**, 1584-1590 (1996).
323 Daniels, J. S., Gates, K. S., Tronche, C. & Greenberg, M. M. Direct evidence for bimodal DNA damage induced by tirapazamine. *Chem Res Toxicol* **11**, 1254-1257, doi:10.1021/tx980184j (1998).

324 Hwang, J. T., Greenberg, M. M., Fuchs, T. & Gates, K. S. Reaction of the hypoxia-selective antitumor agent tirapazamine with a C1'-radical in single-stranded and double-stranded DNA: the drug and its metabolites can serve as surrogates for molecular oxygen in radical-mediated DNA damage reactions. *Biochemistry* **38**, 14248-14255 (1999).
325 Shi, X., Mandel, S. M. & Platz, M. S. On the mechanism of reaction of radicals with tirapazamine. *Journal of the American Chemical Society* **129**, 4542-4550, doi:10.1021/ja0647405 (2007).
326 Avendaño, C. & Menéndez, J. C. in *Medicinal Chemistry of Anticancer Drugs (Second Edition)* (eds Carmen Avendaño & J. Carlos Menéndez) 133-195 (Elsevier, 2015).
327 Brown, J. M. SR 4233 (tirapazamine): a new anticancer drug exploiting hypoxia in solid tumours. *Br J Cancer* **67**, 1163-1170 (1993).
328 Durand, R. E. & Olive, P. L. Physiologic and cytotoxic effects of tirapazamine in tumor-bearing mice. *Radiation oncology investigations* **5**, 213-219, doi:10.1002/(sici)1520-6823(1997)5:5<213::Aid-roi1>3.0.Co;2-0 (1997).
329 Siim, B. G., Menke, D. R., Dorie, M. J. & Brown, J. M. Tirapazamine-induced cytotoxicity and DNA damage in transplanted tumors: relationship to tumor hypoxia. *Cancer Res* **57**, 2922-2928 (1997).
330 Lartigau, E. & Guichard, M. Does tirapazamine (SR-4233) have any cytotoxic or sensitizing effect on three human tumour cell lines at clinically relevant partial oxygen pressure? *International journal of radiation biology* **67**, 211-216 (1995).
331 Brown, J. M. & Lemmon, M. J. Potentiation by the Hypoxic Cytotoxin SR 4233 of Cell Killing Produced by Fractionated Irradiation of Mouse Tumors. *Cancer Research* **50**, 7745 (1990).
332 Zhang, M. & Stevens, G. Effect of radiation and tirapazamine (SR-4233) on three melanoma cell lines. **8**, 510-516 (1998).
333 Shibata, T. *et al.* Tirapazamine: hypoxic cytotoxicity and interaction with radiation as assessed by the micronucleus assay. *The British journal of cancer. Supplement* **27**, S61-64 (1996).
334 Shibata, T. *et al.* Comparison of in vivo Efficacy of Hypoxic Cytotoxin Tirapazamine and Hypoxic Cell Radiosensitizer KU-2285 in Combination with Single and Fractionated Irradiation. *Japanese Journal of Cancer Research* **87**, 98-104, doi:10.1111/j.1349-7006.1996.tb00206.x (1996).
335 Maxim, P. G. *et al.* Enhanced Effectiveness of Radiochemotherapy with Tirapazamine by Local Application of Electric Pulses to Tumors. *Radiation Research* **162**, 185-193, doi:10.1667/RR3200 (2004).
336 Done, M. J. & Brown, J. M. Tumor-specific, Schedule-dependent Interaction between Tirapazamine (SR 4233) and Cisplatin. *Cancer Research* **53**, 4633 (1993).
337 Kovacs, M. S. *et al.* Cisplatin anti-tumour potentiation by tirapazamine results from a hypoxia-dependent cellular sensitization to cisplatin. *Br J Cancer* **80**, 1245-1251, doi:10.1038/sj.bjc.6690492 (1999).
338 Peters, L. J., Rischin, D., Hicks, R. J., Hughes, P. G. & Sizeland, A. M. 8 Extraordinary tumor control in phase I trial of concurrent tirapazamine cisplatin and radiotherapy for far advanced head and neck cancer. *International Journal of Radiation Oncology • Biology • Physics* **45**, 148-149, doi:10.1016/S0360-3016(99)90026-3 (1999).

339 Craighead, P. S., Pearcey, R. & Stuart, G. A phase I/II evaluation of tirapazamine administered intravenously concurrent with cisplatin and radiotherapy in women with locally advanced cervical cancer. *Int J Radiat Oncol Biol Phys* **48**, 791-795 (2000).
340 Rischin, D. *et al.* Phase I trial of concurrent tirapazamine, cisplatin, and radiotherapy in patients with advanced head and neck cancer. *Journal of clinical oncology : official journal of the American Society of Clinical Oncology* **19**, 535-542, doi:10.1200/jco.2001.19.2.535 (2001).
341 Le, Q. T. *et al.* Phase I study of tirapazamine plus cisplatin/etoposide and concurrent thoracic radiotherapy in limited-stage small cell lung cancer (S0004): a Southwest Oncology Group study. *Clin Cancer Res* **10**, 5418-5424, doi:10.1158/1078-0432.Ccr-04-0436 (2004).
342 Senan, S. *et al.* Phase I and pharmacokinetic study of tirapazamine (SR 4233) administered every three weeks. *Clin Cancer Res* **3**, 31-38 (1997).
343 Reddy, S. B. & Williamson, S. K. Tirapazamine: a novel agent targeting hypoxic tumor cells. *Expert opinion on investigational drugs* **18**, 77-87, doi:10.1517/13543780802567250 (2009).
344 Doherty, N. *et al.* Muscle cramping in phase I clinical trials of tirapazamine (SR 4233) with and without radiation. *Int J Radiat Oncol Biol Phys* **29**, 379-382 (1994).
345 Miller, V. A. *et al.* Phase II study of the combination of the novel bioreductive agent, tirapazamine, with cisplatin in patients with advanced non-small-cell lung cancer. *Annals of Oncology* **8**, 1269-1271, doi:10.1023/A:1008219125746 (1997).
346 Reck, M., von Pawel, J., Nimmermann, C., Groth, G. & Gatzemeier, U. [Phase II-trial of tirapazamine in combination with cisplatin and gemcitabine in patients with advanced non-small-cell-lung-cancer (NSCLC)]. *Pneumologie (Stuttgart, Germany)* **58**, 845-849, doi:10.1055/s-2004-830056 (2004).
347 Lee, D. J. *et al.* Concurrent tirapazamine and radiotherapy for advanced head and neck carcinomas: a Phase II study. *Int J Radiat Oncol Biol Phys* **42**, 811-815 (1998).
348 Bedikian, A. Y. *et al.* Phase II trial of tirapazamine combined with cisplatin in chemotherapy of advanced malignant melanoma. *Annals of oncology : official journal of the European Society for Medical Oncology* **8**, 363-367 (1997).
349 Maluf, F. C. *et al.* Phase II study of tirapazamine plus cisplatin in patients with advanced or recurrent cervical cancer. *International journal of gynecological cancer : official journal of the International Gynecological Cancer Society* **16**, 1165-1171, doi:10.1111/j.1525-1438.2006.00454.x (2006).
350 Covens, A., Blessing, J., Bender, D., Mannel, R. & Morgan, M. A phase II evaluation of tirapazamine plus cisplatin in the treatment of recurrent platinum-sensitive ovarian or primary peritoneal cancer: a Gynecologic Oncology Group study. *Gynecologic oncology* **100**, 586-590, doi:10.1016/j.ygyno.2005.09.032 (2006).
351 Smith, H. O. *et al.* Tirapazamine plus cisplatin in advanced or recurrent carcinoma of the uterine cervix: a Southwest Oncology Group study. *International journal of gynecological cancer : official journal of the International Gynecological Cancer Society* **16**, 298-305, doi:10.1111/j.1525-1438.2006.00339.x (2006).
352 Del Rowe, J. *et al.* Single-arm, open-label phase II study of intravenously administered tirapazamine and radiation therapy for glioblastoma multiforme. *Journal of clinical oncology : official journal of the American Society of Clinical Oncology* **18**, 1254-1259, doi:10.1200/jco.2000.18.6.1254 (2000).

353 Rischin, D. *et al.* Tirapazamine, Cisplatin, and Radiation versus Fluorouracil, Cisplatin, and Radiation in patients with locally advanced head and neck cancer: a randomized phase II trial of the Trans-Tasman Radiation Oncology Group (TROG 98.02). *Journal of clinical oncology : official journal of the American Society of Clinical Oncology* **23**, 79-87, doi:10.1200/jco.2005.01.072 (2005).

354 Le, Q.-T. X. *et al.* Phase II study of tirapazamine, cisplatin, and etoposide and concurrent thoracic radiotherapy for limited-stage small-cell lung cancer: SWOG 0222. *Journal of clinical oncology : official journal of the American Society of Clinical Oncology* **27**, 3014-3019, doi:10.1200/JCO.2008.21.3868 (2009).

355 Pawel, J. *et al. Tirapazamine plus cisplatin versus cisplatin in advanced non-small-cell lung cancer: A report of the international CATAPULT I study group. Cisplatin and Tirapazamine in Subjects with Advanced Previously Untreated Non-Small-Cell Lung Tumors*. Vol. 18 (2000).

356 Shepherd, F. *et al.* Comparison of Tirazone (Tirapazamine) and cisplatin vs. etoposide and cisplatin in advanced non-small cell lung cancer (NSCLC): Final results of the international Phase III CATAPULT II Trial. *Lung Cancer* **29**, 28, doi:10.1016/S0169-5002(00)80087-2 (2000).

357 Shulman, L. N. *et al.* Phase I trial of the hypoxic cell cytotoxin tirapazamine with concurrent radiation therapy in the treatment of refractory solid tumors. *Int J Radiat Oncol Biol Phys* **44**, 349-353 (1999).

358 Williamson, S. *et al. Phase III Trial of Paclitaxel Plus Carboplatin With or Without Tirapazamine in Advanced Non-Small-Cell Lung Cancer: Southwest Oncology Group Trial S0003*. Vol. 23 (2006).

359 Rischin, D. *et al.* Tirapazamine, cisplatin, and radiation versus cisplatin and radiation for advanced squamous cell carcinoma of the head and neck (TROG 02.02, HeadSTART): a phase III trial of the Trans-Tasman Radiation Oncology Group. *Journal of clinical oncology : official journal of the American Society of Clinical Oncology* **28**, 2989-2995, doi:10.1200/jco.2009.27.4449 (2010).

360 Brown, J. M. & Lemmon, M. J. Tumor hypoxia can be exploited to preferentially sensitize tumors to fractionated irradiation. *Int J Radiat Oncol Biol Phys* **20**, 457-461 (1991).

361 Hicks, K. O., Pruijn, F. B., Sturman, J. R., Denny, W. A. & Wilson, W. R. Multicellular Resistance to Tirapazamine Is Due to Restricted Extravascular Transport. *Cancer Research* **63**, 5970 (2003).

362 Hicks, K. O., Fleming, Y., Siim, B. G., Koch, C. J. & Wilson, W. R. Extravascular diffusion of tirapazamine: effect of metabolic consumption assessed using the multicellular layer model. *International Journal of Radiation Oncology • Biology • Physics* **42**, 641-649, doi:10.1016/S0360-3016(98)00268-5 (1998).

363 Kyle, A. H. & Minchinton, A. I. Measurement of delivery and metabolism of tirapazamine to tumour tissue using the multilayered cell culture model. *Cancer Chemother Pharmacol* **43**, 213-220, doi:10.1007/s002800050886 (1999).

364 Hicks, K. O., Siim, B. G., Pruijn, F. B. & Wilson, W. R. Oxygen dependence of the metabolic activation and cytotoxicity of tirapazamine: implications for extravascular transport and activity in tumors. *Radiat Res* **161**, 656-666 (2004).

365 Hicks, K. O. *et al.* Use of Three-Dimensional Tissue Cultures to Model Extravascular Transport and Predict In Vivo Activity of Hypoxia-Targeted Anticancer Drugs. *JNCI: Journal of the National Cancer Institute* **98**, 1118-1128, doi:10.1093/jnci/djj306 (2006).

366 Denny, W. A. & Wilson, W. R. Tirapazamine: a bioreductive anticancer drug that exploits tumour hypoxia. *Expert opinion on investigational drugs* **9**, 2889-2901, doi:10.1517/13543784.9.12.2889 (2000).
367 Hicks, K. O. *et al.* Pharmacokinetic/pharmacodynamic modeling identifies SN30000 and SN29751 as tirapazamine analogues with improved tissue penetration and hypoxic cell killing in tumors. *Clinical cancer research : an official journal of the American Association for Cancer Research* **16**, 4946-4957, doi:10.1158/1078-0432.CCR-10-1439 (2010).
368 Wang, J. *et al.* Identification of one-electron reductases that activate both the hypoxia prodrug SN30000 and diagnostic probe EF5. *Biochemical pharmacology* **91**, 436-446, doi:10.1016/j.bcp.2014.08.003 (2014).
369 Chitneni, S. K. *et al.* 18F-EF5 PET imaging as an early response biomarker for the hypoxia-activated prodrug SN30000 combined with radiation treatment in a non-small cell lung cancer xenograft model. *Journal of nuclear medicine : official publication, Society of Nuclear Medicine* **54**, 1339-1346, doi:10.2967/jnumed.112.116293 (2013).
370 Zhao, P. *et al.* PL-W18O49-TPZ Nanoparticles for Simultaneous Hypoxia-Activated Chemotherapy and Photothermal Therapy. *ACS applied materials & interfaces* **10**, 3405-3413, doi:10.1021/acsami.7b17323 (2018).
371 Chang, J., Ajnai, G. & Lin, P.-Y. P 084 - Therapeutic assessment of tirapazamine-induced oxidative stress on gastric cancers. *Free Radical Biology and Medicine* **108**, S46, doi:https://doi.org/10.1016/j.freeradbiomed.2017.04.169 (2017).
372 Wang, Y. *et al.* Tumor-Penetrating Nanoparticles for Enhanced Anticancer Activity of Combined Photodynamic and Hypoxia-Activated Therapy. *ACS nano* **11**, 2227-2238, doi:10.1021/acsnano.6b08731 (2017).
373 Johnson, K. M., Parsons, Z. D., Barnes, C. L. & Gates, K. S. Toward hypoxia-selective DNA-alkylating agents built by grafting nitrogen mustards onto the bioreductively activated, hypoxia-selective DNA-oxidizing agent 3-amino-1,2,4-benzotriazine 1,4-dioxide (tirapazamine). *The Journal of organic chemistry* **79**, 7520-7531, doi:10.1021/jo501252p (2014).
374 Fuchs, T., Chowdhury, G., Barnes, C. L. & Gates, K. S. 3-amino-1,2,4-benzotriazine 4-oxide: characterization of a new metabolite arising from bioreductive processing of the antitumor agent 3-amino-1,2,4-benzotriazine 1,4-dioxide (tirapazamine). *The Journal of organic chemistry* **66**, 107-114 (2001).
375 Denny, W. A. & Wilson, W. R. Considerations for the design of nitrophenyl mustards as agents with selective toxicity for hypoxic tumor cells. *Journal of medicinal chemistry* **29**, 879-887 (1986).
376 Shi, X., Poole, J. S., Emenike, I., Burdzinski, G. & Platz, M. S. Time-resolved spectroscopy of the excited singlet states of tirapazamine and desoxytirapazamine. *The journal of physical chemistry. A* **109**, 1491-1496, doi:10.1021/jp0457040 (2005).
377 Poole, J. S. *et al.* Photochemical electron transfer reactions of tirapazamine. *Photochemistry and photobiology* **75**, 339-345 (2002).
378 Shen, X. *et al.* Exploiting the Inherent Photophysical Properties of the Major Tirapazamine Metabolite in the Development of Profluorescent Substrates for Enzymes That Catalyze the Bioreductive Activation of Hypoxia-Selective Anticancer Prodrugs. *The Journal of organic chemistry* **83**, 3126-3131, doi:10.1021/acs.joc.7b03035 (2018).

379 Mosmann, T. Rapid colorimetric assay for cellular growth and survival: Application to proliferation and cytotoxicity assays. *Journal of Immunological Methods* **65**, 55-63, doi:https://doi.org/10.1016/0022-1759(83)90303-4 (1983).
380 Pfaffl, M. W. A new mathematical model for relative quantification in real-time RT-PCR. *Nucleic acids research* **29**, e45 (2001).
381 Warburg, O. On the origin of cancer cells. *Science (New York, N.Y.)* **123**, 309-314 (1956).
382 Hanahan, D. & Weinberg, R. A. The hallmarks of cancer. *Cell* **100**, 57-70 (2000).
383 Hanahan, D. & Weinberg, R. A. Hallmarks of cancer: the next generation. *Cell* **144**, 646-674, doi:10.1016/j.cell.2011.02.013 (2011).
384 Ouiddir, A., Planès, C., Fernandes, I., VanHesse, A. & Clerici, C. Hypoxia Upregulates Activity and Expression of the Glucose Transporter GLUT1 in Alveolar Epithelial Cells. **21**, 710-718, doi:10.1165/ajrcmb.21.6.3751 (1999).
385 Nagasawa, H. *et al.* Antiangiogenic hypoxic cytotoxin TX-402 inhibits hypoxia-inducible factor 1 signaling pathway. *Anticancer Res* **23**, 4427-4434 (2003).
386 Kumar, P. *et al.* Design, Synthesis, and Preliminary Biological Evaluation of 6-O-Glucose–Azomycin Adducts for Diagnosis and Therapy of Hypoxic Tumors. *Journal of medicinal chemistry* **55**, 6033-6046, doi:10.1021/jm2017336 (2012).
387 Gynther, M. *et al.* Glucose promoiety enables glucose transporter mediated brain uptake of ketoprofen and indomethacin prodrugs in rats. *Journal of medicinal chemistry* **52**, 3348-3353, doi:10.1021/jm8015409 (2009).
388 Barros, L. F. *et al.* Kinetic validation of 6-NBDG as a probe for the glucose transporter GLUT1 in astrocytes. *Journal of neurochemistry* **109 Suppl 1**, 94-100, doi:10.1111/j.1471-4159.2009.05885.x (2009).
389 Ampferl, R., Rodemann, H. P., Mayer, C., Hofling, T. T. A. & Dittmann, K. Glucose starvation impairs DNA repair in tumour cells selectively by blocking histone acetylation. *Radiotherapy and oncology : journal of the European Society for Therapeutic Radiology and Oncology* **126**, 465-470, doi:10.1016/j.radonc.2017.10.020 (2018).
390 Zhang, J. *et al.* Suppression of hypoxia-inducible factor 1alpha (HIF-1alpha) by tirapazamine is dependent on eIF2alpha phosphorylation rather than the mTORC1/4E-BP1 pathway. *PLoS One* **5**, e13910, doi:10.1371/journal.pone.0013910 (2010).
391 Rostovtsev, V. V., Green, L. G., Fokin, V. V. & Sharpless, K. B. A stepwise huisgen cycloaddition process: copper(I)-catalyzed regioselective "ligation" of azides and terminal alkynes. *Angewandte Chemie (International ed. in English)* **41**, 2596-2599, doi:10.1002/1521-3773(20020715)41:14<2596::Aid-anie2596>3.0.Co;2-4 (2002).
392 Huisgen, R., Szeimies, G. & Möbius, L. 1.3-Dipolare Cycloadditionen, XXXII. Kinetik der Additionen organischer Azide an CC-Mehrfachbindungen. **100**, 2494-2507, doi:doi:10.1002/cber.19671000806 (1967).
393 Hein, J. E. & Fokin, V. V. Copper-catalyzed azide-alkyne cycloaddition (CuAAC) and beyond: new reactivity of copper(I) acetylides. *Chemical Society reviews* **39**, 1302-1315, doi:10.1039/b904091a (2010).
394 Jeanquartier, F., Jean-Quartier, C. & Holzinger, A. Integrated web visualizations for protein-protein interaction databases. *BMC bioinformatics* **16**, 195-195, doi:10.1186/s12859-015-0615-z (2015).
395 Szklarczyk, D. *et al.* The STRING database in 2017: quality-controlled protein-protein association networks, made broadly accessible. *Nucleic acids research* **45**, D362-D368, doi:10.1093/nar/gkw937 (2017).

396 Szklarczyk, D. *et al.* STRING v10: protein-protein interaction networks, integrated over the tree of life. *Nucleic acids research* **43**, D447-D452, doi:10.1093/nar/gku1003 (2015).
397 Kerrien, S. *et al.* The IntAct molecular interaction database in 2012. *Nucleic acids research* **40**, D841-846, doi:10.1093/nar/gkr1088 (2012).
398 Schaefer, M. H. *et al.* HIPPIE: Integrating protein interaction networks with experiment based quality scores. *PLoS One* **7**, e31826, doi:10.1371/journal.pone.0031826 (2012).
399 Licata, L. *et al.* MINT, the molecular interaction database: 2012 update. *Nucleic acids research* **40**, D857-861, doi:10.1093/nar/gkr930 (2012).
400 Luo, Q., Pagel, P., Vilne, B. & Frishman, D. DIMA 3.0: Domain Interaction Map. *Nucleic acids research* **39**, D724-729, doi:10.1093/nar/gkq1200 (2011).
401 Niu, Y., Otasek, D. & Jurisica, I. Evaluation of linguistic features useful in extraction of interactions from PubMed; application to annotating known, high-throughput and predicted interactions in I2D. *Bioinformatics (Oxford, England)* **26**, 111-119, doi:10.1093/bioinformatics/btp602 (2010).
402 Lewis, A. C., Saeed, R. & Deane, C. M. Predicting protein-protein interactions in the context of protein evolution. *Molecular bioSystems* **6**, 55-64, doi:10.1039/b916371a (2010).
403 Patra, M., Awuah, S. G. & Lippard, S. J. Chemical Approach to Positional Isomers of Glucose–Platinum Conjugates Reveals Specific Cancer Targeting through Glucose-Transporter-Mediated Uptake in Vitro and in Vivo. *Journal of the American Chemical Society* **138**, 12541-12551, doi:10.1021/jacs.6b06937 (2016).
404 Sano, D. & Myers, J. N. Xenograft models of head and neck cancers. *Head & neck oncology* **1**, 32-32, doi:10.1186/1758-3284-1-32 (2009).
405 Killion, J. J., Radinsky, R. & Fidler, I. J. Orthotopic models are necessary to predict therapy of transplantable tumors in mice. *Cancer Metastasis Rev* **17**, 279-284 (1998).
406 Sano, D. *et al.* Targeted molecular therapy of head and neck squamous cell carcinoma with the tyrosine kinase inhibitor vandetanib in a mouse model. *Head & neck* **33**, 349-358, doi:10.1002/hed.21455 (2011).
407 Sano, D. *et al.* Disruptive TP53 mutation is associated with aggressive disease characteristics in an orthotopic murine model of oral tongue cancer. *Clinical cancer research : an official journal of the American Association for Cancer Research* **17**, 6658-6670, doi:10.1158/1078-0432.CCR-11-0046 (2011).
408 Tuttle, S. *et al.* The chemopreventive and clinically used agent curcumin sensitizes HPV (-) but not HPV (+) HNSCC to ionizing radiation, in vitro and in a mouse orthotopic model. *Cancer biology & therapy* **13**, 575-584, doi:10.4161/cbt.19772 (2012).

APPENDIX-A

Table A1: LC-MS/MS analysis for hypoxic whole cell clicked lysate (expanded table)

Accession	Description	Score	Coverage	# Proteins	#Unique Peptides	# Peptides	# PSMs	# AAs	MW [kDa]	calc. pI
Q9BQE3	Tubulin alpha-1C chain	278.57	60.36	2	3	18	164	449	49.9	5.10
Q09666	Neuroblast differentiation-associated protein AHNAK	195.14	33.94	1	92	100	176	5890	628.7	6.15
P78371	T-complex protein 1 subunit beta	159.23	57.01	1	23	23	93	535	57.5	6.46
Q9BUF5	Tubulin beta-6 chain	125.93	41.48	1	9	13	83	446	49.8	4.88
P78527	DNA-dependent protein kinase catalytic subunit	124.97	19.16	1	61	61	91	4128	468.8	7.12
O43707	Alpha-actinin-4	124.93	42.26	1	18	31	98	911	104.8	5.44
P68032	Actin, alpha cardiac muscle 1	121.08	46.68	1	3	12	151	377	42.0	5.39
Q14204	Cytoplasmic dynein 1 heavy chain 1	103.32	16.44	1	54	55	82	4646	532.1	6.40
O75369	Filamin-B	97.50	26.56	1	40	43	76	2602	278.0	5.73
P54652	Heat shock-related 70 kDa protein 2	94.35	19.72	1	3	12	81	639	70.0	5.74
P34932	Heat shock 70 kDa protein 4	90.21	32.50	1	20	21	54	840	94.3	5.19
P18206	Vinculin	90.20	36.24	1	30	30	67	1134	123.7	5.66
P46940	Ras GTPase-activating-like protein IQGAP1	90.18	31.93	1	38	38	77	1657	189.1	6.48
P22102	Trifunctional purine biosynthetic protein adenosine-3	88.07	33.37	1	25	25	57	1010	107.7	6.70
B7ZAR1	T-complex protein 1 subunit	87.76	46.72	3	14	15	57	503	55.3	5.48
P11413	Glucose-6-phosphate 1-dehydrogenase	86.32	48.93	1	19	19	69	515	59.2	6.84
Q02878	60S ribosomal protein L6	83.85	36.46	1	9	9	45	288	32.7	10.58
P19338	Nucleolin	80.66	22.82	1	15	15	61	710	76.6	4.70
P05783	Keratin, type I cytoskeletal 18	80.61	39.30	1	13	14	63	430	48.0	5.45
P42704	Leucine-rich PPR motif-containing protein, mitochondrial [LPPRC_HUMAN]	78.96	29.91	1	29	29	64	1394	157.8	6.13
P05787	Keratin, type II cytoskeletal 8	78.80	39.96	1	18	20	58	483	53.7	5.59
P22314	Ubiquitin-like modifier-activating enzyme 1	76.86	31.29	1	19	19	62	1058	117.8	5.76
O75533	Splicing factor 3B subunit 1 [SF3B1_HUMAN]	68.05	23.85	1	23	23	48	1304	145.7	7.09
Q01518	Adenylyl cyclase-associated protein 1 GN=CAP1 PE=1 SV=5	67.59	30.32	1	13	13	49	475	51.9	8.06

Accession	Description	Score	Coverage	# Proteins	#Unique Peptides	# Peptides	# PSMs	# AAs	MW [kDa]	calc. pI
P04843	Dolichyl-diphosphooligosaccharide--protein glycosyltransferase subunit 1	66.25	33.11	1	14	14	47	607	68.5	6.38
Q14974	Importin subunit beta-1	66.05	19.52	1	13	13	45	876	97.1	4.78
P30101	Protein disulfide-isomerase A3	65.34	38.02	1	17	17	47	505	56.7	6.35
P17066	Heat shock 70 kDa protein 6	64.01	23.79	1	1	12	46	643	71.0	6.14
P08727	Keratin, type I cytoskeletal 19	63.82	55.50	1	11	18	48	400	44.1	5.14
A6NLN1	Polypyrimidine tract binding protein 1, isoform CRA_b	62.96	35.10	3	9	9	47	527	56.5	9.38
P26639	Threonine--tRNA ligase, cytoplasmic	62.89	20.47	1	14	14	60	723	83.4	6.67
P13010	X-ray repair cross-complementing protein 5	62.71	32.92	1	16	16	50	732	82.7	5.81
P05023	Sodium/potassium-transporting ATPase subunit alpha-1	61.26	27.86	1	20	20	37	1023	112.8	5.49
P63241	Eukaryotic translation initiation factor 5A-1	59.15	61.69	1	9	9	61	154	16.8	5.24
Q16658	Fascin	58.89	35.50	1	11	11	36	493	54.5	7.24
P37802	Transgelin-2	57.76	63.82	2	10	11	39	199	22.4	8.25
P07814	Bifunctional glutamate/proline--tRNA ligase	56.11	23.61	1	24	24	40	1512	170.5	7.33
P49321	Nuclear autoantigenic sperm	55.82	24.75	1	11	11	35	788	85.2	4.30
A0A087WSW9	Thioredoxin reductase 1, cytoplasmic	55.66	41.79	3	13	13	36	548	60.0	6.68
P06748	Nucleophosmin	55.44	28.57	1	6	6	32	294	32.6	4.78
P40227	T-complex protein 1 subunit zeta	54.79	50.09	1	18	19	57	531	58.0	6.68
P55072	Transitional endoplasmic reticulum ATPase	54.61	31.27	1	18	18	53	806	89.3	5.26
P40926	Malate dehydrogenase, mitochondrial	53.50	36.69	1	9	9	35	338	35.5	8.68
P22626	Heterogeneous nuclear ribonucleoproteins A2/B1	53.33	34.28	1	11	12	32	353	37.4	8.95
P30153	Serine/threonine-protein phosphatase 2A 65 kDa regulatory subunit A alpha isoform	51.23	18.85	1	10	10	33	589	65.3	5.11
E9PDF6	Unconventional myosin-Ib	50.69	24.48	2	18	18	35	1107	128.4	9.31

Accession	Description	Score	Coverage	# Proteins	#Unique Peptides	# Peptides	# PSMs	# AAs	MW [kDa]	calc. pI
A0A087WTT1	Polyadenylate-binding protein]	50.36	30.84	2	9	13	35	522	58.5	9.26
P13929	Beta-enolase	49.11	19.35	1	1	5	33	434	47.0	7.71
E9PK01	Elongation factor 1-delta (Fragment)	48.88	32.57	11	6	6	26	261	28.8	5.02
P60842	Eukaryotic initiation factor 4A-I	48.33	48.28	1	7	13	38	406	46.1	5.48
P31150	Rab GDP dissociation inhibitor alpha	48.01	35.12	1	5	11	27	447	50.6	5.14
P18669	Phosphoglycerate mutase 1	47.48	69.29	1	13	13	31	254	28.8	7.18
Q9Y490	Talin-1	47.32	15.27	1	22	22	30	2541	269.6	6.07
Q14697	Neutral alpha-glucosidase AB	47.10	29.34	1	19	19	47	944	106.8	6.14
P63244	Receptor of activated protein C kinase 1	47.09	62.78	1	12	12	32	317	35.1	7.69
Q15149	Plectin	46.76	9.93	1	34	35	37	4684	531.5	5.96
A0A0A0MSQ0	Plastin-3	45.96	34.20	2	10	15	38	617	69.3	5.94
Q9NZM1	Myoferlin	45.46	16.50	1	25	25	34	2061	234.6	6.18
Q00839	Heterogeneous nuclear ribonucleoprotein U	45.25	19.15	1	10	11	35	825	90.5	6.00
P47895	Aldehyde dehydrogenase family 1 member A3	45.23	27.73	1	14	14	40	512	56.1	7.25
P55060	Exportin-2	45.16	27.19	1	19	19	46	971	110.3	5.77
Q9UL46	Proteasome activator complex subunit 2	44.93	46.44	2	8	8	28	239	27.4	5.73
P09972	Fructose-bisphosphate aldolase C	44.49	41.21	2	5	10	28	364	39.4	6.87
Q7KZF4	Staphylococcal nuclease domain-containing protein 1	44.36	31.10	1	19	20	42	910	101.9	7.17
P53396	ATP-citrate synthase	43.93	23.34	1	17	17	38	1101	120.8	7.33
P05141	ADP/ATP translocase 2	43.69	37.58	1	5	9	38	298	32.8	9.69
B4DY09	Interleukin enhancer-binding factor 2	43.54	32.95	2	7	7	24	352	38.9	4.94
P31947	14-3-3 protein sigma	43.01	66.94	1	11	12	32	248	27.8	4.74
Q32Q12	Nucleoside diphosphate kinase	43.01	55.14	1	8	8	46	292	32.6	8.48
P35580	Myosin-10	42.46	11.39	1	9	16	33	1976	228.9	5.54
Q99832	T-complex protein 1 subunit eta	42.44	46.96	1	18	18	50	543	59.3	7.65
P34897	Serine hydroxymethyltransferase, mitochondrial	42.36	36.11	1	13	13	34	504	56.0	8.53
A0A087WWU8	Tropomyosin alpha-3 chain	41.83	24.23	2	5	9	18	227	26.4	4.78

Accession	Description	Score	Coverage	# Proteins	#Unique Peptides	# Peptides	# PSMs	# AAs	MW [kDa]	calc. pI
G5E972	Lamina-associated polypeptide 2, isoforms beta/gamma	41.79	29.23	2	2	7	25	414	46.3	9.03
P36578	60S ribosomal protein L4	41.71	34.19	1	14	14	29	427	47.7	11.06
Q08211	ATP-dependent RNA helicase A	41.52	17.09	1	15	15	29	1270	140.9	6.84
Q96QK1	Vacuolar protein sorting-associated protein 35	41.05	25.25	1	16	16	41	796	91.6	5.49
Q86VP6	Cullin-associated NEDD8-dissociated protein 1	40.84	16.50	1	14	14	36	1230	136.3	5.78
P17987	T-complex protein 1 subunit alpha	40.70	52.34	1	19	19	42	556	60.3	6.11
P62979	Ubiquitin-40S ribosomal protein S27a	40.45	44.87	1	6	6	26	156	18.0	9.64
P36871	Phosphoglucomutase-1	40.00	30.60	1	9	9	26	562	61.4	6.76
A0A087X054	Hypoxia up-regulated protein 1	39.90	22.09	2	15	15	28	937	104.7	5.72
Q13200	26S proteasome non-ATPase regulatory subunit 2	39.85	27.20	1	13	13	35	908	100.1	5.20
P30048	Thioredoxin-dependent peroxide reductase, mitochondrial	39.83	40.23	1	7	7	26	256	27.7	7.78
P20618	Proteasome subunit beta type-1	39.59	43.57	1	7	7	28	241	26.5	8.13
Q15029	116 kDa U5 small nuclear ribonucleoprotein component	39.36	16.87	1	11	12	23	972	109.4	5.00
P32119	Peroxiredoxin-2	39.28	31.82	1	4	5	19	198	21.9	5.97
P61204	ADP-ribosylation factor 3	39.12	59.67	2	5	10	27	181	20.6	7.43
Q8TEX9	Importin-4	39.10	17.48	1	13	13	26	1081	118.6	4.96
O60701	UDP-glucose 6-dehydrogenase	39.00	40.28	1	13	13	30	494	55.0	7.12
O75643	U5 small nuclear ribonucleoprotein 200 kDa helicase	38.37	11.99	1	19	19	29	2136	244.4	6.06
P51149	Ras-related protein Rab-7a	37.76	43.48	1	8	8	19	207	23.5	6.70
P31946	14-3-3 protein beta/alpha	37.59	46.34	1	7	9	31	246	28.1	4.83
P08758	Annexin A5	37.51	57.81	1	16	16	41	320	35.9	5.05
P26038	Moesin	37.40	32.41	1	10	15	31	577	67.8	6.40
P67809	Nuclease-sensitive element-binding protein 1	37.35	38.27	1	7	7	18	324	35.9	9.88
P36957	Dihydrolipoyllysine-residue succinyltransferase component of 2-oxoglutarate	37.01	18.10	1	7	7	20	453	48.7	8.95

Accession	Description	Score	Coverage	# Proteins	#Unique Peptides	# Peptides	# PSMs	# AAs	MW [kDa]	calc. pI
	dehydrogenase complex, mitochondrial									
H0Y4R1	Inosine-5'-monophosphate dehydrogenase 2 (Fragment)	36.52	22.98	2	10	10	27	470	51.0	8.18
P49588	Alanine--tRNA ligase, cytoplasmic	36.39	20.14	1	13	13	29	968	106.7	5.53
Q92616	eIF-2-alpha kinase activator GCN1	36.38	11.98	1	20	20	34	2671	292.6	7.47
O60814	Histone H2B type 1-K	36.02	19.84	10	2	2	35	126	13.9	10.32
O60506	Heterogeneous nuclear ribonucleoprotein Q	36.00	26.00	1	12	15	37	623	69.6	8.59
P31939	Bifunctional purine biosynthesis protein PURH	35.65	26.69	1	10	10	24	592	64.6	6.71
Q8WUM4	Programmed cell death 6-interacting protein	35.55	17.63	1	12	12	24	868	96.0	6.52
P13647	Keratin, type II cytoskeletal 5	35.31	21.19	1	8	11	27	590	62.3	7.74
H0YNW5	Deoxyuridine 5'-triphosphate nucleotidohydrolase, mitochondrial	34.81	46.71	3	6	6	19	167	17.8	7.28
H0Y8E6	DNA helicase (Fragment)	34.72	21.65	2	13	13	26	836	94.0	6.24
Q92945	Far upstream element-binding protein 2	34.70	24.33	1	11	11	23	711	73.1	7.30
E7EX73	Eukaryotic translation initiation factor 4 gamma 1	34.69	17.76	4	18	18	39	1436	158.5	5.21
Q12931	Heat shock protein 75 kDa, mitochondrial	34.66	29.26	1	11	12	23	704	80.1	8.21
P54886	Delta-1-pyrroline-5-carboxylate synthase	34.59	17.74	1	10	10	22	795	87.2	7.12
P13645	Keratin, type I cytoskeletal 10	34.45	28.08	1	8	10	38	584	58.8	5.21
C9JMC5	Aldehyde dehydrogenase, dimeric NADP-preferring (Fragment)	34.37	24.73	4	7	7	28	372	41.6	5.31
D6RG13	40S ribosomal protein S3a (Fragment)	34.33	38.57	2	8	8	26	223	25.6	9.66
P09661	U2 small nuclear ribonucleoprotein A'	34.28	42.35	1	9	9	21	255	28.4	8.62
O14980	Exportin-1	34.24	20.82	1	15	15	35	1071	123.3	6.06
P00491	Purine nucleoside phosphorylase	34.16	42.21	1	8	8	21	289	32.1	6.95
P62701	40S ribosomal protein S4, X isoform	33.90	37.26	1	9	9	25	263	29.6	10.15
P42166	Lamina-associated polypeptide 2, isoform alpha	33.64	18.73	1	3	8	22	694	75.4	7.66

Accession	Description	Score	Coverage	# Proteins	#Unique Peptides	# Peptides	# PSMs	# AAs	MW [kDa]	calc. pI
P17655	Calpain-2 catalytic subunit	33.58	17.43	1	8	8	18	700	79.9	4.98
Q14152	Eukaryotic translation initiation factor 3 subunit A	33.15	14.91	1	17	19	37	1382	166.5	6.79
P20700	Lamin-B1	32.72	29.35	1	13	13	23	586	66.4	5.16
Q96AE4	Far upstream element-binding protein 1	32.46	20.34	2	10	10	22	644	67.5	7.61
Q9Y265	RuvB-like 1	32.38	22.37	1	7	7	20	456	50.2	6.42
A0A140T936	Valine--tRNA ligase (Fragment)	32.03	14.29	2	11	11	20	1183	131.9	7.49
Q15393	Splicing factor 3B subunit 3	31.76	16.52	1	13	13	21	1217	135.5	5.26
P62191	26S protease regulatory subunit 4	31.75	18.18	1	4	5	17	440	49.2	6.21
P04264	Keratin, type II cytoskeletal 1	31.67	23.60	1	13	15	30	644	66.0	8.12
Q9UJZ1	Stomatin-like protein 2, mitochondrial	31.35	42.98	1	10	10	21	356	38.5	7.39
Q04695	Keratin, type I cytoskeletal 17	31.29	46.06	1	11	16	31	432	48.1	5.02
Q9NY33	Dipeptidyl peptidase 3	31.23	24.29	3	11	11	20	737	82.5	5.10
M0R0F0	40S ribosomal protein S5 (Fragment)	31.06	43.50	2	6	7	21	200	22.4	9.55
O00410	Importin-5	30.71	15.13	2	10	10	34	1097	123.5	4.94
J3KR24	Isoleucine--tRNA ligase, cytoplasmic	30.49	14.50	3	15	15	20	1152	131.7	6.11
Q9NTK5	Obg-like ATPase 1	30.26	30.56	2	8	8	26	396	44.7	7.81
O15067	Phosphoribosylformylglycinamidine synthase	30.13	14.05	1	12	12	18	1338	144.6	5.76
Q99986	Serine/threonine-protein kinase VRK1	29.94	30.81	1	8	8	18	396	45.4	8.91
Q15181	Inorganic pyrophosphatase	29.87	32.53	1	6	6	19	289	32.6	5.86
P49591	Serine--tRNA ligase, cytoplasmic	29.86	25.68	2	10	10	25	514	58.7	6.43
P62333	26S protease regulatory subunit 10B	29.74	31.88	2	9	9	26	389	44.1	7.49
E9PK47	Alpha-1,4 glucan phosphorylase	29.62	16.24	2	7	10	23	819	94.0	7.31
J3KTF8	Rho GDP-dissociation inhibitor 1 (Fragment)	29.43	27.98	3	5	5	20	193	21.5	5.49
P35241	Radixin	29.34	18.18	1	4	9	22	583	68.5	6.37
P46783	40S ribosomal protein S10	29.21	32.73	1	5	5	21	165	18.9	10.15
Q99497	Protein deglycase DJ-1	29.19	56.08	1	9	9	28	189	19.9	6.79
P27695	DNA-(apurinic or apyrimidinic site) lyase	29.00	38.05	1	8	8	23	318	35.5	8.12

Accession	Description	Score	Coverage	# Proteins	#Unique Peptides	# Peptides	# PSMs	# AAs	MW [kDa]	calc. pI
E9PCY7	Heterogeneous nuclear ribonucleoprotein H	28.93	22.14	3	4	5	17	429	47.1	6.34
J3KTA4	Probable ATP-dependent RNA helicase DDX5	28.62	23.45	2	7	12	23	614	69.0	8.85
Q7Z406	Myosin-14	28.53	6.32	1	4	9	24	1995	227.7	5.60
A0A0D9SFB3	ATP-dependent RNA helicase DDX3X	28.49	15.78	4	6	7	15	640	70.8	7.36
Q96KP4	Cytosolic non-specific dipeptidase	28.12	26.11	1	9	9	20	475	52.8	5.97
P15559	NAD(P)H dehydrogenase [quinone] 1	27.78	40.15	1	9	9	18	274	30.8	8.88
Q9H0U4	Ras-related protein Rab-1B	27.74	62.69	1	7	9	25	201	22.2	5.73
E9PM69	26S protease regulatory subunit 6A	27.68	39.80	3	12	12	28	397	44.3	5.05
P61160	Actin-related protein 2	27.65	34.01	1	10	10	20	394	44.7	6.74
Q86UP2	Kinectin	27.64	20.04	1	20	20	28	1357	156.2	5.64
P62081	40S ribosomal protein S7	27.58	31.44	2	5	5	17	194	22.1	10.10
P50454	Serpin H1	27.01	27.75	1	7	7	16	418	46.4	8.69
B4DXW1	Actin-related protein 3	26.92	25.07	2	7	7	13	367	42.0	5.62
P40939	Trifunctional enzyme subunit alpha, mitochondrial	26.85	24.90	1	12	12	15	763	82.9	9.04
G8JLD5	Dynamin-1-like protein	26.72	26.83	2	12	12	22	712	79.6	7.08
P20290	Transcription factor BTF3	26.66	47.57	1	4	4	15	206	22.2	9.38
P62263	40S ribosomal protein S14	26.65	30.46	1	5	5	13	151	16.3	10.05
P41250	Glycine--tRNA ligase	26.46	22.87	1	10	10	19	739	83.1	7.03
P54136	Arginine--tRNA ligase, cytoplasmic	26.38	24.70	1	13	13	18	660	75.3	6.68
Q06323	Proteasome activator complex subunit 1	26.30	46.18	1	11	11	21	249	28.7	6.02
F8W6I7	Heterogeneous nuclear ribonucleoprotein A1	26.25	29.32	2	6	7	18	307	33.1	9.13
K7ENT6	Tropomyosin alpha-4 chain (Fragment)	26.14	23.46	2	2	6	12	179	20.6	4.61
P22234	Multifunctional protein ADE2	25.67	31.53	2	12	12	20	425	47.0	7.23
O95433	Activator of 90 kDa heat shock protein ATPase homolog 1	25.63	38.46	1	9	9	14	338	38.3	5.53
P62826	GTP-binding nuclear protein Ran	25.37	37.96	3	8	8	23	216	24.4	7.49
G3XAM7	Catenin (Cadherin-associated protein), alpha 1, 102kDa, isoform CRA_a	25.30	20.33	2	10	12	15	841	92.7	5.52

Accession	Description	Score	Coverage	# Proteins	#Unique Peptides	# Peptides	# PSMs	# AAs	MW [kDa]	calc. pI
F8VZJ2	Nascent polypeptide-associated complex subunit alpha	24.91	51.47	4	5	5	23	136	15.0	4.91
Q6P2Q9	Pre-mRNA-processing-splicing factor 8	24.90	9.98	1	17	18	24	2335	273.4	8.84
O43809	Cleavage and polyadenylation specificity factor subunit 5	24.74	42.73	1	6	6	15	227	26.2	8.82
P05198	Eukaryotic translation initiation factor 2 subunit 1	24.33	39.68	1	11	11	16	315	36.1	5.08
P13928	Annexin A8	24.32	35.47	2	9	9	17	327	36.9	5.78
P19105	Myosin regulatory light chain 12A	24.30	47.37	3	7	7	15	171	19.8	4.81
P62424	60S ribosomal protein L7a	24.25	21.05	1	5	5	13	266	30.0	10.61
P61106	Ras-related protein Rab-14	23.98	52.56	2	6	7	16	215	23.9	6.21
J3KMX5	40S ribosomal protein S13	23.84	23.65	2	4	4	14	148	16.7	10.51
P00533	Epidermal growth factor receptor	23.83	8.76	3	8	8	17	1210	134.2	6.68
A0A0G2JH68	Protein diaphanous homolog 1	23.64	16.35	4	15	15	19	1272	141.3	5.39
P62829	60S ribosomal protein L23	23.57	46.43	1	6	6	14	140	14.9	10.51
P33176	Kinesin-1 heavy chain	23.48	16.82	1	12	12	20	963	109.6	6.51
P52597	Heterogeneous nuclear ribonucleoprotein F	23.45	19.76	1	3	4	16	415	45.6	5.58
P04844	Dolichyl-diphosphooligosaccharide--protein glycosyltransferase subunit	23.45	17.59	1	6	6	14	631	69.2	5.69
P05455	Lupus La protein	23.03	39.22	1	14	14	24	408	46.8	7.12
P33993	DNA replication licensing factor MCM7	22.98	13.77	1	7	7	10	719	81.3	6.46
K4DI93	Cullin 4B, isoform CRA_e	22.93	9.89	2	7	7	16	900	102.7	8.03
Q14651	Plastin-1	22.85	16.53	1	3	7	17	629	70.2	5.41
P25205	DNA replication licensing factor MCM3]	22.80	14.73	2	8	8	18	808	90.9	5.77
A0A087WWT3	Serum albumin	22.77	6.06	7	3	3	18	396	45.1	6.10
P62753	40S ribosomal protein S6	22.45	20.08	1	4	4	13	249	28.7	10.84
G3V1C3	Apoptosis inhibitor 5	22.37	12.75	2	4	4	14	510	57.5	6.09
O00299	Chloride intracellular channel protein 1	22.16	45.64	1	7	8	18	241	26.9	5.17
Q15233	Non-POU domain-containing octamer-binding protein	22.02	13.80	1	4	4	10	471	54.2	8.95
P62805	Histone H4	21.95	43.69	1	7	7	16	103	11.4	11.36

Accession	Description	Score	Coverage	# Proteins	#Unique Peptides	# Peptides	# PSMs	# AAs	MW [kDa]	calc. pI
Q6NZI2	Polymerase I and transcript release factor	21.94	15.64	1	5	5	12	390	43.4	5.60
E9PKZ0	60S ribosomal protein L8 (Fragment)	21.91	22.93	2	3	3	10	205	22.4	10.76
P61019	Ras-related protein Rab-2A	21.80	38.21	1	6	6	13	212	23.5	6.54
P11908	Ribose-phosphate pyrophosphokinase 2	21.78	19.50	1	4	4	18	318	34.7	6.61
P30041	Peroxiredoxin-6	21.75	62.95	1	12	12	20	224	25.0	6.38
P12270	Nucleoprotein TPR	21.71	10.62	1	18	18	26	2363	267.1	5.02
O43242	26S proteasome non-ATPase regulatory subunit 3	21.68	14.61	1	6	6	10	534	60.9	8.44
Q9Y262	Eukaryotic translation initiation factor 3 subunit L	21.67	21.45	3	10	10	18	564	66.7	6.34
P53999	Activated RNA polymerase II transcriptional coactivator p15	21.57	30.71	1	5	5	21	127	14.4	9.60
P61221	ATP-binding cassette sub-family E member 1	21.55	14.52	1	6	6	15	599	67.3	8.34
B1ANR0	Polyadenylate-binding protein	21.42	22.11	2	5	9	15	615	67.9	9.45
P16152	Carbonyl reductase [NADPH] 1	21.40	42.96	1	7	8	12	277	30.4	8.32
P16615	Sarcoplasmic/endoplasmic reticulum calcium ATPase 2	21.35	13.92	1	11	11	14	1042	114.7	5.34
Q92841	Probable ATP-dependent RNA helicase DDX17	21.15	14.54	2	4	9	13	729	80.2	8.27
Q12906	Interleukin enhancer-binding factor 3	20.90	10.74	1	7	7	13	894	95.3	8.76
F5H6E2	Unconventional myosin-Ic	20.88	14.63	2	9	9	16	1039	118.9	9.41
P51991	Heterogeneous nuclear ribonucleoprotein A3	20.75	23.81	1	6	6	13	378	39.6	9.01
Q99714	3-hydroxyacyl-CoA dehydrogenase type-2	20.62	72.03	1	11	11	15	261	26.9	7.78
P23246	Splicing factor, proline- and glutamine-rich	20.58	14.57	1	7	7	17	707	76.1	9.44
P52907	F-actin-capping protein subunit alpha-1	20.52	47.90	1	8	8	16	286	32.9	5.69
H0Y2W2	ATPase family AAA domain-containing protein 3A (Fragment)	20.51	9.79	2	5	6	11	572	64.3	9.44
E9PLK3	Puromycin-sensitive aminopeptidase	20.27	12.57	2	7	7	15	915	102.9	5.60
Q86V81	THO complex subunit 4	20.20	29.18	2	4	4	17	257	26.9	11.15

Accession	Description	Score	Coverage	# Proteins	#Unique Peptides	# Peptides	# PSMs	# AAs	MW [kDa]	calc. pI
C9JPM4	ADP-ribosylation factor 4 (Fragment)	20.18	64.57	2	3	8	15	127	14.5	8.12
P46777	60S ribosomal protein L5	20.10	30.30	1	5	5	18	297	34.3	9.72
P56192	Methionine--tRNA ligase, cytoplasmic	19.91	17.00	1	9	10	17	900	101.1	6.16
P56537	Eukaryotic translation initiation factor 6	19.76	40.82	1	6	6	12	245	26.6	4.68
Q01813	ATP-dependent 6-phosphofructokinase, platelet type	19.70	14.03	1	7	9	16	784	85.5	7.55
Q04917	14-3-3 protein eta	19.42	23.58	1	3	4	13	246	28.2	4.84
P51148	Ras-related protein Rab-5C	19.42	30.56	1	3	5	12	216	23.5	8.41
F8W1A4	Adenylate kinase 2, mitochondrial	19.40	44.83	3	8	8	20	232	25.6	7.83
P14868	Aspartate--tRNA ligase, cytoplasmic	19.36	23.95	1	9	10	17	501	57.1	6.55
P28070	Proteasome subunit beta type-4	19.21	36.36	1	6	6	12	264	29.2	5.97
Q7Z4W1	L-xylulose reductase	19.18	27.46	1	4	4	14	244	25.9	8.10
P25787	Proteasome subunit alpha type-2	19.14	37.18	1	6	6	12	234	25.9	7.43
Q01469	Fatty acid-binding protein, epidermal	19.00	48.15	1	7	7	14	135	15.2	7.01
I3L3U9	Ribosomal L1 domain-containing protein 1 (Fragment)	18.66	24.66	3	5	5	11	296	33.9	10.01
A0A0J9YYL3	Poly(U)-binding-splicing factor PUF60 (Fragment)	18.65	21.39	5	7	7	11	505	54.6	5.34
P61086	Ubiquitin-conjugating enzyme E2 K	18.64	59.50	1	7	8	12	200	22.4	5.44
Q9UHD8	Septin-9	18.61	20.65	1	8	8	20	586	65.4	8.97
P17858	ATP-dependent 6-phosphofructokinase, liver type	18.43	14.49	1	6	8	15	780	85.0	7.50
Q9NUQ9	Protein FAM49B	18.39	23.15	1	6	6	13	324	36.7	6.06
P09960	Leukotriene A-4 hydrolase	18.30	18.17	1	7	7	17	611	69.2	6.18
P59998	Actin-related protein 2/3 complex subunit 4	18.30	42.26	2	5	5	11	168	19.7	8.43
K7ENG2	Splicing factor U2AF 65 kDa subunit	18.27	27.69	2	6	6	13	307	33.9	5.03
P30084	Enoyl-CoA hydratase, mitochondrial	18.17	37.93	1	8	8	13	290	31.4	8.07

Accession	Description	Score	Coverage	# Proteins	#Unique Peptides	# Peptides	# PSMs	# AAs	MW [kDa]	calc. pI
Q01650	Large neutral amino acids transporter small subunit 1	18.12	9.66	1	4	4	7	507	55.0	7.72
P47897	Glutamine--tRNA ligase	18.08	19.61	1	11	11	19	775	87.7	7.15
Q9NYU2	UDP-glucose:glycoprotein glucosyltransferase 1	17.99	11.38	1	12	12	14	1555	177.1	5.63
B1AK87	Capping protein (Actin filament) muscle Z-line, beta, isoform CRA_a	17.98	40.00	2	8	8	10	260	29.3	6.92
Q92499	ATP-dependent RNA helicase DDX1	17.97	19.46	3	9	9	15	740	82.4	7.23
O00303	Eukaryotic translation initiation factor 3 subunit F	17.94	15.13	1	3	3	10	357	37.5	5.45
Q07021	Complement component 1 Q subcomponent-binding protein, mitochondrial	17.82	31.56	1	5	5	13	282	31.3	4.84
P12236	ADP/ATP translocase 3	17.78	32.21	1	3	7	24	298	32.8	9.74
Q04837	Single-stranded DNA-binding protein, mitochondrial	17.69	41.22	1	4	4	10	148	17.2	9.60
Q14019	Coactosin-like protein	17.63	21.13	1	3	3	12	142	15.9	5.67
P52209	6-phosphogluconate dehydrogenase, decarboxylating	17.47	26.50	1	10	10	18	483	53.1	7.23
Q15046	Lysine--tRNA ligase	17.47	13.57	1	7	7	13	597	68.0	6.35
P41091	Eukaryotic translation initiation factor 2 subunit 3	17.44	20.55	1	5	5	11	472	51.1	8.40
P53618	Coatomer subunit beta	17.41	11.96	1	7	7	13	953	107.1	6.05
A0A0A0MR02	Voltage-dependent anion-selective channel protein 2 (Fragment)	17.40	42.55	2	8	8	21	282	30.3	7.81
J3QR09	Ribosomal protein L19	17.37	13.99	3	3	3	9	193	23.1	11.47
Q86UE4	Protein LYRIC	17.37	14.43	1	7	7	17	582	63.8	9.32
P23381	Tryptophan--tRNA ligase, cytoplasmic	17.30	19.53	1	6	6	13	471	53.1	6.23
Q96C19	EF-hand domain-containing protein D2	17.27	27.08	1	5	5	9	240	26.7	5.20
Q14566	DNA replication licensing factor MCM6	17.26	13.03	1	8	8	15	821	92.8	5.41
P54578	Ubiquitin carboxyl-terminal hydrolase 14	17.26	19.84	2	6	6	9	494	56.0	5.30

Accession	Description	Score	Coverage	# Proteins	#Unique Peptides	# Peptides	# PSMs	# AAs	MW [kDa]	calc. pI
P55809	Succinyl-CoA:3-ketoacid coenzyme A transferase 1, mitochondrial	17.21	9.42	1	2	3	7	520	56.1	7.46
O95373	Importin-7	17.18	11.37	1	8	8	19	1038	119.4	4.82
Q9UQE7	Structural maintenance of chromosomes protein 3	17.12	16.35	1	13	14	16	1217	141.5	7.18
H7C469	Uncharacterized protein (Fragment)	17.10	17.86	8	4	4	8	336	35.9	5.40
Q9UHB9	Signal recognition particle subunit SRP68	17.08	10.85	1	5	5	10	627	70.7	8.56
H7C3T4	Peroxiredoxin-4 (Fragment)	17.02	46.58	2	4	6	14	161	18.3	6.19
B4DJ81	NADH-ubiquinone oxidoreductase 75 kDa subunit, mitochondrial	16.92	16.37	2	7	7	10	611	66.9	5.38
B4DGU4	Catenin beta-1	16.87	9.17	2	4	5	11	774	84.7	5.92
P60228	Eukaryotic translation initiation factor 3 subunit E	16.83	16.18	1	5	5	14	445	52.2	6.04
P16403	Histone H1.2	16.67	17.84	3	4	6	20	213	21.4	10.93
P49755	Transmembrane emp24 domain-containing protein 10	16.66	32.42	1	7	7	12	219	25.0	7.44
P35527	Keratin, type I cytoskeletal 9	16.40	21.83	1	7	7	19	623	62.0	5.24
P62244	40S ribosomal protein S15a	16.22	53.85	1	6	6	10	130	14.8	10.13
P38919	Eukaryotic initiation factor 4A-III	16.16	17.03	1	5	6	10	411	46.8	6.73
P17812	CTP synthase 1	16.11	15.91	1	6	6	12	591	66.6	6.46
P61353	60S ribosomal protein L27	16.09	36.76	1	5	5	11	136	15.8	10.56
P62266	40S ribosomal protein S23	16.00	35.66	1	5	5	8	143	15.8	10.49
A0A0C4DGS1	Dolichyl-diphosphooligosaccharide--protein glycosyltransferase 48 kDa subunit	16.00	16.17	2	6	6	12	439	48.8	5.69
P30044		15.94	40.65	1	9	9	16	214	22.1	8.70
H0YN26	Acidic leucine-rich nuclear phosphoprotein 32 family member A	15.89	47.46	2	5	6	9	177	20.0	4.58
P35998	26S protease regulatory subunit 7	15.87	20.79	1	7	7	11	433	48.6	5.95
P31689	DnaJ homolog subfamily A member 1	15.79	14.36	1	3	3	8	397	44.8	7.08
P13796	Plastin-2	15.79	10.53	1	2	5	10	627	70.2	5.43
P30043	Flavin reductase (NADPH)	15.77	26.21	1	3	3	6	206	22.1	7.65

Accession	Description	Score	Coverage	# Proteins	#Unique Peptides	# Peptides	# PSMs	# AAs	MW [kDa]	calc. pI
P61224	Ras-related protein Rap-1b	15.72	55.43	3	8	8	19	184	20.8	5.78
E5RI99	60S ribosomal protein L30 (Fragment)	15.68	35.09	2	3	3	14	114	12.6	9.55
P23193	Transcription elongation factor A protein 1	15.60	35.88	1	8	8	12	301	33.9	8.38
P48047	ATP synthase subunit O, mitochondrial	15.57	20.66	2	4	4	8	213	23.3	9.96
Q9UNM6	26S proteasome non-ATPase regulatory subunit 13	15.55	17.55	4	5	5	14	376	42.9	5.81
P31153	S-adenosylmethionine synthase isoform type-2	15.40	18.99	1	5	5	13	395	43.6	6.48
O76094	Signal recognition particle subunit SRP72	15.31	7.30	2	3	3	8	671	74.6	9.26
Q07955	Serine/arginine-rich splicing factor 1	15.22	29.03	2	5	5	12	248	27.7	10.36
P30086	Phosphatidylethanolamine-binding protein 1	15.21	48.13	1	7	7	18	187	21.0	7.53
Q9NSD9	Phenylalanine--tRNA ligase beta subunit	15.17	12.56	1	7	7	13	589	66.1	6.84
O75131	Copine-3	15.14	23.09	1	8	8	11	537	60.1	5.85
Q92688	Acidic leucine-rich nuclear phosphoprotein 32 family member B	15.13	15.94	1	2	3	9	251	28.8	4.06
Q99471	Prefoldin subunit 5	15.12	43.51	2	4	4	8	154	17.3	6.33
Q15691	Microtubule-associated protein RP/EB family member 1	15.06	27.24	1	5	5	12	268	30.0	5.14
P18124	60S ribosomal protein L7	15.03	32.66	1	8	8	11	248	29.2	10.65
Q96HE7	ERO1-like protein alpha	14.99	12.82	1	5	5	7	468	54.4	5.68
Q9Y617	Phosphoserine aminotransferase	14.92	28.11	1	9	9	12	370	40.4	7.66
P28074	Proteasome subunit beta type-5	14.82	31.18	1	6	6	9	263	28.5	6.92
P00367	Glutamate dehydrogenase 1, mitochondrial	14.71	25.45	1	9	9	16	558	61.4	7.80
Q99613	Eukaryotic translation initiation factor 3 subunit C	14.70	13.58	2	10	10	20	913	105.3	5.68
Q5JR07	Rho-related GTP-binding protein RhoC (Fragment)	14.69	59.84	5	6	6	11	127	14.4	4.73
P51858	Hepatoma-derived growth factor	14.67	34.58	1	7	7	11	240	26.8	4.73
J3QLI9	Small nuclear ribonucleoprotein Sm D1	14.64	44.00	2	2	2	10	75	8.4	11.84
P28838	Cytosol aminopeptidase	14.62	14.45	1	6	6	9	519	56.1	7.93

Accession	Description	Score	Coverage	# Proteins	#Unique Peptides	# Peptides	# PSMs	# AAs	MW [kDa]	calc. pI
Q16795	NADH dehydrogenase [ubiquinone] 1 alpha subcomplex subunit 9, mitochondrial	14.58	12.73	1	3	3	9	377	42.5	9.80
P62136	Serine/threonine-protein phosphatase PP1-alpha catalytic subunit	14.47	27.88	1	8	8	13	330	37.5	6.33
P17174	Aspartate aminotransferase, cytoplasmic	14.44	41.16	1	10	10	15	413	46.2	7.01
P20073	Annexin A7	14.40	10.25	1	4	4	8	488	52.7	5.68
F5H157	Ras-related protein Rab-35 (Fragment)	14.38	21.62	2	1	3	8	185	21.2	8.31
Q9UIJ7	GTP:AMP phosphotransferase AK3, mitochondrial	14.28	32.16	1	5	5	10	227	25.5	9.16
P51659	Peroxisomal multifunctional enzyme type 2	14.27	10.73	1	5	5	7	736	79.6	8.84
I3L0H8	ATP-dependent RNA helicase DDX19A	14.26	5.82	3	2	2	6	447	50.5	6.38
Q02539	Histone H1.1	14.24	16.28	1	2	4	12	215	21.8	10.99
Q15785	Mitochondrial import receptor subunit TOM34	14.22	32.04	1	6	6	8	309	34.5	8.98
P15121	Aldose reductase	13.97	21.20	1	4	5	10	316	35.8	6.98
Q6PIU2	Neutral cholesterol ester hydrolase 1	13.89	25.98	3	6	6	10	408	45.8	7.23
P31948	Stress-induced-phosphoprotein 1	13.80	9.02	1	5	5	11	543	62.6	6.80
H7C463	MICOS complex subunit MIC60 (Fragment)	13.79	13.87	4	6	6	10	613	68.1	6.06
Q9HAV4	Exportin-5	13.67	8.55	1	8	8	14	1204	136.2	5.80
A0A087X1I3	Succinate dehydrogenase [ubiquinone] flavoprotein subunit, mitochondrial	13.59	14.45	3	4	4	6	519	56.6	7.50
O14744	Protein arginine N-methyltransferase 5	13.56	14.29	1	7	7	10	637	72.6	6.29
P00390	Glutathione reductase, mitochondrial	13.56	17.24	1	4	4	9	522	56.2	8.50
P09525	Annexin A4	13.55	33.86	1	7	7	8	319	35.9	6.13
P43358	Melanoma-associated antigen 4	13.48	25.24	1	8	8	15	317	34.9	4.69
O00151	PDZ and LIM domain protein 1	13.46	38.30	1	9	9	14	329	36.0	7.02
Q13126	S-methyl-5'-thioadenosine phosphorylase	13.43	27.21	2	4	4	8	283	31.2	7.18

Accession	Description	Score	Coverage	# Proteins	#Unique Peptides	# Peptides	# PSMs	# AAs	MW [kDa]	calc. pI
Q9H4A4	Aminopeptidase B	13.42	17.69	2	10	10	10	650	72.5	5.74
F8W020	Nucleosome assembly protein 1-like 1 (Fragment)	13.37	42.51	6	7	7	19	207	24.4	4.51
O00232	26S proteasome non-ATPase regulatory subunit 12	13.37	19.30	1	5	5	12	456	52.9	7.65
B4DJV2	Citrate synthase	13.35	23.18	2	8	9	13	453	50.4	7.90
P39019	40S ribosomal protein S19	13.28	17.24	1	3	3	6	145	16.1	10.32
Q9Y3F4	Serine-threonine kinase receptor-associated protein	13.20	21.43	1	5	5	9	350	38.4	5.12
Q5T7C4	High mobility group protein B1	13.16	46.84	2	5	6	15	158	18.3	9.70
P53621	Coatomer subunit alpha	13.11	9.56	1	10	10	11	1224	138.3	7.66
B7Z9I1	Medium-chain-specific acyl-CoA dehydrogenase, mitochondrial	13.05	25.71	3	6	6	15	385	42.4	6.43
D6RAN4	60S ribosomal protein L9 (Fragment)	12.99	40.88	3	4	4	12	181	20.8	10.20
P62316	Small nuclear ribonucleoprotein Sm D2	12.96	40.68	1	5	5	10	118	13.5	9.91
P37837	Transaldolase	12.96	23.15	2	8	8	16	337	37.5	6.81
P51571	Translocon-associated protein subunit delta	12.91	24.86	1	3	3	7	173	19.0	6.15
Q13435	Splicing factor 3B subunit 2	12.91	10.50	1	9	9	10	895	100.2	5.67
E5RIW3	Tubulin-specific chaperone A	12.84	45.24	3	5	5	8	84	10.1	4.63
P10644	cAMP-dependent protein kinase type I-alpha regulatory subunit	12.78	14.17	1	3	3	5	381	43.0	5.35
P61289	Proteasome activator complex subunit 3	12.65	25.20	3	5	5	10	254	29.5	5.95
P00492	Hypoxanthine-guanine phosphoribosyltransferase	12.62	34.40	1	6	6	12	218	24.6	6.68
P13804	Electron transfer flavoprotein subunit alpha, mitochondrial	12.61	38.44	1	8	8	10	333	35.1	8.38
P43304	Glycerol-3-phosphate dehydrogenase, mitochondrial	12.60	14.86	1	7	7	13	727	80.8	7.69
P49915	GMP synthase [glutamine-hydrolyzing	12.60	27.42	1	12	12	17	693	76.7	6.87
C9JU14	Ras-related protein Rab-6B (Fragment)	12.58	27.71	4	1	2	7	83	9.7	5.45
K7EM73	Calpain small subunit 1 (Fragment)	12.53	20.86	6	2	2	7	163	15.9	4.91
O75694	Nuclear pore complex protein Nup155	12.52	9.56	1	10	10	11	1391	155.1	6.16

Accession	Description	Score	Coverage	# Proteins	#Unique Peptides	# Peptides	# PSMs	# AAs	MW [kDa]	calc. pI
B7Z7P8	Eukaryotic peptide chain release factor subunit 1	12.52	21.51	2	6	6	11	423	47.4	5.57
P38606	V-type proton ATPase catalytic subunit A	12.49	13.61	1	7	7	9	617	68.3	5.52
P15880	40S ribosomal protein S2	12.48	37.20	2	8	8	17	293	31.3	10.24
P00387	NADH-cytochrome b5 reductase 3	12.45	22.59	1	6	6	14	301	34.2	7.59
X1WI28	60S ribosomal protein L10 (Fragment)	12.36	29.50	2	4	4	11	200	23.0	10.01
F8W1R7	Myosin light polypeptide 6	12.33	49.66	7	6	6	15	145	16.3	4.65
E9PN17	ATP synthase subunit g, mitochondrial	12.24	36.84	2	2	2	6	76	8.4	10.29
Q12874	Splicing factor 3A subunit 3	12.24	18.76	1	6	6	11	501	58.8	5.38
Q9NX58	Cell growth-regulating nucleolar protein	12.22	10.29	1	2	2	8	379	43.6	9.54
A0A096LNY6	Adenylosuccinate lyase (Fragment)	12.18	13.89	7	3	3	4	360	40.9	7.68
Q9H9B4	Sideroflexin-1	12.16	26.09	1	5	5	5	322	35.6	9.07
O15144	Actin-related protein 2/3 complex subunit 2	12.14	35.00	1	8	8	11	300	34.3	7.36
Q9Y678	Coatomer subunit gamma-1	12.12	14.76	1	7	8	14	874	97.7	5.47
P61604	10 kDa heat shock protein, mitochondrial	12.12	43.14	2	4	4	12	102	10.9	8.92
P14550	Alcohol dehydrogenase [NADP(+)]	12.04	18.15	1	4	5	9	325	36.5	6.79
P60866	40S ribosomal protein S20	12.03	22.69	1	3	3	7	119	13.4	9.94
P08754	Guanine nucleotide-binding protein G(k) subunit alpha	11.99	21.47	1	4	6	19	354	40.5	5.69
D6RA82	Annexin	11.99	29.93	2	8	8	12	284	32.1	5.94
P52292	Importin subunit alpha-1	11.94	26.65	1	7	7	14	529	57.8	5.40
Q8N1G4	Leucine-rich repeat-containing protein 47	11.91	15.44	1	6	6	7	583	63.4	8.28
P11166	Solute carrier family 2, facilitated glucose transporter member 1	11.84	11.99	1	3	4	8	492	54.0	8.72
A0A087X1K9	Acyl-protein thioesterase 1	11.83	16.27	3	2	2	5	166	18.0	5.06
P62249	40S ribosomal protein S16	11.77	38.36	2	5	5	12	146	16.4	10.21
P33991	DNA replication licensing factor MCM4	11.77	11.24	1	6	6	10	863	96.5	6.74
Q92597	Protein NDRG1	11.73	20.30	1	5	5	10	394	42.8	5.82
H3BRG4	Cytochrome b-c1 complex subunit 2, mitochondrial	11.73	27.43	2	8	8	13	412	44.6	9.00

Accession	Description	Score	Coverage	# Proteins	#Unique Peptides	# Peptides	# PSMs	# AAs	MW [kDa]	calc. pI
P50995	Annexin A11	11.72	13.07	1	5	5	7	505	54.4	7.65
Q13724	Mannosyl-oligosaccharide glucosidase	11.64	10.99	1	5	5	7	837	91.9	8.90
Q13283	Ras GTPase-activating protein-binding protein 1	11.62	15.24	1	4	4	8	466	52.1	5.52
P62241	40S ribosomal protein S8	11.61	41.35	1	7	7	16	208	24.2	10.32
P60900	Proteasome subunit alpha type-6	11.61	20.73	2	5	5	11	246	27.4	6.76
P26232	Catenin alpha-2	11.57	8.08	1	1	5	10	953	105.2	5.71
P11388	DNA topoisomerase 2-alpha	11.53	7.58	1	9	9	11	1531	174.3	8.72
K7ES52	Thymidine kinase	11.51	25.00	4	3	3	6	180	19.8	8.29
P02786	Transferrin receptor protein 1	11.51	9.47	1	6	6	8	760	84.8	6.61
C9JIG9	Serine/threonine-protein kinase OSR1	11.41	9.40	2	3	3	5	468	51.8	7.80
P16422	Epithelial cell adhesion molecule	11.36	24.84	2	4	4	10	314	34.9	7.46
A0A087WVM4	Monofunctional C1-tetrahydrofolate synthase, mitochondrial	11.33	15.66	3	9	9	9	913	99.2	7.27
Q9Y224	UPF0568 protein C14orf166	11.32	24.18	1	4	4	9	244	28.1	6.65
P28066	Proteasome subunit alpha type-5	11.30	34.85	1	6	6	13	241	26.4	4.79
Q8N163	Cell cycle and apoptosis regulator protein 2	11.30	10.83	1	6	6	7	923	102.8	5.22
P23921	Ribonucleoside-diphosphate reductase large subunit	11.26	17.30	1	8	8	9	792	90.0	7.15
P27797	Calreticulin	11.25	21.10	1	5	5	13	417	48.1	4.44
Q96P70	Importin-9	11.24	4.42	1	2	2	5	1041	115.9	4.81
Q16531	DNA damage-binding protein 1	11.19	8.68	1	9	9	10	1140	126.9	5.26
Q15459	Splicing factor 3A subunit 1	11.15	9.96	1	5	5	9	793	88.8	5.22
P82979	SAP domain-containing ribonucleoprotein	11.14	23.33	2	4	4	6	210	23.7	6.42
Q15427	Splicing factor 3B subunit 4	11.11	12.97	1	3	3	8	424	44.4	8.56
C9J3L8	Translocon-associated protein subunit alpha	11.11	9.81	5	2	2	6	265	29.6	4.30
E9PLL6	60S ribosomal protein L27a	11.04	38.89	2	5	5	10	108	12.2	11.46
M0QXS5	Heterogeneous nuclear ribonucleoprotein L (Fragment)	11.04	13.96	2	4	4	20	530	58.4	6.79

Accession	Description	Score	Coverage	# Proteins	#Unique Peptides	# Peptides	# PSMs	# AAs	MW [kDa]	calc. pI
P10599	Thioredoxin	11.02	48.57	1	5	5	8	105	11.7	4.92
Q15907	Ras-related protein Rab-11B	11.00	27.98	1	5	5	8	218	24.5	5.94
Q15758	Neutral amino acid transporter B(0)	10.99	12.38	1	4	4	6	541	56.6	5.48
O96008	Mitochondrial import receptor subunit TOM40 homolog	10.98	9.14	1	3	3	7	361	37.9	7.25
Q8WXF1	Paraspeckle component 1	10.94	13.58	2	4	5	13	523	58.7	6.67
O14818	Proteasome subunit alpha type-7	10.92	28.23	1	5	5	7	248	27.9	8.46
O75475	PC4 and SFRS1-interacting protein	10.90	6.79	1	2	3	7	530	60.1	9.13
Q99798	Aconitate hydratase, mitochondrial	10.90	11.03	2	6	6	10	780	85.4	7.61
P07099	Epoxide hydrolase 1	10.84	7.69	1	2	3	5	455	52.9	7.25
F2Z2Y4	Pyridoxal kinase	10.83	26.10	2	4	4	9	272	30.6	6.65
Q9HDC9	Adipocyte plasma membrane-associated protein	10.82	23.32	2	5	5	7	416	46.5	6.16
P48444	Coatomer subunit delta	10.81	8.61	2	5	5	8	511	57.2	6.21
Q96AG4	Leucine-rich repeat-containing protein 59	10.78	34.53	1	7	7	10	307	34.9	9.57
P62851	40S ribosomal protein S25	10.77	16.80	1	3	3	12	125	13.7	10.11
B4E3S0	Coronin	10.76	20.33	2	4	4	9	369	41.6	6.73
I3L1P8	Mitochondrial 2-oxoglutarate/malate carrier protein (Fragment)	10.75	20.61	2	6	6	7	296	32.2	9.77
Q13045	Protein flightless-1 homolog	10.68	4.10	1	4	4	6	1269	144.7	6.05
Q92973	Transportin-1	10.64	9.24	1	6	6	8	898	102.3	4.98
Q12797	Aspartyl/asparaginyl beta-hydroxylase	10.62	11.74	1	5	5	11	758	85.8	5.01
Q9BSJ8	Extended synaptotagmin-1	10.55	9.24	1	6	6	7	1104	122.8	5.83
P20339	Ras-related protein Rab-5A	10.52	24.19	1	2	4	6	215	23.6	8.15
H7BXH2	Serine/threonine-protein phosphatase 6 regulatory subunit 3	10.50	4.72	3	3	3	6	827	92.4	4.63
P07384	Calpain-1 catalytic subunit	10.49	18.35	1	10	10	15	714	81.8	5.67
P63173	60S ribosomal protein L38	10.48	52.86	3	5	5	9	70	8.2	10.10
P30520	Adenylosuccinate synthetase isozyme 2	10.42	23.25	1	7	7	9	456	50.1	6.55

Accession	Description	Score	Coverage	# Proteins	#Unique Peptides	# Peptides	# PSMs	# AAs	MW [kDa]	calc. pI
P31930	Cytochrome b-c1 complex subunit 1, mitochondrial	10.40	15.00	1	5	5	9	480	52.6	6.37
P49721	Proteasome subunit beta type-2	10.37	22.39	1	3	3	5	201	22.8	7.02
O15371	Eukaryotic translation initiation factor 3 subunit D	10.36	15.33	1	4	5	7	548	63.9	6.05
H3BQZ7	HCG2044799	10.35	10.99	2	5	5	6	746	84.6	4.93
Q14008	Cytoskeleton-associated protein 5	10.32	4.38	1	7	7	8	2032	225.4	7.80
P35606	Coatomer subunit beta'	10.30	6.29	1	5	5	8	906	102.4	5.27
H7BXY3	Putative ATP-dependent RNA helicase DHX30	10.27	3.60	2	2	2	4	1166	130.5	8.56
P19012	Keratin, type I cytoskeletal 15	10.25	13.38	1	1	7	13	456	49.2	4.77
O43390	Heterogeneous nuclear ribonucleoprotein R	10.21	15.01	1	4	7	15	633	70.9	8.13
K7ERZ3	Perilipin-3 (Fragment)	10.19	31.51	2	5	5	7	292	32.0	5.14
E7EPB3	60S ribosomal protein L14	10.19	19.35	2	2	2	5	124	14.5	10.21
H0YHS6	Tyrosine--tRNA ligase (Fragment)	10.17	20.27	2	4	4	8	291	32.2	8.40
C9JZR2	Catenin delta-1	10.16	11.19	2	7	7	12	938	104.8	6.87
P62857	40S ribosomal protein S28	10.07	30.43	1	2	2	7	69	7.8	10.70
Q9H0A0	RNA cytidine acetyltransferase	10.03	7.80	2	4	4	7	1025	115.7	8.27
A0A0C4DG79	Constitutive coactivator of PPAR-gamma-like protein 1 (Fragment)	10.02	8.10	2	3	3	6	494	54.2	9.33
O00629	Importin subunit alpha-3	9.99	11.32	1	3	3	11	521	57.9	4.96
Q9UBT2	SUMO-activating enzyme subunit 2	9.98	7.81	1	4	4	6	640	71.2	5.29
Q9NSE4	Isoleucine--tRNA ligase, mitochondrial	9.91	9.58	1	7	7	10	1012	113.7	7.20
Q92538	Golgi-specific brefeldin A-resistance guanine nucleotide exchange factor 1	9.84	2.10	1	3	3	5	1859	206.3	5.73
E9PGT6	COP9 signalosome complex subunit 8	9.81	51.45	2	5	5	9	173	19.3	5.53
P25786	Proteasome subunit alpha type-1	9.80	29.66	1	5	5	8	263	29.5	6.61
P07741	Adenine phosphoribosyltransferase	9.79	38.33	1	4	4	7	180	19.6	6.02

Accession	Description	Score	Coverage	# Proteins	#Unique Peptides	# Peptides	# PSMs	# AAs	MW [kDa]	calc. pI
P08574	Cytochrome c1, heme protein, mitochondrial	9.79	22.15	1	4	4	10	325	35.4	9.00
Q9H845	Acyl-CoA dehydrogenase family member 9, mitochondrial	9.76	10.14	1	4	5	8	621	68.7	7.96
P13798	Acylamino-acid-releasing enzyme	9.75	7.10	2	4	4	6	732	81.2	5.48
O75489	NADH dehydrogenase [ubiquinone] iron-sulfur protein 3, mitochondrial	9.74	23.86	1	5	5	5	264	30.2	7.50
P05387	60S acidic ribosomal protein P2	9.67	59.13	1	4	4	6	115	11.7	4.54
P38117	Electron transfer flavoprotein subunit beta	9.67	18.82	1	4	4	6	255	27.8	8.10
Q9H0S4	Probable ATP-dependent RNA helicase DDX47	9.66	6.15	1	2	2	5	455	50.6	9.10
P60953	Cell division control protein 42 homolog	9.65	35.60	1	4	4	8	191	21.2	6.55
P35637	RNA-binding protein FUS	9.65	10.46	2	6	6	10	526	53.4	9.36
D6R9A6	High mobility group protein B2 (Fragment)	9.64	29.10	2	3	4	6	134	15.4	9.79
Q99459	Cell division cycle 5-like protein	9.62	7.61	1	4	4	5	802	92.2	8.18
P43686	26S protease regulatory subunit 6B	9.56	23.44	1	4	4	9	418	47.3	5.21
P09758	Tumor-associated calcium signal transducer 2	9.53	10.84	1	3	3	6	323	35.7	8.87
P26373	60S ribosomal protein L13	9.51	19.91	2	4	4	10	211	24.2	11.65
O00505	Importin subunit alpha-4	9.48	11.52	1	3	3	12	521	57.8	4.94
P11498	Pyruvate carboxylase, mitochondrial	9.39	6.54	1	5	5	5	1178	129.6	6.84
A0A087WXM6	60S ribosomal protein L17 (Fragment)	9.39	27.22	5	4	4	10	169	19.6	10.04
P08243	Asparagine synthetase [glutamine-hydrolyzing]	9.38	3.57	1	2	2	6	561	64.3	6.86
P11216	Glycogen phosphorylase, brain form	9.33	12.46	1	4	7	13	843	96.6	6.86
P46087	Probable 28S rRNA (cytosine(4447)-C(5))-methyltransferase	9.33	6.40	1	4	4	6	812	89.2	9.23
O15131	Importin subunit alpha-6	9.27	4.66	3	2	2	6	536	60.3	5.16

Accession	Description	Score	Coverage	# Proteins	#Unique Peptides	# Peptides	# PSMs	# AAs	MW [kDa]	calc. pI
O43143	Pre-mRNA-splicing factor ATP-dependent RNA helicase DHX15	9.22	6.92	1	5	5	9	795	90.9	7.46
H0YMZ1	Proteasome subunit alpha type (Fragment)	9.22	44.55	3	7	7	7	220	24.5	6.77
C9JXB8	60S ribosomal protein L24	9.12	26.45	3	3	3	8	121	14.4	11.31
C9JQ41	Coiled-coil domain-containing protein 58	9.05	34.62	3	3	3	5	130	15.3	8.88
P54577	Tyrosine--tRNA ligase, cytoplasmic	9.03	9.85	1	4	4	7	528	59.1	7.05
X6RAC9	Eukaryotic translation initiation factor 1A, X-chromosomal	9.03	12.93	3	2	2	6	116	13.2	4.83
P21281	V-type proton ATPase subunit B, brain isoform	9.01	9.00	1	3	3	5	511	56.5	5.81
K7EKI8	Periplakin	8.95	7.53	3	9	10	14	1754	204.4	5.62
J3QLE5	Small nuclear ribonucleoprotein-associated protein N (Fragment)	8.92	14.20	3	3	3	7	169	17.5	9.99
O43399	Tumor protein D54	8.89	35.44	1	4	4	6	206	22.2	5.36
E7ETK0	40S ribosomal protein S24	8.89	29.77	3	3	3	10	131	15.2	10.89
Q14764	Major vault protein	8.85	12.32	1	6	6	7	893	99.3	5.48
P61758	Prefoldin subunit 3	8.85	28.43	1	4	4	8	197	22.6	7.11
Q9P2J5	Leucine--tRNA ligase, cytoplasmic	8.85	11.90	1	8	8	9	1176	134.4	7.30
Q9UKX7	Nuclear pore complex protein Nup50	8.84	14.32	1	3	3	6	468	50.1	7.06
O14579	Coatomer subunit epsilon	8.84	31.49	1	5	5	5	308	34.5	5.12
Q08J23	tRNA (cytosine(34)-C(5))-methyltransferase	8.79	11.99	1	5	5	7	767	86.4	6.77
G3V4F2	Acyl-coenzyme A thioesterase 1	8.77	17.22	5	5	5	5	395	43.7	6.99
P55263	Adenosine kinase	8.73	28.45	1	5	5	10	362	40.5	6.70
A0A0A0MRA5	Heterogeneous nuclear ribonucleoprotein U-like protein 1	8.71	4.44	3	2	2	3	766	85.9	8.78
E9PKG1	Protein arginine N-methyltransferase 1	8.67	24.00	3	6	6	9	325	37.7	6.15
P17931	Galectin-3	8.64	20.40	1	4	4	5	250	26.1	8.56
P04792	Heat shock protein beta-1	8.64	18.05	1	3	3	4	205	22.8	6.40

Accession	Description	Score	Coverage	# Proteins	#Unique Peptides	# Peptides	# PSMs	# AAs	MW [kDa]	calc. pI
O75400	Pre-mRNA-processing factor 40 homolog A	8.60	7.52	1	6	6	7	957	108.7	7.56
P14314	Glucosidase 2 subunit beta	8.60	8.33	2	4	4	7	528	59.4	4.41
C9J1E7	AP-1 complex subunit beta-1 (Fragment)	8.55	13.67	2	3	6	10	578	65.3	5.19
C9JFR7	Cytochrome c (Fragment)	8.54	47.52	2	6	6	10	101	11.3	9.66
O43598	2'-deoxynucleoside 5'-phosphate N-hydrolase 1	8.54	38.51	2	3	3	8	174	19.1	5.05
F8WJN3	Cleavage and polyadenylation-specificity factor subunit 6	8.52	10.25	2	3	3	7	478	52.2	6.43
P47985	Cytochrome b-c1 complex subunit Rieske, mitochondrial	8.51	12.77	1	2	2	6	274	29.6	8.32
P51572	B-cell receptor-associated protein 31	8.51	9.76	1	3	3	7	246	28.0	8.44
C9JVE2	DCN1-like protein	8.44	17.21	6	3	3	7	244	28.3	4.98
O60313	Dynamin-like 120 kDa protein, mitochondrial	8.42	6.04	5	4	4	4	960	111.6	7.87
Q9P258	Protein RCC2	8.41	8.05	1	4	4	6	522	56.0	8.78
O15511	Actin-related protein 2/3 complex subunit 5	8.39	39.74	1	3	3	9	151	16.3	5.67
P36542	ATP synthase subunit gamma, mitochondrial	8.38	29.53	1	6	6	7	298	33.0	9.22
P63000	Ras-related C3 botulinum toxin substrate 1	8.29	19.79	1	2	3	5	192	21.4	8.50
P62318	Small nuclear ribonucleoprotein Sm D3	8.29	30.95	1	3	3	5	126	13.9	10.32
Q8WVC2	40S ribosomal protein S21	8.26	34.57	2	3	3	4	81	8.8	8.50
A0A087X0K1	Calcium-binding protein 39	8.24	5.90	2	2	2	5	339	39.4	7.11
E9PNC7	Dr1-associated corepressor (Fragment)	8.22	14.84	4	3	3	5	155	16.6	7.43
Q02750	Dual specificity mitogen-activated protein kinase kinase 1	8.21	9.67	1	2	2	4	393	43.4	6.62
P62158	Calmodulin	8.20	35.57	4	5	5	11	149	16.8	4.22
Q14558	Phosphoribosyl pyrophosphate synthase-associated protein 1	8.16	12.08	1	3	3	6	356	39.4	7.20
K7EQ02	DAZ-associated protein 1 (Fragment)	8.15	9.48	4	2	2	5	327	35.0	7.85

Accession	Description	Score	Coverage	# Proteins	#Unique Peptides	# Peptides	# PSMs	# AAs	MW [kDa]	calc. pI
J3QLH6	26S protease regulatory subunit 8 (Fragment)	8.13	19.07	5	2	3	4	215	24.2	7.97
F8W031	Uncharacterized protein (Fragment)	8.11	17.87	4	3	4	5	263	29.2	7.01
Q9Y295	Developmentally-regulated GTP-binding protein 1	8.08	15.80	1	3	3	4	367	40.5	8.90
P31949	Protein S100-A11	8.05	34.29	1	3	3	9	105	11.7	7.12
A5YKK6	CCR4-NOT transcription complex subunit 1	8.05	2.44	1	4	5	6	2376	266.8	7.11
Q9C0C2	182 kDa tankyrase-1-binding protein	8.04	5.26	1	6	6	6	1729	181.7	4.86
P55769	NHP2-like protein 1	8.03	19.53	2	3	3	5	128	14.2	8.46
K7ENK9	Vesicle-associated membrane protein 2	8.02	35.29	7	2	2	3	68	7.8	8.79
P30085	UMP-CMP kinase	8.01	35.20	2	6	6	9	196	22.2	5.57
P13473	Lysosome-associated membrane glycoprotein 2	8.00	4.88	1	2	2	4	410	44.9	5.63
P41567	Eukaryotic translation initiation factor 1	7.98	25.66	2	2	2	4	113	12.7	7.44
A0A1B0GWA2	Alkyldihydroxyacetonephosphate synthase, peroxisomal (Fragment)	7.98	6.45	2	2	2	5	543	60.9	6.25
Q7L576	Cytoplasmic FMR1-interacting protein 1	7.96	3.67	1	4	4	5	1253	145.1	6.90
A0A087WW66	26S proteasome non-ATPase regulatory subunit 1	7.95	11.02	2	6	7	10	953	105.8	5.41
O00264	Membrane-associated progesterone receptor component 1	7.91	16.92	1	4	4	5	195	21.7	4.70
A0A087WXM8	Basal cell adhesion molecule	7.87	10.71	2	5	5	6	588	63.7	6.10
P35908	Keratin, type II cytoskeletal 2 epidermal	7.87	7.36	1	2	4	7	639	65.4	8.00
Q9Y3U8	60S ribosomal protein L36	7.86	28.57	1	5	5	9	105	12.2	11.59
Q08257	Quinone oxidoreductase	7.86	18.24	2	3	3	4	329	35.2	8.44
Q93009	Ubiquitin carboxyl-terminal hydrolase 7	7.85	6.53	1	4	4	5	1102	128.2	5.55
P63092	Guanine nucleotide-binding protein G(s) subunit alpha isoforms short	7.83	17.26	2	3	4	7	394	45.6	5.82
E5RJR5	S-phase kinase-associated protein 1	7.82	26.38	2	3	3	5	163	18.7	4.70

Accession	Description	Score	Coverage	# Proteins	#Unique Peptides	# Peptides	# PSMs	# AAs	MW [kDa]	calc. pI
P62750	60S ribosomal protein L23a	7.81	31.41	6	4	4	6	156	17.7	10.45
Q03252	Lamin-B2	7.79	11.94	1	6	6	7	620	69.9	5.59
P19367	Hexokinase-1	7.72	7.31	1	4	6	11	917	102.4	6.80
Q15819	Ubiquitin-conjugating enzyme E2 variant 2	7.67	24.83	2	3	3	8	145	16.4	8.09
H7C2W9	60S ribosomal protein L31 (Fragment)	7.62	29.63	5	3	3	6	108	12.8	11.00
G3V1U5	Golgi transport 1 homolog B (S. cerevisiae), isoform CRA_c	7.59	20.27	3	2	2	4	74	8.2	10.26
P09874	Poly [ADP-ribose] polymerase 1	7.58	7.30	1	5	5	6	1014	113.0	8.88
Q9BT78	COP9 signalosome complex subunit 4	7.54	13.05	2	3	3	5	406	46.2	5.83
P04908	Histone H2A type 1-B/E OS=Homo sapiens GN=HIST1H2AB PE=1 SV=2 - [H2A1B_HUMAN]	7.54	57.69	3	1	5	9	130	14.1	11.05
Q96KK5	Histone H2A type 1-H	7.54	58.59	7	1	5	9	128	13.9	10.89
P16104	Histone H2AX	7.54	47.55	1	1	4	8	143	15.1	10.74
H3BR35	Eukaryotic peptide chain release factor GTP-binding subunit ERF3A (Fragment)	7.49	17.47	2	4	4	8	475	52.9	5.63
B5MCW2	60S ribosomal protein L3 (Fragment)	7.49	20.22	3	4	5	12	272	31.2	9.96
K7EIG1	Clustered mitochondria protein homolog (Fragment)	7.48	5.92	2	7	7	9	1251	140.5	6.40
Q9BPX5	Actin-related protein 2/3 complex subunit 5-like protein	7.47	16.34	1	2	2	3	153	16.9	6.60
Q13011	Delta(3,5)-Delta(2,4)-dienoyl-CoA isomerase, mitochondrial	7.43	16.16	1	3	3	4	328	35.8	8.00
Q92990	Glomulin	7.42	12.12	1	4	4	5	594	68.2	5.33
O75874	Isocitrate dehydrogenase [NADP] cytoplasmic	7.41	23.19	1	7	7	13	414	46.6	7.01
P13693	Translationally-controlled tumor protein	7.39	29.65	3	4	4	8	172	19.6	4.93
Q92542	Nicastrin	7.39	6.35	1	3	3	4	709	78.4	5.99
A2A2D0	Stathmin (Fragment)	7.30	31.76	2	3	3	8	85	9.8	7.42

Accession	Description	Score	Coverage	# Proteins	#Unique Peptides	# Peptides	# PSMs	# AAs	MW [kDa]	calc. pI
F8VVM2	Phosphate carrier protein, mitochondrial	7.29	11.11	2	3	3	4	324	36.1	9.26
E9PGT1	Translin	7.26	21.97	2	4	4	8	223	25.6	6.89
Q7Z6Z7	E3 ubiquitin-protein ligase HUWE1	7.25	1.30	1	3	4	4	4374	481.6	5.22
Q9BZE1	39S ribosomal protein L37, mitochondrial	7.24	6.86	2	2	2	11	423	48.1	8.59
E7ES33	Septin-7	7.22	18.23	6	4	5	10	417	48.7	8.73
P04899	Guanine nucleotide-binding protein G(i) subunit alpha-2	7.21	26.76	1	4	6	15	355	40.4	5.54
O60869	Endothelial differentiation-related factor 1	7.20	15.54	1	2	2	3	148	16.4	9.95
Q9NZL9	Methionine adenosyltransferase 2 subunit beta	7.20	23.35	1	5	5	7	334	37.5	7.36
Q9Y266	Nuclear migration protein nudC	7.19	18.43	1	4	4	7	331	38.2	5.38
P25788	Proteasome subunit alpha type-3	7.16	24.31	1	5	5	7	255	28.4	5.33
P25398	40S ribosomal protein S12	7.13	28.03	1	3	3	5	132	14.5	7.21
P21912	Succinate dehydrogenase [ubiquinone] iron-sulfur subunit, mitochondrial	7.12	11.07	1	3	3	4	280	31.6	8.76
D6RHZ5	Protein transport protein Sec31A	7.10	3.53	4	2	2	3	877	96.4	6.38
Q96C90	Protein phosphatase 1 regulatory subunit 14B	7.09	26.53	1	3	3	5	147	15.9	4.86
G3V153	Caprin-1	7.09	10.99	3	4	4	11	628	70.3	5.02
P78347	General transcription factor II-I	7.06	4.71	1	2	2	3	998	112.3	6.39
Q06210	Glutamine--fructose-6-phosphate aminotransferase [isomerizing] 1	7.05	9.30	1	4	4	6	699	78.8	7.11
Q15843	NEDD8	7.04	34.57	1	2	2	7	81	9.1	8.43
O60888	Protein CutA	7.03	22.91	1	2	2	4	179	19.1	5.50
Q15424	Scaffold attachment factor B1	7.02	5.14	1	3	3	7	915	102.6	5.47
Q9HB71	Calcyclin-binding protein	7.02	25.44	1	3	3	3	228	26.2	8.25
P61088	Ubiquitin-conjugating enzyme E2 N	7.01	43.42	1	5	5	7	152	17.1	6.57

Accession	Description	Score	Coverage	# Proteins	#Unique Peptides	# Peptides	# PSMs	# AAs	MW [kDa]	calc. pI
Q14232	Translation initiation factor eIF-2B subunit alpha	6.99	32.46	1	5	5	6	305	33.7	7.33
Q9HCY8	Protein S100-A14	6.98	44.23	1	4	4	7	104	11.7	5.24
K7EN20	Hsp70-binding protein 1 (Fragment)	6.96	37.11	2	2	2	3	97	10.6	7.80
M0R3D6	60S ribosomal protein L18a (Fragment)	6.95	21.99	5	3	3	6	141	16.7	10.77
O95831	Apoptosis-inducing factor 1, mitochondrial	6.93	8.16	1	3	3	4	613	66.9	8.95
Q6NUK1	Calcium-binding mitochondrial carrier protein SCaMC-1	6.92	10.27	1	3	3	3	477	53.3	6.33
Q5T985	Inter-alpha-trypsin inhibitor heavy chain H2	6.89	3.21	2	2	2	4	935	105.2	7.03
A0A0D9SFS3	2-oxoglutarate dehydrogenase, mitochondrial]	6.88	6.09	4	5	5	6	1001	113.2	7.08
C9J8H1	V-type proton ATPase subunit E 1 (Fragment)	6.87	16.75	2	2	2	5	203	23.5	9.04
P19404	NADH dehydrogenase [ubiquinone] flavoprotein 2, mitochondrial	6.84	9.24	2	2	2	4	249	27.4	8.06
Q5T4S7	E3 ubiquitin-protein ligase UBR4	6.83	2.59	1	8	8	8	5183	573.5	6.04
Q96FQ6	Protein S100-A16	6.81	40.78	1	3	3	4	103	11.8	6.79
Q13409	Cytoplasmic dynein 1 intermediate chain 2	6.80	6.43	1	2	2	10	638	71.4	5.20
A0A1B0GUC3	Alpha-ketoglutarate-dependent dioxygenase FTO	6.78	7.33	7	2	2	7	450	51.8	5.16
P55957	BH3-interacting domain death agonist	6.77	29.74	1	3	3	4	195	22.0	5.44
P62304	Small nuclear ribonucleoprotein E	6.76	25.00	1	2	2	5	92	10.8	9.44
O96019	Actin-like protein 6A	6.74	15.62	1	5	5	5	429	47.4	5.60
P14324	Farnesyl pyrophosphate synthase	6.74	7.64	1	3	3	4	419	48.2	6.15
Q9H2P9	Diphthine methyl ester synthase	6.72	13.33	1	2	2	7	285	31.6	5.31
Q9NP72	Ras-related protein Rab-18	6.70	29.61	2	4	4	4	206	23.0	5.24
H3BLU7	Aflatoxin B1 aldehyde reductase member 2 (Fragment)	6.70	10.83	2	2	2	3	314	34.7	7.18

Accession	Description	Score	Coverage	# Proteins	#Unique Peptides	# Peptides	# PSMs	# AAs	MW [kDa]	calc. pI
Q9UBX3	Mitochondrial dicarboxylate carrier	6.69	14.98	3	3	3	3	287	31.3	9.54
E7EQ69	N-alpha-acetyltransferase 50	6.69	25.00	2	4	4	4	168	19.3	8.81
E9PN51	NADH dehydrogenase [ubiquinone] iron-sulfur protein 8, mitochondrial (Fragment)	6.66	28.18	5	3	3	4	110	12.4	9.98
A0AVT1	Ubiquitin-like modifier-activating enzyme 6	6.65	3.52	1	3	3	4	1052	117.9	6.14
Q86U28	Iron-sulfur cluster assembly 2 homolog, mitochondrial	6.65	20.78	1	3	3	3	154	16.5	5.25
E7EMS6	Catechol O-methyltransferase (Fragment)	6.64	33.18	2	4	4	6	223	24.8	5.58
P10620	Microsomal glutathione S-transferase 1	6.60	27.10	1	3	3	3	155	17.6	9.39
P54727	UV excision repair protein RAD23 homolog B	6.59	21.03	1	6	6	11	409	43.1	4.84
Q15404	Ras suppressor protein 1	6.59	11.91	1	2	2	3	277	31.5	8.65
P24539	ATP synthase F(0) complex subunit B1, mitochondrial	6.57	28.52	2	5	5	5	256	28.9	9.36
C9JVN9	L-2-hydroxyglutarate dehydrogenase, mitochondrial	6.57	13.38	2	4	4	5	441	48.4	8.65
P09382	Galectin-1	6.56	20.74	1	2	2	3	135	14.7	5.50
A6NCQ0	ADP-sugar pyrophosphatase	6.55	16.11	4	3	3	5	180	19.9	4.75
Q92621	Nuclear pore complex protein Nup205	6.55	2.44	1	4	4	5	2012	227.8	6.19
P29966	Myristoylated alanine-rich C-kinase substrate	6.54	19.88	1	3	3	4	332	31.5	4.45
A0A087WYS1	UTP--glucose-1-phosphate uridylyltransferase	6.53	8.66	3	3	3	7	508	56.9	7.88
F8VY02	Endoplasmic reticulum resident protein 29	6.53	41.88	2	5	5	8	160	18.1	8.00
P19013	Keratin, type II cytoskeletal 4	6.51	7.30	1	2	3	5	534	57.2	6.61
P43490	Nicotinamide phosphoribosyltransferase	6.46	9.16	1	3	3	7	491	55.5	7.15
Q86SX6	Glutaredoxin-related protein 5, mitochondrial	6.45	21.02	1	2	2	4	157	16.6	6.79
Q9P0J0	NADH dehydrogenase [ubiquinone] 1 alpha subcomplex subunit 13	6.44	25.00	1	3	3	4	144	16.7	8.43

Accession	Description	Score	Coverage	# Proteins	#Unique Peptides	# Peptides	# PSMs	# AAs	MW [kDa]	calc. pI
Q16836	Hydroxyacyl-coenzyme A dehydrogenase, mitochondrial	6.43	18.79	3	3	3	5	314	34.3	8.85
P67775	Serine/threonine-protein phosphatase 2A catalytic subunit alpha isoform	6.41	23.95	1	5	5	6	309	35.6	5.54
C9IZU3	Septin-2 (Fragment)	6.39	53.44	4	4	4	11	131	14.8	5.96
P55884	Eukaryotic translation initiation factor 3 subunit B	6.37	11.55	1	6	6	10	814	92.4	5.00
P11233	Ras-related protein Ral-A	6.36	35.44	2	6	6	6	206	23.6	7.11
Q9NQG5	Regulation of nuclear pre-mRNA domain-containing protein 1B	6.34	16.87	1	4	4	5	326	36.9	5.97
E5RH50	La-related protein 1 (Fragment)	6.33	9.34	3	4	4	6	610	69.7	6.47
Q9NPH2	Inositol-3-phosphate synthase 1	6.33	9.68	1	4	4	7	558	61.0	5.76
H0Y630	Serine/threonine-protein kinase 24 (Fragment)	6.31	12.47	4	3	3	11	369	40.9	6.32
A0A087X0X3	Heterogeneous nuclear ribonucleoprotein M	6.30	7.40	4	3	3	3	730	77.5	8.78
O43678	NADH dehydrogenase [ubiquinone] 1 alpha subcomplex subunit 2	6.29	31.31	1	2	2	3	99	10.9	9.57
Q9Y446	Plakophilin-3	6.26	7.03	1	3	3	5	797	87.0	9.32
P37108	Signal recognition particle 14 kDa protein	6.26	38.24	1	3	3	5	136	14.6	10.04
P26196	Probable ATP-dependent RNA helicase DDX6	6.23	10.35	1	4	4	4	483	54.4	8.66
B0QZ43	Erlin-1 (Fragment)	6.22	10.55	2	2	2	3	275	31.1	7.96
P55327	Tumor protein D52	6.22	22.77	1	1	3	5	224	24.3	4.83
B4DXZ6	Fragile X mental retardation syndrome-related protein 1	6.21	13.49	4	6	6	12	608	68.3	6.05
Q9UMS4	Pre-mRNA-processing factor 19	6.21	10.91	1	3	3	7	504	55.1	6.61
P23588	Eukaryotic translation initiation factor 4B	6.19	16.20	2	6	6	10	611	69.1	5.73
P09110	3-ketoacyl-CoA thiolase, peroxisomal	6.19	15.57	1	5	5	5	424	44.3	8.44
Q00059	Transcription factor A, mitochondrial	6.17	13.41	1	3	3	4	246	29.1	9.72

Accession	Description	Score	Coverage	# Proteins	#Unique Peptides	# Peptides	# PSMs	# AAs	MW [kDa]	calc. pI
A0A087X2D0	Serine/arginine-rich-splicing factor 3	6.16	49.47	2	4	4	11	95	10.3	5.14
Q07960	Rho GTPase-activating protein 1	6.13	10.02	1	2	2	3	439	50.4	6.29
Q9NQP4	Prefoldin subunit 4	6.12	20.15	2	2	2	4	134	15.3	4.53
C9J931	GTP-binding protein Rheb	6.11	32.91	2	2	2	3	79	8.7	6.02
P53004	Biliverdin reductase A	6.09	22.30	1	4	4	5	296	33.4	6.44
A0A087X0K9	Tight junction protein ZO-1	6.09	1.97	4	2	2	3	1676	187.7	6.70
Q9UBF2	Coatomer subunit gamma-2	6.07	7.92	1	3	4	6	871	97.6	5.81
H0YL72	Isocitrate dehydrogenase [NAD] subunit alpha, mitochondrial	6.07	11.78	3	3	3	4	331	35.8	6.44
Q6PI48	Aspartate--tRNA ligase, mitochondrial	6.05	6.36	1	3	3	4	645	73.5	8.02
Q6ZRP7	Sulfhydryl oxidase 2	6.04	6.02	1	3	3	3	698	77.5	7.72
P08708	40S ribosomal protein S17	6.03	41.48	1	3	3	5	135	15.5	9.85
O94826	Mitochondrial import receptor subunit TOM70	6.03	4.77	1	2	2	4	608	67.4	7.12
Q9BR76	Coronin-1B	6.03	11.25	1	3	3	6	489	54.2	5.88
Q15075	Early endosome antigen 1	6.03	8.01	1	8	9	11	1411	162.4	5.68
P49792	E3 SUMO-protein ligase RanBP2	6.03	1.46	1	3	3	3	3224	358.0	6.20
A6PVH9	Copine-1	6.02	11.23	4	4	4	8	481	53.0	5.82
P16435	NADPH--cytochrome P450 reductase	6.01	9.75	3	4	4	4	677	76.6	5.58
P46778	60S ribosomal protein L21	5.98	27.50	3	3	3	4	160	18.6	10.49
C9JJT5	Protein ATP5J2-PTCD1	5.98	44.44	4	2	2	3	54	5.9	9.32
G3V1D1	Ferritin	5.96	32.74	3	4	4	8	113	12.9	5.30
A0A0C4DFU2	Superoxide dismutase	5.95	16.67	3	3	3	5	222	24.7	8.25
P13489	Ribonuclease inhibitor	5.92	13.67	1	4	4	5	461	49.9	4.82
G8JLG1	Structural maintenance of chromosomes protein	5.91	2.89	2	2	2	2	1211	140.8	7.40
A0A087WXR5	NADH dehydrogenase [ubiquinone] 1 alpha subcomplex subunit 5	5.91	53.25	4	3	3	6	77	8.8	4.96
O75947	ATP synthase subunit d, mitochondrial	5.90	26.71	1	3	3	5	161	18.5	5.30
F8W726	Ubiquitin-associated protein 2-like	5.89	2.22	2	2	2	4	1079	113.6	6.68

Accession	Description	Score	Coverage	# Proteins	#Unique Peptides	# Peptides	# PSMs	# AAs	MW [kDa]	calc. pI
Q8N1F7	Nuclear pore complex protein Nup93	5.89	5.74	1	3	3	3	819	93.4	5.72
P12830	Cadherin-1	5.88	6.80	4	3	3	3	882	97.4	4.73
Q7Z7H8	39S ribosomal protein L10, mitochondrial	5.87	11.11	1	2	2	3	261	29.3	9.58
Q9NUJ1	Mycophenolic acid acyl-glucuronide esterase, mitochondrial	5.87	21.24	1	4	4	6	306	33.9	8.57
D3YTB1	60S ribosomal protein L32 (Fragment)	5.87	21.05	3	3	3	4	133	15.6	11.44
G3V198	Nuclear pore complex protein Nup160 (Fragment)	5.84	2.82	2	3	3	4	1314	148.9	5.57
K7EJE8	Lon protease homolog, mitochondrial	5.84	4.95	3	3	3	5	829	93.2	6.49
E9PD53	Structural maintenance of chromosomes protein	5.83	5.94	2	6	6	6	1263	144.4	7.12
H0Y5R6	Uroporphyrinogen decarboxylase (Fragment)	5.82	23.25	3	4	4	5	228	25.4	5.31
H0YC42	Uncharacterized protein	5.81	16.19	1	2	4	5	278	31.2	6.19
Q96TC7	Regulator of microtubule dynamics protein 3	5.81	8.30	1	2	2	2	470	52.1	5.10
Q96A33	Coiled-coil domain-containing protein 47	5.81	16.15	1	6	6	7	483	55.8	4.87
F5GX77	Multifunctional methyltransferase subunit TRM112-like protein	5.80	38.68	2	3	3	4	106	12.0	8.07
A0A0U1RR22	Protein kinase C and casein kinase substrate in neurons protein 2 (Fragment)	5.80	6.87	2	3	3	4	451	51.8	5.34
F2Z388	60S ribosomal protein L35	5.78	23.96	2	2	2	7	96	10.6	10.29
Q8WVM8	Sec1 family domain-containing protein 1	5.74	10.28	1	3	3	4	642	72.3	6.27
O15143	Actin-related protein 2/3 complex subunit 1B	5.73	6.18	1	2	2	3	372	40.9	8.35
F8W7S5	Ribosome-binding protein 1	5.73	6.79	4	3	4	6	751	84.3	5.01
Q5TEJ7	Replication protein A 32 kDa subunit (Fragment)	5.71	21.79	2	2	2	2	179	19.4	6.07
P04080	Cystatin-B	5.69	33.67	1	2	2	6	98	11.1	7.56
E9PHA6	DNA mismatch repair protein	5.69	3.37	2	2	2	4	921	103.1	6.09
J3QT28	Mitotic checkpoint protein BUB3 (Fragment)	5.68	22.66	2	5	5	7	278	31.7	8.16

Accession	Description	Score	Coverage	# Proteins	#Unique Peptides	# Peptides	# PSMs	# AAs	MW [kDa]	calc. pI
Q9ULC4	Malignant T-cell-amplified sequence 1	5.68	36.46	1	4	4	6	181	20.5	8.82
P55145	Mesencephalic astrocyte-derived neurotrophic factor	5.65	22.53	2	4	4	5	182	20.7	8.69
F8VR50	Actin-related protein 2/3 complex subunit 3 (Fragment)	5.62	28.57	3	2	2	5	84	9.7	7.93
A0A087WYD1	AP-2 complex subunit beta (Fragment)	5.62	13.62	5	2	5	8	639	70.9	5.06
R4GN49	Protein S100-A2	5.61	26.56	2	2	2	5	64	7.3	4.49
H0YJW7	SRA stem-loop-interacting RNA-binding protein, mitochondrial (Fragment)	5.59	52.63	6	3	3	6	76	8.7	9.06
B4E1C5	Histidine--tRNA ligase, cytoplasmic	5.57	10.63	3	4	4	5	395	43.9	5.10
P20674	Cytochrome c oxidase subunit 5A, mitochondrial	5.53	18.00	2	4	4	5	150	16.8	6.79
V9GYR2	Sodium/potassium-transporting ATPase subunit beta (Fragment)	5.52	19.23	2	2	2	3	130	15.1	6.16
P49748	Very long-chain specific acyl-CoA dehydrogenase, mitochondrial	5.50	13.28	1	6	6	6	655	70.3	8.75
E9PKV2	39S ribosomal protein L17, mitochondrial (Fragment)	5.50	11.27	2	2	2	2	142	16.4	10.48
J3KQ96	Treacle protein (Fragment)	5.48	2.48	3	3	3	4	1414	144.0	8.29
P10606	Cytochrome c oxidase subunit 5B, mitochondrial	5.47	24.81	1	3	3	7	129	13.7	8.81
F5GXJ9	CD166 antigen	5.40	12.22	2	3	3	4	532	59.5	6.10
H7C024	Glypican-1 (Fragment)	5.36	11.22	3	2	2	3	294	32.9	7.40
Q9NT62	Ubiquitin-like-conjugating enzyme ATG3	5.36	7.32	1	2	2	3	314	35.8	4.74
P22307	Non-specific lipid-transfer protein	5.33	7.68	2	4	4	4	547	59.0	6.89
O76070	Gamma-synuclein	5.32	29.13	1	3	3	3	127	13.3	4.86
M0QYS1	60S ribosomal protein L13a (Fragment)	5.31	15.71	4	3	3	4	210	24.2	10.86
Q96HS1	Serine/threonine-protein phosphatase PGAM5, mitochondrial	5.30	6.23	1	2	2	3	289	32.0	8.68

Accession	Description	Score	Coverage	# Proteins	#Unique Peptides	# Peptides	# PSMs	# AAs	MW [kDa]	calc. pI
C9JIZ0	LSM8 homolog, U6 small nuclear RNA associated (S. cerevisiae), isoform CRA_a	5.29	57.33	2	2	2	2	75	8.1	4.35
Q9H223	EH domain-containing protein 4	5.29	6.65	1	3	3	4	541	61.1	6.76
Q96EL3	39S ribosomal protein L53, mitochondrial	5.27	27.68	1	2	2	3	112	12.1	8.76
P63096	Guanine nucleotide-binding protein G(i) subunit alpha-1	5.26	16.10	1	2	4	13	354	40.3	5.97
P55011	Solute carrier family 12 member 2	5.26	2.56	1	2	2	2	1212	131.4	6.40
Q14498	RNA-binding protein 39	5.23	10.00	1	4	4	5	530	59.3	10.10
Q14914	Prostaglandin reductase 1	5.23	11.25	1	2	2	3	329	35.8	8.29
P30622	CAP-Gly domain-containing linker protein 1	5.22	3.55	1	4	4	4	1438	162.1	5.36
Q9Y3L5	Ras-related protein Rap-2c	5.22	16.94	1	3	3	3	183	20.7	4.94
H3BPC4	SUMO-conjugating enzyme UBC9 (Fragment)	5.21	51.43	4	4	4	5	70	8.0	9.72
P0C0S5	Histone H2A.Z	5.20	46.09	2	2	4	10	128	13.5	10.58
Q5U5X0	Complex III assembly factor LYRM7	5.17	25.96	1	2	2	2	104	11.9	9.66
P30405	Peptidyl-prolyl cis-trans isomerase F, mitochondrial	5.16	37.20	1	3	3	11	207	22.0	9.38
H0Y394	Vigilin (Fragment)	5.12	4.01	3	2	2	2	973	108.8	7.80
O00203	AP-3 complex subunit beta-1	5.12	5.03	1	5	5	6	1094	121.2	6.04
Q9BRA2	Thioredoxin domain-containing protein 17	5.12	30.08	3	3	3	5	123	13.9	5.52
P27144	Adenylate kinase 4, mitochondrial	5.11	17.49	1	3	3	4	223	25.3	8.40
Q9UMX0	Ubiquilin-1	5.10	4.92	1	2	2	2	589	62.5	5.11
A0A087X1A9	Vesicle-trafficking protein SEC22b (Fragment)	5.09	18.99	2	2	2	2	79	8.8	5.19
I3L3Q4	Glyoxalase domain-containing protein 4 (Fragment)	5.07	27.75	3	3	4	5	227	25.5	7.01
Q8WUM0	Nuclear pore complex protein Nup133	5.06	2.77	1	3	3	3	1156	128.9	5.10
P13861	cAMP-dependent protein kinase type II-alpha regulatory subunit	5.01	7.92	1	2	2	2	404	45.5	5.07

Accession	Description	Score	Coverage	# Proteins	#Unique Peptides	# Peptides	# PSMs	# AAs	MW [kDa]	calc. pI
Q92905	COP9 signalosome complex subunit 5	5.00	4.79	1	2	2	3	334	37.6	6.54
Q9Y5M8	Signal recognition particle receptor subunit beta	4.98	29.52	1	5	5	5	271	29.7	9.04
C9J4Z3	60S ribosomal protein L37a	4.97	44.12	2	2	2	4	68	7.6	10.01
C9JBI3	Phosphoserine phosphatase (Fragment)	4.88	24.60	2	4	4	4	187	20.7	6.93
P30837	Aldehyde dehydrogenase X, mitochondrial	4.87	9.09	1	3	3	5	517	57.2	6.80
Q9BQA1	Methylosome protein 50	4.86	10.53	1	2	2	2	342	36.7	5.17
K7EKW4	Isochorismatase domain-containing protein 2 (Fragment)	4.85	35.96	2	3	3	3	178	19.4	8.10
Q53GQ0	Very-long-chain 3-oxoacyl-CoA reductase	4.85	35.58	2	7	7	7	312	34.3	9.32
Q5RKV6	Exosome complex component MTR3	4.84	11.40	1	2	2	2	272	28.2	6.28
O75348	V-type proton ATPase subunit G 1	4.83	16.95	1	2	2	2	118	13.7	8.79
Q99615	DnaJ homolog subfamily C member 7	4.82	7.29	4	3	3	3	494	56.4	6.96
Q12904	Aminoacyl tRNA synthase complex-interacting multifunctional protein 1	4.82	16.99	1	3	3	3	312	34.3	8.43
E7ER77	Endoplasmic reticulum metallopeptidase 1	4.81	5.47	3	3	3	4	841	93.1	8.09
O15355	Protein phosphatase 1G	4.80	5.31	1	2	2	2	546	59.2	4.36
Q9Y5B9	FACT complex subunit SPT16	4.79	3.53	1	2	2	2	1047	119.8	5.66
A6PVN7	Serine/threonine-protein phosphatase 2A activator (Fragment)	4.77	35.94	10	2	2	3	64	7.4	8.47
J3KN66	Torsin-1A-interacting protein 1	4.76	4.51	1	2	2	2	599	67.8	7.90
Q8IZ83	Aldehyde dehydrogenase family 16 member A1	4.76	3.12	1	2	2	3	802	85.1	6.79
B1AKZ5	Astrocytic phosphoprotein PEA-15	4.75	24.07	1	2	2	3	108	12.5	5.17
A0A0C4DGY8	Enolase-phosphatase E1	4.74	28.19	3	2	2	2	149	16.5	6.38
Q13617	Cullin-2	4.74	3.49	2	2	2	2	745	86.9	6.92
Q08945	FACT complex subunit SSRP1	4.70	3.67	1	2	2	2	709	81.0	6.87

Accession	Description	Score	Coverage	# Proteins	#Unique Peptides	# Peptides	# PSMs	# AAs	MW [kDa]	calc. pI
Q96DG6	Carboxymethylenebutenolidase homolog	4.70	20.82	1	2	3	3	245	28.0	7.18
Q99598	Translin-associated protein X	4.69	9.66	1	2	2	5	290	33.1	6.55
Q9UJA5	tRNA (adenine(58)-N(1))-methyltransferase non-catalytic subunit TRM6	4.68	6.04	1	2	2	3	497	55.8	7.55
K7EQA1	Programmed cell death protein 5	4.66	40.23	2	3	3	3	87	10.0	9.00
Q9NVJ2	ADP-ribosylation factor-like protein 8B	4.65	17.74	1	3	3	4	186	21.5	8.43
H0YAC6	Lipopolysaccharide-responsive and beige-like anchor protein (Fragment)	4.65	1.73	3	2	2	2	1505	166.8	5.64
E5RHG9	Cytochrome b-c1 complex subunit 7	4.65	31.58	3	2	2	2	76	9.2	8.12
Q9H444	Charged multivesicular body protein 4b	4.63	12.05	1	2	2	2	224	24.9	4.82
J3KTL8	Structural maintenance of chromosomes flexible hinge domain-containing protein 1 (Fragment)	4.61	2.38	2	3	3	3	1388	155.5	8.02
P40616	ADP-ribosylation factor-like protein 1	4.58	19.89	2	3	3	6	181	20.4	5.72
Q9P287	BRCA2 and CDKN1A-interacting protein	4.56	10.83	1	2	2	2	314	36.0	4.61
Q15645	Pachytene checkpoint protein 2 homolog	4.56	8.33	1	2	2	2	432	48.5	6.09
O00487	26S proteasome non-ATPase regulatory subunit 14	4.56	6.45	1	2	2	3	310	34.6	6.52
Q9BXP5	Serrate RNA effector molecule homolog	4.55	3.54	1	2	2	5	876	100.6	5.96
C9JW69	Regulator of chromosome condensation (Fragment)	4.52	7.26	2	2	2	2	372	39.6	8.37
O95573	Long-chain-fatty-acid--CoA ligase 3	4.51	6.11	1	3	3	5	720	80.4	8.38
H0YAX3	39S ribosomal protein L13, mitochondrial (Fragment)	4.50	74.47	3	3	3	3	47	5.8	4.65
P69849	Nodal modulator 3	4.49	2.95	6	2	2	2	1222	134.0	5.67
Q9BRG1	Vacuolar protein-sorting-associated protein 25	4.48	35.80	2	3	3	4	176	20.7	6.34
X6RJ95	Prostaglandin E synthase 2 (Fragment)	4.47	15.47	2	2	2	5	265	29.1	9.67
Q8WUT1	POLDIP3 protein	4.47	13.10	4	2	2	2	229	24.8	10.70

Accession	Description	Score	Coverage	# Proteins	#Unique Peptides	# Peptides	# PSMs	# AAs	MW [kDa]	calc. pI
Q9UDY2	Tight junction protein ZO-2	4.46	4.62	2	4	4	4	1190	133.9	7.40
Q96C01	Protein FAM136A	4.46	23.19	2	2	3	3	138	15.6	7.61
P67870	Casein kinase II subunit beta	4.45	13.02	2	2	2	2	215	24.9	5.55
A0A087WUL2	Proteasome subunit beta type-3 (Fragment)	4.45	45.52	4	4	4	13	145	16.2	8.43
Q07065	Cytoskeleton-associated protein 4	4.45	4.49	1	2	2	2	602	66.0	5.92
Q9BTT0	Acidic leucine-rich nuclear phosphoprotein 32 family member E	4.41	13.06	1	2	2	2	268	30.7	3.85
A0A0U1RQD1	Chromosome 12 open reading frame 5, isoform CRA_b	4.41	22.27	2	2	2	2	211	23.6	7.28
Q16540	39S ribosomal protein L23, mitochondrial	4.39	29.41	4	3	3	3	153	17.8	9.69
P51665	26S proteasome non-ATPase regulatory subunit 7	4.39	8.33	1	2	2	2	324	37.0	6.77
Q99848	Probable rRNA-processing protein EBP2	4.38	7.19	2	2	2	2	306	34.8	10.10
O43747	AP-1 complex subunit gamma-1	4.36	7.42	1	3	4	8	822	91.3	6.80
F5H6P7	Protein mago nashi homolog 2	4.35	55.88	5	4	4	5	102	11.8	5.52
K7EJR3	26S proteasome non-ATPase regulatory subunit 8 (Fragment)	4.33	10.00	3	2	2	4	250	28.0	8.18
A0A1B0GV75	Carnitine O-palmitoyltransferase 2, mitochondrial	4.31	9.03	5	3	3	3	598	67.1	8.57
F5H796	Diablo homolog, mitochondrial (Fragment)	4.30	19.87	3	3	3	4	156	17.7	4.89
Q96A35	39S ribosomal protein L24, mitochondrial	4.29	12.50	1	2	2	2	216	24.9	9.29
Q9Y570	Protein phosphatase methylesterase 1	4.29	6.99	1	2	2	2	386	42.3	5.97
Q06124	Tyrosine-protein phosphatase non-receptor type 11	4.28	8.04	1	3	3	3	597	68.4	7.30
P61599	N-alpha-acetyltransferase 20	4.28	11.24	1	2	2	2	178	20.4	5.03
Q9H773	dCTP pyrophosphatase 1	4.27	26.47	1	3	3	5	170	18.7	5.03
O75531	Barrier-to-autointegration factor	4.26	19.10	1	3	3	5	89	10.1	6.09

Accession	Description	Score	Coverage	# Proteins	#Unique Peptides	# Peptides	# PSMs	# AAs	MW [kDa]	calc. pI
J3QL26	Serine/threonine-protein phosphatase 4 regulatory subunit 1 (Fragment)	4.25	19.26	4	2	2	2	135	15.5	5.03
Q16204	Coiled-coil domain-containing protein 6	4.24	6.54	1	2	2	2	474	53.3	7.34
Q92878	DNA repair protein RAD50	4.24	3.05	1	3	3	3	1312	153.8	6.89
Q3MHD2	Protein LSM12 homolog	4.24	13.85	2	2	2	2	195	21.7	7.74
Q12996	Cleavage stimulation factor subunit 3	4.23	4.18	1	2	2	2	717	82.9	8.12
Q16850	Lanosterol 14-alpha demethylase	4.23	8.95	2	3	3	3	503	56.8	8.53
Q96E11	Ribosome-recycling factor, mitochondrial	4.22	18.70	1	3	3	4	262	29.3	9.79
Q96CN7	Isochorismatase domain-containing protein 1	4.22	11.07	1	2	2	2	298	32.2	7.39
E9PF63	Rho-associated protein kinase 2	4.21	4.19	3	4	4	4	1145	133.2	5.78
Q9H2G2	STE20-like serine/threonine-protein kinase	4.20	1.86	1	2	2	2	1235	142.6	5.15
Q9P0I2	ER membrane protein complex subunit 3	4.18	9.58	1	2	2	3	261	29.9	6.81
P52657	Transcription initiation factor IIA subunit 2	4.18	22.94	1	2	2	2	109	12.4	6.62
D6R967	Inorganic pyrophosphatase 2, mitochondrial (Fragment)	4.17	15.71	3	2	2	4	191	21.4	6.79
A0A0B4J1W3	N-alpha-acetyltransferase 15, NatA auxiliary subunit	4.16	6.13	2	3	3	9	865	101.1	7.42
P62906	60S ribosomal protein L10a	4.15	23.04	1	4	4	7	217	24.8	9.94
Q16401	26S proteasome non-ATPase regulatory subunit 5	4.15	13.10	1	4	4	4	504	56.2	5.48
E9PB90	Hexokinase-2	4.15	7.20	2	3	5	6	889	98.9	6.04
G5E9W7	28S ribosomal protein S22, mitochondrial	4.14	14.11	3	3	3	3	319	36.8	6.81
Q13308	Inactive tyrosine-protein kinase 7	4.14	2.34	1	2	2	2	1070	118.3	7.09
P50416	Carnitine O-palmitoyltransferase 1, liver isoform	4.14	9.18	1	5	5	5	773	88.3	8.65
Q8NEW0	Zinc transporter 7	4.14	6.91	1	2	2	2	376	41.6	6.95
P22061	Protein-L-isoaspartate(D-aspartate) O-methyltransferase	4.12	11.89	3	2	2	3	227	24.6	7.21

Accession	Description	Score	Coverage	# Proteins	#Unique Peptides	# Peptides	# PSMs	# AAs	MW [kDa]	calc. pI
P24752	Acetyl-CoA acetyltransferase, mitochondrial	4.11	12.18	1	4	4	5	427	45.2	8.85
Q9Y2X3	Nucleolar protein 58	4.10	8.88	1	3	3	3	529	59.5	8.92
I3L378	Ketosamine-3-kinase (Fragment)	4.10	13.71	2	2	2	2	124	13.9	5.67
Q96CS3	FAS-associated factor 2	4.10	8.76	1	3	3	3	445	52.6	5.62
C9J0K6	Sorcin	4.09	13.55	2	2	2	3	155	17.6	5.60
O43765	Small glutamine-rich tetratricopeptide repeat-containing protein alpha	4.09	12.46	2	3	3	3	313	34.0	4.87
Q9UHD1	Cysteine and histidine-rich domain-containing protein 1	4.09	18.37	1	4	4	4	332	37.5	7.87
Q6IAK0	Selenoprotein T	4.08	24.82	3	2	2	5	137	15.8	6.67
Q15050	Ribosome biogenesis regulatory protein homolog	4.08	12.33	1	2	3	4	365	41.2	10.70
Q9H3K6	BolA-like protein 2	4.07	29.07	6	2	2	3	86	10.1	6.52
B1AH77	Ras-related C3 botulinum toxin substrate 2	4.07	16.89	4	2	3	4	148	16.8	8.06
H0YAL7	Eukaryotic translation elongation factor 1 epsilon-1 (Fragment)	4.06	13.24	4	2	2	2	136	15.3	8.40
Q9H061	Transmembrane protein 126A	4.05	28.72	1	3	3	3	195	21.5	9.26
Q13136	Liprin-alpha-1	4.05	3.33	1	3	3	3	1202	135.7	6.29
G5EA06	28S ribosomal protein S27, mitochondrial	4.04	15.36	2	3	3	6	358	41.3	5.52
P21283	V-type proton ATPase subunit C 1	4.04	10.99	1	3	3	3	382	43.9	7.46
Q9UL25	Ras-related protein Rab-21	4.04	21.33	1	3	3	3	225	24.3	7.94
A0A024QZ42	HCG1985580, isoform CRA_c	4.04	17.36	2	2	2	3	121	14.4	5.29
Q8NBS9	Thioredoxin domain-containing protein 5	4.03	9.26	1	3	3	4	432	47.6	5.97
O75822	Eukaryotic translation initiation factor 3 subunit J	4.03	19.77	1	4	4	5	258	29.0	4.83
Q8TBA6	Golgin subfamily A member 5	4.01	2.87	1	2	2	2	731	83.0	5.83
Q15008	26S proteasome non-ATPase regulatory subunit 6	4.00	6.17	1	2	2	3	389	45.5	5.62

Accession	Description	Score	Coverage	# Proteins	#Unique Peptides	# Peptides	# PSMs	# AAs	MW [kDa]	calc. pI
O60341	Lysine-specific histone demethylase 1A	4.00	2.93	1	2	2	2	852	92.8	6.52
O60271	C-Jun-amino-terminal kinase-interacting protein 4	3.95	1.89	1	2	2	2	1321	146.1	5.15
O43920	NADH dehydrogenase [ubiquinone] iron-sulfur protein 5	3.94	22.64	1	2	2	2	106	12.5	9.14
V9GYP5	Uncharacterized protein (Fragment)	3.94	19.82	3	3	3	3	217	23.8	9.31
D3YTI2	Low molecular weight phosphotyrosine protein phosphatase	3.92	54.12	1	1	3	3	85	9.4	8.35
E9PNM1	Squalene synthase	3.92	6.59	2	2	2	2	410	47.3	6.54
Q13177	Serine/threonine-protein kinase PAK 2	3.91	7.82	1	3	3	4	524	58.0	5.96
Q9NS69	Mitochondrial import receptor subunit TOM22 homolog	3.90	36.62	1	3	3	3	142	15.5	4.34
Q9NP97	Dynein light chain roadblock-type 1	3.90	29.17	2	2	2	2	96	10.9	7.25
Q8WWM7	Ataxin-2-like protein	3.89	4.56	1	3	3	4	1075	113.3	8.59
E9PFH4	Transportin-3	3.89	6.53	2	3	3	4	857	96.6	5.66
Q9NYQ6	Cadherin EGF LAG seven-pass G-type receptor 1	3.89	1.06	1	2	2	2	3014	329.3	5.92
H0YDD4	Acetyltransferase component of pyruvate dehydrogenase complex (Fragment)	3.89	16.08	3	4	4	6	479	51.2	8.51
Q9UBQ5	Eukaryotic translation initiation factor 3 subunit K	3.88	18.81	3	3	3	4	218	25.0	4.93
H3BRL3	Ubiquitin domain-containing protein UBFD1	3.87	11.00	2	3	3	5	300	32.6	5.96
F5H1S8	Malectin (Fragment)	3.87	26.03	2	3	3	5	146	16.7	5.57
A0MZ66	Shootin-1	3.87	3.33	1	2	2	2	631	71.6	5.33
P26006	Integrin alpha-3	3.87	3.43	1	3	3	3	1051	116.5	6.77
O75746	Calcium-binding mitochondrial carrier protein Aralar1	3.87	7.08	1	4	4	4	678	74.7	8.38
Q15717	ELAV-like protein 1	3.87	13.50	1	4	4	5	326	36.1	9.17
P11387	DNA topoisomerase 1	3.86	4.44	1	3	3	5	765	90.7	9.31
Q7Z2W9	39S ribosomal protein L21, mitochondrial	3.83	14.15	1	2	2	2	205	22.8	9.89

Accession	Description	Score	Coverage	# Proteins	#Unique Peptides	# Peptides	# PSMs	# AAs	MW [kDa]	calc. pI
P78417	Glutathione S-transferase omega-1	3.83	13.69	1	3	3	3	241	27.5	6.60
P27105	Erythrocyte band 7 integral membrane protein	3.83	19.10	1	3	3	4	288	31.7	7.88
C9IZ80	Basic leucine zipper and W2 domain-containing protein 1 (Fragment)	3.83	12.93	2	2	2	3	294	33.4	7.85
Q96DA6	Mitochondrial import inner membrane translocase subunit TIM14	3.82	19.83	1	2	2	2	116	12.5	10.10
A0A087X1F5	Protein SYNJ2BP-COX16 (Fragment)	3.80	38.82	4	5	5	5	152	17.2	5.15
G5E9R5	Acid phosphatase 1, soluble, isoform CRA_d	3.79	65.00	2	2	4	4	80	9.0	8.34
D6RAY7	Glucosamine-6-phosphate isomerase (Fragment)	3.79	10.13	4	2	2	2	237	27.0	6.52
Q9UKR5	Probable ergosterol biosynthetic protein 28	3.78	20.00	1	2	2	3	140	15.9	9.83
Q8N5K1	CDGSH iron-sulfur domain-containing protein 2	3.75	31.11	1	4	4	4	135	15.3	9.61
Q59FY4	Acetyl-CoA carboxylase 1 (Fragment)	3.75	4.61	2	2	3	3	998	114.5	6.73
B1AHB1	DNA helicase	3.74	10.56	2	5	5	6	691	77.5	8.60
P36952	Serpin B5	3.74	14.40	1	4	4	5	375	42.1	6.05
C9JXZ7	Replication factor C subunit 4 (Fragment)	3.73	23.58	5	2	2	2	123	13.3	9.26
Q9UBI6	Guanine nucleotide-binding protein G(I)/G(S)/G(O) subunit gamma-12	3.72	25.00	1	2	2	3	72	8.0	8.97
P16401	Histone H1.5	3.72	14.60	1	3	3	8	226	22.6	10.92
A0A0B4J1Z1	Serine/arginine-rich-splicing factor 7	3.70	30.66	3	3	3	5	137	15.8	9.80
Q9NZ45	CDGSH iron-sulfur domain-containing protein 1	3.70	25.93	1	2	2	3	108	12.2	9.09
P61009	Signal peptidase complex subunit 3	3.69	17.78	1	3	3	3	180	20.3	8.62
P07954	Fumarate hydratase, mitochondrial	3.67	6.47	1	2	2	2	510	54.6	8.76
P00403	Cytochrome c oxidase subunit 2	3.67	13.22	1	2	2	5	227	25.5	4.82
Q01105	Protein SET	3.66	23.10	4	4	4	9	290	33.5	4.32

Accession	Description	Score	Coverage	# Proteins	#Unique Peptides	# Peptides	# PSMs	# AAs	MW [kDa]	calc. pI
Q9BU61	NADH dehydrogenase [ubiquinone] 1 alpha subcomplex assembly factor 3	3.66	11.96	1	2	2	2	184	20.3	8.22
B8ZZA8	Glutaminase kidney isoform, mitochondrial	3.65	14.20	1	2	2	2	169	18.6	6.86
Q96I99	Succinate--CoA ligase [GDP-forming] subunit beta, mitochondrial	3.60	14.35	1	4	4	4	432	46.5	6.39
Q8TAT6	Nuclear protein localization protein 4 homolog	3.60	10.69	1	4	4	6	608	68.1	6.38
J3QQY2	Calcium load-activated calcium channel	3.59	27.88	3	2	2	5	104	11.4	9.66
P55036	26S proteasome non-ATPase regulatory subunit 4	3.59	7.16	2	2	2	2	377	40.7	4.79
Q9H8Y8	Golgi reassembly-stacking protein 2	3.57	8.41	1	2	2	2	452	47.1	4.82
E7EPN9	Protein PRRC2C	3.55	1.42	2	3	3	3	2819	308.6	9.07
F8VPD4	CAD protein	3.54	1.67	2	3	3	3	2162	235.9	6.55
Q04760	Lactoylglutathione lyase	3.54	21.20	1	3	3	5	184	20.8	5.31
E7EU96	Casein kinase II subunit alpha	3.54	7.79	3	2	2	4	385	45.3	7.94
P68402	Platelet-activating factor acetylhydrolase IB subunit beta	3.53	12.23	1	2	2	5	229	25.6	5.92
Q9Y230	RuvB-like 2	3.52	23.76	1	8	8	12	463	51.1	5.64
Q6NXT2	Histone H3.3C	3.51	13.33	1	2	2	3	135	15.2	11.11
P62873	Guanine nucleotide-binding protein G(I)/G(S)/G(T) subunit beta-1	3.51	6.76	1	2	2	2	340	37.4	6.00
E7EQV9	Ribosomal protein L15 (Fragment)	3.50	29.31	3	4	4	7	174	20.5	11.28
Q9NR31	GTP-binding protein SAR1a	3.50	31.82	2	4	4	7	198	22.4	6.68
C9J9W2	LIM and SH3 domain protein 1 (Fragment)	3.47	15.06	2	2	2	4	166	19.0	9.01
H3BR27	RNA-binding motif protein, X chromosome	3.45	44.87	7	3	3	6	78	8.6	5.49
Q5T8U5	Surfeit 4	3.45	15.59	2	2	2	4	186	21.1	6.52
F8WBG8	Drebrin-like protein	3.43	20.31	2	2	2	3	128	13.7	7.21
Q13185	Chromobox protein homolog 3	3.43	16.39	1	2	2	5	183	20.8	5.33

Accession	Description	Score	Coverage	# Proteins	#Unique Peptides	# Peptides	# PSMs	# AAs	MW [kDa]	calc. pI
Q8TCS8	Polyribonucleotide nucleotidyltransferase 1, mitochondrial	3.42	8.81	1	5	5	5	783	85.9	7.77
Q9P2I0	Cleavage and polyadenylation specificity factor subunit 2	3.41	3.45	1	2	2	3	782	88.4	5.11
P19623	Spermidine synthase	3.41	6.95	1	2	2	2	302	33.8	5.49
O60762	Dolichol-phosphate mannosyltransferase subunit 1	3.37	10.38	3	2	2	3	260	29.6	9.57
P18031	Tyrosine-protein phosphatase non-receptor type 1	3.37	8.28	1	3	3	3	435	49.9	6.27
A0A075B730	Epiplakin	3.35	6.06	3	3	3	4	5063	552.8	5.60
G8JLP4	Meiosis arrest female protein 1	3.32	2.16	3	2	3	4	1577	174.9	7.28
Q9UMX5	Neudesin	3.27	13.95	1	2	2	2	172	18.8	5.69
Q96TA1	Niban-like protein 1	3.24	4.96	1	2	3	4	746	84.1	6.19
Q92734	Protein TFG	3.18	12.50	1	2	2	3	400	43.4	5.10
J3QQV6	Pyridoxine-5'-phosphate oxidase (Fragment)	3.17	17.50	2	2	2	2	120	13.9	7.87
P39748	Flap endonuclease 1	3.16	11.32	1	2	2	2	380	42.6	8.62
E9PLT0	Cold shock domain-containing protein E1	3.15	5.54	2	2	2	7	668	74.5	6.09
E7ETJ9	Nucleolysin TIAR (Fragment)	3.10	21.21	2	2	2	2	132	14.6	8.15
H0YDP7	39S ribosomal protein L49, mitochondrial (Fragment)	3.07	20.47	2	2	2	2	127	14.7	10.21
Q14739	Lamin-B receptor	3.04	7.32	1	3	3	3	615	70.7	9.36
P52788	Spermine synthase	3.00	26.78	1	5	5	6	366	41.2	5.02
O75663	TIP41-like protein	2.89	10.66	1	2	2	2	272	31.4	5.91
Q15056	Eukaryotic translation initiation factor 4H	2.88	14.92	1	2	2	2	248	27.4	7.23
Q9UBB4	Ataxin-10	2.87	20.63	1	5	6	6	475	53.5	5.25
D6R991	Matrin-3 (Fragment)	2.78	12.24	4	3	3	5	433	48.1	7.50
Q99959	Plakophilin-2	2.77	3.75	1	2	2	2	881	97.4	9.33
Q8N766	ER membrane protein complex subunit 1	2.76	3.22	1	2	2	2	993	111.7	7.66
Q6IAA8	Ragulator complex protein LAMTOR1	2.76	16.15	1	2	2	3	161	17.7	5.15

Accession	Description	Score	Coverage	# Proteins	#Unique Peptides	# Peptides	# PSMs	# AAs	MW [kDa]	calc. pI
Q93034	Cullin-5	2.71	6.54	1	3	3	3	780	90.9	7.94
B7Z6D5	Probable ATP-dependent RNA helicase DDX27	2.71	3.66	2	2	2	2	765	86.6	9.25
C9JQD4	Peptidyl-prolyl cis-trans isomerase (Fragment)	2.69	34.72	2	4	4	4	144	15.8	8.72
H0YD13	CD44 antigen	2.69	12.14	3	2	2	3	206	22.7	8.19
Q5K651	Sterile alpha motif domain-containing protein 9	2.68	2.27	1	2	2	2	1589	184.2	7.83
P61970	Nuclear transport factor	2.67	29.13	1	2	2	4	127	14.5	5.38
H0YA83	Beta-hexosaminidase subunit beta (Fragment)	2.63	18.24	3	2	2	2	170	19.5	5.71
P62310	U6 snRNA-associated Sm-like protein LSm3	2.62	19.61	1	2	2	2	102	11.8	4.70
O60306	Intron-binding protein aquarius	2.60	2.49	1	2	2	2	1485	171.2	6.37
Q9BSD7	Cancer-related nucleoside-triphosphatase	2.58	18.42	2	2	2	2	190	20.7	9.54
A0A087WZK9	Eukaryotic translation initiation factor 3 subunit H	2.57	10.89	3	2	2	2	349	39.6	6.39
P49790	Nuclear pore complex protein Nup153	2.53	3.25	1	3	3	3	1475	153.8	8.73
Q96HY6	DDRGK domain-containing protein 1	2.52	9.87	1	2	2	2	314	35.6	5.12
P62993	Growth factor receptor-bound protein 2	2.51	11.98	1	2	2	2	217	25.2	6.32
Q9Y3B4	Splicing factor 3B subunit 6	2.46	20.00	1	2	2	2	125	14.6	9.38
P68036	Ubiquitin-conjugating enzyme E2 L3	2.44	51.95	1	4	4	5	154	17.9	8.51
P53634	Dipeptidyl peptidase 1	2.43	5.62	1	2	2	2	463	51.8	6.99
E9PS17	N-terminal kinase-like protein	2.43	3.48	3	2	2	3	775	85.7	5.67
P48147	Prolyl endopeptidase	2.42	4.37	1	2	2	3	710	80.6	5.86
P11279	Lysosome-associated membrane glycoprotein 1	2.41	5.04	1	2	2	5	417	44.9	8.75
A0A087X020	Ribosome maturation protein SBDS	2.38	21.20	2	4	4	6	250	28.8	8.75
Q9UGP8	Translocation protein SEC63 homolog	2.37	4.61	1	2	2	3	760	87.9	5.31
F6RFD5	Destrin	2.37	20.74	2	2	2	3	135	15.4	8.59

Accession	Description	Score	Coverage	# Proteins	#Unique Peptides	# Peptides	# PSMs	# AAs	MW [kDa]	calc. pI
P11177	Pyruvate dehydrogenase E1 component subunit beta, mitochondrial	2.37	8.91	1	2	2	2	359	39.2	6.65
A0A0A0MRA3	Titin	2.37	0.10	3	2	2	2	27118	3012.1	6.71
O75083	WD repeat-containing protein 1	2.37	7.26	2	3	3	3	606	66.2	6.65
Q9P2B2	Prostaglandin F2 receptor negative regulator	2.35	2.73	1	2	2	2	879	98.5	6.61
C9JRP1	Anion exchange protein (Fragment)	2.35	2.76	4	2	2	2	1051	118.4	7.31
Q9NQR4	Omega-amidase NIT2	2.33	32.61	1	6	6	6	276	30.6	7.21
F5GYN4	Ubiquitin thioesterase OTUB1	2.32	10.37	4	2	2	3	241	28.0	5.29
E7EPW2	28S ribosomal protein S25, mitochondrial	2.31	20.00	2	2	2	2	110	12.9	9.74
P48507	Glutamate--cysteine ligase regulatory subunit	2.31	10.58	1	2	2	2	274	30.7	6.02
P61923	Coatomer subunit zeta-1	2.31	28.25	8	4	4	4	177	20.2	4.81
P35270	Sepiapterin reductase	2.29	19.54	1	3	3	3	261	28.0	8.05
Q01082	Spectrin beta chain, non-erythrocytic 1	2.29	0.97	2	1	2	2	2364	274.4	5.57
G5EA31	Protein transport protein Sec24C	2.28	4.89	2	3	3	4	1042	111.9	6.37
F5H365	Protein transport protein Sec23A	2.28	6.25	2	3	3	4	736	82.9	7.46
Q15813	Tubulin-specific chaperone E	2.28	7.59	1	2	2	6	527	59.3	6.76
P61163	Alpha-centractin	2.27	15.16	2	3	3	3	376	42.6	6.64
P50552	Vasodilator-stimulated phosphoprotein	2.27	10.53	1	2	3	4	380	39.8	8.94
P01111	GTPase NRas	2.25	19.58	2	2	2	4	189	21.2	5.17
Q9UI09	NADH dehydrogenase [ubiquinone] 1 alpha subcomplex subunit 12	2.25	20.00	1	2	2	2	145	17.1	9.63
P30740	Leukocyte elastase inhibitor	2.25	11.08	1	3	3	3	379	42.7	6.28
B4DE93	NADH dehydrogenase [ubiquinone] flavoprotein 1, mitochondrial	2.24	5.23	3	2	2	2	363	39.4	6.46
A0A087X1A5	Double-stranded RNA-binding protein Staufen homolog 1	2.24	5.07	3	2	2	2	493	54.9	9.67

Accession	Description	Score	Coverage	# Proteins	#Unique Peptides	# Peptides	# PSMs	# AAs	MW [kDa]	calc. pI
H7BZ20	Thymidylate kinase (Fragment)	2.23	11.98	2	2	2	2	192	21.8	8.18
B4DIH5	COP9 signalosome complex subunit 2	2.23	15.57	2	4	4	5	379	44.2	5.87
Q5T3Q7	HEAT repeat-containing protein 1	2.23	1.36	2	2	2	2	2063	233.1	6.60
P31937	3-hydroxyisobutyrate dehydrogenase, mitochondrial	2.23	8.04	1	2	2	2	336	35.3	8.13
A0A0A0MRM8	Unconventional myosin-VI	2.22	2.47	4	2	2	3	1253	144.9	8.56
Q9NTX5	Ethylmalonyl-CoA decarboxylase	2.22	9.45	1	2	2	2	307	33.7	8.21
E9PE82	Short-chain-specific acyl-CoA dehydrogenase, mitochondrial	2.21	9.31	2	2	2	2	408	44.0	8.35
A0A0A6YYA0	Protein TMED7-TICAM2	2.20	16.49	2	2	2	2	188	21.2	6.20
P50897	Palmitoyl-protein thioesterase 1	2.19	9.48	1	2	2	2	306	34.2	6.52
Q15006	ER membrane protein complex subunit 2	2.19	9.76	1	2	2	2	297	34.8	6.57
Q9H2W6	39S ribosomal protein L46, mitochondrial	2.16	15.77	1	3	3	4	279	31.7	7.05
A0A0A0MSW4	Phosphatidylinositol transfer protein beta isoform	2.15	20.66	4	3	3	5	271	31.6	6.87
C9JLU1	DNA-directed RNA polymerases I, II, and III subunit RPABC3 (Fragment)	2.14	19.59	2	2	2	3	148	16.9	4.68
J3KTJ8	60S ribosomal protein L26 (Fragment)	2.13	27.08	9	4	4	4	96	11.5	10.90
C9JVB6	Mitochondrial ribonuclease P protein 1 (Fragment)	2.12	7.37	2	2	2	4	312	36.8	9.16
O60264	SWI/SNF-related matrix-associated actin-dependent regulator of chromatin subfamily A member 5	2.12	2.38	1	2	2	3	1052	121.8	8.09
Q9P1F3	Costars family protein ABRACL	2.12	19.75	1	2	2	3	81	9.1	6.29
O95837	Guanine nucleotide-binding protein subunit alpha-14	2.11	9.58	2	2	2	2	355	41.5	6.07
Q15637	Splicing factor 1	2.11	5.32	1	2	2	3	639	68.3	8.98
P62253	Ubiquitin-conjugating enzyme E2 G1	2.10	25.88	1	2	2	2	170	19.5	5.30

Accession	Description	Score	Coverage	# Proteins	#Unique Peptides	# Peptides	# PSMs	# AAs	MW [kDa]	calc. pI
P35237	Serpin B6	2.10	9.31	3	2	2	2	376	42.6	5.27
Q6ZXV5	Transmembrane and TPR repeat-containing protein 3	2.08	2.40	1	2	2	2	915	103.9	8.87
G3XAH6	Poly(A) polymerase alpha	2.07	4.14	2	2	2	3	724	80.6	8.10
Q15020	Squamous cell carcinoma antigen recognized by T-cells 3	2.07	2.39	1	2	2	3	963	109.9	5.57
P46977	Dolichyl-diphosphooligosaccharide--protein glycosyltransferase subunit STT3A	2.05	4.54	1	2	2	3	705	80.5	8.07
B4DWA1	Brain-specific angiogenesis inhibitor 1-associated protein 2	2.05	9.07	3	2	2	2	375	40.6	9.06
Q9H3N1	Thioredoxin-related transmembrane protein 1	2.05	8.93	1	2	2	3	280	31.8	4.98
A0A0G2JS82	AP-2 complex subunit alpha-2 (Fragment)	2.04	3.71	2	2	2	2	917	101.6	6.86
Q3LXA3	Triokinase/FMN cyclase	2.04	4.87	1	2	2	2	575	58.9	7.49
P35573	Glycogen debranching enzyme	2.04	1.63	1	2	2	2	1532	174.7	6.76
E9PFT6	Hemoglobin subunit delta	2.03	13.48	3	2	2	3	141	15.4	7.91
P06730	Eukaryotic translation initiation factor 4E	2.02	8.29	2	2	2	2	217	25.1	6.15
H7BZI1	Nucleobindin-1 (Fragment)	2.02	8.14	2	2	2	2	295	34.9	5.21
Q13155	Aminoacyl tRNA synthase complex-interacting multifunctional protein 2	2.02	18.44	3	3	3	4	320	35.3	8.22
P62280	40S ribosomal protein S11	2.02	36.08	2	5	5	6	158	18.4	10.30
H7BZT7	S-formylglutathione hydrolase (Fragment)	2.02	17.83	3	2	2	2	230	25.5	6.86
Q9BRX8	Redox-regulatory protein FAM213A	2.01	17.47	1	4	4	4	229	25.7	8.84
Q9NQH7	Probable Xaa-Pro aminopeptidase 3	2.00	4.73	1	1	2	7	507	57.0	6.83
Q5SZE2	Ceramide synthase 2 (Fragment)	2.00	19.53	6	2	2	2	128	15.3	9.69
E7EMB6	Aspartyl aminopeptidase	2.00	9.76	3	2	2	3	410	45.0	6.79
Q9HCC0	Methylcrotonoyl-CoA carboxylase beta chain, mitochondrial	1.99	3.91	1	2	2	2	563	61.3	7.68

Accession	Description	Score	Coverage	# Proteins	#Unique Peptides	# Peptides	# PSMs	# AAs	MW [kDa]	calc. pI
H0YNG3	Signal peptidase complex catalytic subunit SEC11	1.98	17.79	4	3	3	4	163	18.6	9.55
Q13423	NAD(P) transhydrogenase, mitochondrial	1.94	2.58	1	2	2	2	1086	113.8	8.09
O00743	Serine/threonine-protein phosphatase 6 catalytic subunit	1.94	9.18	1	2	2	2	305	35.1	5.69
F8W7Q4	Protein FAM162A	1.93	21.53	2	2	2	3	144	16.5	9.77
Q70UQ0	Inhibitor of nuclear factor kappa-B kinase-interacting protein	1.93	8.29	1	2	2	2	350	39.3	9.17
Q9P0L0	Vesicle-associated membrane protein-associated protein A	1.92	11.24	1	2	3	4	249	27.9	8.62
H3BP78	Fanconi anemia group I protein (Fragment)	1.90	1.56	3	1	2	2	1090	122.9	6.52
F5GWX5	Chromodomain-helicase-DNA-binding protein 4	1.90	2.15	3	3	3	3	1905	217.0	5.81
P00568	Adenylate kinase isoenzyme 1	1.89	20.10	2	3	3	4	194	21.6	8.63
E9PES6	High mobility group protein B3 (Fragment)	1.86	35.95	4	3	4	5	153	17.5	9.79
Q9NX63	MICOS complex subunit MIC19	1.86	11.45	3	2	2	2	227	26.1	8.28
Q9Y3D6	Mitochondrial fission 1 protein	1.86	21.71	1	3	3	3	152	16.9	8.79
P58546	Myotrophin	1.86	43.22	2	3	3	5	118	12.9	5.52
Q9NTI5	Sister chromatid cohesion protein PDS5 homolog B	1.85	3.94	1	4	4	4	1447	164.6	8.47
P05556	Integrin beta-1	1.84	6.27	1	4	4	5	798	88.4	5.39
R4GN98	Protein S100 (Fragment)	1.84	17.65	2	2	2	2	85	9.7	5.45
Q7L014	Probable ATP-dependent RNA helicase DDX46	1.84	3.69	2	3	3	3	1031	117.3	9.29
C9JA36	Sodium/potassium-transporting ATPase subunit beta-3 (Fragment)	1.84	19.55	2	2	2	3	133	15.0	5.22
H0YFY6	Nuclear mitotic apparatus protein 1 (Fragment)	1.82	2.18	2	2	2	2	964	107.3	9.09
P60983	Glia maturation factor beta	1.82	19.72	2	2	2	4	142	16.7	5.29
Q13618	Cullin-3	1.79	5.99	1	3	3	3	768	88.9	8.48
M0R0P1	rRNA 2'-O-methyltransferase fibrillarin (Fragment)	1.78	18.42	6	3	3	4	228	24.5	10.11

Accession	Description	Score	Coverage	# Proteins	#Unique Peptides	# Peptides	# PSMs	# AAs	MW [kDa]	calc. pI
P06396	Gelsolin	1.78	4.48	1	2	2	2	782	85.6	6.28
O75306	NADH dehydrogenase [ubiquinone] iron-sulfur protein 2, mitochondrial	1.77	6.70	1	2	2	3	463	52.5	7.55
O95292	Vesicle-associated membrane protein-associated protein B/C	1.77	12.35	1	2	3	3	243	27.2	7.30
Q13243	Serine/arginine-rich splicing factor 5	1.76	13.24	1	1	3	4	272	31.2	11.59
P30419	Glycylpeptide N-tetradecanoyltransferase 1	1.76	5.44	1	2	2	2	496	56.8	7.80
O00515	Ladinin-1	1.76	6.77	2	3	3	3	517	57.1	9.67
Q13247	Serine/arginine-rich splicing factor 6	1.75	8.72	1	2	3	6	344	39.6	11.43
A0A087X2B5	Basigin (Fragment)	1.75	17.19	3	3	3	3	221	23.9	5.25
E1CEI4	Glutamate--cysteine ligase catalytic subunit	1.75	3.34	2	2	2	2	599	68.6	5.94
Q96DC0	DCI protein	1.75	11.93	2	3	3	3	243	27.0	6.77
B1AJY5	26S proteasome non-ATPase regulatory subunit 10	1.73	18.38	3	2	2	2	185	20.2	5.58
O15481	Melanoma-associated antigen B4	1.72	6.07	1	1	2	5	346	38.9	9.25
K7ER90	Eukaryotic translation initiation factor 3 subunit G (Fragment)	1.72	9.69	3	3	3	3	227	25.4	5.49
P13726	Tissue factor	1.71	21.36	1	3	3	4	295	33.0	7.03
A0A087WXS7	ATPase ASNA1	1.71	5.74	2	2	2	2	331	37.1	5.14
Q00765	Receptor expression-enhancing protein 5	1.70	9.52	1	2	2	2	189	21.5	8.10
M0QXU7	Mitochondrial import inner membrane translocase subunit TIM44 (Fragment)	1.70	10.99	2	3	3	3	273	31.1	9.48
F8VR84	UPF0160 protein MYG1, mitochondrial	1.70	9.39	3	2	2	3	213	24.0	5.39
P48163	NADP-dependent malic enzyme	1.69	5.24	1	2	2	5	572	64.1	6.13
P35244	Replication protein A 14 kDa subunit	1.68	51.24	2	4	4	4	121	13.6	5.08
P52732	Kinesin-like protein KIF11	1.67	4.36	1	2	3	4	1056	119.1	5.64
H0YJH9	Polyadenylate-binding protein 2 (Fragment)	1.67	26.04	4	2	2	2	96	11.1	11.27

Accession	Description	Score	Coverage	# Proteins	#Unique Peptides	# Peptides	# PSMs	# AAs	MW [kDa]	calc. pI
M0R0C3	Mitochondrial import inner membrane translocase subunit TIM50 (Fragment)	1.67	26.92	3	2	2	3	104	12.0	7.25
Q00688	Peptidyl-prolyl cis-trans isomerase FKBP3	1.66	14.29	1	3	3	3	224	25.2	9.28
E9PQK4	CUGBP Elav-like family member 1 (Fragment)	1.65	34.48	5	2	2	2	87	9.9	6.52
C9J0J7	Profilin	1.65	31.87	5	2	2	2	91	9.8	9.17
O00231	26S proteasome non-ATPase regulatory subunit 11	1.65	25.59	2	8	8	9	422	47.4	6.48
P52888	Thimet oligopeptidase	1.65	3.05	1	2	2	2	689	78.8	6.05
O14874	[3-methyl-2-oxobutanoate dehydrogenase [lipoamide]] kinase, mitochondrial	1.64	6.31	1	2	2	3	412	46.3	8.82
A0A087X142	Septin-8	1.64	3.99	5	1	2	4	426	49.3	6.20
H0Y3P2	Eukaryotic translation initiation factor 4 gamma 2	1.64	3.45	3	2	2	5	869	98.1	6.99
P42677	40S ribosomal protein S27	1.64	38.10	2	3	3	5	84	9.5	9.45
Q08380	Galectin-3-binding protein	1.64	7.52	1	3	3	3	585	65.3	5.27
Q13347	Eukaryotic translation initiation factor 3 subunit I	1.64	11.69	1	3	3	3	325	36.5	5.64
P49756	RNA-binding protein 25	1.62	4.98	1	3	3	4	843	100.1	6.32
E5RIZ4	39S ribosomal protein L15, mitochondrial (Fragment)	1.62	16.88	3	3	3	3	237	27.2	9.57
O75940	Survival of motor neuron-related-splicing factor 30	1.62	13.03	1	2	2	3	238	26.7	7.24
Q8N3D4	EH domain-binding protein 1-like protein 1	1.62	2.10	1	2	2	2	1523	161.8	4.83
O14656	Torsin-1A	1.61	7.53	1	2	2	2	332	37.8	6.99
P69905	Hemoglobin subunit alpha	1.61	16.90	1	2	2	2	142	15.2	8.68
P48637	Glutathione synthetase	1.60	10.55	1	3	3	3	474	52.4	5.92
Q8NC51	Plasminogen activator inhibitor 1 RNA-binding protein	1.60	6.62	1	2	2	4	408	44.9	8.65
P84090	Enhancer of rudimentary homolog	0.00	30.77	1	2	2	2	104	12.3	5.92
P83876	Thioredoxin-like protein 4A	0.00	21.83	1	2	2	3	142	16.8	5.85
Q16537	Serine/threonine-protein phosphatase 2A 56 kDa	0.00	5.78	1	2	2	2	467	54.7	6.95

Accession	Description	Score	Coverage	# Proteins	#Unique Peptides	# Peptides	# PSMs	# AAs	MW [kDa]	calc. pI
	regulatory subunit epsilon isoform									
O00170	AH receptor-interacting protein	0.00	7.27	1	2	2	2	330	37.6	6.29
Q9BPX3	Condensin complex subunit 3	0.00	2.76	1	2	2	2	1015	114.3	5.59
O43237	Cytoplasmic dynein 1 light intermediate chain 2	0.00	6.30	1	2	2	2	492	54.1	6.38
Q7L2H7	Eukaryotic translation initiation factor 3 subunit M	0.00	12.03	3	3	3	7	374	42.5	5.63
Q9BS26	Endoplasmic reticulum resident protein 44	0.00	6.40	1	2	2	2	406	46.9	5.26
Q13158	FAS-associated death domain protein	0.00	20.19	1	3	3	3	208	23.3	5.69
P06241	Tyrosine-protein kinase Fyn	0.00	4.10	1	1	2	4	537	60.7	6.67
O76003	Glutaredoxin-3	0.00	12.84	1	3	3	3	335	37.4	5.39
Q8TCT9	Minor histocompatibility antigen H13	0.00	9.02	1	2	2	2	377	41.5	6.43
Q13907	Isopentenyl-diphosphate Delta-isomerase 1	0.00	14.10	1	2	2	2	227	26.3	6.34
P20042	Eukaryotic translation initiation factor 2 subunit 2	0.00	8.41	1	2	2	3	333	38.4	5.80
Q9Y4Z0	U6 snRNA-associated Sm-like protein LSm4	0.00	17.27	2	2	2	2	139	15.3	9.99
Q9Y2Q5	Ragulator complex protein LAMTOR2	0.00	40.00	1	2	2	4	125	13.5	5.40
Q9Y316	Protein MEMO1	0.00	9.43	1	2	2	2	297	33.7	7.14
Q9Y6C9	Mitochondrial carrier homolog 2	0.00	13.86	2	3	3	3	303	33.3	7.97
P22033	Methylmalonyl-CoA mutase, mitochondrial	0.00	3.20	1	2	2	2	750	83.1	6.93
Q14CX7	N-alpha-acetyltransferase 25, NatB auxiliary subunit	0.00	2.37	1	2	2	2	972	112.2	6.64
Q09161	Nuclear cap-binding protein subunit 1	0.00	3.29	1	2	2	3	790	91.8	6.43
Q9Y2A7	Nck-associated protein 1	0.00	3.46	1	2	2	2	1128	128.7	6.62
Q9BV86	N-terminal Xaa-Pro-Lys N-methyltransferase 1	0.00	10.76	1	2	2	2	223	25.4	5.52
Q01970	1-phosphatidylinositol 4,5-bisphosphate phosphodiesterase beta-3	0.00	2.35	1	2	2	2	1234	138.7	5.90
Q92900	Regulator of nonsense transcripts 1	0.00	2.57	1	2	2	3	1129	124.3	6.61

Accession	Description	Score	Coverage	# Proteins	#Unique Peptides	# Peptides	# PSMs	# AAs	MW [kDa]	calc. pI
Q8IXM3	39S ribosomal protein L41, mitochondrial	0.00	27.74	1	4	4	4	137	15.4	9.57
P82930	28S ribosomal protein S34, mitochondrial	0.00	11.93	2	2	2	2	218	25.6	9.98
P08579	U2 small nuclear ribonucleoprotein B"	0.00	16.44	1	2	2	2	225	25.5	9.72
P60903	Protein S100-A10	0.00	27.84	1	2	2	4	97	11.2	7.37
O95347	Structural maintenance of chromosomes protein 2	0.00	6.10	1	6	6	6	1197	135.6	8.43
Q96JX3	Protein SERAC1	0.00	4.43	1	2	2	2	654	74.1	7.68
Q9UEW8	STE20/SPS1-related proline-alanine-rich protein kinase	0.00	4.22	1	2	2	2	545	59.4	6.29
O43776	Asparagine--tRNA ligase, cytoplasmic	0.00	5.66	1	2	2	2	548	62.9	6.25
P29144	Tripeptidyl-peptidase 2	0.00	2.80	2	2	2	3	1249	138.3	6.32
Q9Y2W1	Thyroid hormone receptor-associated protein 3	0.00	2.30	1	2	2	2	955	108.6	10.15
O95881	Thioredoxin domain-containing protein 12	0.00	17.44	1	2	2	3	172	19.2	5.40
Q9Y4E8	Ubiquitin carboxyl-terminal hydrolase 15	0.00	2.85	1	2	2	2	981	112.3	5.22
P07947	Tyrosine-protein kinase Yes	0.00	5.16	2	1	2	3	543	60.8	6.74
E7EWK3	ATP-dependent RNA helicase DHX36 (Fragment)	0.00	3.14	2	2	2	2	797	91.4	7.28
B4DFG0	Protein DEK	0.00	6.92	3	3	3	3	347	39.5	8.51
B5MCT8	40S ribosomal protein S9	0.00	19.42	3	4	4	4	139	16.6	11.06
C9JFE4	COP9 signalosome complex subunit 1	0.00	7.22	5	3	3	4	471	53.3	6.74
J3KT68	Transmembrane protein 97	0.00	25.00	2	2	2	2	92	11.0	7.97
H3BTA2	Serine/threonine-protein phosphatase (Fragment)	0.00	8.99	2	2	2	2	267	30.5	5.31
F8VZN8	Protein phosphatase 1 regulatory subunit 12A (Fragment)	0.00	3.76	4	3	3	4	692	76.5	5.31
C9K0M0	Trifunctional enzyme subunit beta, mitochondrial (Fragment)	0.00	23.81	5	2	2	2	84	9.3	10.77
J3QL05	Serine/arginine-rich-splicing factor 2 (Fragment)	0.00	11.54	4	2	2	3	130	15.1	10.96

Accession	Description	Score	Coverage	# Proteins	#Unique Peptides	# Peptides	# PSMs	# AAs	MW [kDa]	calc. pI
X6RM00	ELKS/Rab6-interacting/CAST family member 1	0.00	2.87	4	2	2	2	976	111.9	6.49
B8ZZZ0	3-hydroxyisobutyryl-CoA hydrolase, mitochondrial (Fragment)	0.00	9.16	2	2	2	2	273	30.0	10.48
F8WAU4	Elongation factor G, mitochondrial	0.00	3.09	3	2	2	2	453	50.9	9.31
B5MBZ8	Protein phosphatase 1 regulatory subunit 7	0.00	14.60	5	2	2	3	274	31.3	4.63
J3KS15	Protein MRPL58 (Fragment)	0.00	12.50	2	2	2	2	192	21.9	9.72
C9J2Z4	EH domain-containing protein 1 (Fragment)	0.00	10.13	4	2	2	2	306	34.7	6.14
H7C3G1	Protein ECT2 (Fragment)	0.00	11.96	2	1	2	2	209	24.0	7.91
H7C3Z9	Anterior gradient protein 2 homolog (Fragment)	0.00	23.53	3	2	2	2	119	13.5	6.35
H7BY36	RNA-binding protein EWS (Fragment)	0.00	9.42	5	2	2	4	308	32.2	9.82
E9PC52	Histone-binding protein RBBP7	0.00	5.77	2	2	2	4	416	46.9	5.07
A8MX29	Kinesin light chain 2	0.00	12.91	2	2	2	2	333	36.6	6.34
A0A087X1B2	U4/U6.U5 tri-snRNP-associated protein 2]	0.00	6.98	3	2	2	2	487	56.4	8.38
E7ENN3	Nesprin-1	0.00	0.54	3	2	3	5	8392	964.2	5.54
A0A096LNZ9	Ubiquitin-like protein ISG15 (Fragment)	0.00	23.08	3	2	2	2	143	15.6	6.29
A0A0G2JQN5	1,2-dihydroxy-3-keto-5-methylthiopentene dioxygenase (Fragment)]	0.00	21.21	2	1	2	2	99	11.8	5.80